

SOLID STATE POLYMERIZATION OF CALCIUM ACRYLATE

THE MECHANISM OF SOLID-STATE POLYMERIZATION  
OF CALCIUM ACRYLATE

by

Patrice J. Grisard

A thesis submitted to the Faculty of Graduate  
Studies and Research in partial fulfilment of  
the requirements for the degree of  
Doctor of Philosophy

Department of Chemistry,  
McGill University

Montréal, Canada  
September, 1976

Ils m'ont permis de commencer ...

mes parents

Elle m'a permis de finir ...

Michelle

Patrice J. Grisard

THE MECHANISM OF SOLID-STATE POLYMERIZATIONOF CALCIUM ACRYLATEABSTRACT

The mechanisms of post-irradiation polymerization of calcium acrylate were investigated in the solid state across the hydration range (0-2).

The study of molecular weights distributions and inhibition by oxygen established the existence of at least 2 chemical polymerization mechanisms, radical and ionic.

Polymerization, although it was concluded from crystallography to be impossible in the dihydrate lattice, was found to proceed nevertheless rapidly in the bulk of the solid along with the growth of a new phase. The study of molecular mobility by NMR and of oxygen diffusion by ESR led to the proposal of a model involving motions of the macromolecules inside a "disruption sleeve" or a cavity, which is consistent with the absence of stereotacticity measured by  $^{13}\text{C}$ -NMR.

Initiation and termination were concluded from kinetical and other considerations to be governed by physical rather than chemical factors.

The maximum in polymer yield around 0.5  $\text{H}_2\text{O}$  was rationalized in terms of a maximization of the interphase boundary area and of the radical concentration at that composition.

Patrice J. Grisard

MECANISME DE POLYMERISATION DE L'ACRYLATE DE CALCIUM EN PHASE SOLIDERésumé

Les mécanismes de polymérisation radiochimique de l'acrylate de calcium en phase solide ont été étudiés en fonction du degré d'hydratation (0-2).

L'étude des distributions des poids moléculaires, et celle de l'inhibition par l'oxygène, ont démontré l'existence d'au moins 2 mécanismes chimiques, radicalaire et ionique.

La polymérisation, bien qu'impossible dans le réseau du dihydrate d'après l'analyse cristallographique, s'effectue néanmoins rapidement au cœur du solide en conjonction avec la croissance d'une phase nouvelle. L'étude de la mobilité moléculaire par RMN et celle de la diffusion de l'oxygène par RPE, permirent l'élaboration d'un modèle impliquant des mouvements des macromolécules à l'intérieur d'une "manche de dislocation" ou d'une cavité. L'absence de stéréotacticité du polymère, établie par RMN du  $^{13}\text{C}$ , vient confirmer ce modèle.

Des considérations cinétiques et autres ont permis de conclure que l'initiation et la terminaison dépendaient de facteurs physiques plutôt que chimiques.

Le maximum du taux de conversion en polymère près de  $0.5 \text{ H}_2\text{O}$  a été expliqué en fonction de l'aire interfaciale et de la concentration en radicaux libres, qui sont maximisés à cette composition.

## ACKNOWLEDGEMENTS

This work was carried out under the supervision of Professor L.E. St. Pierre, whom the author wishes to thank for his friendliness and generous assistance. Thanks are also due to McGill University Chemistry Department for a teaching assistantship and for laboratory facilities and services; and to the Université de Montréal for the use of an ESR spectrometer.

The author wishes to express his profound gratitude to Dr. E. Cyr of the Université de Montréal\* for the particular care and time he devoted to teach him the principles and practice of ESR spectroscopy, for his communicating enthusiasm, and for his precious help with the methodology of results interpretation.

Thanks are also due to:

Dr. G. Donnay and S. Fortier for their collaboration and for performing the single-crystal X-ray analysis in the Geology Department;

Dr. R. St. John Manley of the P.P.R.I.C. for his kind assistance with the Debye-Scherrer experiments;

Dr. Yvon Lepage for particularly helpful assistance in the processing and discussion of X-ray data;

Drs. G.K. Hamer and N. Cyr for recording the  $^{13}\text{C}$ -NMR spectra in the P.P.R.I.C. laboratory of Dr. A.S. Perlin;

Dr. D.F.R. Gilson for help with the Wide-Line NMR work; and finally to Dr. D. Patterson, Dr. T. Okazawa and colleagues F. Watine and P. Saviotti for many helpful discussions.

---

\* Now at the N.R.C. Research Center in Ottawa.

TABLE OF CONTENTS

	<u>Page</u>
<u>CHAPTER I: INTRODUCTION</u>	
I-1 Historical Background	1
I-2 Motivations for the SSP studies	2
I-3 The factors of SSP	5
1) Intermolecular distances and lattice parameters	5
2) Size and quality of monomer crystals	6
3) Molecular mobility, annealing, and reanimation	8
4) Additives, copolymerization and eutectics	10
5) Physical parameters of the environment	11
I-4 The different types of SSP	12
Classified according to:	
1) Phase state of the reaction	12
2) Initiation and propagation mechanisms	13
3) Polymerization types and kinetic types	18
I-5 Specific difficulties and means of investigation	18
1) Difficulties specific to the field of SSP	18
2) Techniques of investigation in the solid state	20
I-6 Statement of the problem	21
1) Previous studies in the field	21
2) Choice of the calcium acrylate and aims of the present study	27
3) Structure of the Thesis	29

CHAPTER II: EXPERIMENTAL

II-1	<u>Preparation and characterization of a stock of monomer common to all experiments.</u>	30
a)	Purification of acrylic acid	30
b)	Neutralization	31
c)	Crystallization	31
d)	Characterization and storage	32
II-2	<u>Preparation and characterization of heavy-water dihydrate.</u>	33
II-3	<u>Evacuation and dehydration procedures</u>	34
a)	Dihydrate under vacuum and air	34
b)	Anhydrate under vacuum and air	36
c)	Intermediate hydrates	36
d)	Treatment of small samples	37
II-4	<u>Irradiation with <math>\gamma</math>-rays</u>	38
II-5	<u>Post-irradiation polymerization and product recovery</u>	40
II-6	<u>Differential Scanning Calorimetry (D.S.C.)</u>	41
II-7	<u>Wide-Line Nuclear Magnetic Resonance (N.M.R.)</u>	41
II-8	<u>Mass spectrometry experiments</u>	42
II-9	<u>Electron Spin Resonance (E.S.R.)</u>	44
a)	Technique	44
b)	Preparation of the samples	44
c)	Annealing of the quartz and post-irradiation treatment	45
II-10	<u>Molecular weights measurements by Viscometry</u>	47

II-11 <u>Molecular weights measurements by Exclusion Chromatography</u>	48
a) Samples preparation and solubilization	48
b) Recovery of the poly-acid	48
c) Bypassing the recovery	49
d) Choice of the eluant	49
e) Technicalities and injection procedures	50
f) Choice of the columns	51
g) Dextran calibration standards	52
II-12 <u><sup>13</sup>Carbon NMR Spectroscopy</u>	53
II-13 <u>Crystallography</u>	54
a) Debye-Scherrer powder patterns	54
b) Single-crystal structure analysis	54
 <u>CHAPTER III: THE MONOMER AND THE INITIATION STAGES</u>	
III-1 <u>Crystalline structure of the monomer</u>	57
III-1-1 Previous crystallographic studies	57
III-1-2 Crystallographic experiments	64
a) Debye-Scherrer powder patterns	64
b) Single crystal structure analysis	70
III-1-3 Discussion of the results	74
a) Structure stability and dehydration	76
b) Diffusion of water and inhibitor molecules	78
c) Di-, tri- and polymerization	81
III-2 <u>Oxygen diffusion in the monomer</u>	84
III-2-1 Oxygen diffusion investigated by ESR	84
a) Dihydrate	85
b) Anhydrate	88

III-2-2	Effect of oxygen and thorough degassing on the polymer yield	91
<u>III-3</u>	<u>Physical and phase changes in calcium acrylate hydrates</u>	94
III-3-1	Physical and phase changes as a function of dehydration	94
	a) Previous studies	94
	b) Thermal analysis of the dehydration	99
	c) Disruption of the crystals	106
	d) Molecular motions as a function of dehydration	108
III-3-2	Phase changes and molecular motion at low temperature	115
	a) Low-temperature thermal analysis	115
	b) Molecular motions at low temperature	115
III-3-3	Phase changes and molecular motion as a result of irradiation	119
	a) Thermal analysis of irradiated monomers at low temperatures	119
	b) Molecular motion in the irradiated monomers	119
<u>III-4</u>	<u>Chemical effects of irradiation on the monomer</u>	120
III-4-1	The radicals formed upon irradiation	120
	a) Saturation considerations	121
	b) Annealing at 195°K and kinetics of decay	126
	c) Radical concentrations versus hydration levels	130
	d) Location of the radicals in the irradiated monomer	138
III-4-2	The chemical involvement of water	140
	a) Origins of the initiating radicals	140
	b) Analysis of the radiolysis gases	147

CHAPTER IV: THE POLYMERIZATION MECHANISMS AND THE POLYMER

IV-1	<u>Oxygen diffusion and location of the radicals at the limiting conversion stage</u>	152
IV-1-1	In the dihydrate	153
IV-1-2	In the anhydrate	157
IV-1-3	Conclusions.	157
IV-2	<u>Molecular motions during polymerization</u>	160
IV-2-1	Mobility of the water	163
IV-2-2	Mobility of the monomer	165
IV-2-3	Mobility of the polymer	170
IV-2-4	Conclusion: physical mechanism of SSP	172
IV-3	<u>Stereotacticity of the polymerization</u>	173
IV-3-1	Effect of the pH of observation	175
IV-3-2	Effect of the temperature of observation	177
IV-3-3	Analysis of the results	177
IV-3-4	Fit with Bernoullian statistics	181
IV-3-5	Fit with higher-order statistics	185
IV-3-6	Conclusion: Tacticity control by SSP	187
IV-4	<u>The molecular weight of the polymer and the chemical mechanism of polymerization</u>	187
IV-4-1	Molecular weights measurements by viscometry	188
	a) Viscometry in p-dioxane	188
	b) Viscometry in 0.2 N HCl	192
IV-4-2	Molecular weights distribution measurements by Exclusion Chromatography	195
	a) Benoit's calibration	197
	b) $\bar{M}_V$ distributions of polymers from dihydrate in vacuo and in air	203
	c) $\bar{M}_V$ distributions of polymers from anhydrate in vacuo and in air	212

	<u>Page</u>
IV-4-3 Conclusion: chemical polymerization mechanisms and kinetic parameters	217
a) Chemical polymerization mechanisms	217
b) Kinetic parameters	221

#### CHAPTER V: SUMMARY AND CONCLUSIONS

V-1 <u>Summarizing discussion</u>	223
a) Dehydration mechanisms	223
b) Chemical polymerization mechanisms	225
c) Physical polymerization mechanism	227
V-2 <u>Short conclusions</u>	230
V-3 <u>Contributions to original knowledge</u>	232
V-4 <u>Suggestions for further work</u>	234

<u>REFERENCES</u>	236
-------------------	-----

#### APPENDICES

A <u>Preliminary mass spectrometric experiments</u>	245
A-1 Analysis of water	245
A-2 Analysis of D <sub>2</sub> O	247
A-3 Analysis of a model mixture H <sub>2</sub> O/D <sub>2</sub> O	249
B <u>Mass spectrometric analysis of the vapours above irradiated CaAc, 2 D<sub>2</sub>O</u>	253
B-1 Analysis at 77°K	253
B-2 Analysis at 20°C	253
B-3 Miscellaneous irradiation products	256
C <u>Notes on the direct synthesis of calcium acrylate anhydrate</u>	260
D <u>Tables of supporting data</u>	262

INDEX OF FIGURESPageCHAPTER I:

- Fig. I-6-1-a: Post-polymerization curves of calcium acrylate hydrates in various atmospheres 23
- Fig. I-6-1-b: Post-polymerization curves of barium methacrylate hydrates in various atmospheres 24

CHAPTER II:

- Fig. II-3-1: Types of vessels used for the evacuation and dehydration of the calcium acrylate hydrates samples 35
- Fig. II-4-1: Spatial isodose distribution inside the  $^{60}\text{Co}$  Gammacell 220, giving the positional factor  $f_p$ , in %, as obtained from the AEC 39
- Fig. II-8-1: Sample vessel for the mass spectrometry experiments 43
- Fig. II-9-1: Special vessels for the ESR study of radical scavenging and oxygen diffusion 46

CHAPTER III:

- Fig. III-1-1: Comparison between the dehydration models proposed by Costaschuk and by Watine 60
- Fig. III-1-2: Densitometric measurements of the crystallinity contents of calcium acrylate hydrates, from the Debye-Scherrer powder patterns 61
- Fig. III-1-3: Micro-densitometric analysis of the Debye-Scherrer powder patterns of two anhydrous calcium acrylate samples 66
- Fig. III-1-4: Calcium-calcium distances, in Å, in calcium acrylate dihydrate, as measured from the Debye-Scherrer powder patterns by X-rays 69
- Fig. III-1-5: Calcium acrylate dihydrate unit cell, projection on the ac plane. 73
- Fig. III-1-6: Cross-section of the calcium ribbons stretching along b in the structure of  $\text{CaAc} \cdot 2\text{H}_2\text{O}$ , showing the two types of water present 75
- Fig. III-2-1: Oxygen diffusion through  $\text{CaAc} \cdot 2\text{H}_2\text{O}$ , investigated by ESR 86

Fig. III-2-2:	Oxygen diffusion through CaAc anhydrate, investigated by ESR	89
Fig. III-3-1:	Previous dehydration thermograms of CaAc, 2 H <sub>2</sub> O and BaMa, H <sub>2</sub> O obtained by Differential Scanning Calorimetry <sup>2</sup> in regular sample pans	95
Fig. III-3-2:	Thermograms of barium methacrylate monohydrate, obtained by D.S.C. and T.G.A.	97
Fig. III-3-3:	Dehydration thermograms and simultaneous effluent analyses of CuSO <sub>4</sub> · 5 H <sub>2</sub> O recorded in standard and special sample pans	101
Fig. III-3-4:	Differential Scan <sup>g</sup> Calorimetry Thermogram of a polycrystalline sample of calcium acrylate dihydrate	103
Fig. III-3-5:	Wide-Line N.M.R. spectra of calcium acrylate monomers, recorded at room temperature	110
Fig. III-3-6:	Wide-Line N.M.R. spectra of calcium acrylate monomers, recorded at liquid nitrogen temperature	111
Fig. III-3-7:	Second moments of the Wide-Line curves as a function of the degree of hydration, for 77 and 295°K	112
Fig. III-3-8:	Wide-Line NMR second moment of calcium acrylate samples as a function of temperature	117
Fig. III-4-1:	Effect of Radio-Frequency saturation on the ESR spectra of calcium acrylate dihydrate at 77°K	123
Fig. III-4-2:	Effect of R.F. power saturation on the apparent relative radical concentrations in the various fractional hydrates	124
Fig. III-4-3:	Initial ESR spectra of calcium acrylate samples at 77°K	127
Fig. III-4-4:	ESR spectra of calcium acrylate samples annealed at 195°K for one week	128
Fig. III-4-5:	Effect of annealing on the relative radical concentration as a function of the hydration level	129
Fig. III-4-6:	S.S. Polymerization model involving 3 kinds of radicals	134
Fig. III-4-7:	Radiochemical involvement of the water of hydration: effect of deuteration on the initial ESR spectra at low temperature	143
Fig. III-4-8:	Difference spectrum computed from CaAc, 2H <sub>2</sub> O and CaAc, 2D <sub>2</sub> O	146

CHAPTER IV:

Fig. IV-1-1:	ESR study of oxygen diffusion at 25°C through CaAc, 2 H <sub>2</sub> O at the limiting conversion stage	154
Fig. IV-1-2:	Kinetics of oxygen diffusion through CaAc at the limiting conversion stage, as measured by the rate of oxidation of the acrylate radicals at 25°C	155
Fig. IV-1-3:	ESR study of oxygen diffusion at 25°C through CaAc anhydrate at the limiting conversion stage	158
Fig. IV-2-1:	Wide-Line NMR spectra of irradiated calcium acrylate, 2 H <sub>2</sub> O after various times of post-polymerization at 50°C in vacuo	161
Fig. IV-2-2:	Wide-Line NMR spectra of irradiated calcium acrylate, 2 D <sub>2</sub> O after various times of post-polymerization at 50°C in vacuo	162
Fig. IV-2-3:	Peak-to-Peak height of the NMR narrow line in CaAc dihydrates, during the post-irradiation polymerization stage at 50°C	164
Fig. IV-2-4:	Schematic representation of a physical model of S.S.P.	166
Fig. IV-2-5:	Proportionality between the normalized height of the narrow component of the NMR spectra and the polymer yield	169
Fig. IV-2-6:	Wide-Line NMR spectra of pure poly(calcium acrylate) at 25°C	171
Fig. IV-3-1:	Effect of pH on the <sup>13</sup> C-NMR spectra of poly(acrylic acid) in D <sub>2</sub> O at 353°K	176
Fig. IV-3-2:	<sup>13</sup> C-NMR spectra of poly(acrylic acid) samples made by SSP from calcium acrylates under different conditions; recorded in D <sub>2</sub> O at pH 9, 353°K	179
Fig. IV-3-3:	Triad probability (%) for a Bernoullian polymer, as a function of the placement probability P <sub>m</sub> of the last adding monomer	183
Fig. IV-4-1:	Viscometry of poly(acrylic acid) in p-dioxane at 30.00±0.02°C	191
Fig. IV-4-2:	Viscometry of poly(acrylic acid) in 0.2 N HCl at 24.00±0.02°C	193

Fig. IV-4-3:	"Benoit calibration plot" for the Dextran standards	198
Fig. IV-4-4:	Viscometry of poly(acrylic acid) in the phosphoric buffer used for the exclusion chromatography experiments (pH 3 and $24.00 \pm 0.02^\circ\text{C}$ )	200
Fig. IV-4-5:	Effect of the chemical nature of the solutes on their elution volumes, in exclusion chromatography over porous glass columns	202
Fig. IV-4-6:	Practical molecular weights calibration curve for the exclusion chromatography experiments, at $25^\circ\text{C}$ in the pH 3 buffer	204
Fig. IV-4-7:	Polymerization curves of calcium acrylate dihydrate in vacuo and in air	205
Fig. IV-4-8:	Exclusion chromatograms of polyacids from dihydrate in vacuo, after various times of post-irradiation polymerization at $50^\circ\text{C}$	207
Fig. IV-4-9:	Exclusion chromatograms of polyacids from dihydrate in air, after various times of post-irradiation polymerization at $50^\circ\text{C}$	208
Fig. IV-4-10:	E.C. elution volumes as a function of post-polymerization times	209
Fig. IV-4-11:	Exclusion chromatograms of polyacids from anhydrate in vacuo after various times of post-irradiation polymerization at $50^\circ\text{C}$	213 & 214
Fig. IV-4-12:	Exclusion chromatograms of polyacids from anhydrate in air after various times of post-irradiation polymerization at $50^\circ\text{C}$	215 & 216
Fig. IV-4-13:	E.C. elution volumes as a function of post-polymerization times	218
Fig. IV-4-14:	Polymerization curves of calcium acrylate anhydrate in vacuo and in air	219

INDEX OF TABLES

(xi)

Page

CHAPTER II:

Table II-11-1:	Characteristics of the porous glass columns	51
Table II-11-2:	Characteristics of the Dextran calibration standards	52

CHAPTER III:

Table III-1-1:	Cell parameters of calcium acrylate dihydrate at 183°K	71
Table III-1-2-a:	Atomic coordinates of calcium acrylate dihydrate at 183°K	72
Table III-1-2-b:	Interatomic distances (in Å)	72
Table III-1-3-a:	Dimensional data (Å)	80
Table III-1-3-b:	Dimensions of the envelopes of molecules considered in the study of diffusion	80
Table III-2-1	Calcium acrylate post-polymerization yields under various atmospheres	92

CHAPTER IV:

Table IV-3-1:	<sup>13</sup> C chemical shifts (in ppm) of poly-acrylic acid, relative to dioxane	175
---------------	--	-----

APPENDICES:

Table A-1:	Mass spectrometric analysis of water: Peak intensities and relative abundances of the ions	246
Table A-2:	Mass spectrometric analysis of heavy water: peak intensities and relative abundances of the ions	248
Table A-3:	Fragmentation probabilities of the three isotopes of water in the mass spectrometer	248
Table A-4:	Mass spectrometric analysis of a model mixture of 50% H <sub>2</sub> O + 50% D <sub>2</sub> O: relative peak intensities <sup>2</sup> at equilibrium	250
Table A-5:	Relative abundances of the 3 isotopes of water at equilibrium in a model mixture of 50% H <sub>2</sub> O + 50% D <sub>2</sub> O	252

		<u>Page</u>
Table B-1:	Mass spectrometric analysis at 77°K of the gases above irradiated calcium acrylate di-deuterohydrate	254
Table B-2:	Mass spectrometric analysis at 20°C of the gases above irradiated calcium acrylate di-deutero hydrate	255
Table B-3-1:	Carbon dioxide	257
Table B-3-3:	Ethylene	258
Table B-3-4:	Acetylene	259

DATA FOR THE FIGURES OF THE THESIS:

Data for Fig. III-3-7	262
Data for Fig. III-3-8	263
Data for Fig. III-4-2	264
Data for Fig. III-4-5	264
Data for Fig. IV-1-2	265
Data for Fig. IV-2-3	266
Data for Fig. IV-2-5	266
Data for Fig. IV-4-1, IV-4-2, IV-4-4	267
Data for Fig. IV-4-5	268
Data for Fig. IV-4-7, IV-4-14	268

CHAPTER I

---

INTRODUCTION

## I-1 Historical background

Until recently, solid-state polymerization was considered to be a laboratory curiosity or a puzzling exception. Indeed, most modern scientific curricula in Universities still do not even mention the possibility of chemical reactions in the solid state, let alone polymerizations. However, twenty-five years, have elapsed since Schmitz and Lawton<sup>(1)</sup> irradiated a series of polycrystalline acrylates and methacrylates with fast electrons and obtained surprisingly large (and sometimes explosive) polymerization rates. This was enough to attract general attention to the subject, and in 1954, two groups reported the polymerization of  $\gamma$ -irradiated acrylamide (Mesrobian et al.<sup>(2)</sup> and Henglein and Schulz<sup>(3)</sup>).

Meanwhile, Gerhard M.J. Schmidt, who was to figure prominently in this field, became fascinated by the possibility of using the spacial orientation of molecules in a crystal to carry out stereospecific organic reactions. These ideas were formulated in 1957 in the first part of a thirty-five-article series to appear on the newly named field of "Topochemistry"<sup>(4)</sup>. Since then, the solid-state-polymerization (to be henceforth abbreviated as SSP) has become a field in its own right, and its literature has known the exponential growth rate typical of scientific publications. Vinyl and heterocyclic monomers were the most studied, but more particular ones such as diacetylenics, distyrylpyrazine, etc. are also well represented. The once exceptional behaviour has almost become the rule, and as early as 1962, Magat<sup>(5)</sup> listed forty monomers suitable for SSP, out of the fifty he reviewed.

Unfortunately, general patterns were slow to emerge because of the large number of parameters governing SSP and of the unusual nature of the

problems and experimental techniques involved. In view of the general scantiness of such pertinent information as given by the molecular weight distribution analysis of the polymer products and by the crystallographic analysis of the host monomer, it is not surprising to note that most reviews published on the subject are mainly limited to an enumeration of particular cases.

#### I-2 Motivations for the SSP studies

The rapid initial development of research on SSP was spurred by a number of hopes. Although all of them have eventually been fulfilled by various individual monomers, it can be said nevertheless that as a field, the study of SSP has produced results falling considerably short of the expectations. All these disillusionments can be tracked down to one initial false assumption, which was that the "frozen" state of the monomer molecules in the solid state, particularly in crystals, would provide for some degree of geometrical control over the respective orientation of the reacting species.

This control can assume two forms. On the molecular level, one might expect that the intermolecular forces present could impose a certain stereochemical configuration to the adding monomer, thereby conveniently giving rise to the formation of a crystallizable polymer of a high stereotactic purity. On the macroscopic level, one might envisage that the polymerization could be induced to take place along certain directions of the host monomer lattice favoured by shorter intermolecular distances or by reduced potential barriers. The resulting "topotactic reaction" would thus produce layered or fibrous polymer structures with unusual mechanical

and physical properties. The controls of the stereotacticity and/or of the topotacticity of the polymerization obviously represent a highly attractive proposition in view of their many industrial and theoretical applications.

Indeed, SSP appears thusfar to be the only possible method to obtain polymer single crystals exhibiting an extended-chain morphology. As was pointed out by Morawetz<sup>(20)</sup>, SSP is consequently of considerable theoretical interest to polymer science in general, since the usual crystallization techniques yield only folded-chain polymer single crystals.

Unfortunately, most SSP systems yield an amorphous and atactic product. Topotacticity has been reported in only a few cases (heterocycles: oxetanes, trioxane<sup>(6-11)</sup>; more recently: diacetylenic compounds<sup>(12-14)</sup> and distyrylpyrazine<sup>(15)</sup>). Even then, some of these claims to topotacticity have been subsequently disproved by the recent studies of Keggenhoff and Wegner<sup>(16)</sup> who have shown that apparent topotacticity may be an artefact (this will be developed in section I-5-1).

As a consequence of the prevailing lack of topotacticity, all attempts at gaining a fundamental understanding of the solid-state reactions in general by using the polymer product as a "photograph" of the successive reaction steps proved to be in vain. By and large, the use of SSP to prepare novel polymers or new forms of known polymers and copolymers with "abnormal" sequencing proved to be disappointing in spite of the success obtained in a few isolated cases (co-polyoxetanes<sup>(18)</sup>), cis and trans polyacetylene<sup>(19)</sup>.

Some success has been met with in the areas of the suppression of some undesirable side-reactions accompanying liquid-state polymerization,

for example, the cyclopolymerization of vinyluracil is repressed by SSP<sup>(17)</sup>, and the inhibition of radical reactions by oxygen is often reduced or prevented by the difficult diffusion of O<sub>2</sub> in the solid state. A particular case of a suppressed side-reaction is the termination reaction itself. The quasi-impossibility for macroradicals or macroions to terminate bimolecularly by diffusing towards one another often provides for very high molecular weights up to quantitative conversion<sup>(13)</sup> and in some cases for faster rates of polymerization in the solid than in the liquid state.

There are two areas where the SSP is clearly superior to any other method. The first is high-purity polymerization. Operating in the solid state can free the experimenter from the worry that various residues such as solvent, catalysts or other impurities might become incorporated into the polymer. The crystalline state is specifically useful in this regard, as the crystallization process itself typically excludes impurities. The second area is post-irradiation polymerization. Whether irradiation by U.V., X-rays,  $\gamma$ -Rays or particle bombardment is chosen as an initiation technique for its specific merits or just convenience, the problem arises that the continued irradiation might interfere with the polymer already produced, by causing branching, crosslinking or depolymerization. The solid state, by trapping the primary initiating species at low temperature, allows the experimenter to study the polymerization that occurs upon warming up the sample after it has been removed from the irradiation source. The amount of "in source" polymerization at low temperature is usually small enough to be neglected.

The solid-state post-irradiation polymerization technique thus enables

the scientist to make full use of the inherent advantages of  $\gamma$  irradiation over other initiation techniques. These advantages are:

- formation of initiating species throughout the thickness of the solid, instead of only on the surface as a chemical process would do.
- capacity to initiate both ionic and radical reactions (however, this can sometimes be a disadvantage as well).
- effectiveness over a very wide range of temperatures, including very low ones.
- freedom from contamination of the polymer by catalysts, solvents and other residues.

### I-3 The factors of SSP

#### I-3-1 Intermolecular distances and lattice parameters

From a detailed study of the cyclodimerization of a great many olefines, Gerhard Schmidt and his group<sup>(21,22)</sup> were able to show that a maximum distance of less than approximately 4 Angströms between adjacent reactive double bonds is required for polymerization to take place. When compared to the 1.5 Angströms of the C-C bond formed in the process, this critical distance appears remarkably large. This remark suggests that a considerable spacial rearrangement is needed, in addition to the change of the hybridization level of the carbon. It is therefore obvious that molecular orientations and lattice parameters of the monomer crystals are bound to be important factors in determining their rates of polymerization. Indeed, in the cases where one monomer may be prepared under more than one crystallographic modification, differences

are often observed in their behaviour<sup>(23-26,46)</sup>. However, in the absence of a thorough study, it is difficult to attribute these differences solely to the lattice parameters or to the various amounts and types of molecular mobility present.

### I-3-2 Size and quality of monomer crystals

Many authors have reported the influence of monomer crystal size and quality upon SSP, as well as upon other organic and inorganic reactions.

This influence may manifest itself in three domains: the rate of conversion, the extent of the limiting conversion, and the molecular weight of the polymer product. The effect of an increase in the quality of the monomer crystal varies from inhibiting to promoting the above parameters, but has seldom been reported to be without influence.

The effects of particle size of polycrystalline samples are difficult to interpret. This difficulty originates from the way the crystal size control is achieved. Small crystallites may either be obtained by growing them small or by crushing larger crystals in a mortar. In the first case, the usual method is to provoke an abundant nucleation and a fast phase separation, such as is given by shock-cooling the monomer melt or solution. This procedure also results in a decrease in the quality of the crystals, and the effects of size and quality are hard to distinguish from one another. In the second case, the powdering of monocrystals may distort the observations in two ways: the grinding action itself may degrade the monomer by thermal build-up or radical generation, and secondly the fractures may leave exposed surfaces that are qualitatively different from the natural faces of virgin monocrystals.

In the cases where polymerization begins, takes place or ends at the surface, one can expect the polymerization parameters to be related to the surface area per unit volume. Otherwise, large and more perfect crystals will either tend to show an enhanced rate, extent and degree of polymerization<sup>(6,8,29-32,47)</sup> or the opposite<sup>(27,28)</sup>.

The types of defects found in crystals are: electronic defects (electrons in the conductance band and the positive holes left behind), point defects (vacancies, substitutions or interstitial insertion of a foreign molecule, atom or ion), line defects (edge and screw dislocations) and plane defects (phase boundaries, crystal boundaries with the outside or with another twinned crystal). The study of crystal defects constitutes a specialty in itself, and a number of books are available on the subject<sup>(33-35)</sup>.

Crystal defects influence SSP in two ways: they are themselves privileged places in a crystal lattice, and they influence the lattice around them. The defects are surrounded by regions of both compressive and tensile stress. They can affect the polymerization reaction by providing a favourable free energy, as the perfect lattice opposes a higher energy barrier to the nucleation of a new phase. This is specially true in the most common case where polymer density and inter-atomic distances are very different from those of the monomer. Since most polymers are not isomorphous with their host monomer, propagation will tend to take advantage of the lesser strain build-up required along the dislocations. There also, the mobility of the monomer molecules is considerably greater, and their migration towards the active chain-end may become fast enough to make propagation feasible.

The way crystal defects influence the lattice around them is equally important. Even if minimized by taking place at a dislocation, the strain build-up still accumulates with the polymer growth. This energy may be released by the lattice in two ways: the creation of new dislocations and the migration of existing ones. Such mechanisms are apparently the basis of plastic deformation in solids. Plastic deformation is orders of magnitudes easier in dislocated rather than perfect crystals, and may be favored by the inclusion of additives.

### I-3-3 Molecular mobility, annealing, and reanimation

A few aspects of molecular mobility have already been discussed above. However, certain others will be considered now in some more detail.

The average molecular mobility in solids is obviously much lower than in the usual liquid phases, the first consequence of this being an increase in the likelihood that the self-diffusion of the monomer will be the rate-determining step of the reaction. The second consequence is that the lifetimes of the reactive species are orders of magnitude longer in the solids than the usual ones, and may even appear indefinite. Bimolecular termination reactions are either reduced or inhibited altogether since the probability of two living chain ends meeting together is vanishingly small in a rigid matrix. This implies that establishment of a steady-state process in solid systems is highly unlikely, which renders most traditional kinetic approaches invalid. Chapiro<sup>(36)</sup> finds evidence to this effect in the existence of auto-accelerated polymerization curves with rate law exponents larger than one.

The average molecular mobility may not always be of direct consequence to SSP. In fact, many authors have suggested that in the common case

where the polymer is not isomorphous with the monomer, the lattice may nevertheless be a site of initiation, eventually followed by propagation along the defects. In this case, the molecular mobility at the dislocations is more relevant than the average mobility in the crystal lattice. Even then, however, general molecular reorientation may be indirectly important because it affects the migration of the dislocations involved in plastic deformation. This is a possible mechanism by which the mobility within the crystal may affect the polymer growth in areas outside of the lattice, through assistance to stress relief and annealing. Many systems exhibit the so-called "reanimation" effect, by which a sample having reached its limiting conversion may be reactivated by heating at a higher temperature, without any change in the radical concentration<sup>(40-42,67)</sup>.

It has been suggested by analogy with the work hardening of metals and sucrose caramelization<sup>(43)</sup> that the multiplication of the dislocations could be responsible for the existence of a low conversion limit. This limit would reflect an equilibrium between the strain-generating power of SSP and the strain-relieving power of thermal annealing. Although this explanation has not yet been positively demonstrated, it is consistent with experimental evidence gathered on methacrylamide, isobutyramide<sup>(37)</sup>, on a series of acrylic acid salts studied recently by P.P. Savio in this University<sup>(39)</sup> and on many other monomers, among which the one studied in the present investigation. The inclusion of an elastic strain free-energy term has been judged mandatory in a calculation of interphase free-energy for trioxane<sup>(38)</sup>.

Such remarks have prompted the use of wide-line NMR and ESR to correlate SSP behaviour with various crystallographic forms, allotropic

phase transitions and temperature dependence.

#### I-3-4 Additives, copolymerizations and eutectics

The use of additives has always been of great help in studying traditional polymerizations. For SSP however, the problem is complicated by many factors.

First, most additives are excluded from the crystalline lattice, unless they happen to be isomorphous with the monomer. Small fractions of heteromorphous compounds may be incorporated during crystallization, but are then likely to either create lattice defects or to concentrate preferentially therein. The resulting lattice inhomogeneity is likely to complicate the interpretation by affecting specific reaction steps or stages, as well as by combining physical and chemical effects. Solid-solid phase transition may even result<sup>(35)</sup>.

Second, the use of any additive in radiation-initiated SSP presents problems. The radiochemistry of the additive itself may sometimes obscure its chemical or physical effects. Even so called "inert" additives like carbon black or silica may play a complex role of energy transfer, storage and redistribution to the surrounding lattice.

Third, even if the additive is apparently isomorphous, some lattice distortions are inevitable. Physical plasticization has been invoked as the cause of the rate and yield increase when the "inert" propionamide is co-crystallized with acrylamide<sup>(44,27)</sup>, or when the "inert" propionitrile (or isopropanol) is co-crystallized with acrylonitrile<sup>(45,46)</sup>.

Copolymerization may be attempted between isomorphous or co-crystallizable monomers. Whether co-monomers or other additives are used, most binary compositions of organic compounds form eutectic mixtures. X-ray

diffraction shows that they are constituted by the juxtaposition of microcrystals of both components, which gives more importance to boundary regions and to imperfections. Usually, a maximum in the rate and polymer yield is observed around the eutectic composition<sup>(50,36,48)</sup>. Block copolymerization is observed in the eutectic, along with homopolymerization in the crystallites of the excess phase. Sometimes a sharp maximum may be observed for a composition different from the eutectic<sup>(49)</sup>.

In this context, it is interesting to remark that the polymer itself is a foreign admixture that may display characteristics of isomorphism<sup>(13)</sup> or even eutectic formation with its monomer. This eventuality may be invoked to account for the presence of distinct kinetic periods as polymerization proceeds, such as those observed on acrylic salts by Saviotti<sup>(39)</sup>. Usually, those monomers that polymerize faster in the presence of additives also exhibit auto-accelerated conversion curves<sup>(36)</sup>. "Dormant" radicals may become activated by the approach of the polymerizing front<sup>(28,109)</sup>. In acrylamide, the growth of new islands of polymer ahead of the living front was observed by polarizing microscopy. The progress of the reaction was not smooth but occurred in jumps.

#### I-3-5 Physical parameters of the environment

Several physical parameters have been cited in SSP studies.

The temperature is of course the most important. Most monomers present a maximum in polymerization rate just below their melting point. The interpretation of thermal data and of activation energies is extremely complex, since the temperature, besides affecting the chemical reaction step itself, also governs such crucial factors as average molecular mobility, local mobility at defects, diffusion rate of active species and rate

of relaxation of the stress accumulated by the growth of an heteromorphous polymer (this could also be named rate of annealing, or rate of dislocation migration). Activation energies encountered range from 0.1 to 0.3 kcal/mole for low-temperature in-source polymerization, 1 to 2 kcal/mole for a first group of monomers, and 5 to 40 kcal/mole for the post-polymerization of another group. Chapiro suggested that these widely different ranges could correspond to various polymerization mechanisms.

Mechanical pressure has been found by Bamford et al.<sup>(51)</sup> to slow down considerably the SSP of acrylic and methacrylic acids. Inhibition at early stages coupled with enhancement at later stages, as well as other remarkable effects have been investigated subsequently by the group of Y. Tabata on various other vinyl monomers<sup>(52-54)</sup>. The pressure applied seemed to influence SSP via its effect upon molecular mobility in defect regions and upon stress annealing by dislocation migration.

Magnetic and electric<sup>(62)</sup> fields have also been observed to influence SSP. Experiments on several monomers disclosed complex effects<sup>(110)</sup> which are still the subject of much controversy. The influence of these fields either on the orientation and the diffusion of the active species, or on the collective excitation state of the monomer has been invoked to explain the observed phenomena.

#### I-4 The different types of SSP

The solid-state polymerizations may be classified according to various criteria, among which are:

##### I-4-1 Phase state of the reaction

Most of the SSP studies so far have actually been conducted in the

crystalline phase state. Several studies, however, have been carried out in canal complexes (clathrates) of urea and thiourea<sup>(55)</sup>, in the nematic phase (liquid crystals)<sup>(56)</sup> or in the glassy phase. The hypothesis that "crystalline phase" polymerization actually occurs only in the amorphous-like dislocations for some systems has prompted many authors to further investigate glasses.

However, the literature abounds with confusion on this subject. Few systems appear to have been studied in which the monomer itself could be obtained as a glass. Instead, investigators usually freeze solutions of monomers in glass-forming solvents such as alcohols or amides<sup>(57,58)</sup> or oils<sup>(68)</sup>. Monomer complexes or aggregates due to hydrogen bonding may form<sup>(68)</sup>, eventually giving rise to the formation of stereotactic polymers that could not be obtained from the pure crystalline monomer<sup>(57)</sup>. Kaetsu et al.<sup>(59)</sup> combined these two approaches by using polyfunctional hydroxylated monomers. Other authors froze an emulsion of the monomer into a glassy matrix. A recent study however indicates that monomers may be kept in a liquid state by the supercooling phenomenon as much as 80°C below their melting point<sup>(68)</sup>.

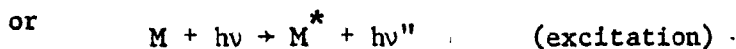
These remarks point towards the need for caution when examining the results of so-called "glassy state" SSP studies.

#### I-4-2 Initiation and propagation mechanisms

Initiation of SSP may be brought about by a great variety of means. Depending on the particular system, heat, ionic or radical initiators, U.V. light with or without sensitizers, particle or molecular bombardment, ultrasonic or shock waves and electrical discharges may be used just as successfully as radiations such as X-rays or gamma-rays and several other miscella-

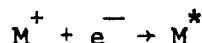
neous techniques. Depending on the experimental conditions, the active species thus formed may be trapped in the solid until released by heating (post-polymerization) or be free to react immediately (in-source polymerization).

Several of these initiation techniques are ambiguous in the sense that they produce throughout the solid free radicals as well as ions of both signs, and general electronic excitation. The high-energy radiations are conspicuous in this respect. By Compton scattering, an electron from the monomer M is ejected:

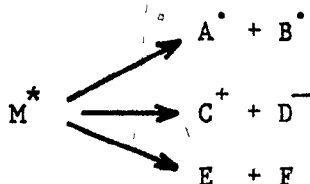


(with  $\nu' < \nu$ ,  $\nu'' < \nu$ )

The ejected ("secondary") electron usually has enough kinetic energy to migrate in the solid, causing further ionization and excitation along its track. When this energy is exhausted, recombination may take place, producing unstable excited species:



which decompose, forming ions, radicals or neutral molecules:





methacrylate). These results clearly demonstrate that chain propagation is not governed by the same factors as the first initiation steps.

Consequently, mechanistic interpretations of ESR results are very delicate for SSP. Possible mechanisms are listed below:

- radical: believed to be a contributing if not the single mechanism at work in most vinyl systems.

- ionic: as high-energy radiations produce ions as well as free radicals, ionic mechanisms of SSP should be at least objectively envisaged. However, some systems, particularly heterocycles, are exceedingly sensitive to minute traces of polar impurities such as water, which might explain why ionic mechanisms have often escaped recognition. Recently, "superdry" monomers have been studied by a number of authors, with the result that ionic mechanisms of both signs have been found in many cases<sup>(111)</sup> (cationic<sup>(32)</sup>, anionic<sup>(60,61)</sup>).

- mixed ionic/radical: exclusion chromatography (gel permeation or other) has recently been used to study molecular weights distributions of the SSP products.

Many systems exhibited binodal or multinodal distributions, which have been linked with the behaviour of superdry monomers to indicate the presence of at least two polymerization mechanisms. Bensasson et al.<sup>(62)</sup> observed that oxygen sometimes acts as an inhibitor even on reactions that are assumed ionic. In a series of articles, Westlake and Huang<sup>(63)</sup> as well as Machi et al.<sup>(64)</sup> agreed to conclude for a combination mechanism (cationic/radical) for styrene SSP. Teramachi and Ushiyama<sup>(65)</sup> proposed a mixed anionic/radical mechanism for the styrene-acrylonitrile system in ethyl bromide at low temperature. In all these examples, it was found that the ratio of the polymer formed by ionic and by radical mechanisms is a func-

tion of the temperature<sup>(110,66)</sup> and of the water content. However, total inhibition even in "wet" samples was not observed, which is of particular significance in the context of the present thesis. Finally, it is to be noted that a mixed mechanism can possibly result from either the presence of the two species independently, or from a radical-ion. Morawetz<sup>(69)</sup> remarked that even if the number of radicals is measured to be equal to the number of polymer chains, it does not necessarily mean that the radical end is the growing one.

- "electronic" mechanism: A collective molecular excitation process has been proposed by Tabata and his group, to account for the occurrence of polymerization even at very low temperatures "in source". The extremely small activation energies, the rapid achievement of limiting conversions and the high molecular weights attained led them to develop the theory and the implications of a very fast collective polymerization under excitation of the monomer crystal as a whole<sup>(110)</sup>.

- "energetic chain" mechanisms: Using the same conditions, Semenov<sup>(70)</sup> proposed that highly excited monomers may attack adjacent units. The heat of reaction, concentrated by the poor thermal conductivity of solids, would be used up for the electronic excitation required by the next step. This would account for low energies of activation. In a modification proposed by Magat and Chachaty, the heat of reaction would create a local temperature elevation allowing conventional reaction after the equivalent of a local "sublimation". In another modification of the energetic chain theory, called the "hot track" theory, a whole polymer molecule would be produced in less than  $10^{-8}$  sec. under a metastable form along the spur of a  $\delta$  electron. Relaxation would then occur, shortening the intermonomer distances

from their lattice values to their polymer bond values. The details of these theories are exposed and discussed in a review by Tabata<sup>(110)</sup>. Recent Moessbauer experiments by Goldansky et al.<sup>(71)</sup> seem to give support to an ionic/electronic mechanism in a methacrylic glass.

#### I-4-3 Polymerization types and kinetic types

In addition to the classifications according to the phase state and the chemical mechanism of the reaction, solid-state polymerization may be further categorized as:

- Topotactic if the orientation of the polymer chains may be related directly to the crystallographic axes of the monomer.
- Stereotactic if the polymer chain units exhibit a configuration which is either constant or related to other neighbouring units.
- Isomorphous if the polymer happens to co-crystallize in a one-phase solid solution with its host monomer.
- Auto-accelerated, -retarded or linear according to the shape of the kinetic conversion curves.

#### I-5 Specific difficulties and means of investigation

##### I-5-1 Difficulties specific to the field of SSP

The exothermicity of SSP and the poor thermal conductivity in solids lead to the possibility that in organic crystals having relatively low melting points, local melting could allow the polymerization to actually take place in the liquid state, followed by a subsequent recrystallization in the mold of the surrounding lattice. This is similar to (in its premises) but not to be confused with the mechanism mentioned earlier in section I-4-2 (Magat and Chachaty<sup>(110)</sup>). It is believed that this problem may be solved

by the use of high-melting monomers, to ascertain a "true" SSP.

- Product recovery in SSP experiments lends itself to many criticisms. The first danger is that the trapped ionic or radical species might react rapidly when one tries to melt or dissolve the remaining monomer away, thus giving the illusion that a SSP has occurred. This danger may usually be averted by operating very fast, in a divided state, and by including inhibitors in the solvent. The second danger is that the phase state, degree of crystallinity and apparent topotacticity of the polymer product may be altered, reversed or destroyed at the recovery stage. Keggenhof and Wegner<sup>(16)</sup> have shown recently that the widely claimed "topotactic" SSP of oxetane-series monomers is an artefact. The initially amorphous polymer product recrystallizes during recovery because of the anisotropic swelling of unconverted monomer at the extraction stage. The apparent "topotacticity" is therefore now believed to be only coincidental in this system.

- Traditional kinetic laws and their interpretation of experimental results often do not apply to SSP, or need to be strongly adapted to do so. Concepts such as concentrations and homogeneity (whether macroscopically or between the 3 crystallographic axes), and all the concepts based upon statistical probabilities of collision such as the idea of steady-state need to be properly redefined to have a physical meaning for SSP. For example, the reactivity of a chemical species in the solid state need not be proportional to its overall concentration.

- Limitations in the choice of experiments are placed upon the investigators by the inability to vary concentrations by solvent dilution. The usual inhibitors, catalysts, initiators, co-monomers and other additives

are restricted in SSP to the very few that happen to be tolerated in the crystal network. Many classical techniques such as U.V., I.R. or visible spectroscopy, etc., may not be applied to SSP because of the lack of transparency of polycrystalline samples.

#### I-5-2 Techniques of investigation in the solid state

The choice of techniques utilized for the study of SSP is limited by the specific difficulties discussed above. It includes destructive (polymer recovery for analysis) and non-destructive methods (spectroscopies).

Among the destructive methods may be included the gravimetry and the various analyses of the polymer formed:

- Exclusion Chromatography is a most valuable tool of mechanism elucidation, for its ability to disclose the molecular weights distributions in addition to their average values.
- Carbon-13 NMR is a powerful tool in determining the stereoconfiguration of the polymer products of SSP, and relating it to other parameters.

Among the non-destructive methods may be included picnometry (if the change in density upon polymerization is homogenous enough), X-ray, and the magnetic spectroscopies such as ESR and NMR.

- Electron Spin Resonance (ESR) is the most widely used technique. It gives access to such vital data as radical concentrations (local or average), configuration, conformation, spacing and orientation, as well as to the local molecular motion and diffusion.
- Nuclear Magnetic Resonance (NMR), especially the Wide-Line NMR, gives information about average molecular motion and solid-solid phase

transitions, specially when connected with crystallographic data. A narrow line is sometimes seen superimposed on the wide-line spectra, and is proportional to the polymer concentration. This makes wide-line NMR one of the precious few non-destructive techniques for following polymer conversion kinetics.

Very recent articles by Chachaty, Forchioni and Latimier<sup>(40)</sup> exemplify clearly (acrylic and methacrylic acids, acrylamide) the latest benefits that the three fundamental electromagnetic spectroscopies can bring to the understanding of SSP;

#### I-6 Statement of the problem

##### I-6-1 Previous studies in the field

Several authors have studied various salts of acrylic and methacrylic acids<sup>(72-75)</sup>. Some have studied hydrated salts, like Ca, Zn, and Ba<sup>(76-83)</sup>. But only very few have become interested in the various hydration levels of the same salt, and their potential influence on SSP. Their findings will be briefly summarized here.

Lando and Morawetz<sup>(77,78)</sup> first attempted to prepare various polymorphic and hydrated forms of calcium acrylate and barium methacrylate, and to study their SSP behaviour. Unfortunately, it was shown later that they made a number of errors and omissions that severely undermine the validity of their conclusions<sup>(84)</sup>.

F. Costaschuk<sup>(84)</sup> established the true hydration levels of calcium acrylate (Ca Ac) and barium methacrylate (Ba MA). He was the first to study the SSP of these two salts as a function of a continuous variation of hydration. His thermogravimetric, differential scanning calorimetric

and crystallographic results were interpreted in terms of the dehydration occurring in one single step with no formation of intermediate compound. Although Ba MA forms a monohydrate and Ca Ac a dihydrate, and although the anhydrous Ba MA is crystalline whereas the anhydrous Ca Ac is "pseudo-amorphous", both compounds exhibited a maximum in polymer yield at the same hydration level of 25% of the full hydration (Fig. I-6-1-a and b). When performed in air instead of in vacuo, the post-polymerization exhibited a quasi-total inhibition at this same particular hydration level (Fig. I-6-1-a and b). Costaschuk proposed a model of dehydration involving 2 phases (pure dihydrate, pure anhydrate) and a very thin boundary layer of intermediate "x" composition recessing towards the core of each grain as dehydration proceeds. He also proposed a polymerization model, where the total rate of polymerization is the sum of three factors, which are the rates R and volumes V corresponding to each phase:

$$R_{\text{Total}} = R_2 V_2 + R_0 V_0 + R_x V_x$$

(where subscript 2 is dihydrate; 0: anhydrate; x: boundary layer)

and was led to assume that the small interphase volume  $V_x$  must have a "sphere of influence" extending much beyond its physical boundaries, and varying non-monotonously with the hydration, in order to account for the maximum in the polymer yield curve. His electron-spin-resonance (ESR) experiments indicated that the concentration in free radicals decreased linearly as the composition changed from anhydrate to dihydrate. From this, he concluded that the interphase boundary played no important role in the formation of the initiating radicals.

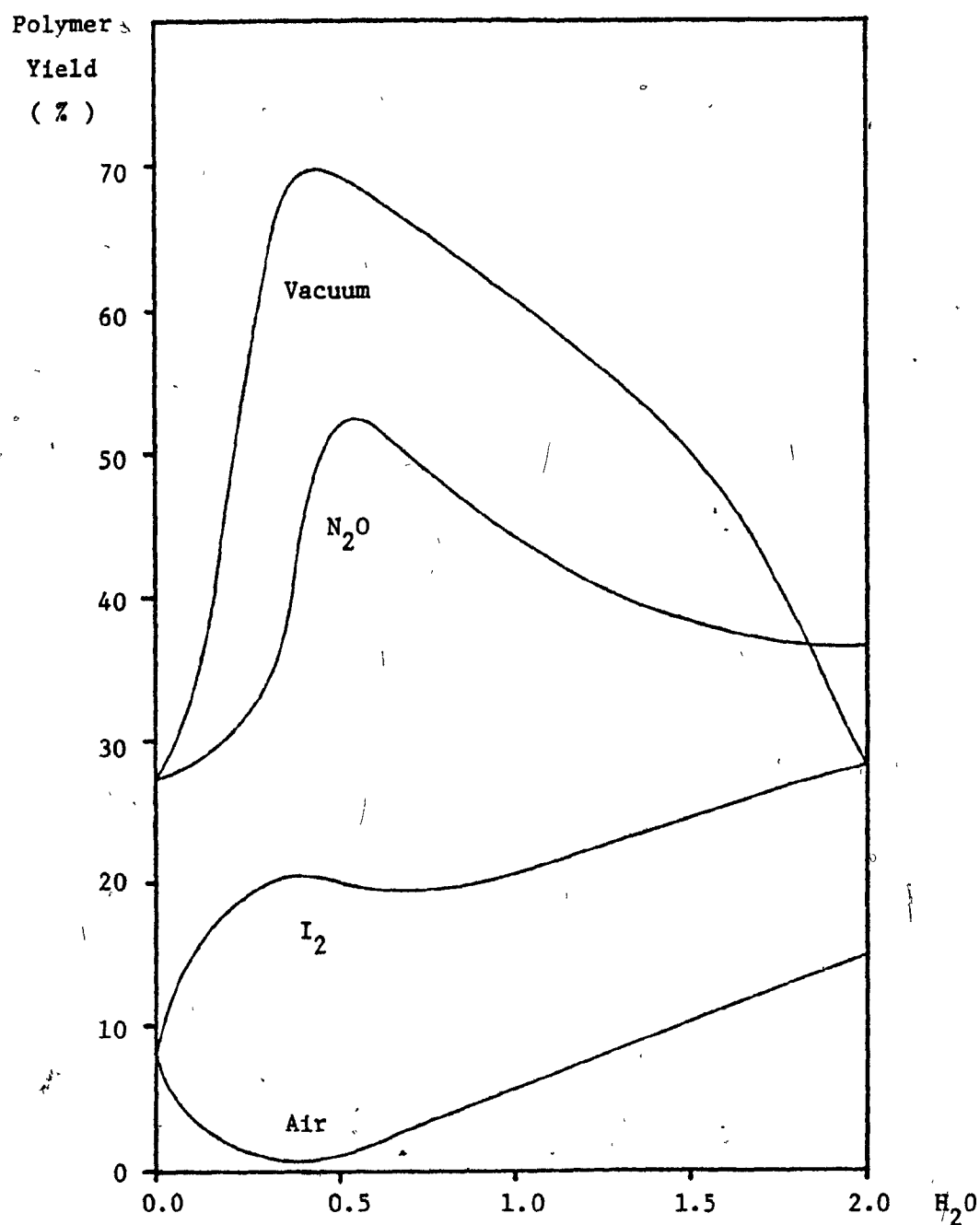


Fig. I-6-1-a : Post-polymerization curves of calcium acrylate hydrates in various atmospheres ( Source : Watine<sup>(85)</sup> p. 53 ) .

Conditions : 0.87 Mrad gamma-irradiation at  $-78^{\circ}\text{C}$

Dose rate :  $3.3 \times 10^5$  rad/hr

Polymerization : 9 days at  $50^{\circ}\text{C}$

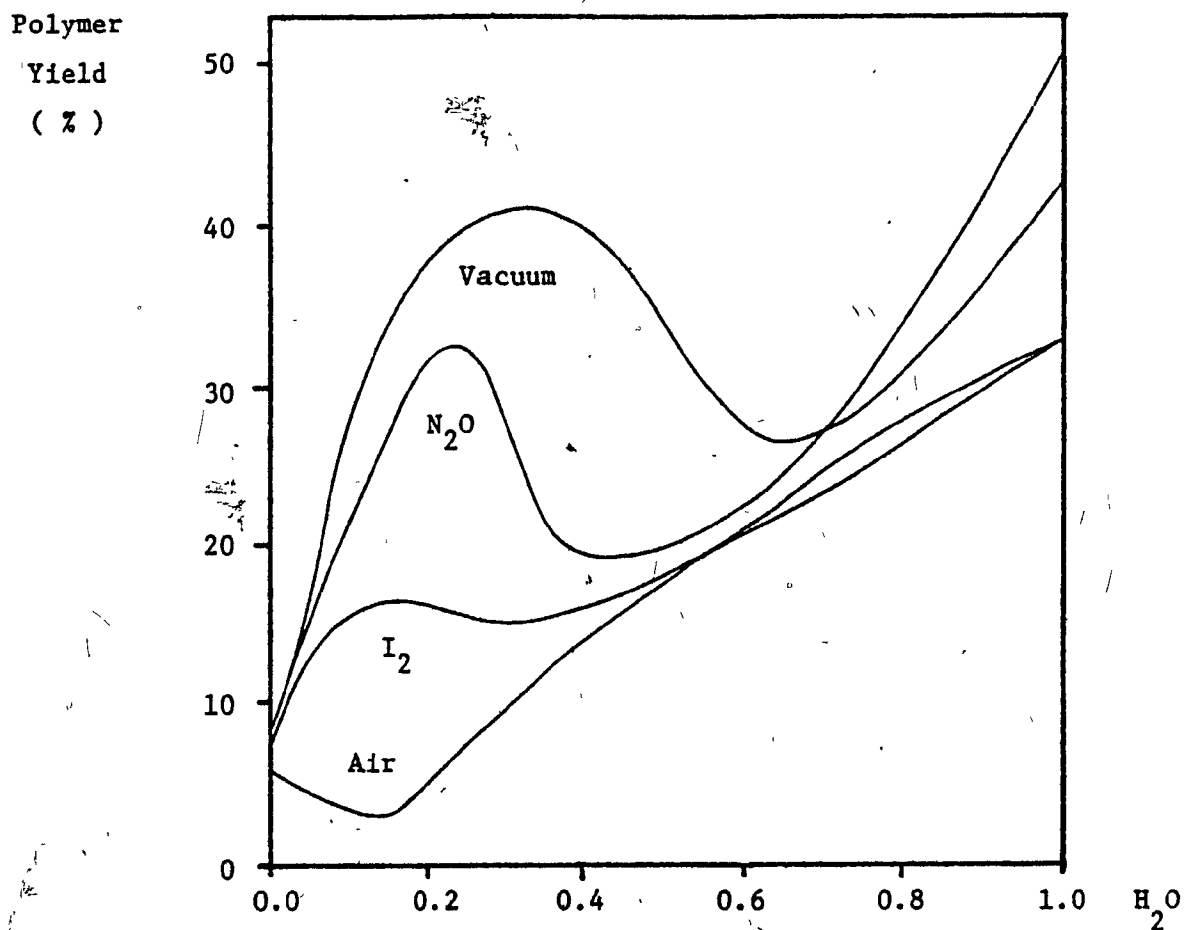


Fig. I-6-1-b : Post-polymerization curves of barium methacrylate hydrates in various atmospheres ( Source : Watine <sup>(85)</sup> p. 130 ) .

Conditions : 0.86 Mrad gamma-irradiation at  $-78^{\circ}\text{C}$

Dose rate :  $3 \times 10^5$  rad/hr

Polymerization : 9 days at  $50^{\circ}\text{C}$

F. Watine<sup>(85)</sup> verified a number of Costaschuk's experiments. He completed the polymerization curves in air and vacuo, and also investigated the inhibition of SSP in the presence of nitrous oxide and iodine (Fig. I-6-1-a and b). The results kept open the possibility of having an ionic mechanism concurrently with the radical one.

His ESR study of heavy-water hydrates indicated that the water of hydration was chemically involved in the initiation step of polymerization, and he speculated that water might also act as a radical scavenger or an electron trap.

X-rays powder diagrams were analysed densitometrically across the hydration range. Assuming a linear additive behaviour, the results were interpreted as indicating that the crystallinity of Ca Ac varied non-linearly with the hydration level, a large step occurring above the special composition of  $0.5 \text{ H}_2\text{O}$  mentioned earlier. Infra-red spectroscopy and gravimetry established that the water of hydration, although hydrogen-bonded in calcium acrylate di-deuterohydrate, was readily exchangeable with the atmospheric humidity.

As a conclusion, F. Watine proposed two models for the dehydration and polymerization mechanisms. On the grounds of the alleged extreme mobility of the water of hydration and of the alleged non-linearity of the crystallinity and density curves, the dehydration model featured a 3-phase system, where a phase of intermediate composition  $0.5 \text{ H}_2\text{O}$  replaces gradually and totally the dihydrate phase as dehydration proceeds. As it goes on below the  $0.5 \text{ H}_2\text{O}$  level, the intermediate phase would then give way to the anhydrate phase.

For the polymerization model, Watine proposed that the "active volume"

of the "intermediate 0.5 H<sub>2</sub>O composition" was the only one to be totally diffusible by oxygen. The anhydrate should be somehow less disordered, to account for the lack of total inhibition of the radical polymerization by oxygen. The same lack of O<sub>2</sub> diffusibility applies even more, of course, to the crystalline dihydrate. The maximum polymerization rate occurring at the 0.5 H<sub>2</sub>O level would thus be a consequence of the larger monomer mobility in the maximally disordered "active volume". Ba MA exhibited a behaviour similar to that of Ca Ac.

Finally, Watine developed a set of equations to fit his models and to account for the behaviour of the three phases required by his "active volume" concept.

Bowden and O'Donnell<sup>(81-c)</sup> studied the dehydration of barium methacrylate monohydrate by D.S.C., thermogravimetry, and X-ray analysis. They concluded to a strictly 2-phases system (crystalline anhydrate and monohydrate), but noticed 2 peaks in the D.S.C. experiments which they attributed, as did Costaschuk, to a phase transition to the anhydrate crystalline form followed by the desorption of the water. However, O'Donnell and Sothmann<sup>(83-b)</sup> made a further study in 1972, which showed that the system is more complicated than was believed previously. Their results indicated that although it is basically a 2-phases system, a metastable partial hydrate could exist under certain conditions. A two-steps weight loss occurred in small crystals, as opposed to the one-step dehydration of fine powders. The first dehydration step would occur together with a structural change, and the second dehydration step could then be a kinetic feature resulting from temporary trapping of water molecules in the partly dehydrated structure. After irradiation, the post-polymerization and the

dehydration could be observed separately under no circumstance.

The models proposed by the various above authors will be discussed in greater detail during the course of the thesis, in the light of the experimental results obtained.

#### I-6-2 Choice of the calcium acrylate and aims of the present study

The general orientation of the present study proceeds along two principal directions:

- to acquire a significant gain in the knowledge of the various phenomena governing solid-state polymerizations in general.
- to obtain a better insight in the dehydration process itself, which usually tends to be taken for granted.

To move along the first direction of research, it was felt that the particular system of the calcium acrylate hydrates offered the potentiality of being a model of outstanding interest, for the following reasons:

- it exhibits at least two phase states, crystalline and pseudo-amorphous, allowing the static study of phase influence on the SSP.
- its continuously variable hydration levels give an opportunity to study the physical effects on SSP nearly independently from the chemical variations on a continuum, as well as during the transition (dynamic study).
- its very high melting point is likely to ensure a true solid-state reaction by precluding "local melting".
- it exhibits the post-irradiation polymerization phenomenon whereby initiation and propagation may be conveniently investigated separately.
- its extreme solubility in water allows a very fast separation of the

polymer from the unreacted monomer, thus minimizing the "post-effect" artefact.

To move along the second direction of research, a hydrate is obviously required. It may be argued that by the selection of such a complicated system, the salient features of either SSP or dehydration show a risk of obscuring one another and confusing the interpretation. This has certainly been the case in the past.

However, it was felt that this complexity represented a challenge and that the very duality of the problem could instead be an advantage, if the data gathered along either direction of research could be rationalized in a way bolstering the other one.

The approach taken has therefore been one of systematic study of many aspects of a single system in as much depth as possible, resorting to several powerful and modern techniques, rather than a more limited study of several compounds.

Finally, it was felt that the presence of the peculiar maximum of polymerization around the "quarter hydration" level of both calcium acrylate and barium methacrylate was actually left incompletely explained by Costaschuk<sup>(84)</sup> and by Watine<sup>(85)</sup>, as was the absence of total inhibition by air for the anhydrate. Several other results of Costaschuk (D.S.C., ESR, wide-line NMR, molecular weights determination) as well as Watine (X-ray densitometry, D.S.C., ESR, polymerization in the presence of excess water vapour) appeared to the present author to necessitate reevaluation and reinterpretation.

The present thesis was therefore oriented towards the acquisition of a clear physical understanding of the phenomena involved in this complex

system, in priority over mathematical speculations based on insufficiently documented models.

### I-6-3 Structure of the Thesis

The thesis is presented in five chapters.

Chapter I is the introduction, presenting the necessary background on SSP and the outline of the problems attacked.

Chapter II exposes the experimental methods in slightly more detail than usual, because of the particular impact that sample preparation and experimental technique have on SSP systems.

Chapter III groups the experimental results gathered during the study of the monomer and of the initiation stages, along with the discussion of the conclusions derived from them.

Chapter IV does the same for the polymer and the propagation stages.

Chapter V contains the general conclusion, the proposition of polymerization and dehydration models and the suggestions for further work.

CHAPTER II

---

EXPERIMENTAL

II-1 Preparation and characterization of a stock of monomer common to all experiments

II-1-a Purification of Acrylic Acid

Reagent grade acrylic acid from American Chemicals was purified according to the following procedure in order to remove all traces of polymer and commercial inhibitor.

One litre of the acid was placed in a flask with a quantity of copper sponge to inhibit polymerization. The flask was attached to a vacuum line, the acid was degassed by the freeze-thaw method, and then vacuum distilled. Excessive degassing proved to be a nuisance, as it allowed two troublesome reactions to take place. The first one was polymerization of the acrylic acid vapours as they condensed on the inside walls of the vacuum line. The second one was polymerization of the acrylic acid during the freeze-thaw cycles, if the copper sponge was omitted.

These seem to be two examples of polymerization induced by, or concomitant with, phase changes. This type of phenomenon will be documented further in the conclusion (Chap. V).

The inhibitory effect of copper prompted the use of a test with the complexing indicator para-aminonitrophenol (P.A.N.P.) to verify whether copper had been dissolved in the acid and was carried over by the distillation.

The test was negative for the distilled acid, but positive for the acid that had bathed the copper sponge, attesting to the efficiency of the distillation within the limits of the P.A.N.P. sensitivity.

Polyacrylic acid, which is insoluble in benzene and cyclohexane, was shown to be virtually absent from the distilled acid as no cloudiness was observed on addition of the distillate to these solvents.

#### II-1-b Neutralization

Calcium hydroxide powder (Fisher reagent grade) was slowly added to a cooled, stirred aqueous solution of 3N acrylic acid. The temperature was kept below 20°C by means of an ice jacket. A light brown, muddy solution resulted. The brown colour and the cloudiness probably derive from impurities contained in the  $\text{CaCO}_3$ . At the phenolphthalein endpoint (pH 8.2 to 10) a slight excess of acrylic acid was added to neutralize the solution, which was checked with pH-paper.

The solution was then filtered, with great difficulty, through several paper filters ranging from coarse to ultra-fine. This procedure removed undissolved materials,  $\text{CaCO}_3$  and gel traces. The resulting solution was clear, but pale yellow. P.A.N.P., added to a test sample, turned pink, which suggested that some trace contaminants were present in the  $\text{Ca(OH)}_2$  reagent. Indeed, it also turned pink when added to the original  $\text{Ca(OH)}_2$ , which is stated by Fisher to contain the following: "Fe=0.03%; other heavy metals < 0.003%; Mg and alkalis + 1%".

#### II-1-c Crystallization

The salt was crystallized from this solution by slow evaporation from a dish covered with a paper towel, at room temperature. Three portions were collected after 10, 12 and 30 days. The remaining greenish-yellow mother liquor was discarded. A carbon, hydrogen analysis having given unsatisfactory results, it was decided that a recrystallization of the product was necessary. The three portions were dissolved together, filtered

through ultrafine paper, and the recrystallization procedure was repeated. The crystals (thin white needles 1-20mm long) were collected and air-dried to constant weight.

#### II-1-d Characterization and storage

The P.A.N.P. test performed on the mother liquor proved weakly positive, whereas it was negative when performed on the crystals. This shows that one recrystallization effected an efficient purification.

The hydration level was ascertained by gravimetry. Weight loss upon total dehydration was shown to match the theoretical 16.5% exactly. The raw crystals were crushed using a mortar and pestle, to form a coarse powder. The crushing is designed to get rid of occluded water, which may amount to 30% of the hydration water in large crystals<sup>(81-c)</sup>. When left in the open air at 21°C for 8 days, a finely powdered sample of the dihydrate exhibited a weight stability of better than 0.1%.

The carbon, hydrogen analysis was performed at McGill on a Hewlett-Packard Model 185:

	Found	Calculated
C% :	33.2 ± 0.3%	33.02%
H% :	4.54 ± 0.2%	4.62%

(Calcium acrylate dihydrate)

The crystals were stored in a dessicator, over a saturated CaCl<sub>2</sub> solution. This procedure proved to be satisfactory in a number of dehydration tests made over a period of two years.

## II-2 Preparation and characterization of heavy-water dihydrate

Calcium acrylate dihydrate (70g) was vacuum desiccated at 65°C. After verifying by gravimetry that the dehydration had been complete, the anhydrate was placed in a dry box. The dry box was partially evacuated and filled with dry air several times to remove the atmospheric moisture. Dry nitrogen proved unsuitable for this purpose, since the exclusion of oxygen from the dry box allowed a fairly rapid polymerization of the monomer as soon as the latter had dissolved in the D<sub>2</sub>O. Accordingly, compressed air was passed through a desiccation apparatus consisting of the following: a mercury safety valve, a safety Erlenmeyer trap, a concentrated sulphuric acid bubbling bath and two glass columns (1.20m x 38mm) filled with anhydrous calcium chloride and phosphorus pentoxide respectively. A positive pressure of dry air was maintained inside the dry box at all times.

The anhydrate was dissolved in 150cm<sup>3</sup> of D<sub>2</sub>O. The purity of this D<sub>2</sub>O was ascertained by high-resolution N.M.R. to be better than 99.6%. This solution was then filtered through ultra-fine paper and left to crystallize in a large dish. While the dry air was flushing the dry box continuously, a crust of crystals formed on the surface of the solution, thereby preventing further crystallization. This crust was broken each day for three weeks, whereupon 56g of heavy water hydrate were collected by filtration. The fine white needles were dried in a stream of dry air.

The product was characterized by its weight loss and by its carbon-hydrogen content. Firstly, it was totally dehydrated in vacuo at 63°C for 20 hours. The experimental weight loss was 17.95%. This shows a 99.76% dehydration when compared to the theoretical weight loss of 17.99% calculated.

for a heavy-water dihydrate made from 99.6% D<sub>2</sub>O. Secondly, it was sent to the Schwarzkopf Microanalytical Laboratory<sup>(86)</sup> for elemental analysis.

The results are shown in tabular form below:

	<u>Found</u>	<u>Calculated</u>
C% :	32.6%	32.42%
D% :	6.18%	6.34%

(calcium acrylate, di-deuterohydrate)

The product was stored in a tightly capped container inside the dry box, and under a positive pressure of dry air.

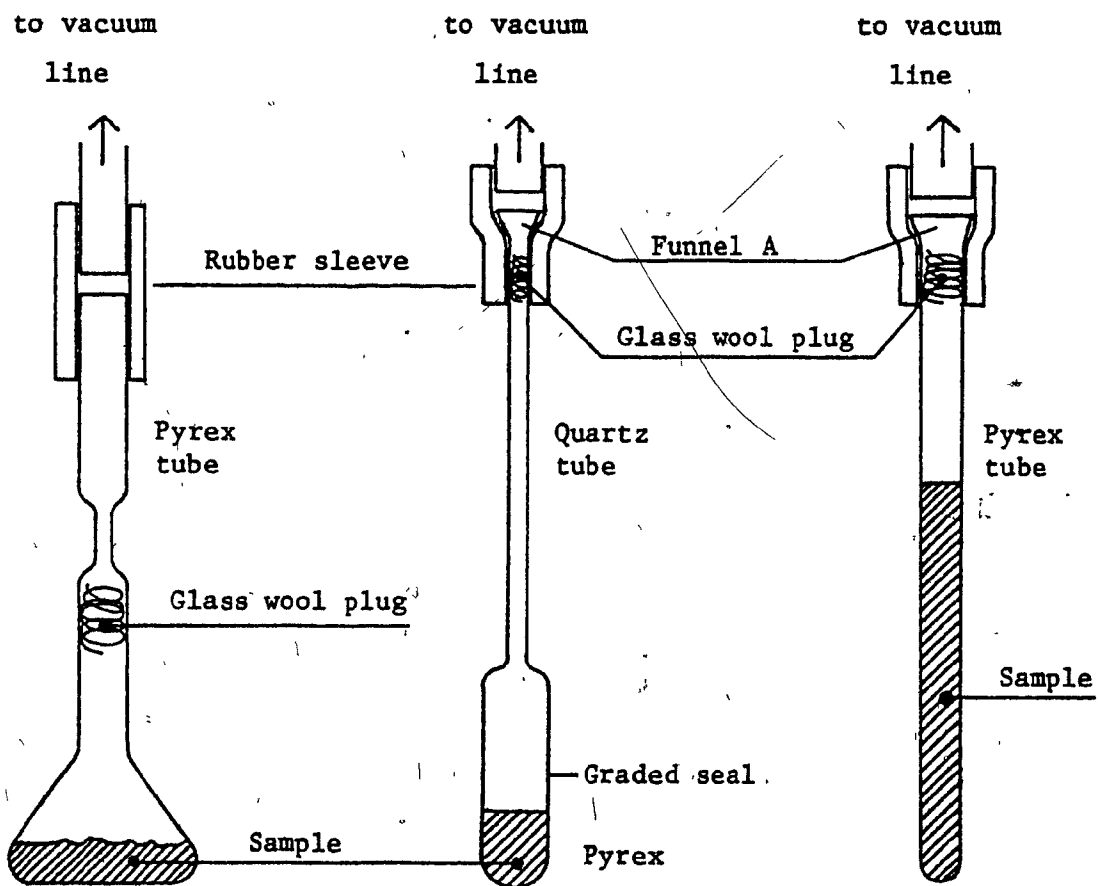
### II-3 Evacuation and dehydration procedures

The dehydration procedures were similar for all the experiments, except for minor details which are described in each section. The vessels used were of various types as shown on Fig. II-3-1.

The necessary amount of sample was weighed into the vessel. The walls of the inlet tube were carefully cleaned with pipe cleaners. Mindful of the possibility of contamination and sample loss, a Pyrex wool plug was inserted into the neck of the sample vessel. The sample vessel was connected to the vacuum line by means of a rubber sleeve whose inside wall was slightly greased.

#### II-3-a Dihydrate under vacuum and air

The pressure above the sample was first quickly reduced to 1/2 atm. to remove any excess atmospheric moisture. The sample was then immediately cooled in liquid nitrogen while the manifold was very slowly opened, allowing



General use and  
Exclusion Chromatography

Regular ESR  
vessels

Wide-Line NMR  
vessels

Fig. II-3-1 : Types of vessels used for the evacuation and dehydration of the calcium acrylate hydrates samples .

the pressure to fall to  $10^{-4}$  mm Hg . The samples were evacuated for 10 more minutes before being sealed off at the constrictions indicated on Figure II-3-1.

The "dihydrate in air" samples were sealed directly under a pressure of 0.9 atm. dry air at room temperature.

#### II-3-b Anhydrate under vacuum and air

The manifold was very slowly opened to the vacuum line. The temperature of the sample was gradually raised from  $25^{\circ}$  to  $60^{\circ}$ C over a period of 12 hrs. by means of a water bath. The samples were left under constant pumping for at least 2 hrs. after the residual pressure fell to  $10^{-4}$  mmHg. It was confirmed by gravimetry that this procedure produced total dehydration. Weight losses of 99.7 to 100% of the calculated value were consistently recorded for experiments conducted during a period of two years, showing the excellent homogeneity and stability of the Ca acrylate dihydrate prepared.

For the "anhydrate in air" samples, the same procedure was followed: then dry air was admitted at a pressure of 0.9 atm. prior to sealing at the constriction.

#### II-3-c Intermediate hydrates

The same procedure as for the anhydrate was used. However, the heating and pumping were interrupted after various lengths of time, determined approximately from a rough calibration curve. To measure the exact extent of the dehydration, the sample vessel was removed from the vacuum line, wiped and weighed after a short period of equilibration. The sample vessel was then reconnected to the vacuum line and either frozen, evacuated and sealed, or filled with dry air at 0.9 atm. and sealed.

This technique of preparation and characterization of the hydrates of intermediate water contents departs from that of Costaschuk<sup>(84)</sup> and of Watine<sup>(85)</sup> in such a way as to significantly affect the precision of the results. Those two authors sealed the sample vessels at the constriction before weighing them. Thus, they needed to apply a correction for the weight of the air lost by evacuation, which was arbitrarily fixed at the same value for all samples.

However, a careful comparative study showed that the unavoidable variability in the glass-blowing allowed the actual correction for air loss to vary between 4 and 9.7 mg. Depending on the degree of dehydration and the size of individual samples, such variations may then be reflected by as much as 5 to 30% error in the calculated hydration level.

Consequently, it is believed that the hydration levels measured in this thesis are significantly more accurate than those of Costaschuk and Watine. This remark could very well explain the important qualitative difference between the ESR results of Costaschuk and those presented in Chap. III.

#### II-3-d Treatment of small samples

For most studies, the typical sample size was approximately 1 g. In such a case, total dehydration corresponded to a weight loss of 165 mg. A 10% dehydration would then amount to a weight loss of 16.5 mg which is still measurable to an acceptable accuracy. However, for some experiments such as the ESR where small samples (0.2 - 0.4 g) were used, it was believed that the accuracy so obtained was not adequate. In these cases, a larger sample (about 1.5 g) was processed in a different container, and an aliquot of the

powder was subsequently transferred to the small ESR tube just prior to sealing. It is known<sup>(84)</sup> that the rate of weight change of these hydrates at room temperature and under atmospheric pressure is negligible, which justifies this modification of the procedure.

#### II-4 Irradiation with $\gamma$ -rays

The irradiations throughout this work were performed by lowering a dewar filled with a suitable coolant into a  $^{60}\text{Co}$  Gammacell 220 of the Atomic Energy of Canada. The actual dose rates received by the sample were calculated from the following factors:

-  $\text{DR}_0 = 0.446 \text{ Mrad/hr}$  on Sept. 16, 1968 as measured by Fricke dosimetry and stated on the certificate of calibration.

- the electron density for the Fricke solution is  $3.33 \times 10^{23} \text{ e}^-/\text{g}$

- the electron density for the Ca acrylate, dihydrate is:

$$\text{E.D.} = \frac{114 \text{ e}^- \times N_{\text{Avo.}}}{\text{Mol. Weight}} = 3.146 \times 10^{23} \text{ e}^-/\text{g}$$

that for the anhydrate being  $3.108 \times 10^{23} \text{ e}^-/\text{g}$ . The average value  $3.127 \times 10^{23} \text{ e}^-/\text{g}$  was used for all samples. Thus the relative electron density  $f_e = 3.127/3.33 = 0.94$

- a uniform  $f_a = 95\%$  factor was applied to account for the absorption of the dewar and dry ice or liq.  $\text{N}_2$ .

- the monthly decay factor  $f_m$  was read from the table accompanying the calibration.

- and finally, the positional factor  $f_p$  was estimated according to the size and position of the individual samples from the following Figure

II-4-1.

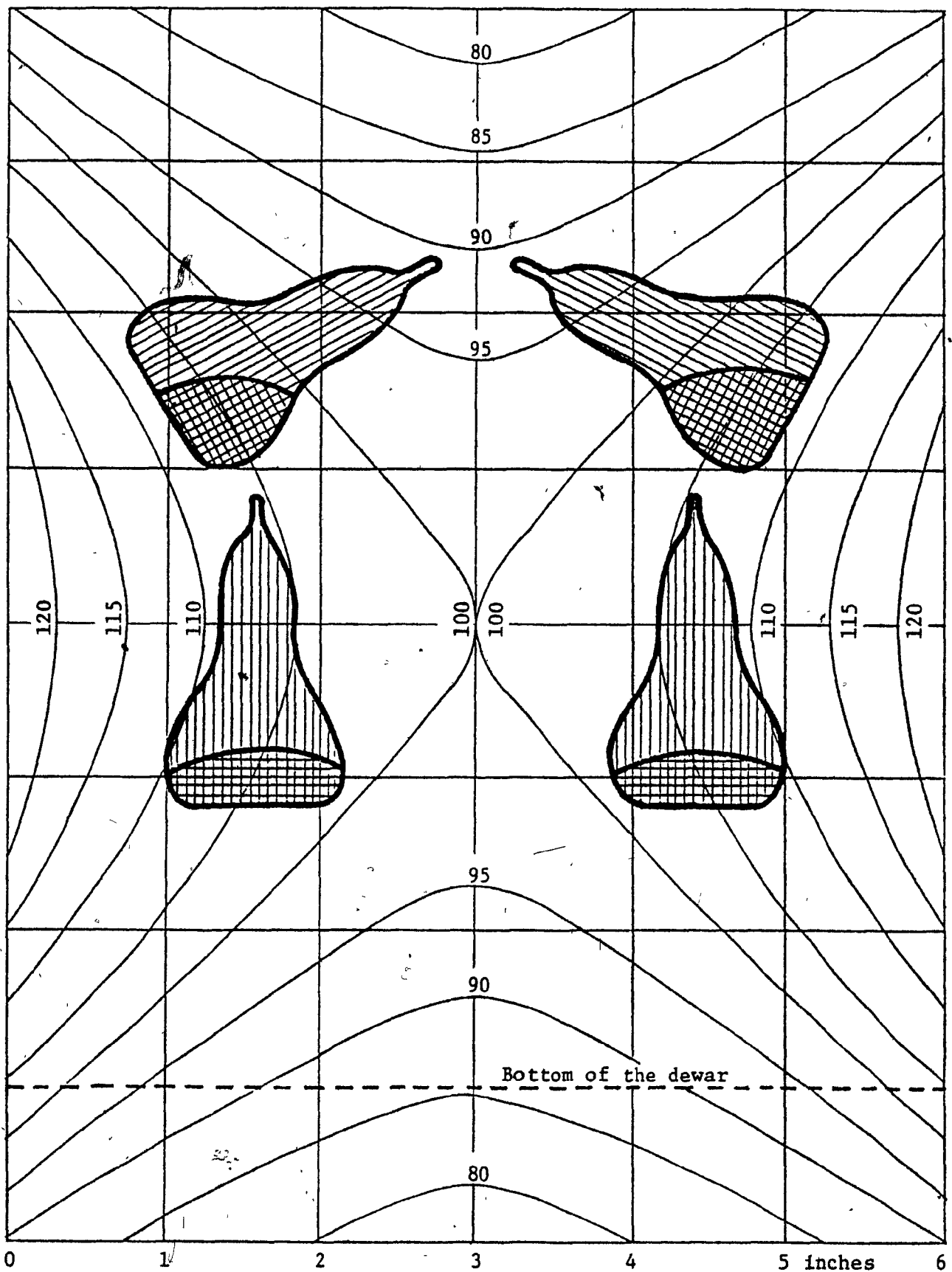


Fig. II-4-1 : Spatial isodose distribution inside the  $^{60}\text{Co}$  Gammacell 220 , giving the positional factor  $f_p$  , in % , as obtained from the AEC (accuracy : 5% )

Consequently, the dose rate was calculated:

$$\begin{aligned} \text{D.R.} &= (\text{DR}_o \times f_e \times f_a) \times f_m \times f_p \\ &= 0.398 \times f_m \times f_p \text{ Mrad/hr} \end{aligned}$$

The accuracy was estimated to be no better than  $\pm 10\%$ , especially in view of the errors inherent in estimating  $f_a$  and  $f_p$ . The typical dose rates ranged from 0.15 to 0.20 Mrad/hr.

#### II-5 Post-irradiation polymerization and product recovery

Unless otherwise specified, the sealed irradiated monomer samples were placed in a water bath thermostatically controlled at  $50.0 \pm 0.1^\circ\text{C}$ . After a predetermined length of time had elapsed, one sample was removed, quickly opened and poured into a large excess of water to which a small amount of hydroquinone had been added. Aided by the finely divided state of the powder and by the rapid stirring of the mixture, the dissolution took place within seconds. The highly soluble monomer (500 g/l) was thus separated from the insoluble polymeric calcium salt.

This procedure was meant to quench the still active radicals, and to minimize any polymerization in the liquid phase that could interfere with the polymerization that had already occurred in the crystalline phase. The polymer usually precipitated as a rubbery swollen mass, leaving a clear solution. It was separated with a spatula, washed and squeezed several times in distilled water against the wall of the beaker in order to remove any traces of occluded monomer. The exclusion chromatography results attest to the efficiency of this procedure; no polymer was found in the clear solution, and only traces of monomer were carried along with the

polymer. This method provided a good reproducibility in the yields.

The poly-(calcium acrylate) was then dried overnight in a vacuum oven at 50°C, and stored for further treatment.

#### II-6 Differential Scanning Calorimetry (D.S.C.)

Differential scanning calorimetry analyses were performed on a Perkin-Elmer DSC-1 machine, using the low-temperature plug-in. The samples (2 - 5 mg) were sealed in the special "volatile sample pans" by means of a crimping press rather than in the regular pans, for reasons explained in Chap. III. A pinhole was pierced through the cover with a sharp needle. Dry nitrogen was used as a purge gas in the measuring chamber of the DSC-1. The instrument was calibrated by using pure water and several spectrograde-quality organic solvents.

For the experiments at low temperature, the samples were irradiated in liquid nitrogen, and then placed quickly in the pre-cooled measuring cell of the instrument under the protection of a plastic "glove bag" filled with dry nitrogen. It was found necessary to so protect the instrument and the sample during the transfer, to exclude the atmospheric moisture and the resulting spurious signals.

#### II-7 Wide-line nuclear magnetic resonance (N.M.R.)

Samples for wide-line N.M.R. measurements were prepared by the evacuation and dehydration procedures described in Chap. II-3, packed and sealed in 9 mm O.D. pyrex tubes.

The temperature was varied by passing a heated or cooled nitrogen stream around the sample and monitored by copper-constantan thermocouples

placed up- and down-stream from the probe coils. The temperature of the sample was calculated from its position, assuming a linear gradient between the two thermocouples. Variations during the recording of a spectrum were estimated to be  $\pm 0.5^\circ\text{K}$ .

The spectra were recorded at 60 MHz using a spectrometer built essentially from Varian components. The samples proved quite susceptible to R.F. saturation at low temperatures. Accordingly, saturation checks were made every  $40^\circ\text{K}$  and the radiofrequency power was maintained 10 dB below the power where distortion of the spectra was last observable. R.F. powers thus used ranged 20 - 53 dB below full power. Modulation amplitudes were kept below 25% of the line width as much as permitted by the poor signal-to-noise ratio. Each spectrum was scanned at least twice at the slow rate of 1 G/min, with a noise filtration time constant low enough to insure freedom from hysteresis.

The experimental second moments were calculated from the first derivative traces with the aid of a computer program containing a correction for finite modulation broadening.

## II-8 Mass spectrometry experiments

The analysis of the gases engendered by the irradiation of calcium acrylate heavy water dihydrate, was carried out on an AEI MS 920 mass spectrometer.

It was found necessary to remove the three-l expansion flask from the spectrometer as well as to reduce the dead volume above the sample to 25 ml. This had two beneficial effects. First, it increased the partial pressures of the sample gases by a factor of several hundreds, thus bringing

them above the detection threshold of the spectrometer sensitivity .  
 Secondly , it helped reduce the problems of background interference  
 caused by water adsorbed onto the Pyrex walls .

A sample of 2.5 g dihydrate , made from heavy water , was ground  
 to a fine powder to facilitate the diffusion of the gases. It was eva-  
 cuated and sealed as usual at S (Fig.II-8-1), and then irradiated in li-  
 quid nitrogen up to a dose of 2.25 Mrad. The vessel was then connected  
 to the mass spectrometer by a B-14 ground joint . The hammer-magnet com-  
 partment was evacuated until the background analysis of the residual  
 gases stabilized. The seal was broken at a time  $t=0$  , and the analysis  
 of the gases above the sample was performed while keeping the sample in  
 liq.  $N_2$  . The sample was subsequently isolated by a valve from the rest  
 of the spectrometer , and allowed to warm up to room temperature for 20  
 minutes . A new analysis was then carried out, concentrating on the peaks  
 of particular interest . Periodic recordings were made over two hours  
 thereafter .

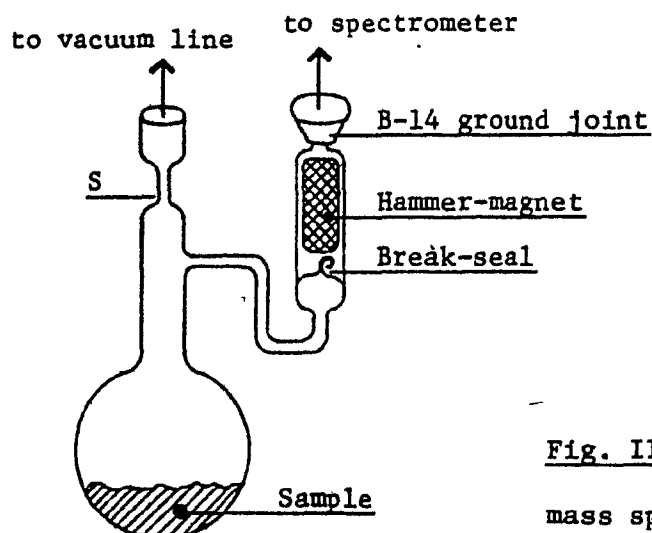


Fig. II-8-1 : Sample vessel for the  
 mass spectrometry experiments .

## II-9 Electron spin resonance (E.S.R.)

### II-9-a Technique

The E.S.R. measurements were taken on a Bruker instrument, whose klystron had been somewhat down-rated by reducing the filament energy to operate at a lower power, where its signal-to-noise ratio was optimal. As a result, the actual radiofrequency power levels were lower than indicated on the attenuator. The detecting diode was selected among several commercial samples for best signal-to-noise characteristics. The signals were recorded on a 60 x 30 cm X-Y recorder. The daily sensitivity of the spectrometer was monitored by recording the spectrum of a standard pitch sample. The curves were integrated using an electromechanical curve reader interfaced to a computer, and were normalized with respect to the pitch standard.

### II-9-b Preparation of the samples

Stock dihydrate was first ground to a very fine powder, one batch being made for all the experiments. The various hydration levels were attained according to the techniques described in Chap. II-3-c and II-3-d. Sufficient sample to fill the spectrometer cavity was weighed and transferred into the experimental vessels through the funnel A.

The quartz tube was then carefully cleaned with several fresh sections of pipe cleaner, until no powder could be seen clinging to the tube walls. This was of paramount importance in preventing the formation of radical-containing charcoals during the step where the quartz was flame-annealed, as well as in protecting the sample from the chemical interference caused by the pyrolysis gases thus produced.

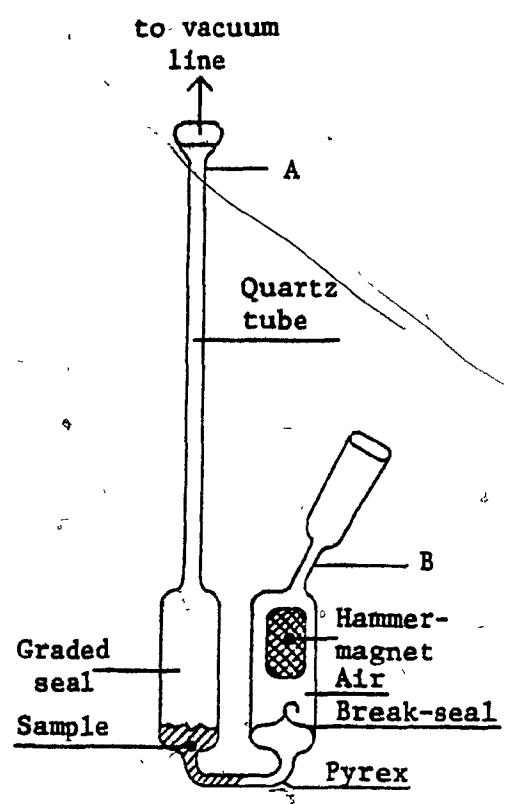
The samples were then connected to the vacuum line by means of a slightly greased sleeve of thick rubber around the funnel, evacuated and sealed in A. Vessels for the study of the diffusion of oxygen had their hammer compartment sealed with 0.9 atm. dry air (Fig. II-9-1-a).

All the vessels for one experiment were irradiated together upright in liq. N<sub>2</sub>. They received 1 Mrad in 6 hr. 22 min. following the regular procedure, with additional care taken not to break the seals.

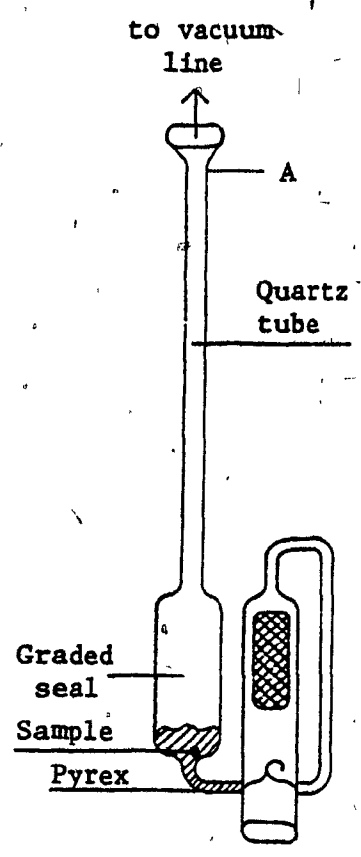
II-9-c Annealing of the quartz and post-irradiation treatment

After the <sup>60</sup>Co irradiation, the vessels were placed in a small dewar so that the bottom part (with the sample) was kept in liq. N<sub>2</sub>, and the quartz tube was accessible. For 10 min., the paramagnetic F centers induced in the quartz by the γ-rays were annealed by heating with a blow-torch, until the quartz started to glow white under examination through the special brown safety glasses. This procedure proved to be 100% effective in removing the strong quartz signal from the E.S.R. spectra.

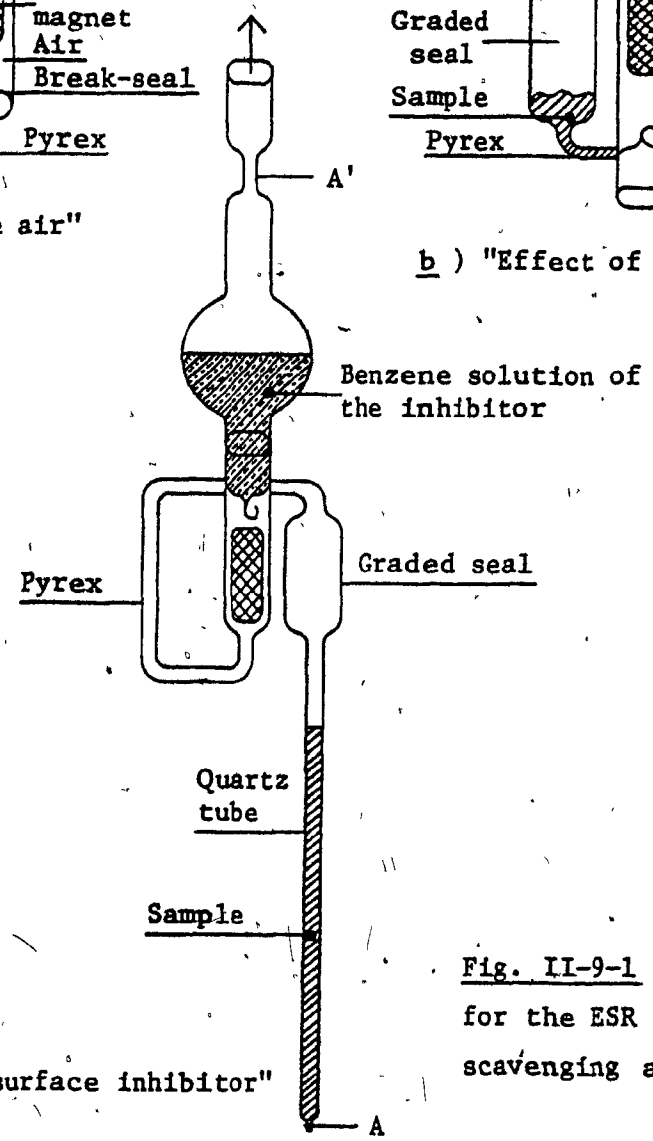
After cooling the whole vessels in liq. N<sub>2</sub>, they were inverted and the sample powder fell into the quartz portion, with the aid of gentle tapping on the tube. At this moment, the samples designed to study the effect of the inhibitor (as on Fig. II-9-1-b) were placed in a dewar, keeping the sample powder in liq. N<sub>2</sub>. An ampoule was connected to the end near the breakseal, then filled with a solution of 0.5% tri-tert. butyl phenol in benzene (Fig. II-9-1-c). This ampoule was connected to the vacuum line, thoroughly degassed by repeated cycles of freezing and thawing under vacuum, and sealed off in A'.



a) "Effect of the air"



b) "Effect of a surface inhibitor"



c) "Effect of a surface inhibitor"

Fig. II-9-1 : Special vessels for the ESR study of radical scavenging and oxygen diffusion

## II-10 Molecular weights measurements by Viscometry

The sample used was a polymeric calcium salt prepared from the dihydrate under vacuum. It was the same as one of those used in the exclusion chromatography experiments, having been postpolymerized at 50°C for 2 days with a yield of 28.6%. It was recovered in the acid form by ion-exchange and freeze-drying. To provide for an accurate weighing, dehydration of the hygroscopic poly-acid was achieved by vacuum dessication for 2 hrs. at 80°C. The weighing was checked against acid-base titration to account for the eventual presence of residual water.

The hydrochloric acid used to make up the sample solution was standardized twice. The two runs gave an identical value of 0.203 N.

The viscosities were measured in an Ubbelohde dilution viscometer, in a water bath maintained at 30.00 or 24.00 ± 0.02°C. The solution was pushed up the capillary with nitrogen pressure rather than aspirated, in order to prevent cooling and concentration of the test solution.

The solutions were injected into the viscometer through an 8 μm filter paper with a syringe.

The corrections for shear rate and kinetic energy were neglected in all cases, as the solvent elution times were very long (400-500 sec.).

After each dilution, the viscometer was agitated and the solution pushed up and down the capillary several times. Elution times were then recorded until they stabilized.

Thereafter, elution times were measured two or three times, and the average of these values was recorded as a point on the graphs shown in the fourth chapter.

The individual times so obtained deviated rarely more than  $\pm 0.2$  s from the mean.

## II-11 Molecular weights measurements by exclusion chromatography

### II-11-a Samples preparation and solubilization

Dihydrate from the common stock was ground to a powder in one batch for all samples. Subsequently, the samples were treated according to the general procedures of evacuation, dehydration, irradiation and post-polymerization as described in the sections II-3, 4 and 5. They received 0.95 Mrad<sup>3</sup> in 5 hr. 40 min. at  $-78^{\circ}\text{C}$ .

In order to perform the Exclusion Chromatography experiments, the sample must be solubilized. The poly-(calcium acrylate) salt itself proved insoluble in anything tried but DMSO, although it swelled to decreasing extents in water, methanol and ethanol. However, it has been reported "soluble in acidified methanol". The explanation for this behavior is likely to lie in its transformation into the poly-acid. The polymeric calcium salt was broken up, and proved indeed soluble 1% in water (and less so in T.H.F. and methanol) provided it was acidified. Complete dissolution was obtained after 2 minutes by the addition of 5% of conc. HCl and overnight by 10% of acetic acid. Caustic bases had no effect. Consequently, the poly-acid form was chosen for the Exclusion Chromatography experiments.

### II-11-b Recovery of the poly-acid

Various methods of recovering the pure poly-acid were tried with no success. Saturation with NaCl yielded an unwieldy, tacky product which was most likely a mixed  $(\text{Na}^+/\text{H}^+)$  composite. An attempt to remove the  $\text{Ca}^{++}$  by adding  $\text{K}_2\text{CO}_3$  failed to precipitate  $\text{CaCO}_3$  before a real end-point was

reached, where a polymer containing  $\text{Ca}^{++}$  was reprecipitated.

The use of a strongly acidic ion-exchange resin of the type Dowex 50W-X8 proved to be an elegant method of separation. The labile acidity contained in 0.1 g polymeric  $\text{Ca}^{++}$  salt is 1.1 milli-equivalents. The resin was stated to have a capacity of 5.1 milli-equivalents per gram of dry weight. An excess by a factor of at least 3 of freshly regenerated resin was used.

After shaking the resin for 10 min. with the polymeric  $\text{Ca}^{++}$  salt previously dissolved in 5% HCl, tests performed by adding KOH or  $\text{K}_2\text{CO}_3$  in excess failed to reprecipitate anything. This showed that all  $\text{Ca}^{++}$  had been removed and that the potassium salts were soluble. Indeed the poly-acid could be recovered from this solution by freeze-drying. It then proved to be readily soluble in water, well in methanol and only poorly in T.H.F. and p-dioxane.

#### II-11-c Bypassing the recovery

The freeze-drying technique is a tedious and time-consuming procedure when many samples are involved. Accordingly, all the samples were prepared as follows: the polymeric  $\text{Ca}^{++}$  salt was broken into grains, weighed, then agitated 4 to 8 hrs. directly with the ion-exchange resin in the phosphoric acid solution at pH 3 used as the eluant in the exclusion chromatograph. The resin shifted the equilibrium in favour of dissolution. One could thus obtain in a single step solutions of an exact concentration and ready to be injected into the exclusion chromatograph.

#### II-11-d Choice of the eluant

The difficulty in solubilizing the freeze-dried poly-acrylic acid in T.H.F. and p-dioxane, the easy technique of simultaneous conversion/

dissolution in the pH 3 buffered solution containing the ion-exchange resin, and the convenience of working with aqueous solutions were all important factors suggesting the use of an aqueous system. A pH 3.0 phosphoric acid buffer was chosen for the following two reasons:

- (i) lack of volatility and corrosiveness of  $H_3PO_4$ .
- (ii) buffering power ensuring a constant pH, and therefore a constant degree of ionization of the sample.

A 25 l glass tank was filled with distilled, deionized water, to which phosphoric acid was added dropwise with agitation, while monitoring the pH with an expanded scale research pH-meter until it read  $3.00 \pm 0.05$  pH units. The pH-meter was calibrated by iterative intercept and slope corrections with 2 standard buffers at pH 7 and pH 4. This "pH 3 buffer" was used to make up the samples, to wash glassware, and as an eluant in the exclusion chromatograph.

#### II-11-e Technicalities and injection procedures

The instrument used was a Waters GPC 200 with a Milton-Roy variable stroke mini-pump, and a differential Refractive Index detector. The reference side of the detector was filled with the carrier fluid, then closed. Before this work started, the machine was found to be fitted with copper tubings and brass fittings. To prevent corrosion by the phosphoric acid and facilitate servicing, it was necessary to completely refit the machine with all-stainless steel parts.

The volume of the injection loop, including the inlet and outlet ports, was 2.6 ml. For drawing the samples a syringe was fitted with a 8  $\mu$ m paper filter to remove any unwanted particles. The syringe was washed and filled with a 10 ml sample which was used first to flush the injection

loop. The syringe was then refilled and the sample was injected exactly at the instant when the chart recorder registered a spike. Each spike on the chart represents 5 ml, the volume of the syphon counter. The injection valve was returned to its normal position on the next spike, thus ensuring the total insertion of the sample into the system. A pump stroke of 50% was used, giving a flow rate of 1.3 ml/min. For all experiments (at room temperature), this gave a satisfactory compromise between a maximum resolution and an acceptable analysis time of about 2 hours.

#### II-11-f Choice of the columns

Corning Porous Glass of controlled porosity, supplied by Electro Nucleonics Inc. <sup>(87)</sup> was chosen for its compatibility with aqueous and organic solvents, its ready availability in a broad pore-size range and its stability towards pressure, solvents and air bubbles. A column can easily be packed dry by one person within  $\frac{1}{2}$  an hour and presents none of the delicate handling problems of the organic crosslinked gels. However, it presented adsorption problems, which will be discussed in Chap. IV. Porous glasses of the following characteristics (Table II-11-1) were tried, all in 120 - 200 Mesh particle size (manufacturer data).

Nominal Pore diam. (Å)	Mean Pore Diam. (Å)	Pore size Distribution (± %)	Pore Volume (cm <sup>3</sup> /g)	Surface Area (m <sup>2</sup> /g)
75	80	13.7	0.52	207.8
240	255	3.7	0.96	95.5
700	729	8.6	0.98	33.9
1000	1012.6	3.7	1.02	27.6
1400	1422	4.5	1.02	17.3
2000	2215	3.1	2.32	27.5

Table II-11-1

The columns were stainless steel cylinders 1.22 m long and 0.78 cm internal diameter thus having a length to diameter ratio of 156.4 (3 times the usually recommended minimum) and an internal volume of 59 cm<sup>3</sup>. Various packing methods were tried in turn: ultrasonic waves, mechanical agitation with an eccentric cam, vibrations and application of a vacuum at one end. All gave poor results. The best packing of the porous glass was obtained by the simple method of filling only 4 cm of the column at a time, then tapping it vigorously with a wrench for 1 minute. The columns were capped with 10  $\mu$ m stainless steel fritted filters. Opening the upstream end of each column after several weeks of wet use under high pressure showed that there was no further compaction. After suitable experimentation a set of 4 columns of 75, 240, 700 and 1400 nominal pore diameter was chosen for use. The 2000 Å column was rejected because it decreased the resolution of the other columns to an unacceptable extent, and also because it considerably increased the analysis time.

#### II-11-g Dextran calibration standards

The characteristics of the five Dextran standards used are given in Table II-11-2 below as furnished by Pharmacia, along with the experimentally determined elution volumes at room temperature in pH 3 phosphoric acid buffer.

$\overline{M}_w$ (g)	$\overline{M}_n$	$\overline{M}_w/\overline{M}_n$	$[\eta]$ (dl/g)	$\log (\eta \times \overline{M}_w)$	$\log (\eta \times \overline{M}_n)$	Elution Volume (counts)
10,500	6,400	1.64	0.098	3.01	2.80	30.7
22,300	15,000	1.49	0.148	3.52	3.35	29.2
39,500	29,500	1.34	0.21	3.92	3.79	27.9
154,000	86,000	1.79	0.37	4.76	4.50	25.1
476,000	188,000	2.53	0.54	5.41	5.01	23.2

Table II-11-2

II-12  $^{13}\text{C}$  Carbon NMR spectroscopy

Five samples of poly-calcium acrylate were prepared according to the usual procedures outlined in section II-5. They were the same as some of the samples for the study of molecular weight distribution by Exclusion Chromatography.

They were transformed into the water-soluble poly-acrylic acid derivative by the ion exchange technique of section II-11-b, using only a few drops of HCl to speed up dissolution. The resulting aqueous solution was freeze-dried, and the poly-acid was redissolved in the minimum amount of  $\text{D}_2\text{O}$  at  $50^\circ\text{C}$  to produce the high concentration required by  $^{13}\text{C}$  spectroscopy. The viscous solution was then transferred to the special large-diameter (10 mm) NMR tubes.

The spectroscopic experiments were carried out by Gordon K. Hamer of the Pulp and Paper Research Institute, in the laboratory of Prof. A.S. Perlín. The instrument was a Bruker WH90 spectrometer with 8000 memory channels equipped for pulsed R-F decay accumulation of scans. The operating frequency was 22.628 MHz, and proton-noise decoupling was applied. Fast-Fourier-Transform was performed on the inboard computer to yield the time-average of some 2000 scans.

The use of  $\text{D}_2\text{O}$  to dissolve the samples was necessary to allow the spectrometer to lock onto the deuterium nucleus frequency, and a drop of dioxane was also added to serve as an internal chemical shift reference. The stored digital data could be displayed on an X-Y recorder at any scale. Large-scale recordings were made to facilitate the cut-and-weigh method of determining peak areas.

## II-13 Crystallography

### II-13-a Debye-Scherrer powder patterns

The treatment of the two anhydrate samples will be described in the text of section III-1-2-a. A dihydrate sample was included for comparison.

The powder patterns were recorded by Dr. St. John Manley of the Pulp and Paper Research Institute of Canada. A circular chamber of 57.3 mm diameter was used, and the experiment was performed at room temperature. The samples received 10 hrs. exposure of the  $\text{CuK}_\alpha$  radiation filtered by Ni. The developed films were then analysed with a microdensitometer as well as inspected visually.

### II-13-b Single-crystal structure analysis

The experiments were performed by Miss Suzanne Fortier in McGill's Geology Department, under the supervision of Prof. Gabrielle Donnay.

A crystal of approximately 0.2 x 0.2 x 0.5 mm was chosen, small enough to give negligible absorption. It was fixed at the end of a copper wire using a low-temperature, high-vacuum silicone rubber glue (G.E. RTV 560 and SR 585). The wire was cooled to  $-90^\circ\text{C}$  in air at a residual pressure of  $10^{-2}$  mm Hg in a AC-1-101-A Cryo-Tip refrigerator of Air Products Inc. Such low temperature was found to be required because calcium acrylate dihydrate is able to polymerize at room temperature under the influence of the X-ray beam. The results of Costaschuck<sup>(84)</sup> indicated that  $-90^\circ\text{C}$  was cold enough to substantially inhibit the polymerization that would otherwise interfere with the measurements.

A 4-circles Picker-Facs I diffractometer was used to collect 915 symmetry-independent intensities with graphite-monochromated  $\text{Mo K}_\alpha$  radiation. The  $\theta - 2\theta$  scan method was used at the rate of  $0.5^\circ/\text{min}$ . All reflections

up to  $2\theta = 45^\circ$  were collected in the quadrant where  $h$  and  $k$  are positive. The Miller indices ranged 0 to 15 for  $h$ , 0 to 6 for  $k$  and -12 to 11 for  $l$ . The two reflections used as standards presented a maximum deviation of 3.5% from their mean value, confirming that the amount of polymerization during the experiment had been minimal.

In order to eliminate the contribution from the copper wire and the glue, the crystal was removed and the intensities remeasured under the same conditions. The values so obtained were subtracted from the previous measurements to furnish the net intensities reflected by the crystal.

590 symmetry-independent reflections had measured intensities larger than twice the standard deviation. The cell dimensions were obtained by least-squares refinement of the angular values of 9 accurately centered reflections. The similarity of the cell parameters and the identity of the space groups observed at 20 and  $-90^\circ\text{C}$  indicate that calcium acrylate dihydrate does not undergo any solid-state transformation between these two temperatures. The absence of any manifestations of phase changes in the Differential Thermal Analysis and molecular motion curves (Wide Line NMR) will be demonstrated in this thesis, and further justifies the procedure employed.

Intensities were corrected for Lorentz and polarization factors, using the scattering factors of Hanson et al. (1964) and the DATRON program of the X-ray 70 system. The calcium ion position was determined from the Patterson synthesis of the intensity data, and was found to be analogous to that proposed by Lando<sup>(77)</sup>. The remaining ions were located by the heavy atom method. Fourier synthesis followed by full matrix least squares and  $\Delta F$  synthesis permitted to locate all the remaining atoms.

Finally, the refinement of the data converged towards a residual of 6.6% on 564 observed reflections. 26 discrepant reflections with  $F_{\text{obs}} \ll |F_{\text{calc}}|$  were eliminated from the least-squares refinement. These discrepancies were attributed to accidental interference of the tubing bringing the refrigerant to the cryo-tip with the X-ray beam.

CHAPTER III

---

THE MONOMER  
AND THE INITIATION STAGES

III-1 Crystalline structure of the monomer

The knowledge of the crystalline structure of the Ca acrylate dihydrate monomer is of fundamental importance if one is to rationalize the phenomena observed during SSP. The question of topotacticity (i.e. whether the monomer matrix imposes orientations on the polymerizing chain) is an obvious one for which such knowledge is required. Furthermore, the study of the dehydration reaction, and that of the polymerization inhibition by deliberately introduced foreign gases, also require a precise knowledge of the diffusability of the monomer crystals by small molecules.

The earlier crystallographic studies of the monomer will be presented first, followed by a description of the experiments performed and finally by the discussion of the results. It will be shown that crystallography supports the results of the other experimental techniques employed in this thesis, and leads to several interesting predictions.

III-1-1 Previous crystallographic studies

The crystallographic structure of calcium acrylate dihydrate was first studied by Lando<sup>(77)</sup>. He found that calcium acrylate is monoclinic and belongs to the space group  $P2_1/a$ , with the following parameters:  $a = 14.36 \text{ \AA}$ ;  $b = 6.56 \text{ \AA}$ ;  $c = 11.62 \text{ \AA}$ ;  $\beta = 118.9^\circ$ ;  $Z = 4$ . The anhydrate was found to be amorphous, and further comments were made later by Lando and Morawetz<sup>(78)</sup> on the nature of the various hydrates they claimed to have prepared.

However, an attentive examination of the crystallographic results of Lando reveals the following facts:

- (a) Lando's structure displays 4 internuclear distances of 1.83  $\text{\AA}$  between the oxygen atoms of different acrylate molecules. Such a short approach between two negative  $\text{CO}_2^-$  ions seems unreasonable, as it would

mean they are separated by a distance closer to the length of an O-O covalent bond (1.5 Å) than to the length of the expected Van der Waals approach (2.8 Å).

(b) Lando found calcium-oxygen internuclear distances of 0.97 Å, which is absolutely impossible in view of the ionic radii concerned (0.99 plus 1.32 Å resp.), which lead to an expected 2.3 - 2.4 Å instead.

(c) The "residual" in Lando's atomic position measurements, which is a measure of the mean discrepancy between observed and calculated structure factors, was 35% for the *h0l* data and 43% for the *0kl* data after least-squares refinement of his data. These values are unusually high compared to the 10-12% generally considered to be the limit of acceptability for the establishment of a new structure.

(d) The calcium ions in Lando's structure lack a clearly defined coordination polyhedron.

A number of these discrepancies may be explained on the basis that Lando carried out his measurements at room temperature. Calcium acrylate dihydrate polymerizes readily under the X-ray beam at room temperature, possibly disrupting the lattice to an extent sufficient to impair the measurements.

On the ground of the above remarks, the crystallographic structure of Lando must clearly be rejected.

Costaschuk<sup>(84)</sup> built a molecular model on Lando's data, and derived from it a number of conclusions. Unfortunately, as Lando's data have been shown erroneous, it is now clear that this model and the conclusions based on it must be totally reconsidered.

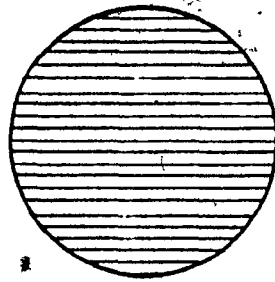
In an effort to gain understanding of the dehydration process, Costas-

chuk also analysed the Debye-Scherrer powder patterns of the intermediate hydration levels (0.95 and 0.28 H<sub>2</sub>O), and that of the anhydrate, which was found to consist of 4 halos.

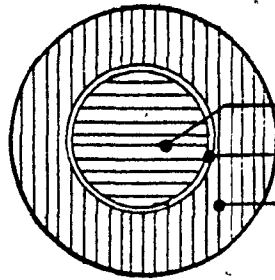
The intermediate patterns were found by Costaschuk to consist of the simple additive superposition of the dihydrate and anhydrate patterns at reduced intensities. He also measured the densities of the various hydrate levels, and found it decreased some 15% from the dihydrate (1.461 g/cm<sup>3</sup>) to the anhydrate (1.425 g/cm<sup>3</sup>) in a smooth linear manner. The dehydration reaction was concluded to proceed by a dihydrate-to-anhydrate transition, with little or no distinct intermediate compound produced (2-phase system). The dehydration model of Costaschuk is depicted schematically on the left half of Fig. III-1-1.

Watine<sup>(85)</sup> attempted a quantitative study of the crystallinity variation with dehydration. He defined the crystallinity of his samples as proportional to the intensity of the peaks occurring at  $2\theta = 12.48^\circ$  and  $15.93^\circ$  in the powder patterns. These two angles were chosen for they did not suffer from interference with the anhydrate halos. The percentage crystallinity could thus be measured from the X-ray films with a microdensitometer, assuming 100% and 0% respectively for the dihydrate and anhydrate. The curve obtained is presented on Fig. III-1-2. Watine observed that 60% of the crystallinity loss occurred over only 25% of the hydration range between 0.5 and 1.0 H<sub>2</sub>O.

He concluded that the volume of the dihydrate phase decreased in a non-linear manner with the extent of dehydration, and that accordingly, the 2-phase dehydration model of Costaschuk should be questioned, and possibly rejected to the profit of a 3-phase model involving a large amount of

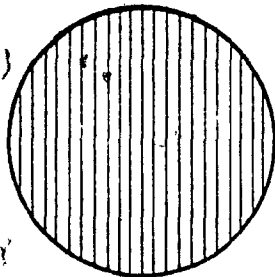
Costaschuk's /dehydration' model :

$\frac{2 H_2O}{}$  :  
(pure dihydrate)

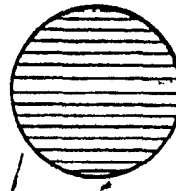


from 2 to 0 H<sub>2</sub>O :

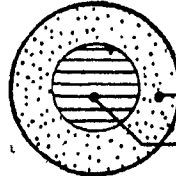
dihydrate core  
thin boundary  
anhydrate shell



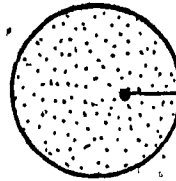
$\frac{0 H_2O}{}$  :  
(pure anhydrate)

Watine's dehydration model :

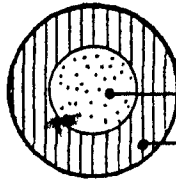
$\frac{2 H_2O}{}$  :  
(pure dihydrate)



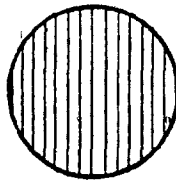
from 2 to 0.5 H<sub>2</sub>O :  
"active volume shell"  
dihydrate core



$\frac{0.5 H_2O}{}$  :  
only "active volume"  
(dynamic structure with  
continuously variable  
composition)



from 0.5 to 0 H<sub>2</sub>O :  
"active volume" core  
anhydrate shell



$\frac{0 H_2O}{}$  :  
(pure anhydrate)

Fig. III-1-1 : Comparison between the dehydration models proposed by Costaschuk (84,p.54) and by Watine (85,p.107)

Crystallinity, (%)

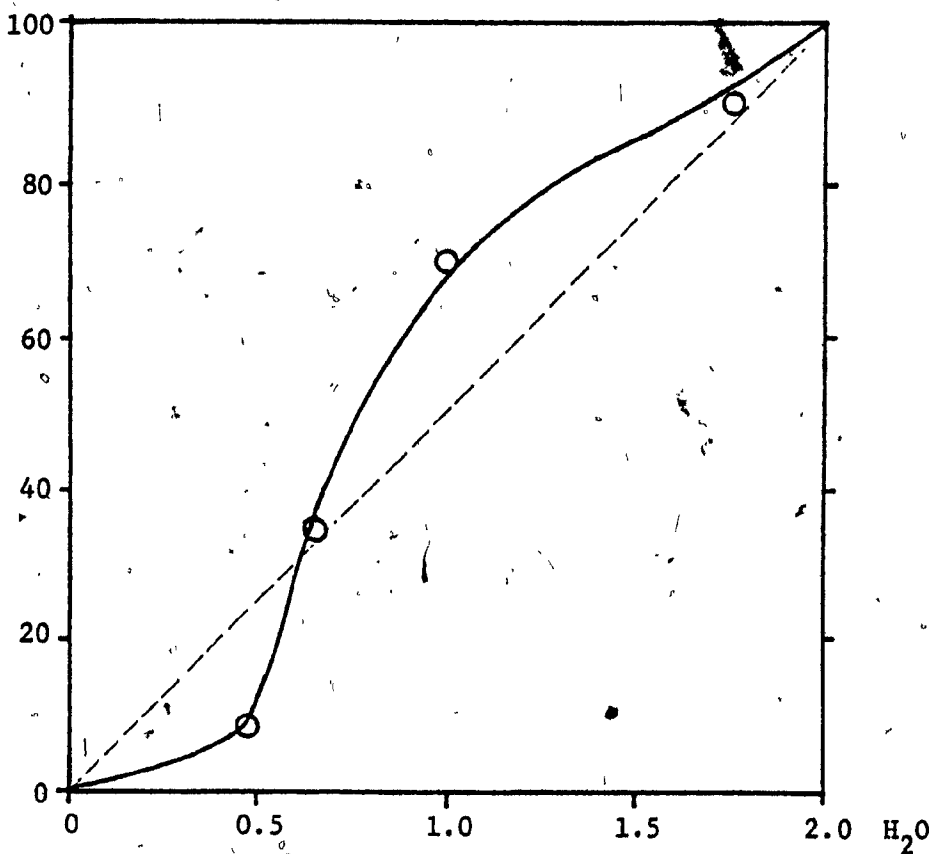


Fig: III-1-2 : Densitometric measurements of the crystallinity contents of calcium acrylate hydrates, from the Debye-Scherrer powder patterns.

Source: Watine (85, p.39)

an intermediate "active phase" of composition  $n \cdot x \text{H}_2\text{O}$ . The two models are compared schematically on Fig. III-1-1.

Several questions may be raised regarding the densitometric measurements of Watine:

(a) the use of a microdensitometric probe involves integrating the optical density of the film over a certain line width corresponding to the opening of the probe slit. As a result, the readings will be incorrect if the actual line width of the measured diffraction line changes from one sample to the next. One practical instance where this can happen is when the dehydration nucleation occurs abundantly by the multiplication of small centers. The width of the dihydrate lines will then increase appreciably when the size of the remaining crystallites will fall below about 1000 Å. This results in an apparent loss of integrated optical density, and in a deviation of the curve below linearity at low water contents.

Indeed, Watine observed such a deviation at the 0.5  $\text{H}_2\text{O}$  level as shown on Fig. III-1-2. It is henceforth suggested that this deviation, far from representing a non-linearity in the crystallinity itself, is instead indicative that dehydration proceeds by an abundant nucleation of independent centers.

(b) By assuming that the two lines he chose could be used for the measurement of the crystallinity content, Watine implicitly assumed that the water oxygens did not contribute to their intensities. In case the water should contribute to these lines, one would expect their intensity to vary anyway upon dehydration regardless of the crystallinity of the surrounding matrix.

Indeed, calculation of the structure factors  $F$  were performed for the (011) line at  $2\theta = 15.93^\circ$  of Watine, based on the single crystal analysis

to be presented in section III-1-2-b. Excellent agreement was observed between the observed total  $F$  ( $60 \pm 6$  electrons) and the calculated  $F$  ( $64 \pm 0.5$  electrons). A strong contribution of the water to this factor was calculated ( $F = -49 \pm 0.5$  electrons). As this contribution is negative, a partial dehydration of  $x\%$  without destruction of the remaining crystal structure would increase the observed intensity  $I$  by the ratio:

$$\frac{I_{2x/100}}{I_{2 H_2O}} = \left( \frac{F - \frac{x}{100} F_{\text{water}}}{F} \right)^2 = (1 + 0.0077 x)^2 \quad \text{Eq. (1)}$$

For small values of  $x$ , this increase ratio may be approximated by  $1 + 0.015 x$ . Only 10% dehydration without collapse of the dihydrate lattice would thus produce a 15% increase in the observed optical density of that line over that of the dihydrate. Such a large effect could not have been missed in Watine's experiment.

On the contrary, Watine observed a decrease in the line intensity upon dehydration. This enables us to conclude that:

- (1) The amount of dehydration that the dihydrate lattice can tolerate without collapsing is very small. This will be shown in section III-1-3-a to be perfectly consistent with the essential role of water in the stability of the crystal.
- (2) This small fraction is nevertheless responsible for some increase in the observed line intensity. Such an increase over the linear behaviour based on a simple additivity of the dihydrate and anhydrate patterns has been indeed observed by Watine in the range 0.7 to 1.8  $H_2O$ . Application of Eq. (1) on Watine's data allows to estimate to 2% or less the fraction  $x$  of dehydration without lattice collapse.

Finally, we may conclude that Watine's observations may all be easily rationalized in the light of simple crystallographic principles. As a consequence, Watine's contention that crystallinity decreases non-linearly with the water content of calcium acrylate, and the resulting deduction as to the existence of an intermediate "active volume" of composition  $x$ , should be seriously questioned and probably rejected. On the contrary, the observation by Costaschuk of a reduced but clear dihydrate pattern all the way down to very low hydration levels, and of the linear decrease of density upon dehydration strongly supports the latter's two-phase dehydration model. It should be kept in mind however that these experiments were all run using finely ground powders, and that the above conclusions cannot formally rule out the existence of a metastable partial hydrate for large monocrystals under certain conditions. This possibility will be discussed later in detail.

### III-1-2 Crystallographic experiments

#### III-1-2-a Debye-Scherrer powder patterns

O'Donnel and Sothmann<sup>(83-b)</sup> made a thorough study of the dehydration of barium methacrylate monohydrate after the preliminary study of Bowden and O'Donnell<sup>(81-c)</sup>. This material is believed to be sufficiently similar in many of its properties to calcium acrylate dihydrate to warrant brief consideration here.

Differential Scanning Calorimetry of barium methacrylate monohydrate exhibited 2 endotherm peaks at 80 and 110°C for small crystals. On the other hand, grinding the samples to a finer powder produced a gradual disappearance of the second endotherm. One of the hypotheses advanced was that the second endotherm might be indicative of an allotropic

transition after the dehydration had taken place, or of a phase transition coupled with a second dehydration step. Such transitions are not uncommon and have been demonstrated to occur during or in between the dehydration steps of  $\text{CuSO}_4 \cdot 5\text{H}_2\text{O}$  (106).

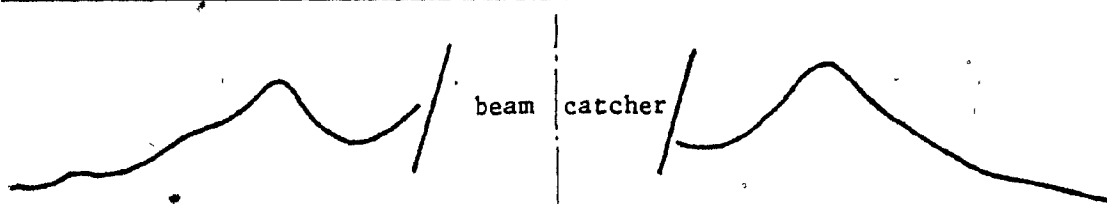
Accrued interest in this hypothesis was sparked by the finding that 2 dehydration endotherms were also present in calcium acrylate dihydrate at substantially the same temperatures of 79.6 and 106°C. All these results will be discussed and illustrated further in section III-3-1.

Accordingly, an experiment was designed to test this hypothesis by comparing the powder patterns of two anhydrate samples. The first sample was prepared by prolonged evacuation of crystalline dihydrate at room temperature, i.e. well below the temperatures of the 2 endotherms. The second sample was dehydrated by evacuation at 60°C, followed by two days annealing at 110°C under vacuum, i.e. at a temperature suitable to allow any eventual recrystallization to take place.

Densitometric traces were obtained by Dr. St. John Manley of the Pulp and Paper Research Institute by the Debye-Scherrer method and are shown on Fig. III-1-3. Both samples exhibited the 4 halos observed by Costaschuk. The outer 3 could only be observed by careful visual inspection of the negatives, but were too weak to be clearly apparent on the densitometric traces. No difference could be found between the patterns of the low and high-temperature samples.

It thus seems necessary to conclude that the second dehydration endotherm of calcium acrylate dihydrate is not associated with a phase transition. As a result, we may say that the Debye-Scherrer experiment devised could not put in evidence the formation of an intermediate structure nor

Anhydrate annealed at high temperature :



Anhydrate prepared at room temperature :

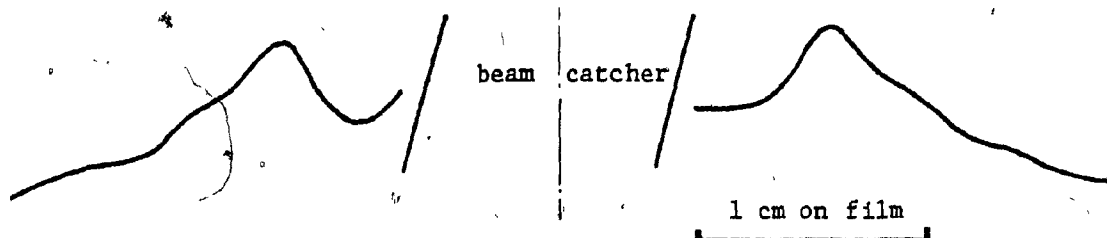


Fig. III-1-3 : Micro-densitometric analysis of the Debye-Scherrer powder patterns of two anhydrous calcium acrylate samples .

the existence of a phase transition overlooked thus far. Nevertheless, some reservations must be made. The observation made by O'Donnell and Sothmann<sup>(83-b)</sup> that grinding the crystals to a fine powder produced the disappearance of the second endotherm suggests that the grinding required to take a Debye-Scherrer pattern may be sufficient to obliterate any structure present. Furthermore, the same authors found that very small doses of  $\gamma$ -irradiation were sufficient to have the same effect.

Consequently, it is felt that the grinding and the X-ray irradiation of the samples, although necessary to run the experiment, could be responsible for the obliteration of any such structure either directly or by inducing polymerization. Therefore we must regard the existence of such a fragile or metastable structure as still possible, and worthy of further investigation. The use of larger crystals and of cooling below  $-100^{\circ}\text{C}$  during the grinding and the recording of the X-ray patterns seems to be indicated, although with no guarantee that it will work.

On the other hand, Debye-Scherrer powder patterns may be exploited to yield information as to the structure of the anhydrate and the features retained from the dihydrate lattice after the removal of water. Costaschuk<sup>(84)</sup> observed the 4 halos of the anhydrate at  $2\theta$  values of 8.3, 23, 30 and  $42^{\circ}$ , corresponding to  $d$  spacings of 10.6, 3.8, 2.9 and 2.2 Å respectively. On the basis of Lando's crystallographic data<sup>(77)</sup>, Costaschuk concluded to the persistence of the (001) reflection throughout the dehydration. It was interpreted that dehydration caused a "substantial loss in crystalline order along the  $a$  and  $b$  axes, but only a minor loss along the  $c$  axis where the lattice spacing remained nearly constant".

As Lando's data have since been shown erroneous, it was deemed neces-

sary to investigate this point again. Although we used the same nickel filtered  $\text{CuK}_\alpha$  radiation, the four anhydrate halos were found, in the current experiments, at  $2\theta$  angles of approximately 12, 15, 20 and  $26^\circ$ , corresponding to  $d$  spacings of 7.4, 5.9, 4.4 and  $3.4 \pm 0.2$  A respectively. These distances were interpreted as the Ca-Ca approaches. They are quite different from those observed by Costaschuk, but they were found to be similar to those measured by the present authors from the dihydrate pattern ( $d = 7.2, 5.9, 6.6$  and  $3.9 \pm 0.1$  A), which match accurately the Ca-Ca approaches independently determined from the dihydrate by the single crystal structure analysis of section III-1-2-b.

The calcium ions will be shown in the next section (III-1-2-b) to form ribbons stretching along the  $b$  axis in the dihydrate. The Ca-Ca distances are noted on Fig. III-1-4, along with the values they assume in the anhydrate (in parentheses). The similarity between the two indicates that the inter-ribbon distances are conserved, therefore supporting their continued existence in the anhydrate. The intra-ribbon distances are markedly shortened as a result of the necessary reorganization of the calcium coordination polyhedra.

In conclusion, we may state in contradiction to the results of Costaschuk, that the dihydrate lattice was found to suffer a complete loss of crystalline order upon dehydration. The preservation of some interatomic distances suggests however that the ribbon-like structure is approximately conserved, although suffering from a 33% contraction along the  $b$  axis and from a 13% contraction of the shortest Ca-Ca distances. These contractions are likely to facilitate polymerization along the ribbons, whereas it was formerly more difficult in the dihydrate. Finally, the persistence of the

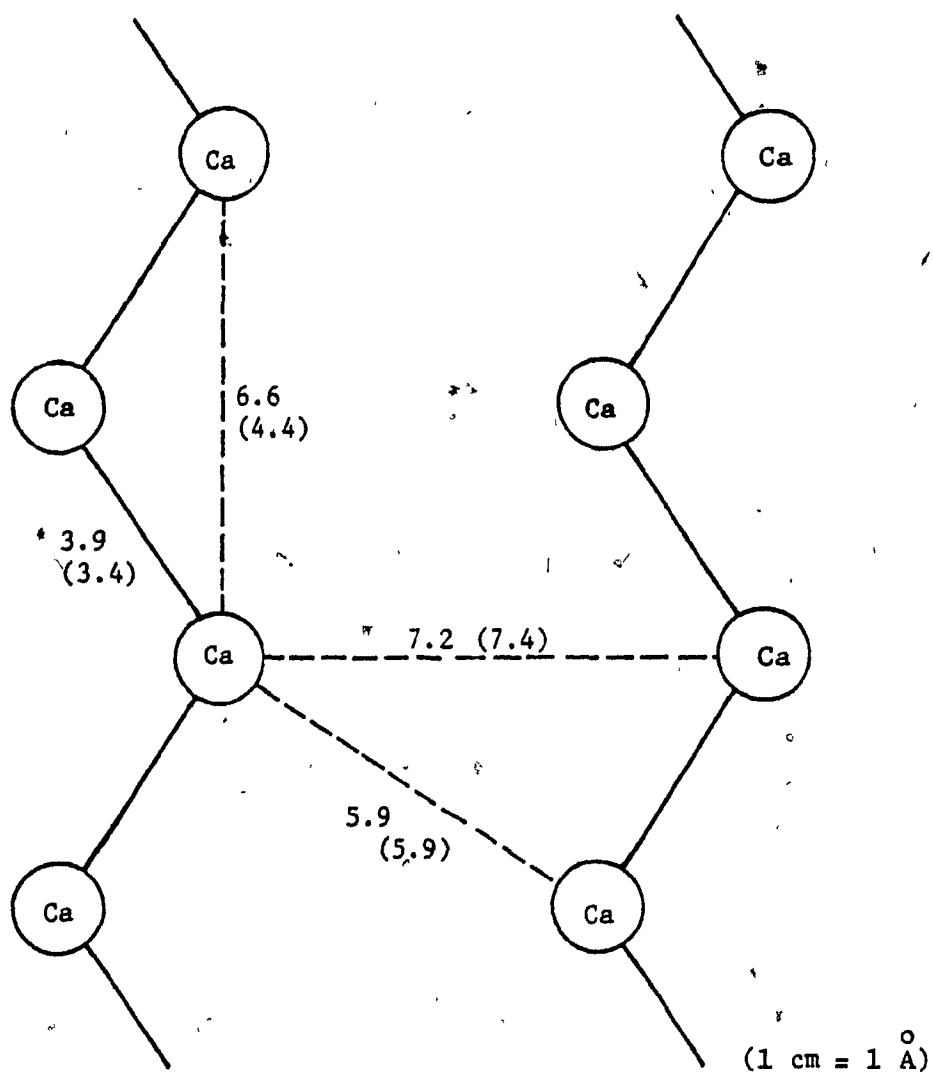


Fig. III-1-4 : Calcium-calcium distances , in Å , in calcium acrylate dihydrate , as measured from the Debye-Scherrer powder patterns by X-rays .

Values shown between brackets are those for the anhydrate .

(001) reflection was not observed, as this reflection is forbidden in the space group of the dihydrate.

#### III-1-2-b Single-crystal structure analysis

The crystal structure analysis of calcium acrylate dihydrate was undertaken at McGill University's Geology Department. The single-crystal experiments were performed by Miss Suzanne Fortier, and the processing of the data by Mr. Yvon Lepage, under the direction of Professor Gabriel-De Donnay. This structure analysis will be the object of a detailed publication by the above authors.

The dihydrate crystals are acicular, fragile and elongated along the  $b$  axis. The cell parameters found are presented in Table III-1-1. The 52 sets of coordinates were generated by this author from the 13 fractional atomic coordinates listed on Table III-1-2-a and from the equivalent positions  $(x, y, z)$ ,  $(-x, -y, -z)$ ,  $(\frac{1}{2}-x, \frac{1}{2}+y, -z)$ ,  $(\frac{1}{2}+x, \frac{1}{2}-y, z)$ . The interatomic distances derived from them are shown on Table III-1-2-b.

A projection of the structure onto the  $ac$  plane was constructed. For clarity of presentation, the unit cell and its immediate vicinity have been completed by applying translations of vectors  $\vec{a}$  and  $\vec{c}$ , and are depicted on Fig. III-1-5.

The structure is made of 10 Å thick layers perpendicular to the plane of the figure and parallel to the (001) plane. Each layer consists of pairs of combs lying with their spines back to back, and staggered along the  $b$  axis at a distance of  $\frac{1}{2}b$  from the opposite comb of the same pair, and of  $1b$  from the corresponding combs of the next pairs above and below. The spines of these combs are rows of calcium ions lying along the  $a$  edges of the unit cell, and form the core of the layers. The teeth of the combs

Space group:  $P2_1/a$

---


$$a = 14.11 \pm 0.02 \text{ \AA}$$

$$b = 6.63 \pm 0.01 \text{ \AA}$$

$$c = 11.76 \pm 0.02 \text{ \AA}$$


---

$$\beta = 118.4 \pm 0.1^\circ$$


---

$$Z = 4 \times \left[ \text{Ca}(\text{CH}_2\text{CHCO}_2)_2 \cdot 2\text{H}_2\text{O} \right] \text{ per cell}$$

$$\text{Formula weight} = 218.23 \text{ g}$$


---

$$\text{Linear absorption coefficient} = 6.27 \text{ cm}^{-1} \text{ for MoK}\alpha$$

$$V \text{ (unit cell volume)} = 967.7 \text{ \AA}^3$$

$$\text{Density (calculated)} = 1.498 \text{ g/cm}^3$$

$$\text{Density (experimental)} = 1.461 \text{ g/cm}^3 \text{ (from Ref. 84)}$$


---

TABLE III-1-1

Cell parameters of calcium acrylate dihydrate at  $183^\circ\text{K}$

Atom	x	y	z
Ca	0.4367 (2)	0.2405 (4)	0.0295 (2)
C <sub>11</sub>	0.1728 (11)	0.0744 (23)	0.5427 (14)
C <sub>21</sub>	0.2108 (9)	0.2404 (23)	0.6185 (10)
C <sub>31</sub>	0.2662 (9)	0.2249 (21)	0.7644 (10)
O <sub>11</sub>	0.2848 (7)	0.0578 (12)	0.8258 (8)
O <sub>21</sub>	0.2988 (7)	0.3887 (13)	0.8257 (7)
C <sub>12</sub>	-0.0132 (12)	0.3824 (23)	0.6424 (14)
C <sub>22</sub>	0.0283 (9)	0.2293 (20)	0.7290 (11)
C <sub>32</sub>	0.0335 (9)	0.2409 (23)	0.8598 (10)
O <sub>12</sub>	0.0490 (7)	0.0807 (13)	0.9240 (8)
O <sub>22</sub>	0.0208 (7)	0.4060 (13)	0.9020 (8)
(H <sub>2</sub> O) <sub>1</sub>	0.6124 (6)	0.2632 (13)	0.2190 (7)
(H <sub>2</sub> O) <sub>1</sub>	0.3201 (7)	0.2305 (13)	0.1266 (8)

TABLE III-1-2-a

Atomic coordinates of calcium acrylate dihydrate at 183°K (in Å, with uncertainties over the last figure expressed shown between brackets).

Calcium coordination polyhedron:

Water molecules and hydrogen bonding:

Ca - O <sub>11</sub>	2.629 (7)	(H <sub>2</sub> O) <sub>1</sub> - O <sub>11</sub>	2.76 (1)	(H <sub>2</sub> O-intra)
O <sub>21</sub>	2.461 (7)	- O <sub>21</sub>	2.79 (1)	
O <sub>12</sub>	2.307 (9)			
O <sub>12</sub>	2.707 (12)			
O <sub>22</sub>	2.339 (9)	(H <sub>2</sub> O) <sub>1</sub> - O <sub>11</sub>	2.83 (1)	(H <sub>2</sub> O-inter)
O <sub>22</sub>	2.509 (12)	- O <sub>21</sub>	3.03 (1)	
(H <sub>2</sub> O) <sub>1</sub>	2.425 (6)			
(H <sub>2</sub> O) <sub>2</sub>	2.409 (12)			

TABLE III-1-2-b

Interatomic distances (in Å)

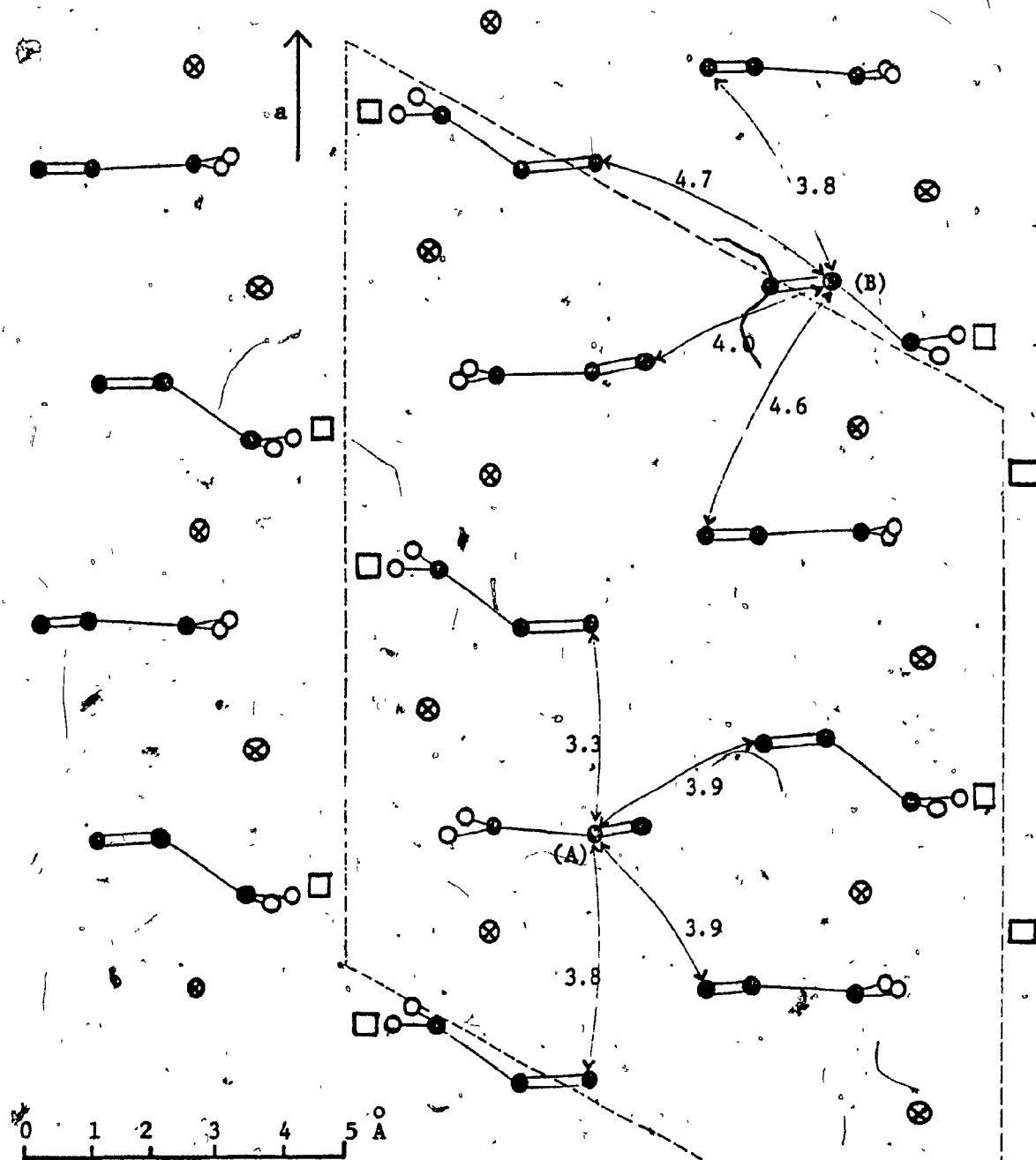


Fig. III-1-5 : Calcium acrylate dihydrate unit cell ,  
 projection on the ac plane . Distances are shown in Å .

- carbon atoms
- oxygen ( $\text{CO}_2^-$ )
- calcium ions
- ⊗ oxygen ( $\text{H}_2\text{O}$ )

are the acrylate molecules, and extend almost perpendicular to the plane of the layers, except for the vinyl double bonds tails which stick alternately above and below the plane of their comb. The surface of the layers is therefore made of the tips of the combs, i.e. the vinyl tails, which engage in Van der Waals bonding with those of the adjacent layer.

The water molecules are interspersed between the teeth of the combs, and are kept close to the spines by the bonds they exchange with the  $\text{Ca}^{++}$  and  $\text{CO}_2^-$  ions.

The sharing by calcium ions of two oxygens (O12 and O22) belonging to different acrylate molecules homologous by a translation of  $\vec{b}$  is responsible for the formation of ribbons of width  $a/2$  extending along  $\vec{b}$ , i.e. vertically above the paper. A cross section of such a ribbon along a vertical plane normal to  $\vec{a}$  is shown on Fig. III-1-6. On this figure, each calcium ion can be seen to be the center of a clear coordination polyhedron of eight elements: six carboxylate oxygens belonging to four different acrylate molecules, and two water molecules.

The bonding scheme of this structure explains the easy (001) and (100) cleavages and the fragility of the crystals. The structure in general and the internal conformation of the acrylate molecules in particular have been found to be reasonable. The factors contributing to the stability and the properties of this structure will be discussed next in greater detail.

### III-1-3 Discussion of the results

The following discussion, and particularly the interpretation of the results directly relevant to dehydration, diffusion, dimerization and polymerization have been established by the present author with the help of discussions with Dr. Yvon Lepage.

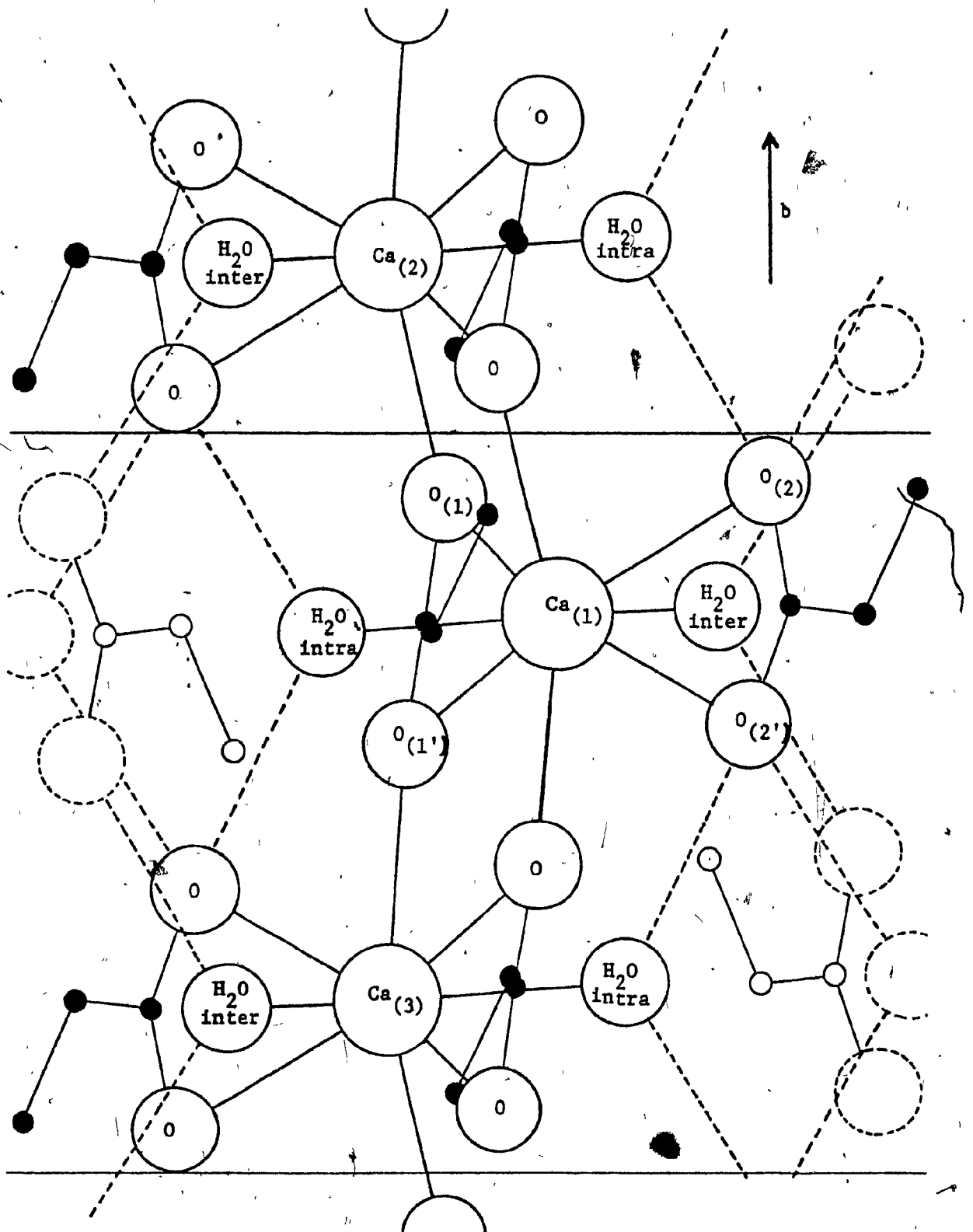


Fig. III-1-6 : Cross-section of the calcium ribbons stretching along  $\vec{b}$  in the structure of  $\text{CaAc} \cdot 2\text{H}_2\text{O}$ , showing the two types of water present.

### III-1-3-a Structure stability and dehydration

A detailed investigation of the crystallographic structure of the dihydrate monomer reveals information as to the stability of this structure along three directions: the principal axis of the crystal ( $\vec{b}$ ); laterally along the plane of the layers (along  $\vec{a}$ ); and between the layers in a direction normal to their planes. The inter-layer stability has been shown to be the result of Van der Waals approaches between the vinyl  $\text{CH}_2$  groups at the tips of the combs' teeth, and needs no further discussion.

Along the principal axis  $\vec{b}$  stretch the ribbons mentioned earlier, organized around the strings of calcium ions. The carboxylate groups are attracted towards these strings, while the vinyl ends of the acrylate molecules point away from them. The forces that hold each ribbon together are of two origins, as may be clearly visualised in the cross-section shown on Fig. III-1-6:

(1) One  $\text{CO}_2^-$  group ( $\text{O}_1$  and  $\text{O}_1'$ ) is shared between three calcium ions labelled  $\text{Ca}_1$ ,  $\text{Ca}_2$ , and  $\text{Ca}_3$  on the figure.  $\text{Ca}_1$  is on the same level, whereas  $\text{Ca}_2$  and  $\text{Ca}_3$  are homologous by a translation of vector  $\vec{b}$  and located  $\frac{1}{2}b$  above and below the carboxylate level. This bonding scheme does not involve any water molecule, and is therefore likely to persist upon dehydration, as has been suggested by the Debye-Scherrer experiments.

(2) The other  $\text{CO}_2^-$  ( $\text{O}_2$  and  $\text{O}_2'$ ) belongs in particular to  $\text{Ca}_1$ , but is linked to  $\text{Ca}_2$  and  $\text{Ca}_3$  indirectly through the H-bonds formed with the water molecules labelled "H<sub>2</sub>O-intra". This bonding scheme will obviously be destroyed upon dehydration, and this destruction is probably responsible for the 33% contraction of the ribbons observed along  $\vec{b}$ .

Laterally, the different ribbons are held together by the water only. The water labelled "H<sub>2</sub>O-inter" on Fig. III-1-6 shares a bond with the calcium Ca<sub>1</sub> of one ribbon, while it forms hydrogen bonds with two carboxylates bound to the calciums Ca'<sub>2</sub> and Ca'<sub>3</sub> of the next ribbon.

The water contributing to the mechanical and electronic stability of each ribbon (H<sub>2</sub>O-intra) is involved in two strong H-bonds of equal length (2.76 and 2.79 ± 0.02 Å), whereas the water which is the only link holding different ribbons together (H<sub>2</sub>O-inter) exchanges weaker H-bonds of unequal length (2.83 and 3.03 ± 0.02 Å). It has been calculated that the fraction of bond valence exchanged by H-bonds between CO<sub>2</sub><sup>-</sup> and H<sub>2</sub>O is close to the fraction exchanged by ionic bond between CO<sub>2</sub><sup>-</sup> and Ca<sup>++</sup>.

In conclusion, water is seen to be clearly indispensable to the stability of the structure. Water is the only strong link between the ribbons, and an important contributor to the stability of each ribbon.

The existence of two non-equivalent types of water has been demonstrated, playing different roles with different bond strengths. On this ground, it would appear that crystallography does not preclude the possibility of a partial dehydration taking place under certain conditions, whereby the weaker-bonded inter-ribbon water could be removed first.

However, even such partial removal would require a complete modification of the coordination polyhedron of the calcium ion, therefore leading to a considerable rearrangement of the whole structure. Indeed, possible intermediate structures such as a monohydrate have eluded isolation and identification thus far. The present structure of the crystalline dihydrate is perfectly consistent with the direct transition to the amorphous anhydrate observed by Costaschuk<sup>(84)</sup> by means of D. S. C., T. G. A., and Debye-

Scherrer powder X-ray analysis. Nevertheless, anomalies in the D.S.C. and T.G.A. curves of a similar sample were observed by O'Donnell and Sothmann<sup>(83-b)</sup>, preventing the complete rejection of the hypothesis that a metastable partial hydrate could exist. These anomalies will be discussed further in section III-3-1-a.

#### III-1-3-b Diffusion of water and inhibitor molecules

The layered structure of the dihydrate leaves a free space between the acrylate molecules homologous by a translation of vector  $\vec{b}$  (6.63 Å). Taking in account the 2.0 Å Van der Waals radius of a  $\text{CH}_2$  group, this leaves a free space of 2.63 Å. However, two opposite factors influence the availability of this free space between the layers of the crystal. First, the vinyl groups are not all at the same altitude with respect to the plane of the combs, thereby reducing the straight line thickness of the free channels and forcing diffusing species to adopt a zig-zag trajectory. Second, wagging of the acrylate molecules around the pivot of the calcium ion is clearly possible, indicating that thermal agitation may help the diffusion by enlarging momentarily the free volume available.

The diffusion behaviour of water and of other small molecules such as inhibitor gases may now be predicted by comparing the dimensions of these molecules with the 2.53 Å free space available.

Watine<sup>(85)</sup> made such an attempt at correlating these parameters with the observed inhibition produced by  $\text{O}_2$ ,  $\text{I}_2$ , and  $\text{N}_2\text{O}$  on the polymerization. However, he based his reasoning on the structure of Lando<sup>(77)</sup>, which has been proved erroneous. Also, he calculated the dimensions of the envelopes of these molecules using the crystalline ionic radii of the elements, where-

as the Van der Waals radii would appear more relevant here. Table III-1-3 lists the dimensions calculated by the two methods.

The Van der Waals diameter of the water molecule is not much different from that of an oxygen atom itself, i.e. 2.80 Å. This is quite close to the 2.63 Å dimension of the channels. Water can therefore be expected to diffuse relatively easily through the crystalline dihydrate lattice, with the help of a little thermal agitation of the acrylate tails. A similar comment can be made for ammonia, which is thus predicted to diffuse only slightly less easily than water.

On the other hand, it is clear that the other molecules such as  $O_2$ ,  $F_2$ ,  $N_2$  and  $N_2O$  will be able to enter the lattice only if they present themselves end first or edgewise. This restriction on their degrees of freedom should greatly restrict the rates of diffusion of these molecules in the order listed.

Furthermore, molecules such as  $O_2$  are capable of forming Van der Waals interactions with the polar acrylate molecules. The first few surface layers of the acrylate crystal could thus very well saturate themselves with oxygen, blocking the channels for further penetration.

Indeed, direct measurement of the rate of diffusion of oxygen in the dihydrate will be shown in section III-2-1 to be close to zero.

As for iodine, its smallest dimension is 63% larger than the thickness of the channel. It should therefore prove completely unable to diffuse in the perfect lattice, and should diffuse more difficultly than oxygen even in a lattice partially disrupted by dehydration. This has been confirmed experimentally by Watine, who showed that iodine had no effect on the polymerization of the dihydrate, whereas it had an inhibitory effect similar to,

Bond	Length	Element	Crystal ionic radius	Van der Waals radius
O-O	1.21	Ca	0.99	-
N≡N	1.10	O	1.32	1.40
N-O in N <sub>2</sub> O	1.19	N	1.71	1.5
N-N in N <sub>2</sub> O	1.13	I	2.20	2.15
I-I	2.66	F	1.33	1.35
F-F	1.42	CH <sub>2</sub>	-	2.0
N-H	1.01			

TABLE III-1-3-a

Dimensional data (Å)

Molecule	Diameter & Length (Å) using ionic radii	Diameter & Length (Å) using Van der Waals radii
H <sub>2</sub> O	~ 2.64	~ 2.80
NH <sub>3</sub>	~ 3.42	~ 3.00
O <sub>2</sub>	2.64 x 3.85	2.80 x 4.01
N <sub>2</sub>	3.42 x 4.52	3.0 x 4.1
I <sub>2</sub>	4.40 x 7.06	4.30 x 6.96
F <sub>2</sub>	2.66 x 4.08	2.70 x 4.12
N <sub>2</sub> O	3.42 x 5.35	3.0 x 5.22

TABLE III-1-3-b

Dimensions of the envelopes of molecules considered in the study of diffusion

but markedly weaker than that of oxygen over the first three-quarters of the dehydration range (Fig. I-6-1) .

In conclusion, it may be stated that the analysis of the crystalline structure has led to several predictions as to the diffusability of the system by small gaseous molecules. Whenever available, independent direct experimental evidence supports the crystallographic conclusions. On this basis, it is here suggested that fluorine should present a diffusion behaviour similar to oxygen, and that ammonia should diffuse nearly as easily as water. The study of polymerization under an atmosphere of ammonia would be of particular interest, since  $\text{NH}_3$  is a specific ionic inhibitor which could be used to investigate the presence of an ionic mechanism of polymerization. Alternately, the synthesis of an ammonia substitution compound of the dihydrate, or of a novel ammonia complex of calcium acrylate would hold the promise of fruitful comparisons between the various systems formed.

#### III-1-3-c Di-, tri- and polymerization

The following is an attempt at predicting the possible reactions of the monomer inside the crystalline calcium acrylate dihydrate. For the sake of simplicity, the discussion will be based on the following assumptions:

- the reactions are radical additions
- the additions are made head-to-tail
- the initiating radical is  $\text{CH}_3\text{-}\dot{\text{C}}\text{H-CO}_2^-$ , which belongs to the general type  $\text{CHX}_2\text{-}\dot{\text{C}}\text{Y-Z}$  that has been identified as the one responsible for S.S. polymerization of a great many vinyl systems including the present one.

The projection of the structure that has been presented on

Fig. III-1-5 showed that because of the various symmetries present, only two different types of radical positions, labelled A and B are identifiable.

In order to interpret this result, the criterion proposed by G. Schmidt<sup>(21,22)</sup> will be retained, namely that reactive double bonds must be less than approximately 4 Å apart for a solid state reaction to take place. In these conditions, reactions along the b axis are very unlikely to take place because of the 6.63 Å distance between adjacent combs. Only the reactions within a single comb (i.e. in the ac plane) need therefore be considered.

The nearest double bonds to a radical placed in a type-A position are 3.3 and 3.8 Å away. They belong to the same comb as the radical, and are tied to the calcium backbone of the comb by their carboxylate ends. Only 30-40° rotation of the acrylate molecules around the carboxylate pivots is enough to bring these double bonds into contact with a type-A radical. It is thus evident that Schmidt's criterion is more than satisfied, and that dimerization of type-A radicals should be easily accomplished with a neighbour of the same comb.

The same case may be made for type-B radicals, although the nearest reactive double bonds are 3.8 and 4.6 Å away. The dimerization is believed to be only slightly more difficult in this case, but is still possible because of the flexibility afforded by the thermal wagging around the carboxylate pivots.

On the other hand, type-A and type-B radicals lie 3.9 and 4.0-4.7 Å away respectively from the nearest double bonds of the molecules in the opposite comb. No amount of rotation is able this time to bring them with-

in reacting distance of the radicals. To achieve dimerization in these conditions, one of the  $\text{Ca}^{++}-\text{CO}_2^-$  bonds must be stretched considerably, which is likely to require much more thermal energy.

As a result, it is concluded from the crystallographic structure that the first reaction to take place upon warming up from a low-temperature irradiation should be a rather easy dimerization of either type-A or type-B radicals with a monomer of the other type placed next to them in the same comb.

This result will be shown to be perfectly consistent with the ESR and Wide-Line NMR data gathered over the range of  $-100$  to  $-50^\circ\text{C}$ .

Once this dimerization is achieved, the radicals become much less reactive, because they are rigidly maintained in a position of the matrix where the nearest neighbours are farther away. Any further reaction now requires the stretching of a calcium-carboxylate ionic bond, and therefore requires much more thermal energy. The breaking of this ionic bond destroys the coordination polyhedron of that calcium, initiating a local crumbling of the structure. This crumbling, associated with the exothermicity of the polymerization, is likely to facilitate the release of water and the release of more acrylates which are thus made available for continuing polymerization.

We may now conclude on the basis of the analysis of the crystallographic structure of the dihydrate that:

- (a) warming up after a low-temperature irradiation first produces dimer radicals.
- (b) further heating is required to initiate the polymerization.
- (c) the polymerization cannot take place in a perfect lattice, but destroys it. The polymer chains are therefore likely to grow in the

middle of a "disruption channel" produced by the growth.

(d) the polymerization is very unlikely to be stereotactic, as no lattice control can be envisaged, and much molecular diffusion is required.

(e) the polymerization is likely to foster dehydration.

(f) conversely, dehydration should facilitate polymerization by loosening the structure, which is a prerequisite for polymerization.

Most of these conclusions will be corroborated by independent experimental evidence presented and further discussed in the sections to follow.

### III-2 Oxygen diffusion in the monomer

F. Costaschuck<sup>(84)</sup> and F. Watine<sup>(85)</sup> have shown that the effect of adding oxygen (air) in the polymerization vessels was a partial inhibition, stronger for the anhydrate than for the dihydrate, and a total inhibition for the intermediate 0.3 hydrate. To aid in understanding these results, it was decided to try to get some insight into the rates of diffusion and reaction of the oxygen, as well as into the kind of product(s) formed by its reaction(s) in the system.

#### III-2-1 Oxygen diffusion investigated by ESR

The acrylate radicals produced by irradiation of the monomer were found to convert readily into peroxide radicals of a distinctly different shape upon contact with the oxygen of the air. Accordingly, it was decided to use this property to monitor the rate and extent of diffusion of  $O_2$  in the monomer by the ESR technique, which is very sensitive and non-destructive.

Samples of dihydrate and anhydrate were prepared under vacuum in

vessels as described in the experimental section Fig. II-9-1-a enabling the experimenter to introduce a quantity of dry air over the sample at liquid nitrogen temperature without removing the sample from the ESR spectrometer. In order to measure the rate of reaction and diffusion of  $O_2$  at low temperature, spectra were recorded in liquid nitrogen for 30 minutes before and after the seal had been broken. The sample was then quickly warmed to  $25^\circ C$ , and spectra recorded for some time to monitor the decay rate at this temperature.

#### III-2-1-a Dihydrate

The initial spectrum of the dihydrate at liquid nitrogen temperature always displayed a narrow group of sharp lines at the center of the acrylate signal, Fig. III-2-1-a. This group has been observed to vary slightly from sample to sample and had the same g factor and line width as a peroxide signal, which is shown superimposed for comparison<sup>(62)</sup>. Its origin may be found in small amounts of air either left over the sample by an imperfect evacuation, or more probably occluded in the lattice during the crystallization of the monomer and thus unable to diffuse out upon evacuation.

Upon breaking the seal and allowing air to enter, the shape of the central part of the spectrum was immediately affected, while the remainder remained unchanged (Fig. III-2-1-b). No more significant changes occurred for 20 more minutes in liquid  $N_2$ . The usual transformation into the propagation triplet occurred then within minutes after warming up to  $25^\circ C$ .

Very little change was to be observed over the next 10 hrs with the sample at  $25^\circ C$  and open to the atmosphere (Fig. III-2-1-c).

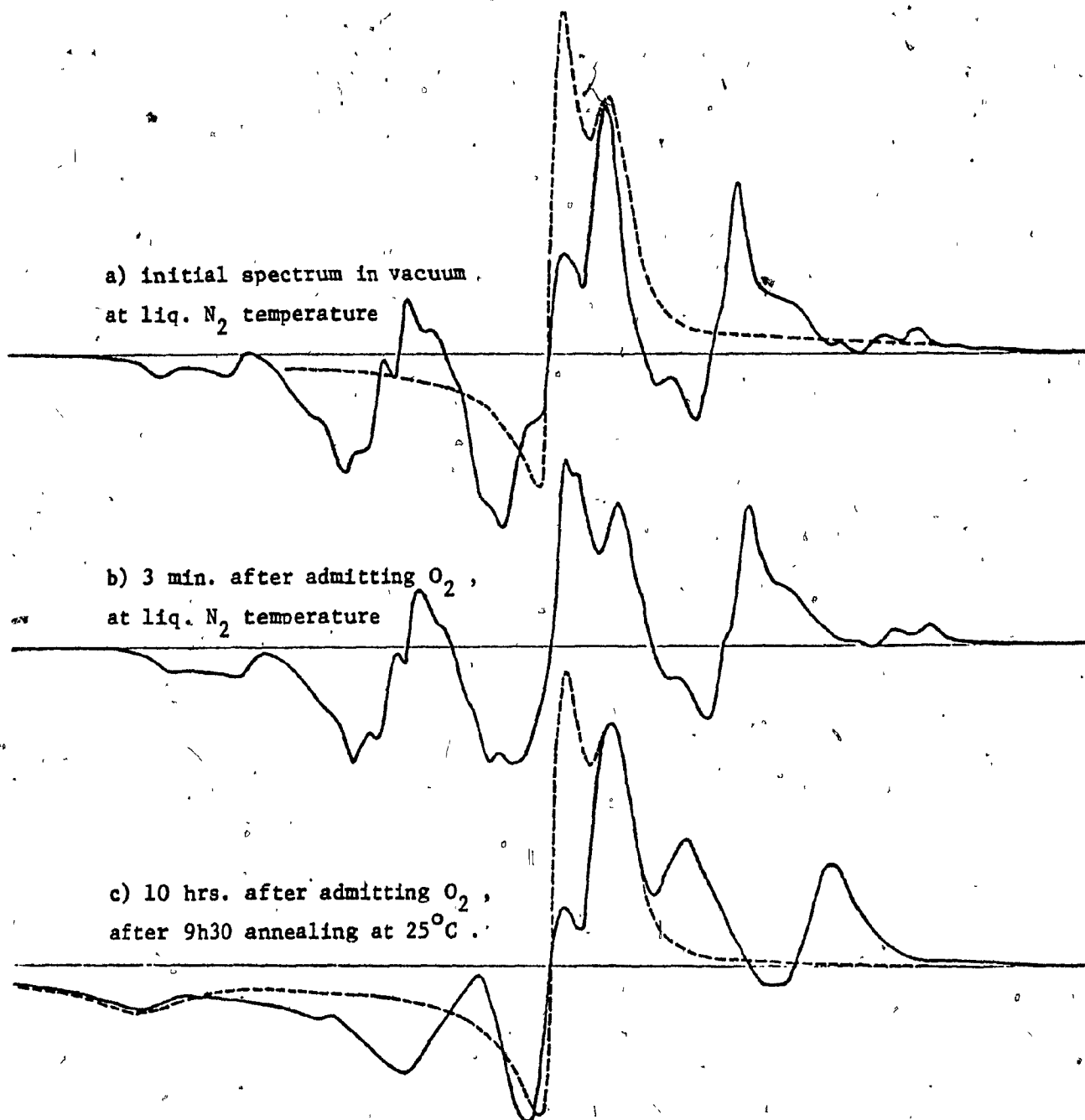


Fig. III-2-1 : Oxygen diffusion through CaAc<sub>2</sub>·2H<sub>2</sub>O , investigated by ESR .  
Peroxide signals are superimposed (in broken line) for comparison .

Quantification was attempted by superimposing a pure peroxide spectrum on the acrylate composite spectrum, making it possible to distinguish between the peroxide and the acrylate components. The number of radicals is proportional to the peak to peak height and to the square of the line width. The narrowest central line (4G width) was chosen to measure the peak to peak height of the peroxide signal because of its characteristic sharp shape, but a total line width of 10G was used to make the estimate. The intensity and line width (60G) of the acrylate part of the spectrum were measured from the two lateral peaks of the main triplet, which are free of interference from the peroxide signal. Thus measured, the concentrations of peroxide radicals relative to that of the acrylate radicals were approximately:

- 1.1% for the initial acrylate @ 77°K in vacuo.
- ⊕ 2.5% 15 min after the seal was broken, at 77°K (stabilized value).
- 3.1% after 10 hours at 25°C (stabilized value).

These figures are to be taken as estimates only, as it is difficult to judge with precision the intensities of two overlapping and rapidly changing multiline spectra. More accuracy could possibly be obtained by using a computer program designed to subtract the two spectra from one another, point by point. The coefficients applied to each spectrum could be varied by trial and error until the difference spectrum matches that of the pure acrylate. Such a program has been developed and tested by the author, but the potential gain in accuracy has been judged unrewarding in the context of the present study.

The first conclusion we can draw from the preceding data is that the rate of chemical transformation of the acrylate radicals into peroxide is

very fast indeed. Even at liquid nitrogen temperature, 70% of the dihydrate radicals ever accessible to oxygen reacted within 15 minutes.

The second conclusion pertains to the ease of diffusion in the system. The dihydrate crystalline lattice appears to be stubbornly closed to diffusion of oxygen. Only 2% of the dihydrate radicals could be reached by oxygen, even at 25°C for a long time.

These radicals could reside within the first few surface layers of the dihydrate crystals. However, the observation by Costaschuk<sup>(84)</sup> that the in-source polymerization amounted to 2% as well suggests that these radicals could rather be those of the polymer, through which oxygen would diffuse easily. This hypothesis will be further substantiated in section IV-1 by results showing that the relationship suggested here holds throughout the polymerization yield range.

#### III-2-1-b Anhydrate

The initial spectrum of the anhydrate at 77°K in *vacuo* also displayed signs of the presence of a small fraction of peroxide signal (Fig. III-2-2-a). However, the intrinsically narrower central line of the anhydrous acrylate is now nearly fused with the peroxy line, and does not allow separate quantitative measurements. No significant change in shape or intensity was observed for 30 min after the air had been admitted through the break-seal (Fig. III-2-2-b).

In view of the quasi-instantaneous reaction of O<sub>2</sub> with the dihydrate radicals, this appears surprising. It seems that even though the amorphous anhydrate is totally diffusible by O<sub>2</sub> at 25°C (as will be shown immediately), the thermal energy at 77°K is too low to allow O<sub>2</sub> in at an observable rate. The 2% acrylate radicals accessible to O<sub>2</sub> in the dihy-

a) initial spectrum in vacuum  
at liq. N<sub>2</sub> temperature

b) 30 min. after admitting O<sub>2</sub> ,  
at liq. N<sub>2</sub> temperature

c) after 40 min. annealing at 25°C

Fig. III-2-2 : Oxygen diffusion through CaAc anhydrate, investigated by ESR .

drate are likely to be also present in the anhydrate, but unfortunately, they cannot be evidenced as easily because the spectral lines now overlap.

Only minutes after warming up to 25°C, the propagation triplet was observed, with a central line now strongly distorted by the peroxide.

Within 40 min, the acrylate lines thus disappeared completely to the benefit of a pure peroxy line (Fig. III-2-2-c) which decayed slowly thereafter. The central peak lost intensity faster than the lateral one, and the line width increased from 9.83 to 10.67 G, which is indicative of some exchange narrowing being removed by dilution of the radicals.

In summary, the study of the diffusion of oxygen through calcium acrylate hydrates has yielded the following information:

- (1) the rate of oxygen reaction with the radicals is very fast.
- (2) the dihydrate lattice is stubbornly closed to the diffusion by oxygen. This confirms the conclusions of the crystallographic study of the lattice dimensions in section III-1-3-b.
- (3) the anhydrate at room temperature is quickly and totally diffusible by oxygen. The diffusability of the anhydrate is a logical consequence of its amorphous nature.

We may further conclude that:

- (4) the less than 2% radicals accessible to oxygen either reside within the surface layers of the dihydrate, or more probably are polymer radicals (as will be shown later).

- (5) the oxygen should be able to fully exert its inhibitory effect on the polymerization of the anhydrate.

However, Watine's polymerization data<sup>(85)</sup> contradicting the proposition (5),

it was decided to further investigate the oxygen inhibition of the polymerization.

### III-2-2 Effect of oxygen and thorough degassing on the polymer yield

Experiments were conducted on dihydrate samples to study the effect of oxygen and of a more or less perfect degassing on the polymer yield.

The dihydrate crystals have been shown by crystallography and ESR to be almost totally impermeable to oxygen at room temperature. However, post-polymerization may allow some  $O_2$  penetration because of two factors: (1) the polymer surrounds itself with a "disruption sleeve" of disordered material, where oxygen may diffuse as easily as through the amorphous anhydrate. This statement is supported by evidence gathered from crystallography (section III-1-3-c) Wide-Line NMR (section IV-2) and ESR (section IV-1).

(2) the higher  $50^\circ C$  temperature at which post-polymerization studies have usually been carried favors molecular motion in the crystal and diffusion.

On the other hand, the anhydrate has been shown in the previous section to be rapidly and totally diffusible by oxygen.

Indeed, a strong but partial inhibition effect of air has been observed by Watine<sup>(85)</sup> over the "in vacuo" polymer yields of the monomers, as well as by the present author. The data are presented below in Table III-2-1.

No significant difference could be found between the yields of dihydrate that had been casually evacuated for 5 min, or that had been thoroughly degassed for 13 hrs of high vacuum with a mercury diffusion pump. In itself, this means that oxygen is either able to diffuse in and out the

Sample, treatment	Polymer Yield (%) from Watina <sup>(85)</sup>	Polymer Yield (%) from this study
Dihydrate, evacuated 5-10 min @ 77°K	29.3	34.9±1.8 (3 samples)
Dihydrate, evacuated 13 hrs @ 77°K	-	34.7±1.8 (3 samples)
Dihydrate, under 1 atm. of air	16	10.7±0.4 (3 samples)
Anhydrate, in vacuo	26 to 29	35 ± 15 (5 samples)
Anhydrate, under 1 atm. of air	4 to 8	6 ± 3 (4 samples)

TABLE III-2-1

Calcium acrylate post-polymerization yields under various atmospheres .

Conditions: 9 days at 50°C, dose 0.86 Mrad.

lattice extremely fast, or not at all. The last suggestion is obviously the correct one.

The differences observed between the results of Watine and of the present author may be rationalized by noting that the samples were taken from different batches, specially regarding the powder particle sizes which were smaller in Watine's case.

Qualitatively, both studies reveal that the inhibition is incomplete. Two reasons might be invoked to explain this:

- (1) the polymerization reaction might be faster than the diffusion rate of oxygen in the "disruption sleeve". Oxygen would thus only be able to interfere with the radicals after the chain has already grown to a sizeable length.
- (2) the polymerization might take place by a combination mechanism such as radical/ionic and the oxygen can only inhibit one of the two mechanisms (the radical one).

Although the first interpretation makes sense for the crystalline dihydrate, it cannot be invoked for the amorphous anhydrate because oxygen has a ready access to all radicals from the start. The failure of oxygen to bring about a total inhibition in the anhydrate may therefore be taken as an indication that another polymerization mechanism than the heretofore accepted radical one is also at work.

The hypothesis according to which the oxygen would be chemically incapable of producing total inhibition must be rejected on the basis of Costaschuk's<sup>(84)</sup> and Watine's<sup>(85)</sup> observation that oxygen is able to completely inhibit the polymerization of the intermediate 0.5 hydrate.

We must therefore conclude that the study of the effects of oxygen

diffusion on the polymer yields of the various hydrates suggests that the SSP of calcium acrylate hydrates proceeds by two concurrential mechanisms, probably an ionic as well as a radical one. The large variability in the yields of the anhydrate samples from one flask to the next may be regarded as a further indication that the second mechanism is ionic, as ionic polymerizations are notably sensitive to variations in the trace amounts of residual water. It is to be remarked that Watine observed a similar variability between his anhydrate samples. On the other hand, the intermediate hydration levels up to 2 did not display such variability, probably because the water is present in a large excess anyway.

The hypothesis of a dual mechanism will be further discussed in section IV-4-2.

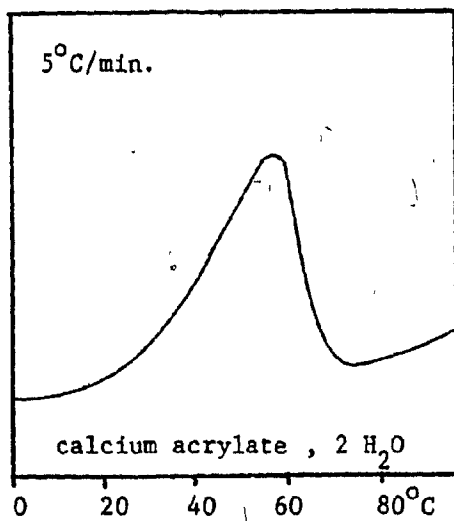
### III-3 Physical and phase changes in calcium acrylate hydrates

#### III-3-1 Physical and phase changes as a function of dehydration

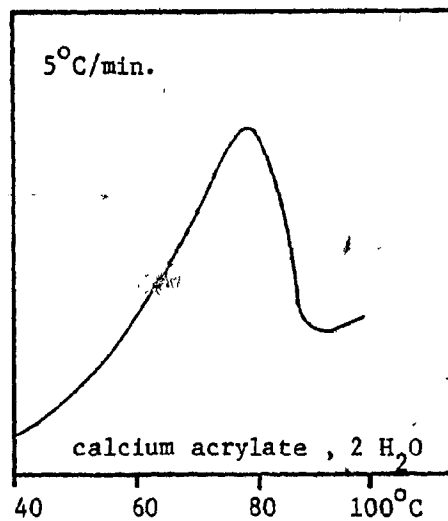
In order to explain the presence of a maximum of the polymerization yield around the 0.5 hydration level, a study of the dehydration process is necessary to disclose the nature of the phases present. Since this maximum is also present in barium methacrylate monohydrate, this salt deserves as much attention as calcium acrylate dihydrate.

##### III-3-1-a Previous studies

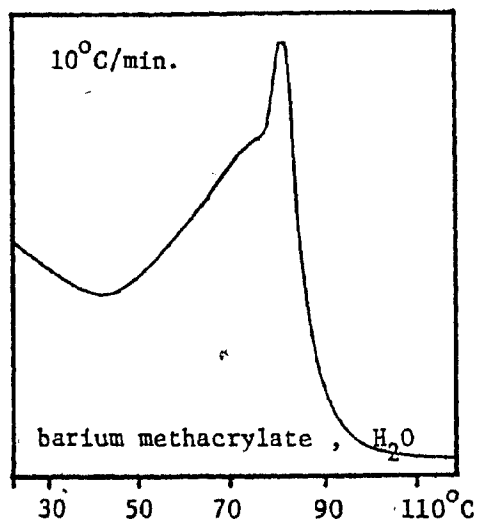
Differential Scanning Calorimetry (D.S.C.) investigations have been performed by Costaschuk<sup>(84)</sup> and Watine<sup>(85)</sup> on calcium acrylate dihydrate and barium methacrylate monohydrate. Their results are depicted on Fig. III-3-1. They indicate that the dehydration of calcium acrylate di-



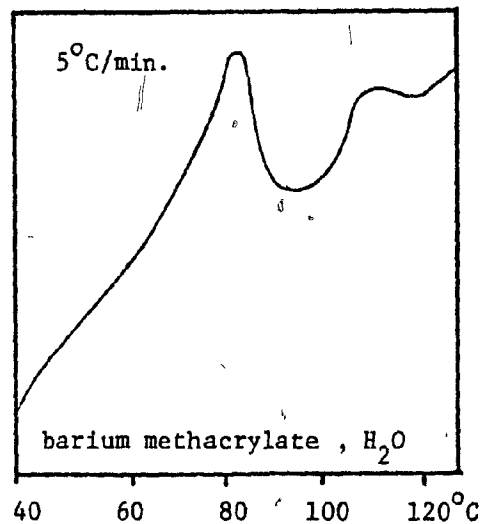
from Costaschuk (84,p.28)



from Watine (85,p.37)



from Costaschuk (84,p.105)



from Watine (85,p.119)

Fig. III-3-1 : Previous dehydration thermograms of CaAc, 2 H<sub>2</sub>O and BaMa, H<sub>2</sub>O obtained by Differential Scanning Calorimetry in-regular sample pans .

hydrate occurs in one step around  $79^{\circ}\text{C}$  (Costaschuk found  $60^{\circ}\text{C}$ , but the calibration of his instrument was shown by Watine to have been incorrect).

A thermogravimetric analysis (TGA) by Costaschuk also confirmed the weight loss occurred in one step.

Barium methacrylate monohydrate exhibited a similar behaviour, except for a second feature in its D.S.C. thermogram in the form of a shoulder or small additional endotherm.

Bowden and O'Donnell<sup>(81-c)</sup> carried out the same investigation; and all four authors concluded the first peak to represent the phase transition from the mono- to the anhydrate, while the additional endotherm would represent the actual desorption of the water.

However, O'Donnell and Sothmann<sup>(83-b)</sup> made a more thorough second study in 1972, showing the system to be more complicated than previously believed. D.S.C. of the barium hydrate displayed two sharp endotherms at  $80$  and  $110^{\circ}\text{C}$  for small crystals, corroborated by a two-step weight loss in TGA (Fig. III-3-2-a). The complexity arises from the observation that the intensities of the second D.S.C. endotherm and of the second TGA step were reduced to the profit of the first ones upon grinding the powder from  $10$  down to  $0.1$  mg particle size.

No shift in temperature was observed until finally, powders finer than  $0.01$  mg ( $-100$  mesh) displayed a shoulder on the side of the remaining D.S.C. endotherm. The resulting trace resembles that obtained by Costaschuk, while the trace for the  $0.3$  mg crystals resembles that observed by Watine, with the two endotherms at the same temperatures (Fig. III-3-1 and III-3-2-a). On the grounds of these observations, the D.S.C. traces obtained by Costaschuk and by Watine may be reconciled by ascribing their

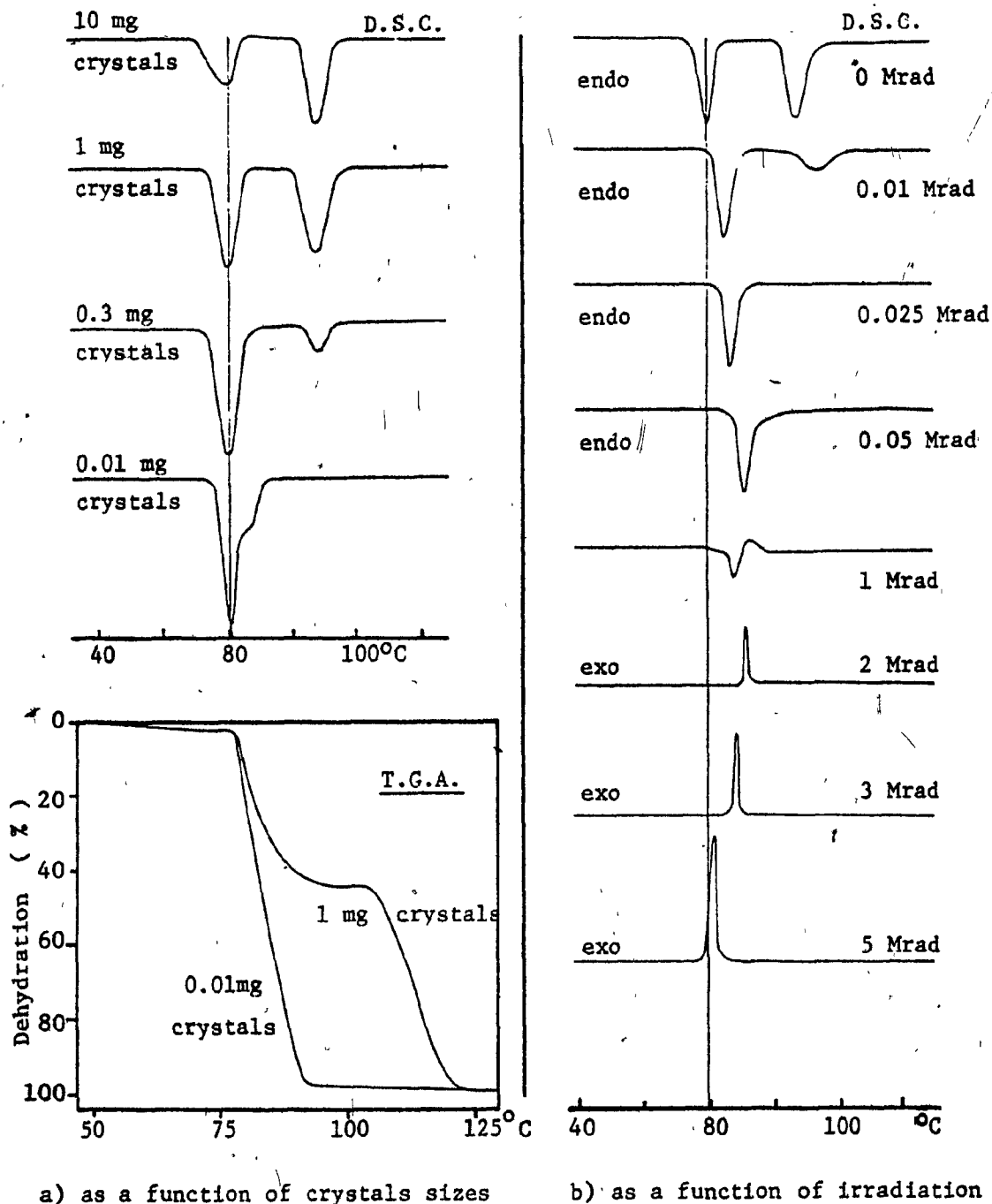


Fig. III-3-2 : Thermograms of barium methacrylate monohydrate , obtained by Differential Scanning Calorimetry (DSC) and Thermo-Gravimetry ( T.G.A. ). Source : O'Donnell and Sothman (83-b)

differences partly to their using powders of different particle sizes.

Two additional observations by O'Donnell and Sothmann deserve particular attention from the point of view of the present thesis.

The first one is their observation that as little as 0.02 Mrad irradiation was sufficient to make the second D.S.C. endotherm vanish altogether, and that 0.05 Mrad was enough to shift the remaining endotherm  $10^{\circ}\text{C}$  higher (Fig. III-3-2-b). Around 1 Mrad, the dehydration endotherm was replaced by a polymerization exotherm at the same temperature. No explanation was given for the disappearance of the second endotherm, but O'Donnell and Sothmann concluded that the post-irradiation polymerization and the dehydration reactions could not be observed separately under any circumstances. This establishes clearly that very strong ties exist between the polymerization and dehydration mechanisms, which appear to be interconnected by some common physical factor.

The second observation is that the dehydration of a partial hydrate occurred more readily and at a lower temperature than that of the monohydrate. In view of the above remark, this is of particular interest since polymerization is known<sup>(84,85)</sup> to also proceed faster and to higher limiting conversions in the intermediate hydrates than in the monohydrate.

O'Donnell and Sothmann have measured the equilibrium water vapour pressure above the barium methacrylate salts. It was found to be constant from near 0 to 1  $\text{H}_2\text{O}$ . They interpreted this to indicate the absence of definite intermediate compounds such as hemi- or quarter-hydrates, and the dehydration was therefore concluded to proceed by a simple 2-phase mechanism.

This points towards the interphase boundary as the possible physical factor interconnecting the polymerization and dehydration mechanisms. The

behaviour of Ba-methacrylate,  $H_2O$  seems to be identical to that of Ca-acrylate,  $2 H_2O$ , which will be discussed next.

### III-3-1-b Thermal analysis of the dehydration

The examination of the dehydration thermograms of calcium acrylate of Costaschuk and of Watine (Fig. III-3-1) reveals two disconcerting facts:

(1) The traces do not return to baseline after the dehydration endotherm, but seem to be at the foot of another peak, right at the temperature where the thermograms displayed have been cut ( $100^\circ C$ ). This is particularly unfortunate since Watine's thermogram of barium methacrylate (which is similar in most respects to the calcium acrylate system) exhibits indeed a second peak around  $110^\circ C$ .

(2) The line widths of the peaks are very broad (30 to  $50^\circ C$ ) whereas dehydration in sealed vessels such as those used throughout the SSP studies is supposed to give rise to a sharp first-order transition.

Accordingly, it was decided to investigate again the thermodynamics of dehydration in general and that of calcium acrylate in particular.

Classical thermodynamics shows that solid hydrates will lose water at any temperature provided the vapour pressure of water above the hydrate is less than the equilibrium vapour pressure at that temperature. In a reasonably unrestricted system such as we have with a standard D.S.C. sample pan, the peak shapes will therefore be very broad, specially on the low temperature side. A peak maximum will be found close to the point where a higher hydrate is completely converted, with the high temperature side much steeper than the low temperature side of the peak.

The observed temperature of a dehydration maximum will therefore be

largely a function of experimental conditions such as:

- the flow rate of the purge gas,
- the temperature scanning rate,
- the particle size of the sample,
- the amount and packing density of the sample,
- the fitting tightness of the sample pan cover.

These considerations are believed to account for the remaining part of the differences noted between the thermograms of Costaschuk and of Watine.

Since the intrusion of so many uncontrollable of instrumental parameters deprive the thermograms of much of their intrinsic thermodynamic significance, the manufacturer of the Differential Scanning Calorimeter recommends the use of special "volatile sample pans", whose covers can be crimped gas-tight in an appropriate press. A very small pinhole needs to be pierced through the cover to allow for pressure equilibration, while ensuring that the sample is surrounded by its own vapour in a quasi-equilibrium condition.

The effect of using a volatile sample pan with a pinhole versus a regular pan is illustrated on Fig. III-3-3, for the classical system  $\text{Cu SO}_4 \cdot 5 \text{H}_2\text{O}$ . The differences are startling, in the number as well as in the shape of the peaks observed. The simultaneous effluent analysis (by a chromatograph-type gas detector) is shown superimposed to the calorimetric trace, and was used jointly with X-ray analysis to interpret the thermograms (106).

The first peak was ascribed to an invariant quadruple point, where no dehydration takes place, but where four phases coexist at equilibrium:  $\text{Cu SO}_4 \cdot 5 \text{H}_2\text{O}$  (solid);  $\text{Cu SO}_4 \cdot 3 \text{H}_2\text{O}$  (solid);  $\text{Cu SO}_4$  (solution);  $\text{H}_2\text{O}$  (vapour).

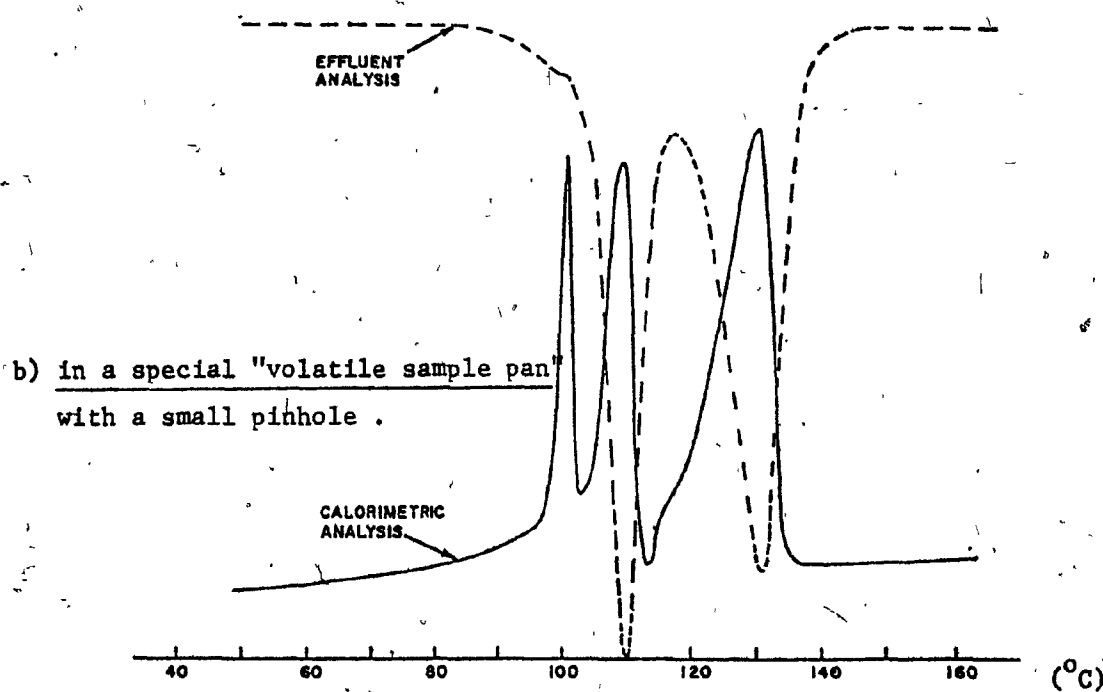
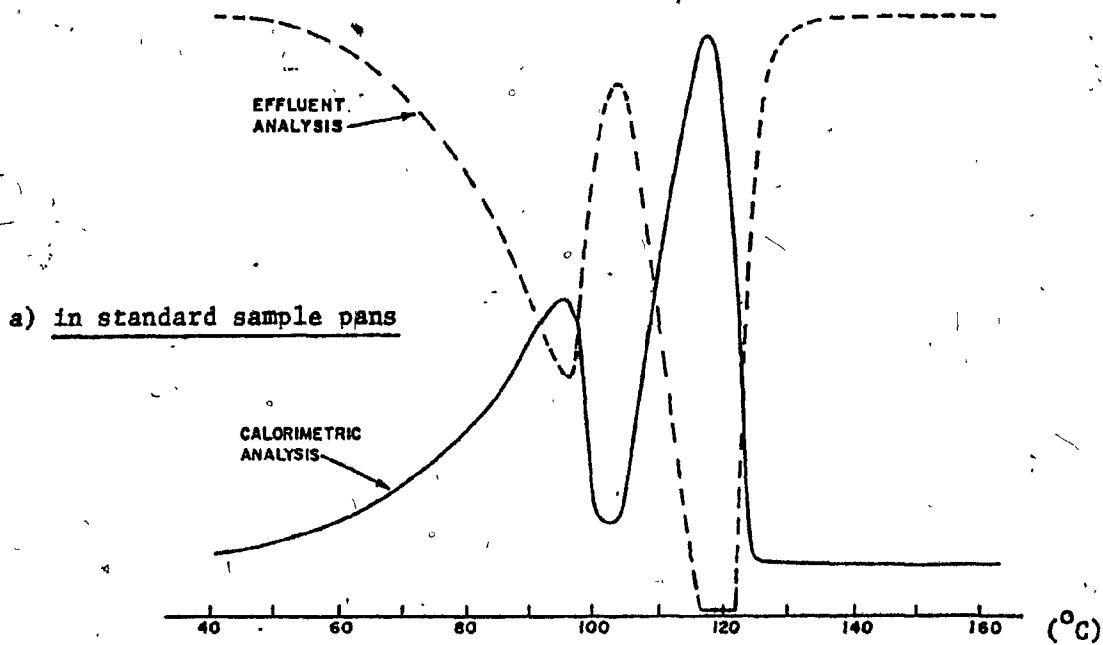


Fig. III-3-3 : Dehydration thermograms and simultaneous effluent analyses of  $\text{CuSO}_4 \cdot 5 \text{H}_2\text{O}$  recorded in standard and special sample pans (Source: (106)).

According to the phase rule, the temperature will rise again only when the pentahydrate is all converted. The second endotherm represents the dehydration of the saturated copper sulphate solution to give more trihydrate, and the third is the dehydration of the trihydrate to the monohydrate, which decomposes only at  $150^{\circ}\text{C}$  (not shown).

On the basis of this information, it was decided to perform the thermal analysis of calcium acrylate dihydrate again, while extending the temperature range upwards and using the special sample pans with a pinhole. The thermogram obtained is presented on Fig. III-3-4.

It is seen that the use of the special pans resulted in a considerably sharper endotherm of only  $2^{\circ}\text{C}$  width, as compared to the  $30\text{-}50^{\circ}\text{C}$  of Costaschuk and Watine. This endotherm was measured at  $79.6^{\circ}\text{C}$  which is the same as that of Watine. Interestingly, it is also very close to the temperature of the first endotherm in barium methacrylate monohydrate measured by Watine and by O'Donnell and Sothmann<sup>(83-b)</sup>.

An additional broad endotherm was disclosed around  $106^{\circ}\text{C}$ , which is also the temperature at which the above authors found a second endotherm in the barium salt. This establishes further the striking similarity between the two systems.

Several interpretations of the thermogram obtained may be advanced.

The first interpretation postulates that water is released at  $79.6^{\circ}\text{C}$  to yield anhydrate. The broad second endotherm should then necessarily be an allotropic phase transition such as a recrystallization of the anhydrate, since the thermal degradation of the acrylate molecule does not occur until much higher temperatures. However, the Debye-Scherrer experiment discussed in section III-1-2-a has shown that no difference could

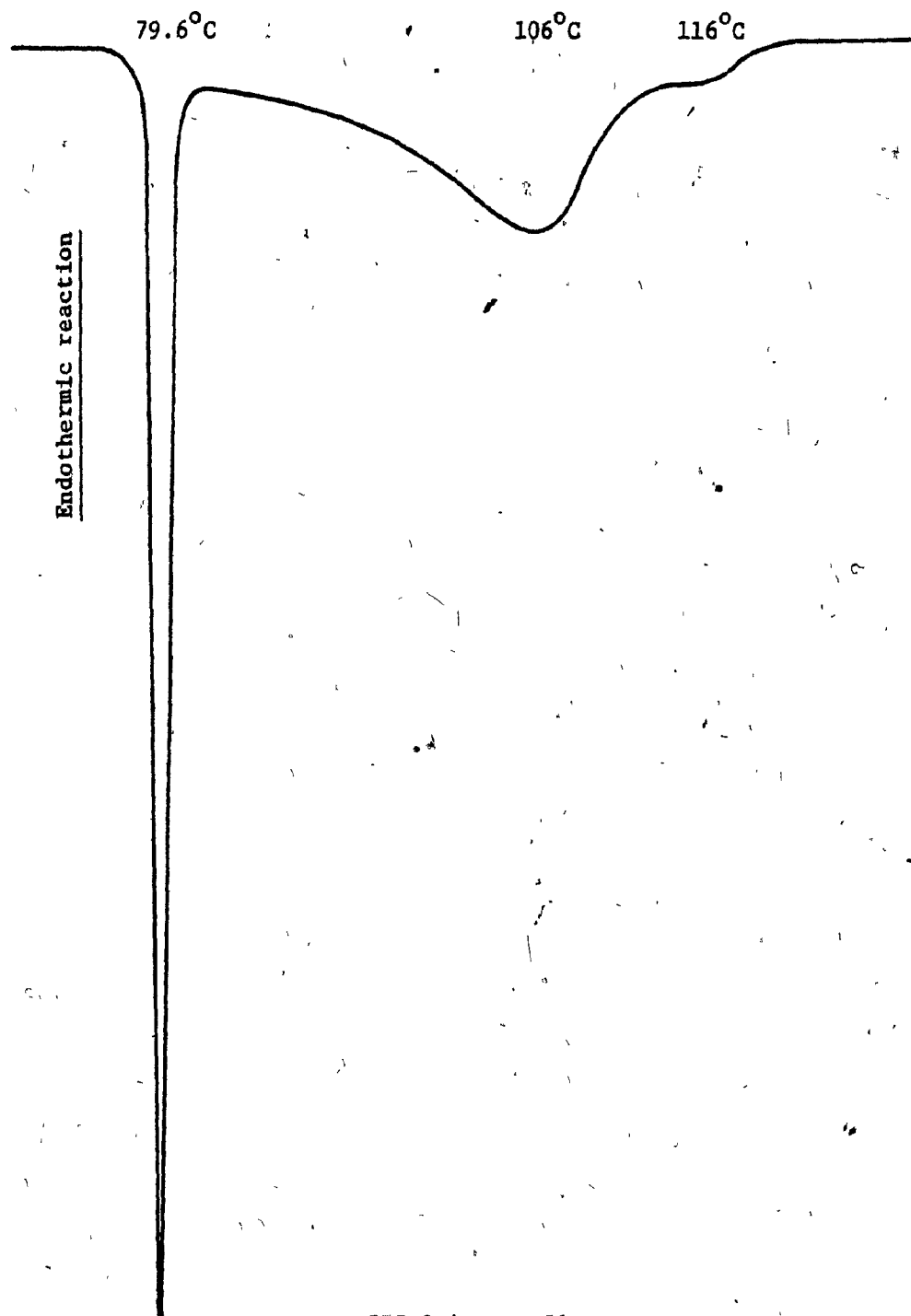


Fig. III-3-4 : Differential Scanning Calorimetry .

Thermogram of a polycrystalline sample of calcium acrylate dihydrate .

Conditions : - 10°C/min. heating rate , in a nitrogen stream  
- volatile sample pan , with a pinhole in the cover

be observed between the X-ray powder patterns of anhydrate prepared either at low temperature or annealed at  $110^{\circ}\text{C}$ . Furthermore, such a phase transition would be expected to give rise to a sharp peak, instead of the broad one found. On these grounds, it appears that the first interpretation (according to which water is released at  $79.6^{\circ}\text{C}$  to yield anhydrate) should be rejected.

The second interpretation postulates that no water is released at  $79.6^{\circ}\text{C}$ , and that the sharp endotherm represents an invariant quadruple point, as in the case of  $\text{CuSO}_4$ :

$\text{CaAc}$ ,  $2 \text{H}_2\text{O}$  (solid);  $\text{CaAc}$  (solution);  $\text{CaAc}$  (anhydrate);  $\text{H}_2\text{O}$  (vapour).

The broad second peak would then represent the dehydration of the saturated  $\text{CaAc}$  solution to yield anhydrate and water vapour. Its broadness would be perfectly consistent with the progressive release of water from the viscous saturated solution and through the amorphous anhydrate solid over the  $80$ - $110^{\circ}\text{C}$  range. It is also consistent with the particle size effect observed by O'Donnell and Sothmann in the similar barium salt, since the grinding of the crystals to a very fine powder is going to accelerate the dehydration and allow it to happen at a lower temperature, resulting in the shoulder observed by them and by Costaschuk on the side of the invariant peak.

According to this interpretation, the disappearance of the second endotherm observed by O'Donnell and Sothmann in the barium salt after irradiation may also be rationalized by the occurrence of a rapid polymerization in the saturated solution formed. Such a hypothesis was tested in the calcium acrylate system by admitting suddenly a small quantity of water into a pre-irradiated dihydrate sample tube. The sample became immediately very hot, attesting to the occurrence of a fast exothermic polymerization. This is believed to be the origin of the replacement of the dehydrat-

ion endotherm by a polymerization exotherm induced at the same temperature by irradiation of the barium salt, as was shown on Fig. III-3-2-b.

In summary, we may state that the second interpretation proposed for the observed thermogram (invariant quadruple point followed by dehydration) seems to be consistent with all the known properties of the two organic systems considered as well as with the established interpretation of the inorganic  $\text{CuSO}_4$  system.

However, some additional complexity arises from the observation of a small shoulder around  $116^\circ\text{C}$  on the thermogram of Fig. III-3-4. This shoulder was found to be reproducible in position and intensity, from sample to sample tested from the same batch.

As crystallography has shown (section III-1-3-a), the two water molecules in calcium acrylate dihydrate occupy different positions in the lattice and engage in bonds of different lengths. Because of this, the existence of a metastable partial hydrate cannot be ruled out, although it could not be deduced directly from the dihydrate structure.

We must therefore accept the possibility of the existence of yet another phase in the system. The three endotherms observed would thus be reinterpreted as follows:

- first peak (sharp,  $79.5^\circ\text{C}$ ): invariant quadruple point involving:  
 $\text{CaAc}$ ,  $2 \text{H}_2\text{O}$  (solid);  $\text{CaAc}$ ,  $x \text{H}_2\text{O}$  (solid);  $\text{CaAc}$  (solution);  $\text{H}_2\text{O}$  (vapour)
- second peak (broad,  $80-110^\circ\text{C}$ ):  
 $\text{CaAc}$ ,  $x \text{H}_2\text{O}$  (solid)  $\rightarrow$   $\text{CaAc}$  (anhydrous solid);  $\text{CaAc}$  (solution);  $\text{H}_2\text{O}$  (vapour)
- third peak (broad shoulder,  $116^\circ$ ):  
 $\text{CaAc}$  (solution)  $\rightarrow$   $\text{CaAc}$  (anhydrous solid);  $\text{H}_2\text{O}$  (vapour).

Unfortunately, the differential scanning calorimeter available was

not equipped for the simultaneous effluent analysis that would be required to test for the presence of the  $(\text{CaAc}, x \text{H}_2\text{O})$  phase. On the other hand, a Debye-Scherrer crystallographic analysis of samples brought to various temperatures between 80 and  $120^\circ\text{C}$  under sealed conditions would prove helpful to untangle the complex factors involved. However, since even the dihydrate lattice is damaged under the X-ray beam at room temperature, and since rapid polymerization occurs in the saturated solution present from 80 to  $110^\circ\text{C}$ , the X-ray analysis should prove particularly difficult to achieve even if low temperatures are employed to stabilize the system.

#### III-3-1-c Disruption of the crystals

Dehydration has been shown by X-ray to bring about a considerable disruption of the dihydrate crystalline lattice. This disruption obviously (and experimentally) favors the penetration of inhibitor gases, but may also be suspected of directly influencing the polymerization even in vacuo.

Accordingly, it was decided to investigate by means of optical microscopy under what form and how soon this disruption appeared during the course of dehydration.

Fresh needles of calcium acrylate dihydrate of sizes up to 2 mm long and 0.2 mm wide were exposed, open to the air, on the glass slide of a hot-stage polarizing microscope. At room temperature, they appeared under 40x magnification as clear glass rods, and could be completely extinguished by rotation of the polarizers in the crossed position.

Heating at the moderately slow rate of  $0.7^\circ\text{C}/\text{min}$  soon produced the first symptoms of crystal dislocation. As low as  $40^\circ\text{C}$ , a series of cracks

or crazes began to appear, running transversely to the long axis of the needle (which is the  $\vec{b}$  crystallographic axis) and sometimes running over the whole width of a needle. Smaller crazes branched sideways along  $\vec{b}$ , sometimes bridging two of the main ones.

These observations are perfectly consistent with the X-ray model, which predicted that the removal of the water would collapse the ribbons (creating crazes normal to  $\vec{b}$ ) and sever the ties between ribbons (creating crazes along  $\vec{b}$ ).

As low as 45-50°C, the pattern became more dense and took on the appearance of birch bark. Already then, crossing the polarizers no longer produced a complete extinction of the needles. The same observations could also be made on a set of fresh crystals having been submitted to less than 30 min evacuation at room temperature.

At 53°C, the crazing had become so fine and dense that the pattern disappeared to the profit of a uniform gray appearance.

A number of conclusions may be derived from these optical observations:

- (1) the dihydrate crystals are very fragile and sensitive to even a very short exposure to vacuum or mild heat, as much as 40°C below the dehydration temperature measured under equilibrium conditions.
- (2) the dehydration does not seem to be uniform, but is more consistent with a multi-phase model such as suggested by Costaschuk (84).
- (3) the nucleation appears to be abundant, which comes to support the interpretation given in section III-1-1 of the non-linearity observed by Watine in the optical density of Debye-Scherrer patterns at low levels of hydration.

III-3-1-d Molecular motions as a function of dehydration

The crystallographic study of the dihydrate has established that polymerization is not possible in the perfect lattice. The fact that polymerization is nevertheless observed in the solid dihydrate draws attention towards the molecular motions that are obviously necessary to bring the reactive species in contact. Molecular diffusion and reorientation thus assume a capital importance for the mechanistic elucidation of SSP.

The existence of a 2-3 fold maximum of polymer yield at the 0.5 hydration level<sup>(84,85)</sup> prompted the investigation of the molecular mobility of the monomer as a function of the hydration level. It was hoped that a motional transition could possibly account for this unexplained maximum.

The technique employed to investigate molecular motions in the solid state involves the measurement of the second moment of the proton NMR absorption line. The second moment is the mean square width  $(\Delta H)^2$  of the normalized line shape  $f(H)$  as the field  $H$  is varied from the center of the resonance line, at a fixed frequency:

$$(\Delta H)^2 = \int_0^{\infty} (H - H_{\text{aver.}})^2 f(H) dH \quad (\text{Ref. 101}).$$

In a solid, each nucleus experiences a local field  $\Delta H$  which is the root mean square value of the local magnetic fields produced by all the other nuclear dipoles. Even in a single crystal, these magnetic dipolar interactions result in a considerable broadening of the resonance line, with little or no resolved structure.

The second moment of the Wide-Line NMR spectra is an indicator of

( ) the amount of motion present, because the dipolar interaction tensor averages to zero for a rapid and random molecular tumbling, producing a narrow line. Non-random or slower motion, however, leads to a partial averaging only, and to a linewidth and a second moment intermediate between the rigid solid and the liquid.

Identical experiments were conducted on  $H_2O$  and  $D_2O$ -hydrates ranging from 2 to 6 waters per calcium. The reason for using  $D_2O$  is that the magnetic moment of the deuteron is very small and that the dipolar interactions involving the heavy water may actually be neglected, which results in a smaller second moment and linewidth. Consequently, the spectra of the  $D_2O$ -hydrates are very nearly representative of only the acrylate molecules, whereas the spectra of the  $H_2O$ -hydrates are representative of both acrylate and water molecules. By comparing the two sets, one is thus able to derive an indication of the compartment of the water itself.

Typical spectra of the monomer at room temperature are presented on Fig. III-3-5 and those at  $-196^\circ C$  are on Fig. III-3-6. The anhydrate line shape was closest to a Gaussian, but all other samples presented clear non-Gaussian features. The expected narrowing effect of the deuteration and of the dehydration on the linewidth was obvious. The low temperature spectra reflected the increased rigidity of the solids by the expected broadening of the lines.

Visual inspection of the spectra cannot yield much more information, but the quantitative measurement of the second moments as a function of the hydration level was performed at the two temperatures for both  $H_2O$  and  $D_2O$  (Fig. III-3-7), and is discussed below.

At both  $77^\circ K$  and  $295^\circ K$ , the  $H_2O$ -hydrates exhibited a second moment

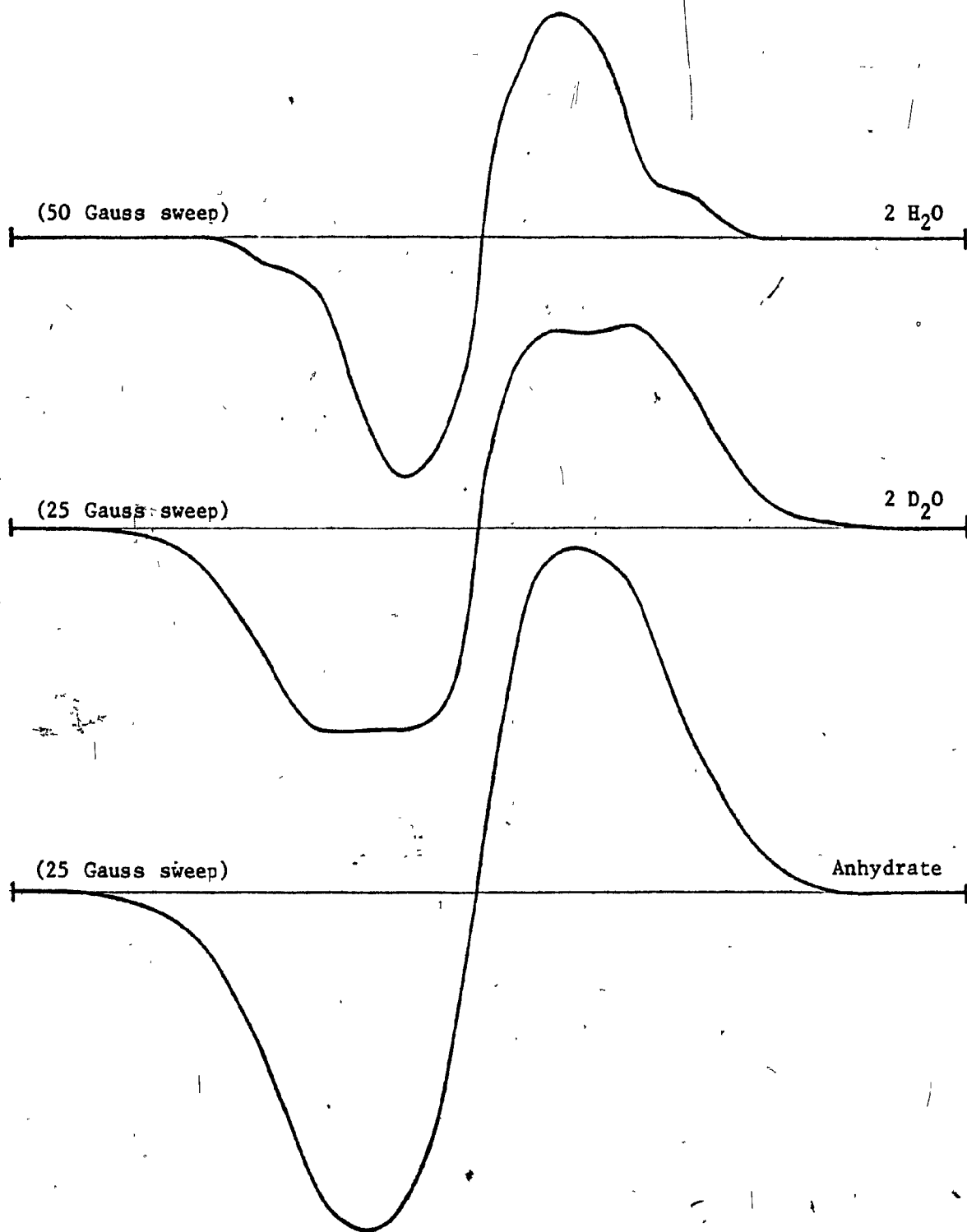


Fig. III-3-5 : Wide-Line N.M.R. spectra of calcium acrylate monomers ,  
recorded at room temperature .

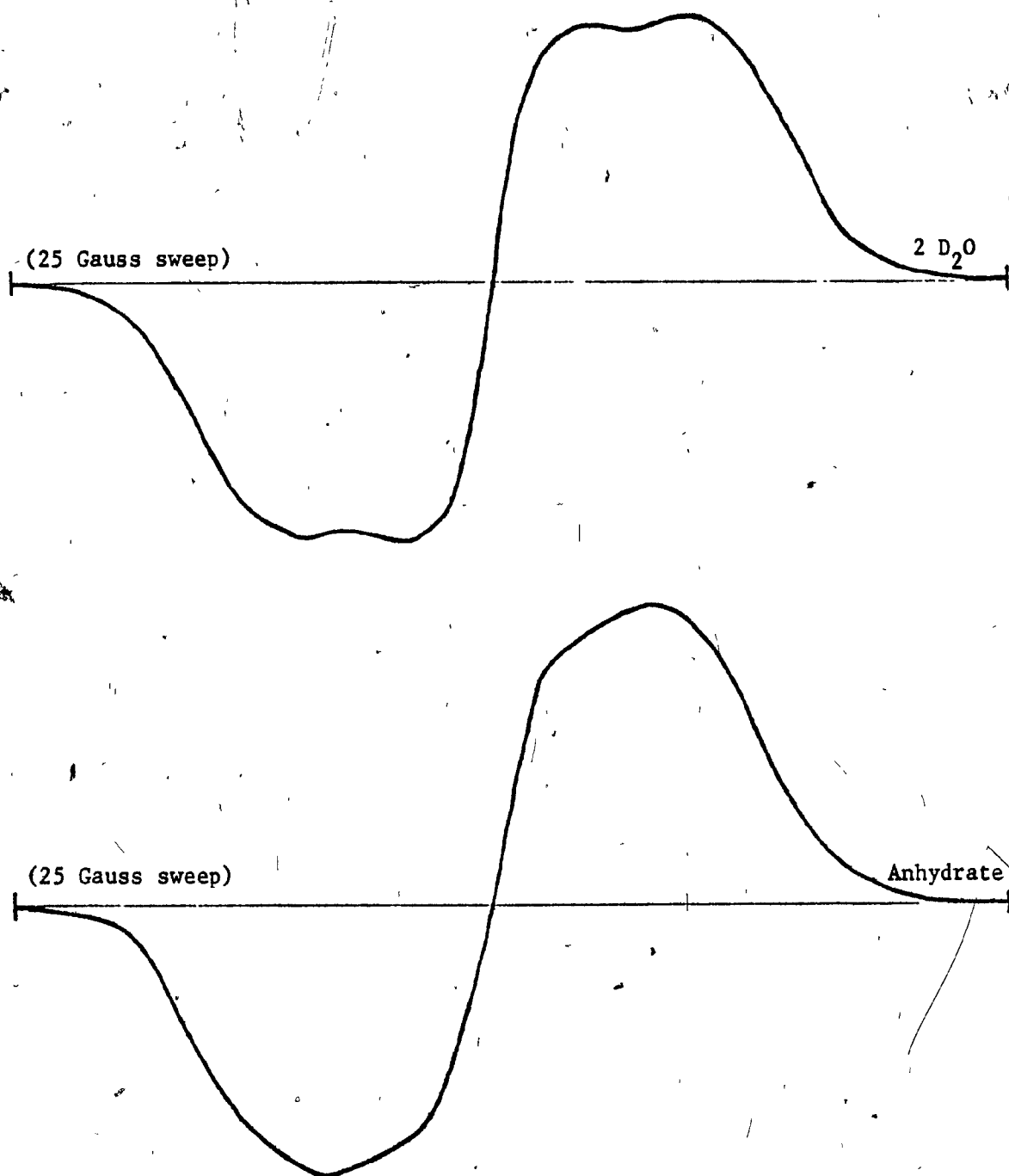


Fig. III-3-6 : Wide-Line N.M.R. spectra of calcium acrylate monomers ,  
recorded at liquid nitrogen temperature .

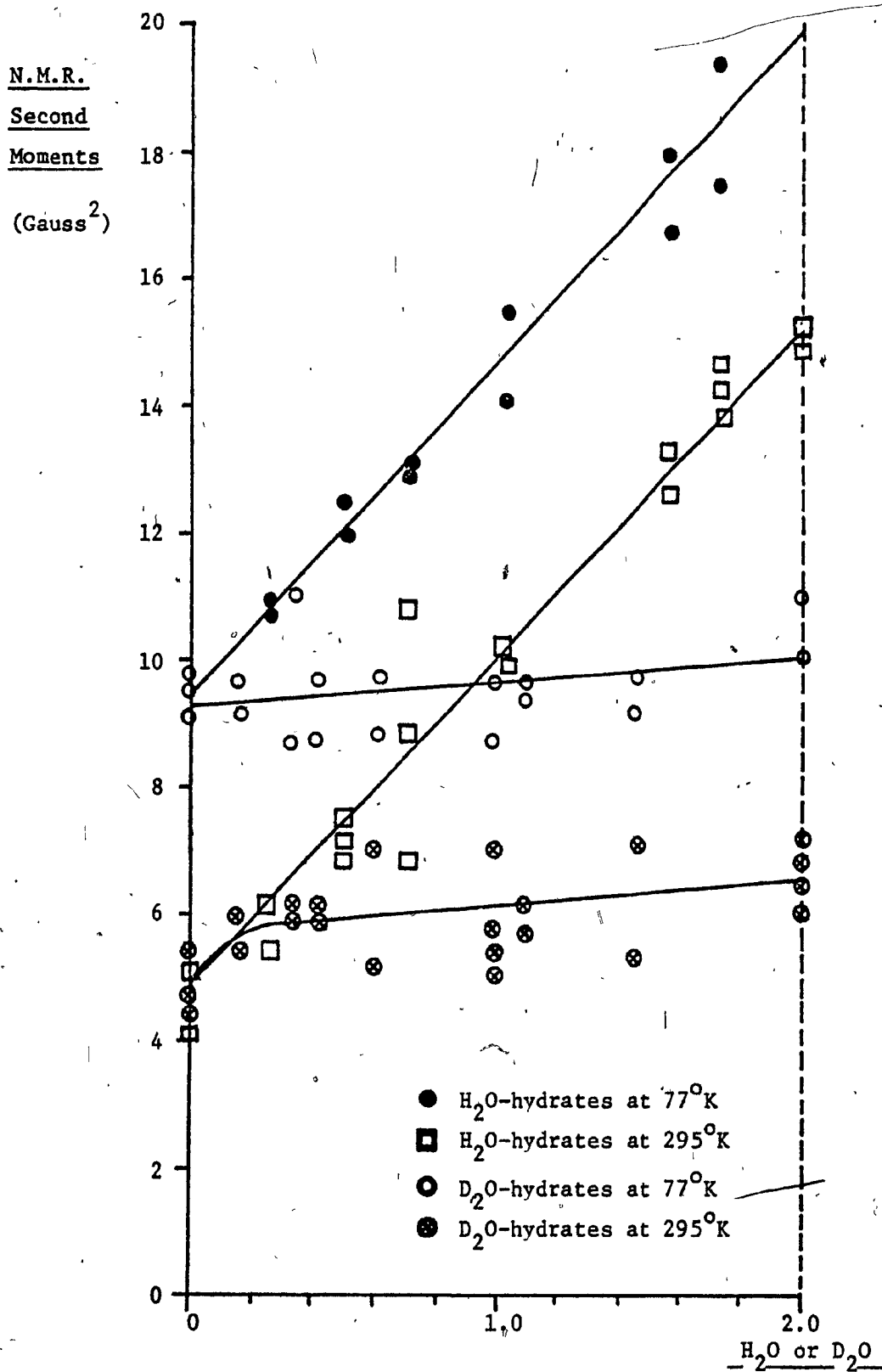


Fig. III-3-7 : Second moments of the Wide-Line curves as a function of the degree of hydration , for 77 and 295°K .

increasing linearly with the hydration level, with equal slopes of  $5.2 \text{ G}^2/\text{H}_2\text{O}$ . The lines shown have been determined by the least squares method. No significant deviation from linearity was observed at either temperature for any particular hydration level. The  $\text{D}_2\text{O}$ -hydrates similarly exhibited two parallel lines at 77 and  $295^\circ\text{K}$ . Their much smaller slope ( $0.4 \text{ G}^2/\text{H}_2\text{O}$ ) reflects the absence of the water contribution to the second moment, thereby giving an account of the acrylate part only.

The most conspicuous feature of these curves is their absence of noteworthy features, with one exception which will be discussed later. The effect of drastically disrupting the crystal lattice by dehydration seems to increase the mobility of the acrylate molecules very little, as shown by the small slopes of the  $\text{D}_2\text{O}$ -hydrates curves. No particular feature was observed that could explain the mysterious 2-3 fold increase in polymer yield around the  $0.5 \text{ H}_2\text{O}$  hydration on the grounds of average molecular mobility in the bulk of the solid monomers, as seen by Wide-Line NMR. The same conclusion may be drawn regarding the average mobility of the water alone, by comparing that of the  $\text{D}_2\text{O}$ -dihydrate with that of the  $\text{H}_2\text{O}$ -dihydrate.

However, Wide-Line NMR is mainly concerned with bulk properties only, and is normally insensitive to the defects and surfaces, which are in low concentration. Hence the results of this experiment could well bring weight to the hypothesis that SSP occurs preferentially at lattice defects either found in the initial dihydrate crystal, or produced as a result of dehydration or polymerization itself. Indeed, crystallography has shown that SSP cannot occur in the perfect dihydrate lattice.

The only exception to the absence of noteworthy features of the curves

on Fig. III-3-7 is the second moment of the anhydrate at room temperature. The average of 16 determinations gave a value of  $4.87 \pm 0.26$  Gauss<sup>2</sup>, which was corroborated by the  $4.82$  Gauss<sup>2</sup> calculated for the intercept of the extrapolated least-squares line of the H<sub>2</sub>O hydrates. On the other hand, the extrapolation of the least-squares line of the D<sub>2</sub>O hydrates, (excluding the anhydrate itself) gave an intercept of  $5.80$  Gauss<sup>2</sup>. It is therefore apparent that although the second moment of the acrylate molecules varies linearly with the hydration level from  $2$  H<sub>2</sub>O down to  $0.2$  H<sub>2</sub>O, the anhydrate itself falls below linearity by more than 3 times the error interval calculated at a 90% confidence level.

The sudden fall of the anhydrate second moment below the line of proportionality seems to be connected with the final collapse of the lattice, as shown by the disappearance of the last traces of crystallinity measured by Watine<sup>(85)</sup> below the  $0.28$  H<sub>2</sub>O level. It is striking to remark that the interpretation presented earlier of Watine's Debye-Scherrer data led to the conclusion that the nucleation of the dehydration was very abundant. The removal of the last  $0.2$  H<sub>2</sub>O will therefore multiply the interfacial boundaries until the concentration of defects (where molecular motions are necessarily easier than in the lattice) becomes no longer negligible as compared to the concentration of the bulk monomer, and may be sensed by NMR.

In conclusion, we may state that the study of the NMR second moments as a function of hydration has concluded to the absence of any phase transition or peculiar change in the bulk monomers and water molecular motions that could be associated with the maximum in polymer yield around  $0.5$  H<sub>2</sub>O.

However, the low sensitivity of Wide-Line NMR to solid defects and the sudden drop of the anhydrate second moment below linear proportionality are consistent with the maximization of motion-prone interfacial defects at low hydrations, that had been concluded from the Debye-Scherrer study.

### III-3-2 Phase changes and molecular motion at low temperatures

Costaschuk<sup>(84)</sup> reported that the calcium acrylate hydrates underwent 2-3% polymerization in source during irradiation at  $-78^{\circ}\text{C}$ , and very little more if any for 10 more days at the same temperature. On the other hand, raising the temperature up to  $25$  or  $50^{\circ}\text{C}$  triggered a post-polymerization to the extent of 20-70%.

Consequently, it was decided to investigate whether a phase or motional transition was present between these temperatures that could account for the observed behaviour. The investigation involved two independent techniques: differential scanning calorimetry and Wide-Line NMR.

#### III-3-2-a Low temperature thermal analysis

Dihydrate and anhydrate samples were analysed by D.S.C. from  $-140^{\circ}\text{C}$  ( $133^{\circ}\text{K}$ ) to room temperature. Heating was applied at rates ranging from 1.25 to  $20^{\circ}\text{K}/\text{min}$ .

None of the samples exhibited any significant feature in the D.S.C. thermograms. In particular, the absence of any peak demonstrates that there are no first-order phase transitions in the raw monomers.

#### III-3-2-b Molecular motion at low temperature

The Wide-Line NMR technique was used to study molecular motions in two samples: the anhydrate and the  $\text{D}_2\text{O}$ -dihydrate. The deuteration was used as a means to enable the comparison of the motion of the acrylate molecules only, because  $\text{D}_2\text{O}$  is virtually transparent to NMR as

explained earlier. The variations of the second moments with temperature are shown on Fig. III-3-8 over the range 77 to 410°K for the anhydrate, and 77 to 295°K only for the dihydrate, because dehydration limits the upper end of the range by giving rise to an additional narrow line.

The D<sub>2</sub>O-dihydrate exhibited a broad step over the 200-300°K range. The broadness and progressiveness of this step establishes that it is not a first-order phase transition of the allotropic type. This constitutes a justification for the 183°K used for the single-crystal crystallography study, as the structure thus determined is going to be the same as at the temperature where post-polymerization was studied. On the other hand, this step represents a motional transition of the acrylate molecules. On the basis of the crystal structure, it is believed that the motion involved is one of oscillation around the axis passing through both oxygens of the carboxylates and is adequate to bring two vinyl tails close enough for dimerization (indeed, dimerization was observed by ESR in the same temperature range).

The anhydrate had a consistently lower second moment, decreasing smoothly with no particular feature over the whole range of temperature tested. The greater amount of molecular mobility is consistent with the greater variety of motions possible in an amorphous material.

The theoretical second moment for a rigid lattice may be computed from the crystallographic data with the use of Van Vleck's formula<sup>(101)</sup>. Unfortunately, the final crystallographic data for calcium acrylate dihydrate have been available too late to be used in such a calculation. Costaschuk<sup>(84)</sup> made such a calculation on the basis of Lando's crystallographic data, but these have been shown erroneous. As a result, the esti-

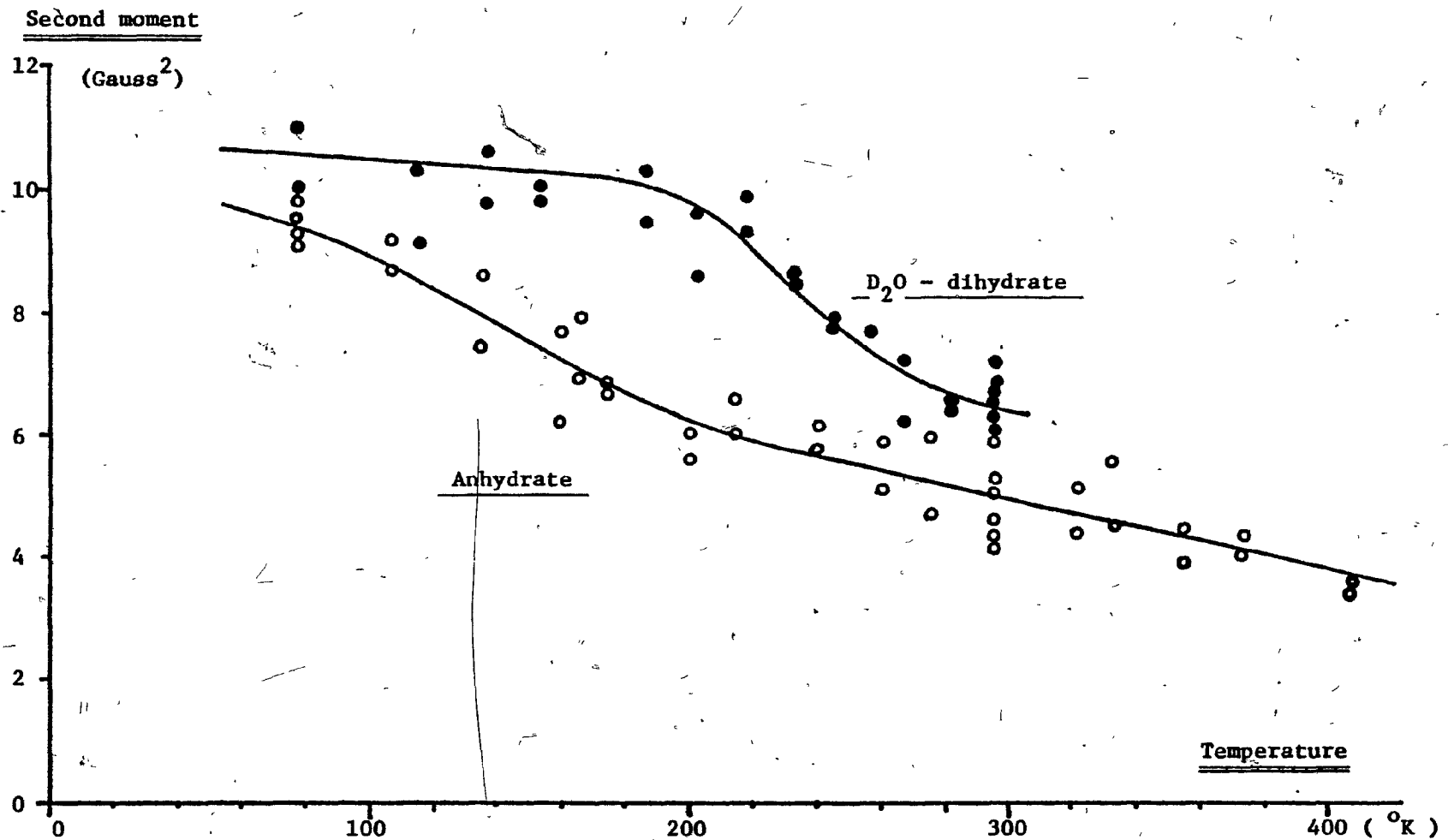


Fig. III-3-8 : Wide-Line NMR second moment of calcium acrylate samples as a function of temperature .

mation of the rigid lattice second moment was attempted the following way.

The magnetic nuclear dipole interactions may be split into their intra - and intermolecular contributions. The calculated intramolecular contribution to the second moment was from 6.4 to 7.1 Gauss<sup>2</sup> depending upon the set of bonds lengths and angles chosen for the acrylate molecule. Estimating the intermolecular contribution presented a problem, as no crystallographic data could be found for similar hydrated systems. However, based on acrylic acid<sup>(108)</sup>, acrylamide<sup>(40-a)</sup> and acrylonitrile<sup>(107)</sup>, 2.8 Gauss<sup>2</sup> seemed a reasonable estimate for acrylic systems.

The resulting 9.2 - 9.9 Gauss<sup>2</sup> estimate for the rigid lattice second moment is believed to be a valid comparison basis for the 10.5 Gauss<sup>2</sup> observed for the di-deutero-hydrate (because of the transparency of deuterium to NMR) and an approximate one for the 9.4 Gauss<sup>2</sup> of the anhydrate at 77°K. According to this estimate, the dihydrate appears to be rigid at 77°K, whereas the anhydrate is not quite so rigid. Indeed, keeping irradiated samples in liquid nitrogen for a week showed that both di- and anhydrate ESR signals underwent very little changes, but that these changes were more apparent in the anhydrate spectrum.

We may now conclude from the study of the NMR second moments as a function of temperature that:

(1) No first-order phase transition was observed in the dihydrate and the anhydrate between the irradiation temperature (77°K) and the post-polymerization temperature (295-320°K).

(2) A broad motional transition sets in the dihydrate around 200°K, involving the oscillation of the acrylate molecules.

(3) The agitation in the anhydrate is always stronger than in the dihydrate, and increases regularly with temperature.

(4) The dihydrate is believed to be rigid at  $77^{\circ}\text{K}$ , whereas the anhydrate is believed to be almost, but not completely rigid.

### III-3-3 Phase changes and molecular motion as a result of irradiation

The irradiation with ionizing radiations such as gamma-rays is able to produce considerable damage to an organic solid, either directly or as a result of the chemical reactions that ensue. Very low doses have been shown to be able to suppress one of the two dehydration endotherms of barium methacrylate<sup>(83-b)</sup>.

As a result, it was decided to investigate the possibility that gamma-rays would produce phase transitions in the irradiated monomers. The techniques employed were the same as in the previous section.

#### III-3-3-a Thermal analysis of irradiated monomers at low temperatures

Dihydrate and anhydrate samples were irradiated in liquid nitrogen with a stronger dose than usual (4 Mrad) in order to make any effect more easily observable. They were analysed in the same conditions as the unirradiated samples (133 to  $295^{\circ}\text{K}$ , heating rates 1.25 to  $20^{\circ}\text{K}/\text{min}$ ).

Again, no significant feature was observed in the smooth thermograms, indicating that irradiation had no effect on the previously established phase behaviour at these temperatures. Furthermore, the thermal effects associated with the formation of dimers above  $173^{\circ}\text{K}$  ( $-100^{\circ}\text{C}$ ) seem to have been too weak or too gradual to be sensed by this technique.

#### III-3-3-b Molecular motion in the irradiated monomers

Samples of dihydrate, di-deuterohydrate and anhydrate were

irradiated (0.86 Mrad at 77°K) and studied by Wide-Line NMR.

The spectra obtained during progressive warm-up to room temperature were identical with those of the un-irradiated samples studied in section III-3-2-b. This fully confirms that irradiation did not affect the phase and motional transition behaviour established previously over 77-295°K. Even at 323°K (50°C) the spectra of the irradiated dihydrates were initially the same as those of the un-irradiated samples.

However, after only 12 hrs post-polymerization, the central part of the dihydrate spectra began to appear distorted.

These changes in the molecular motion observed are therefore clearly associated with the polymerization mechanism rather than with the irradiation itself, and will be discussed in Chapter IV-2.

#### III-4 Chemical effects of irradiation on the monomer

##### III-4-1 The radicals formed upon irradiation

Irradiation with gamma-rays is known to produce both ions and radicals in organic solids. In order to get a better insight into the behaviour of the initiating radicals and their effect on solid-state polymerization, the ESR technique was used in a set of specially designed experiments.

The first experiment was designed to ascertain the effect of the radio-frequency power used on the saturation of the signal. Different samples present different susceptibilities to saturation, and therefore, the knowledge of their saturation behaviour is required to allow an accurate quantitative comparison between their spectra.

The second experiment studied the kinetics of radical decay upon

annealing at 195 and 295°K in order to correlate them with the solids structures and the amount of molecular motion present in them at these temperatures.

The third experiment was designed to measure the relative radical concentrations in the monomer as a function of the hydration level, immediately after irradiation and at low temperature. As a maximum in the polymer conversion was reported at the 0.5 H<sub>2</sub>O hydration level, it was thought to be of the greatest importance to verify whether a corresponding maximum was also present in the radical concentration at the same level.

Finally, the fourth experiment investigated the location of the radicals in the powder grains by attempting a selective surface scavenging with an inhibitor solution.

The samples were prepared from dihydrate and were irradiated in liquid nitrogen up to 0.86 Mrad.

#### III-4-1-a Saturation considerations

Electron Spin Resonance (ESR) spectroscopy is based on the excitation of spin transitions by a microwave radio-frequency field in the presence of a strong permanent magnetic field. If the power of the R.F. field applied is too strong, a saturation of the upper quantum level will result and will prevent the observation of the transition at resonance, producing a weaker and distorted spectral shape. Relaxation of the absorbed energy to the surroundings is required before the transition may be excited and observed again<sup>(102,103)</sup>.

Spectra were recorded at 77°K (-196°C) over the whole range of power available on the ESR spectrometer. The effects of R.F. saturation on the

spectrum of calcium acrylate dihydrate are shown on Fig. III-4-1, from 0.1 to 5 mW. It can be seen that excessive R.F. power distorts the line shape and may even obliterate some of the finely resolved lines. The distortion is not uniform, but affects some parts of the spectrum more than others. The situation is complex, and rather poorly understood<sup>(102)</sup>.

On the other hand, R.F. saturation seemed to affect acrylates samples more at some hydration levels than at others. Fig. III-4-2 presents the relative radical concentrations over the hydration range, as recorded at powers of 0.1, 0.3 and 5 mW. The ratio of the apparent radical concentration of the anhydrate to that of the dihydrate varied from 3.9 at 0.1 mW microwave power to 1.9 at 0.3 mW and to 1.5 at 5 mW, for the same samples analysed in the same conditions. Hence, it is clear that the anhydrate saturates more easily than the dihydrate down to the very low power level of 0.1 mW, i.e. - 33 dB below full klystron power. The greater saturability of the anhydrate may be explained by its looser structure, as spin-lattice relaxation is likely to be less effective in the amorphous anhydrate solid than in the dihydrate crystalline network.

Unfortunately, the limit of saturation could not be determined because the signal-to-noise ratio and the stability of the ESR spectrometer used were not good enough to take reliable quantitative measurements below 0.1 mW. As a result, it was decided to use 0.3 mW R.F. power for the recording of all subsequent spectra, in order to strike a compromise between a power low enough to minimize saturation and a power high enough to ensure a satisfactory signal-to-noise ratio. However, the higher radical concentrations present immediately after irradiation allowed some parts of this study to be carried out at the better power of 0.1 mW as well.

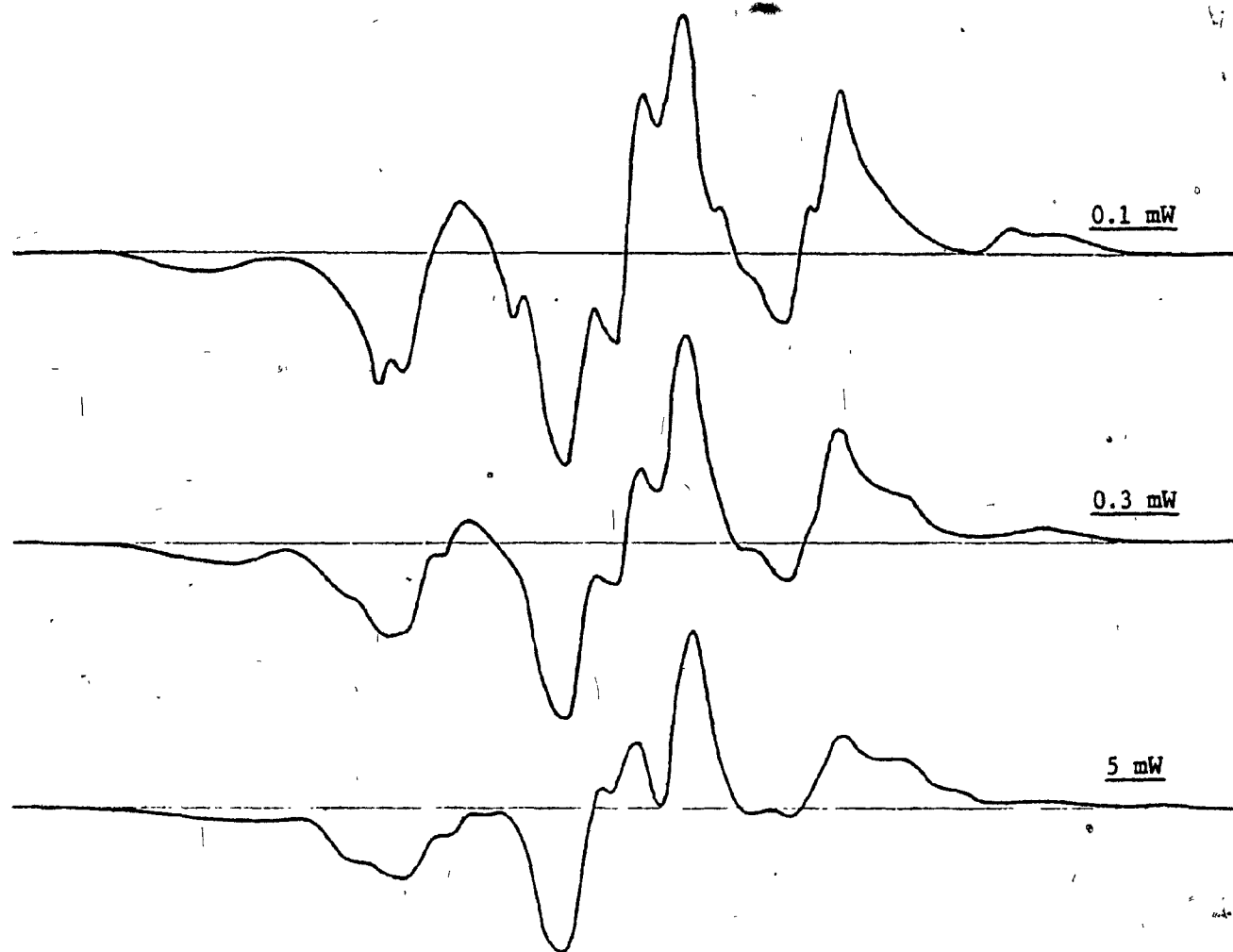


Fig. III-4-1 : Effect of Radio-Frequency saturation on the ESR spectra of calcium acrylate dihydrate at 77°K . Conditions : 0.86 Mrad .

Apparent  
radical  
concentration

(arbitrary  
units)

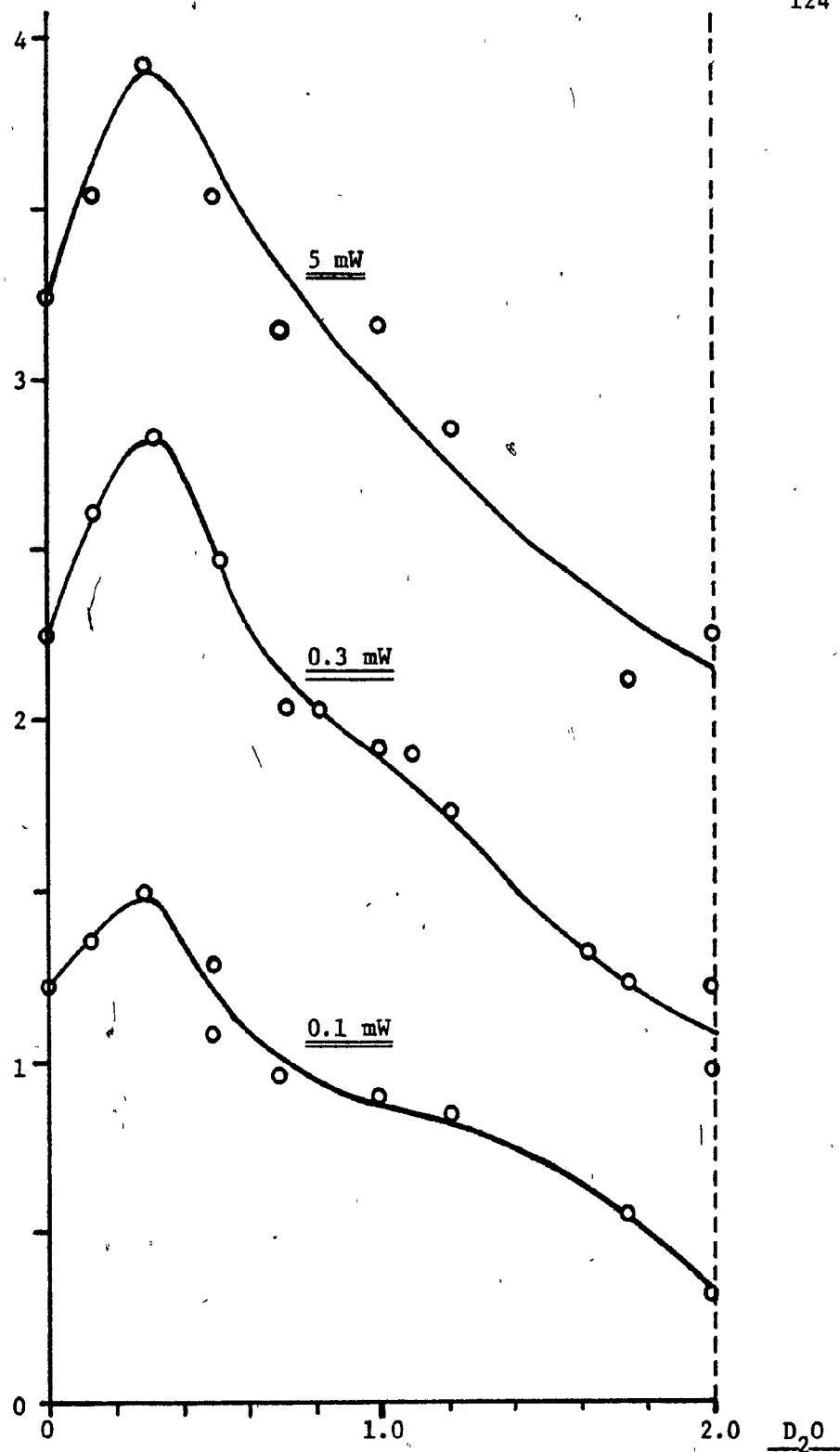


Fig. III-4-2 : Effect of R.F. power saturation on the apparent relative radical concentrations in the various fractional hydrates . ( $77^{\circ}K$ ,  $0.86$  Mrad).

Two major consequences may be drawn from the above considerations. The first one is that nothing indicates that the samples (particularly the anhydrate) were not still saturated even below 0.1 mW R.F. power. Consequently, the measurement of the absolute concentrations of radicals could be inaccurate, yielding apparent values smaller than the actual concentrations by an unknown amount. As a result, only relative radical concentrations have been shown on Fig. III-4-2, and no attempt has been made at calculating the number of radicals per chain.

The second consequence is that the present study is not comparable with the results of Costaschuk<sup>(84)</sup> on the same material. Costaschuk recorded his ESR spectra at a R.F. power of 20 dB below his full klystron power of 300 mW, i.e. at a power of 3 mW. However, the present study established that even power levels thirty times weaker (i.e. 15 dB below yet) were no guarantee against saturation. It must be rightfully admitted that Costaschuk took his measurements at 195°K, where the saturation limit could be higher than at the 77°K used here. Nevertheless, the Wide-Line NMR experiments presented earlier indicated that the dihydrate molecular mobility (and therefore relaxation) is substantially similar at these two temperatures. Hence we believe that the present data, although admittedly not totally free from saturation problems, were nevertheless markedly more so than those of Costaschuk.

This is of major consequence for the study of the radical concentration as a function of the hydration levels, as will be discussed in a subsequent section.

### III-4-1-b Annealing at 195°K and kinetics of decay

Samples were prepared with various degrees of dehydration from D<sub>2</sub>O-dihydrate. The reason for employing heavy water is not of direct relevance here, and will accordingly be discussed in the section (III-4-2) devoted to the chemical involvement of water.

The line shapes recorded at 77°K immediately after irradiation at the same temperature are shown on Fig. III-4-3 for the most noteworthy hydration levels of 2 D<sub>2</sub>O, 0.3 D<sub>2</sub>O and the anhydrate.

Subsequently, the samples were stored in solid carbon dioxide, and new spectra were recorded weekly for one month, at the same temperature of 77°K. The samples were then warmed to room temperature for 5 min and spectra recorded again at 77°K. The line shapes after the first week are shown on Fig. III-4-4. By comparing with the preceding figure, it can be seen that the changes produced by annealing at 195°K are quite large. The complex multiline spectra of the monomers have nearly subsided to the profit of the simple triplet of the dimer (or n-mer), but more so for the anhydrate than for the dihydrate.

Integration of the spectra gave, within the limits of the saturation considerations discussed earlier, a quantitative measurement of the relative total radical concentration. The low R.F. power of 0.1 mW could be used here to minimise saturation effects. The results are plotted on Fig. III-4-5 at various times of annealing and for the different hydration levels.

Concurrently to the changes in line shapes noted above, the ratio of the radical concentration in the anhydrate to that in the dihydrate decreased from 4 initially down to 2.3 after one month annealing. Radicals decayed by 56% in the anhydrate, but only by 26% in the dihydrate.

It is evident that annealing at 195°K had a more pronounced effect

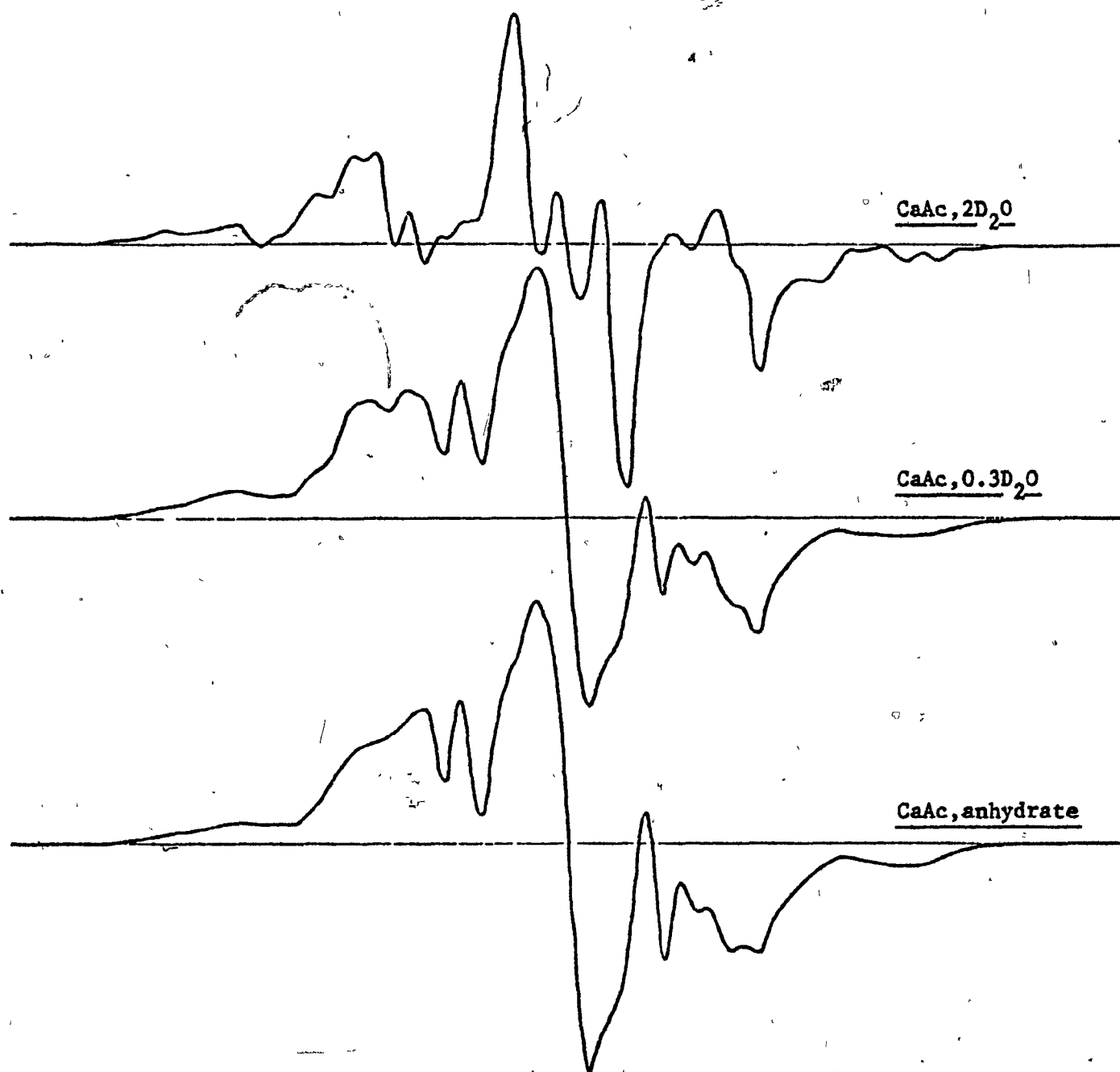


Fig. III-4-3 : Initial ESR spectra of calcium acrylate samples at 77°K .

Conditions : -- immediately after receiving 0.86 Mrad at 77°K  
-- 200 Gauss scanned in 500 s at 9.21 GHz  
-- R.F. power = 0.3 mW ; mod.ampl. = 1.6 Gauss

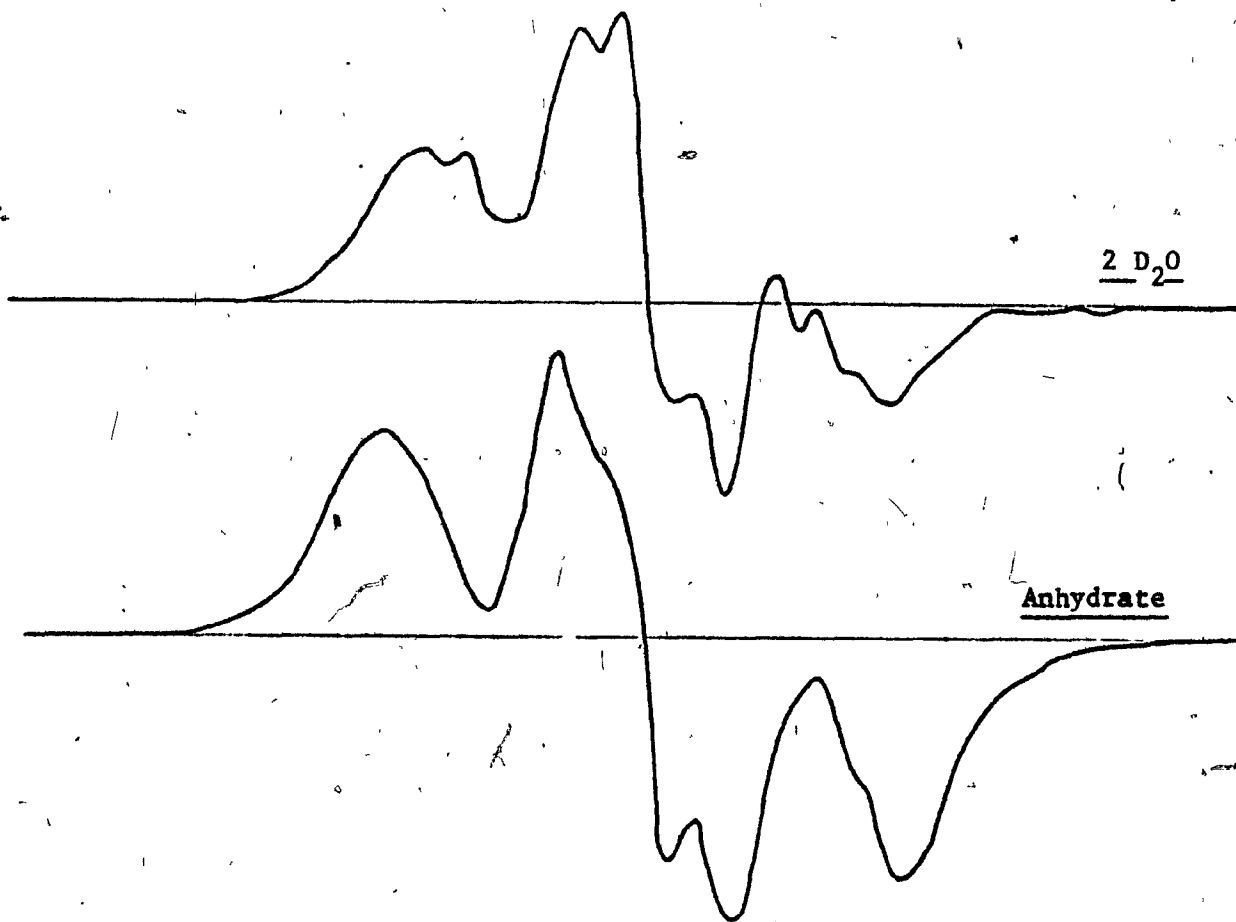


Fig. III-4-4 : ESR spectra of calcium acrylate samples annealed at  $195^{\circ}K$  for one week . Samples are the same as those of Fig. III-4-3 .  
Conditions : spectra recorded at  $77^{\circ}K$  , for accurate comparison .

Relative radical concentration

( arbitrary units )

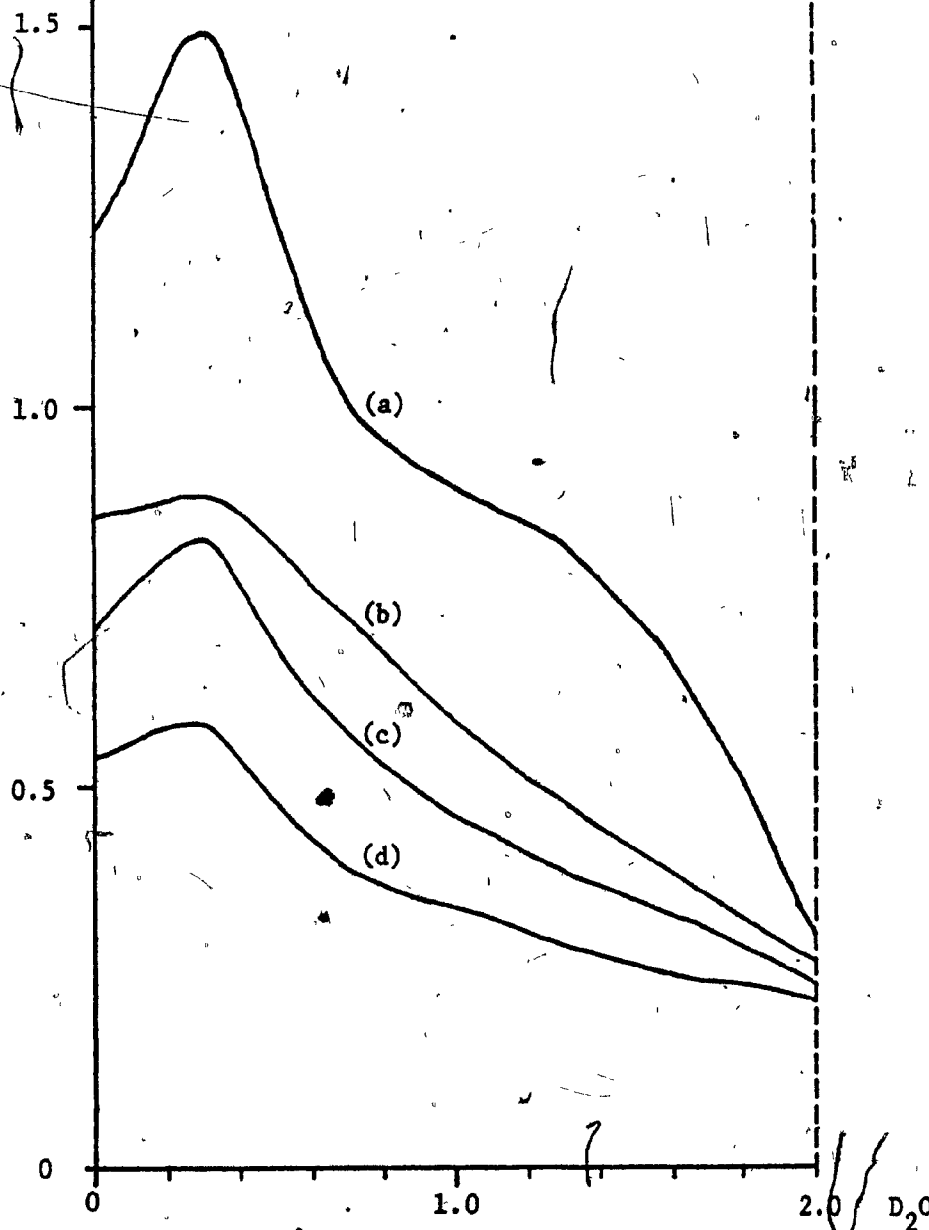


Fig. III-4-5 : Effect of annealing on the relative radical concentration as a function of the hydration level . Conditions : 77°K, 0.1mW RF power. (a) immediately after irradiation, (b) after 1 week annealing at 195°K , (c) after 4 weeks annealing @ 195°K, (d) after warming up to 295°K for 5min.

( ) on the anhydrate than on the dihydrate. These results may be interpreted in the light of the studies of the crystallinity and of the molecular mobility in these samples presented earlier. The rigidity of the dihydrate lattice at 77°K gives way to the easier formation of dimers after the onset of the motional transition around 190°K. But even at 295°K this rigidity is still high enough to prevent more than 26% of the radicals to diffuse within recombination range.

On the other hand, the higher molecular mobility in the amorphous anhydrate at all temperatures explains the faster rate of dimerization, then of decay of the radicals by facilitating self-diffusion and bimolecular recombination.

According to this explanation, the 0.3 hydrate should present even more molecular mobility than the anhydrate, since its rate of radical decay was still faster. The initial 23% excess radicals over the anhydrate dwindled to only 8% after the annealing treatment at 195 and 295°K attesting to a higher occurrence of self-diffusion. However, the Wide-Line NMR study of the monomers (section III-3-1-d) has not revealed any particular increase in molecular motion at the 0.3 hydration level. This apparent contradiction is believed to be a good indication that some of the radicals reside at solid defects, to which Wide-Line NMR is generally insensitive. This hypothesis will be discussed in the next section.

#### III-4-1-c Radical concentrations versus hydration levels

The presence of a maximum in polymer yields around the 0.5 H<sub>2</sub>O hydration level was reported by Costaschuk<sup>(84)</sup> and Watine<sup>(85)</sup>, and prompted the investigation of the corresponding concentrations in initiating radicals. It is of a profound importance to the understanding of the

mechanisms of SSP in general and of this system in particular to determine whether this maximum is the result of a higher number of initiating species or of a higher degree of polymerization.

The relative total radical concentrations as a function of the hydration level have been presented on Fig. III-4-5, initially and after annealing. The general pattern of the curves was retained after 4 weeks annealing at 195°K, and even after warming up to 295°K.

Initially irradiation produced 4 times as many radicals in the anhydrate as in the dihydrate. This fact has been ascribed<sup>(84)</sup> to the greater compactness and solidity of the dihydrate crystalline network, that favors the recombination of the primary radical species in a "local cage". On the contrary, the amorphous nature of the anhydrate allows the primary radiolytic species to migrate away from the ionizing spur, thereby increasing their likelihood to produce secondary initiating monomer radicals in turn and/or reducing the occurrence of initial bimolecular recombination. The greater looseness and the higher molecular mobility in the anhydrate are therefore responsible for the production of more radicals initially, as well as subsequently responsible for their decay faster than in the dihydrate (as discussed previously).

But the most interesting feature of the curves is the presence of a maximum in radical concentration at the 0.3 hydration level. This is similar to the hydration level where a 2.5 fold maximum in polymer yield was observed over those of the dihydrate and anhydrate. We may rationalize the fact that Costaschuk<sup>(84)</sup> did not observe such a maximum in radical concentration by considering the following three remarks:

- (1) Costaschuk used a microwave power of 3 mW, i.e. 30 times larger

than the 0.1 mW used in the present study. According to the saturation considerations presented earlier, it appears that the power he used led to strong saturation of the spectra, thus deteriorating the accuracy of his measurements.

(2) Costaschuk irradiated his samples at 195°K, where considerable molecular mobility is still present in the lower hydrates and allows many in-source reactions to take place before the ESR observations can be made. Specifically, the curves on Fig. III-4-5 show that a small amount of annealing at 195°K produces a considerable reduction in the relative height of the maximum, making it more difficult to observe.

(3) Costaschuk used fewer points to define his curve than in the present study. Furthermore, the discussion presented in the experimental section (II-3-c) has established that the technique he used to measure the hydration levels could lead to as much as 5-30% inaccuracy. The sharpness of the maximum in radical concentration observed on Fig. III-4-5 suggests that it would be easy to miss its observation because of a small error on the hydration level.

As a result it is concluded that the finding of a radical concentration maximum in the present study is not put in question by its non-observation by Costaschuk, and we will turn now towards its interpretation.

After warming up to 295°K, where polymerization is underway, the anhydrate still had 2.3 times more radicals than the dihydrate. This appears surprising at first, since the anhydrate yields approximately as much polymer at 323°K (50°C) as the dihydrate does, and since the average molecular weights of the two polymers are similar (as will be shown in Chap. IV-4). Furthermore, the 0.3 hydrate produces a maximum in polymer yield of 2.5

times that of either anhydrate or dihydrate, whereas it is characterized by only 23% more radicals than the anhydrate initially, dwindling to only 8% excess in the range of temperature where polymerization takes place.

It can be seen that no simple correlation may be deduced between the number of radicals and the polymer yields. However, we have learned from the comparison of the anhydrate and dihydrate systems that the lower number of radicals present in the latter results neither in a lower polymer yield nor in longer polymer chains. Hence, we have to deduce that the system is more complicated than previously believed.

This complexity may derive from two factors, which are not exclusive: the existence of several types of radicals and/or the existence of two types of polymerization mechanisms.

The large discrepancy between the number of radicals and the polymer yields produced by them at various hydration levels may be resolved by assuming there are three kinds of radicals: polymerizable radicals, and two other non-polymerizable kinds. The proposed model is shown schematically on Fig. III-4-6.

The study of oxygen diffusion at the initiation stage (presented already in section III-2) and that made at later polymerization stages (which will be presented in section IV-1) have established that in the dihydrate, the percentage fraction of the radicals accessible to oxygen was roughly equal to the percentage yield of polymer formed, and that they are believed to be polymer radicals. The balance to 100% are dimer radicals trapped in the perfect dihydrate lattice, where polymerization and oxygen diffusion have been found to be impossible. At the limiting conversion stage, the ratio could be measured to be 56% polymer radicals vs 44%

Relative radical concentration  
( arbitrary units )

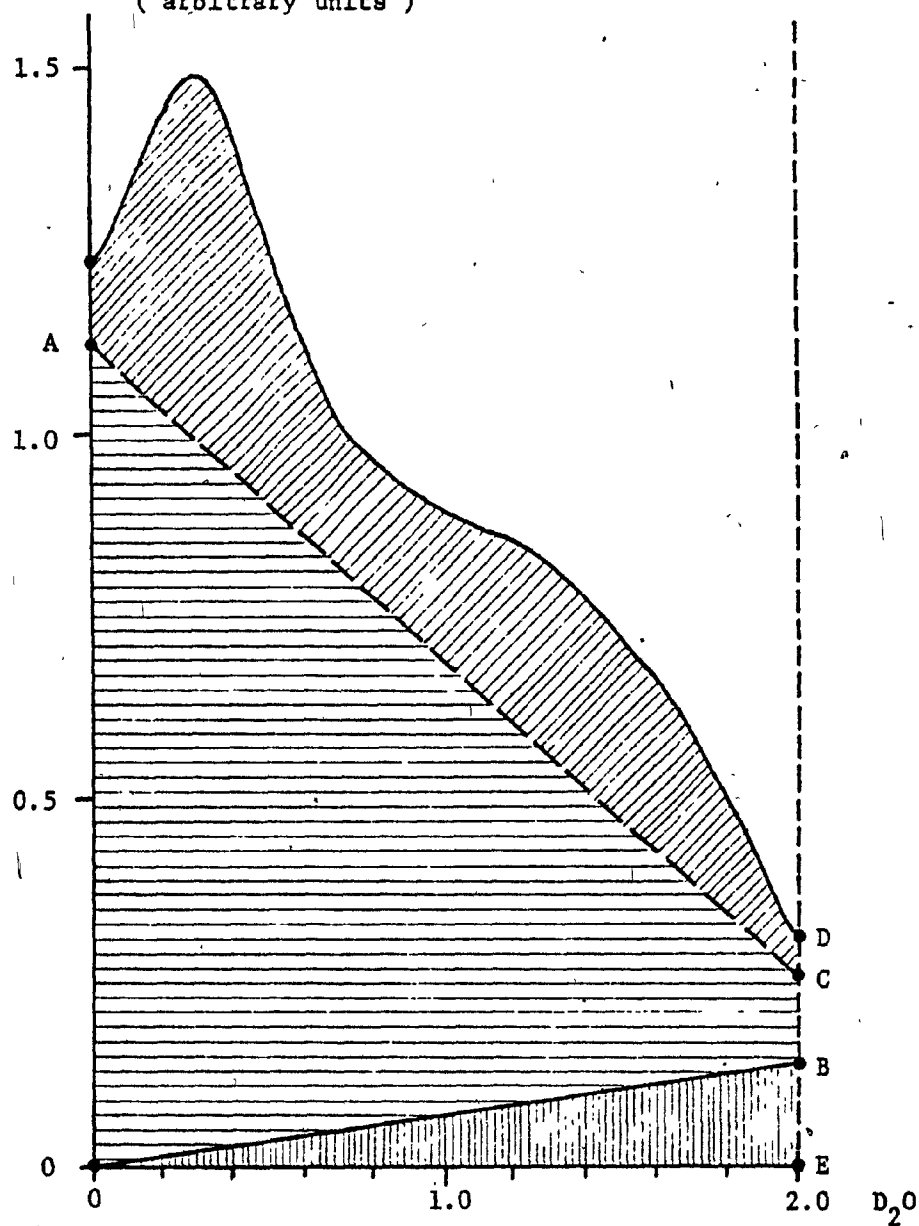
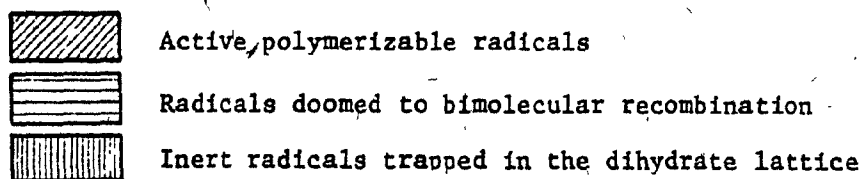


Fig. III-4-6 : S.S. Polymerization model involving 3 kinds of radicals .



trapped dimers. Consequently, the points B and C on the figure are partially defined by the relation  $BE/CD = 44/56$ .

However, it must be recognized that since the amorphous anhydrate is totally diffusible by  $O_2$  at all stages, the measurement of this ratio is made impossible in the anhydrate and in the intermediate hydrates. Nevertheless the Debye-Scherrer experiments of Costaschuk<sup>(84)</sup> and Watine<sup>(85)</sup> have been interpreted in section III-1-1 in terms of a simple two-phase dehydration model. The amount of dimer radicals trapped in the dihydrate lattice is hence concluded to be strictly proportional to the amount of dihydrate phase present and to the hydration level, and has been represented by a straight line from 0 to B on Fig. III-4-6.

On the other hand, the study of the kinetics of radical decay presented in the previous section has established that only a small fraction of the dihydrate radicals underwent bimolecular decay upon annealing and warming up to  $295^\circ K$ . This fraction is represented on the figure by the length of the segment BC, and has been measured to be in the vicinity of 26%. This completes unambiguously the definition of the points B and C. The same fraction was measured to be 56% in the anhydrate shortly after reaching  $295^\circ K$  but the higher molecular mobility in the anhydrate is very likely to foster a continuing bimolecular termination of the radicals during the post-polymerization. The point A on the figure has been accordingly placed to represent an arbitrary fraction of terminating radicals higher than 56%. The shape of the AC curve is also arbitrary at this point.

It can be seen that the model presented can easily account for the polymerization behaviour of the system. The presence of large fractions

of non-polymerizable radicals explains readily why the 0.3 hydrate is able to yield 250% more polymer than the anhydrate even though it exhibits only 23% more radicals initially, and also why the anhydrate yields as much polymer as the dihydrate with 4 times as many radicals initially.

However, the presence of the maximum in radical concentration itself remains to be discussed. According to the interpretation already given, the anhydrate produces more radicals than the dihydrate because its looser structure is less favourable to "local cage recombination" than the dihydrate lattice. Simultaneously, the higher molecular mobility in the anhydrate is believed to be responsible for its faster rate of radical decay by bimolecular recombination. Since the 0.3 hydrate presents both a higher initial radical concentration and a faster rate of recombination than the anhydrate, we must conclude that the 0.3 hydrate is characterized by an even looser structure and an even higher ease of self-diffusion than the amorphous anhydrate itself.

It is here suggested that these conclusions are the direct consequence of the presence of the phase boundary between the dihydrate and anhydrate. The Debye-Scherrer experiments of Costaschuk<sup>(84)</sup> have shown that the pattern of the crystalline dihydrate phase is clearly visible, attenuated but unchanged, all the way down to 0.28 H<sub>2</sub>O. The reinterpretation of Watine's crystallinity measurements<sup>(85)</sup> that was given in section III-1-1 has established that dehydration proceeds by an abundant nucleation of independent small centers. The area of the resulting phase boundary is therefore logically maximized immediately before the disappearance of the last traces of the crystalline phase, i.e. precisely around the 0.3 - 0.5 hydration level.

The phase boundary is certainly characterized by a high interfacial strain energy, and possibly by gaps or voids resulting from the smaller density of the anhydrate phase. These factors definitely contribute to the easier self-diffusion and to the lower "cage effect" that have been observed. They are also likely to make solid-state polymerization easier at the interphase boundary than in the amorphous (but homogeneous) anhydrate phase, possibly resulting in a faster rate of propagation if not necessarily in a higher degree of polymerization.

The fact that polymerization occurs at all in the dihydrate whereas it is known to be impossible in the perfect lattice suggests that it proceeds either at the surface of the powder grains or at crystal defects. The first possibility will be investigated in the next section, concluding to its rejection. The second one appears therefore very likely, especially because polymerization is believed to provoke a local dehydration and the formation of a new phase as it proceeds. Their nucleation would be facilitated by the presence of a defect.

The proposed model involving a phase boundary rationalizes in a satisfactory manner most aspects of the polymerization behaviour of the calcium acrylate hydrates system. The physical nature of the arguments invoked is believed to be sufficiently general to render the model applicable to all other systems presenting enough similarities with the present one. In particular, the proposed model is believed to be applicable to the system of barium methacrylate monohydrate (where Costaschuk<sup>(84)</sup> also observed a maximum in polymer yield at the same hydration level), with the due modifications required by the fact that the anhydrate in this other system is crystalline instead of amorphous as it is here. The pro-

gressive increase in the inhibitory effect of oxygen until it is total as dehydration reaches  $0.5 \text{ H}_2\text{O}$  is perfectly consistent with the model.

However, the failure of oxygen to bring about a total inhibition below  $0.5 \text{ H}_2\text{O}$  cannot be accounted for by the physics of the system and the behavior of the radicals as described by the proposed model. This suggests again that the complexity of this system may derive from yet another factor such as the existence of another polymerization mechanism (i.e. ionic) in addition to the established radical one, as was already discussed in section III-2-2.

#### III-4-1-d Location of the radicals in the irradiated monomer

In an attempt to determine where the reactive species involved in SSP reside, an experiment was designed to detect the presence or absence of free radicals on the surface of the powder at a very early stage of the polymerization, when most of the radicals are believed to be dimers. The picture thus obtained can be assumed very nearly to represent the initiation stage of the SSP.

The basic procedure consisted of wetting the polymerizing powder with a solution of a powerful radical scavenger in an inert solvent, and comparing ESR spectra taken before and after this treatment. The radical scavenger was to be a very bulky molecule to ensure that it could not diffuse into the crystal lattice, therefore confining itself to the surface. Tri-tert.-butylphenol was judged adequate. Benzene was selected as a solvent as it is sufficiently inert towards free radicals, and does not appreciably affect the Q-factor of the microwave cavity.

The samples (one dihydrate and one anhydrate) were prepared under vacuum in vessels of the type shown on Fig. II-9-1-b and -c as described

in the experimental section. They were kept in liquid nitrogen after the irradiation, then quickly warmed up to 25°C for 15 minutes. This delay was judged necessary to allow the ESR signal to stabilize, as it changes very rapidly from the complex low temperature monomer spectrum to the much simple propagation triplet. Spectra were recorded during this interval for further reference as to the rate of radical decay.

Because of the vapour pressure above the dihydrate, it was necessary at this stage to cool again the sample powder temporarily in liquid N<sub>2</sub> before breaking the seal (the anhydrate of course required no such treatment). The inhibitor solution was then pushed by the benzene vapour into the quartz portion of the tube, where it came in contact with the sample. Thus only 10 minutes after the seal was broken, the sample, wet with the inhibitor solution, could be returned to the spectrometer cavity.

Spectra were recorded for two hours thereafter.

The rate of decay of the radicals was measured from the spectra recorded before wetting the sample with the inhibitor. This rate was assumed to be linear over the relatively very short duration of the treatment. Thus, the difference in signal intensity before and after the scavenger was brought to action could be compared with the decay that would have normally occurred during the same period of time.

The results can be summarized very concisely: no effect of the scavenger could be detected in any of the experiments. Whether it be anhydrate or dihydrate, no sudden reduction or alteration of the spectra was observed after the sample powder had been fully wetted with the inhibitor solution.

The conclusion is that no observably significant fraction of the

post-polymerization radicals are located at the surface of the sample powder at the initial stage of the reaction. Hence, we have to conclude that they are trapped somewhere in the bulk of the acrylate, both in the crystalline dihydrate and in the amorphous anhydrate.

#### III-4-2 The chemical involvement of water

The study of the ESR spectra of irradiated Ba-methacrylate,  $D_2O$  by Watine<sup>(85)</sup> has disclosed the presence of lines coming from a deuterated radical in addition to the lines of the regular monomer radical. The interpretation given was that upon irradiation, the water of hydration was contributing to the generation of hydrogen (or deuterium) atoms competitively with those abstracted from the methacrylate.

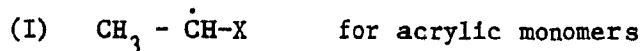
The involvement of the water in the radiochemical events leading to the formation of the initiating monomer radicals is a fundamental aspect of the SSP of hydrated systems. It was therefore decided to investigate this aspect in greater depth, to verify whether the Ca-acrylate system behaved similarly to the barium system, and to make an attempt at measuring quantitatively the extent of this involvement. The investigation undertaken relied upon the synthesis of a heavy-water dihydrate to make the origin of the hydrogens involved clearly apparent in the analyses.

Two analytical techniques were chosen for their unambiguous sensitivity to isotopic substitution: ESR and mass spectrometry.

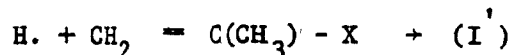
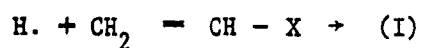
##### III-4-2-a Origins of the initiating radicals

All vinyl monomers submitted to irradiation are submitted to a variety of ionization and homolytic reactions. However, it appears that the complexity of this radiolysis is masked by the rapid completion of secondary reactions. As a result, only one type of monomer initiating

radical (type I) is generally observed by ESR regardless of the monomer:

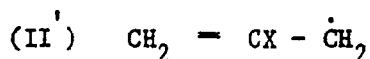
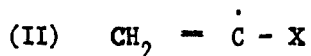


These radicals are believed to be the products of the addition of hydrogen atoms onto the monomer double bonds:

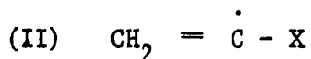


Very few authors have investigated the possible origins of these hydrogen atoms and what would be the fate of the other types of radicals from which they necessarily derive.

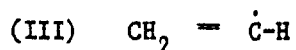
Bensasson et al.<sup>(62)</sup> have calculated the theoretical line ratios in the ESR spectra of several acrylic and methacrylic monomers. The observed ratios were found to deviate from the theoretical ones, and they attributed these deviations to the superposition of lines from a small concentration of the primary species:



Similarly, Bolshakov et al.<sup>(67)</sup> found in acrylic acid and acrylonitrile the radical:



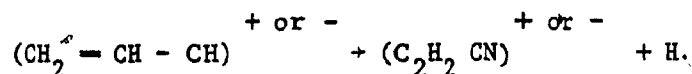
and possibly also:



The intensities of the spectra of (II) and (III) were considerably less than those of the addition radicals of type (I), and they were apparent only at low temperature in mono-crystals, under certain orientations with respect to the field.

Marx and Fenistein<sup>(102)</sup> have investigated the primary radiochemical events in acrylonitrile and alpha-chloroacrylonitrile. It was found that even at 4.2°K, the H atoms produced by the radiolysis were able to diffuse in the solid and react rapidly to form addition radicals of type (I). The absence of vinyl radicals of type (II) in acrylonitrile in the same conditions where they were observed in chloroacrylonitrile was interpreted as follows:

Ionization as well as dissociative capture of electrons of an energy greater than 3.12 eV would lead to the formation of unstable monomer ions, which would subsequently decompose to form hydrogen atoms and keep the charge:



Both charges were believed to be equally rational, in keeping with mass spectrometric analysis of the fragments produced. The in-source polymerization of acrylonitrile at temperatures below 160°K, where the polymerization radicals were not observed, pointed towards the molecular or fragment ions mentioned as the diamagnetic species responsible for the polymerization (ionic mechanism).

In the present study, ESR spectra were taken of the radicals produced immediately after the irradiation at 77°K of calcium acrylate dihydrate and di-deuterohydrate, and are shown on Fig. III-4-7. The clear differences

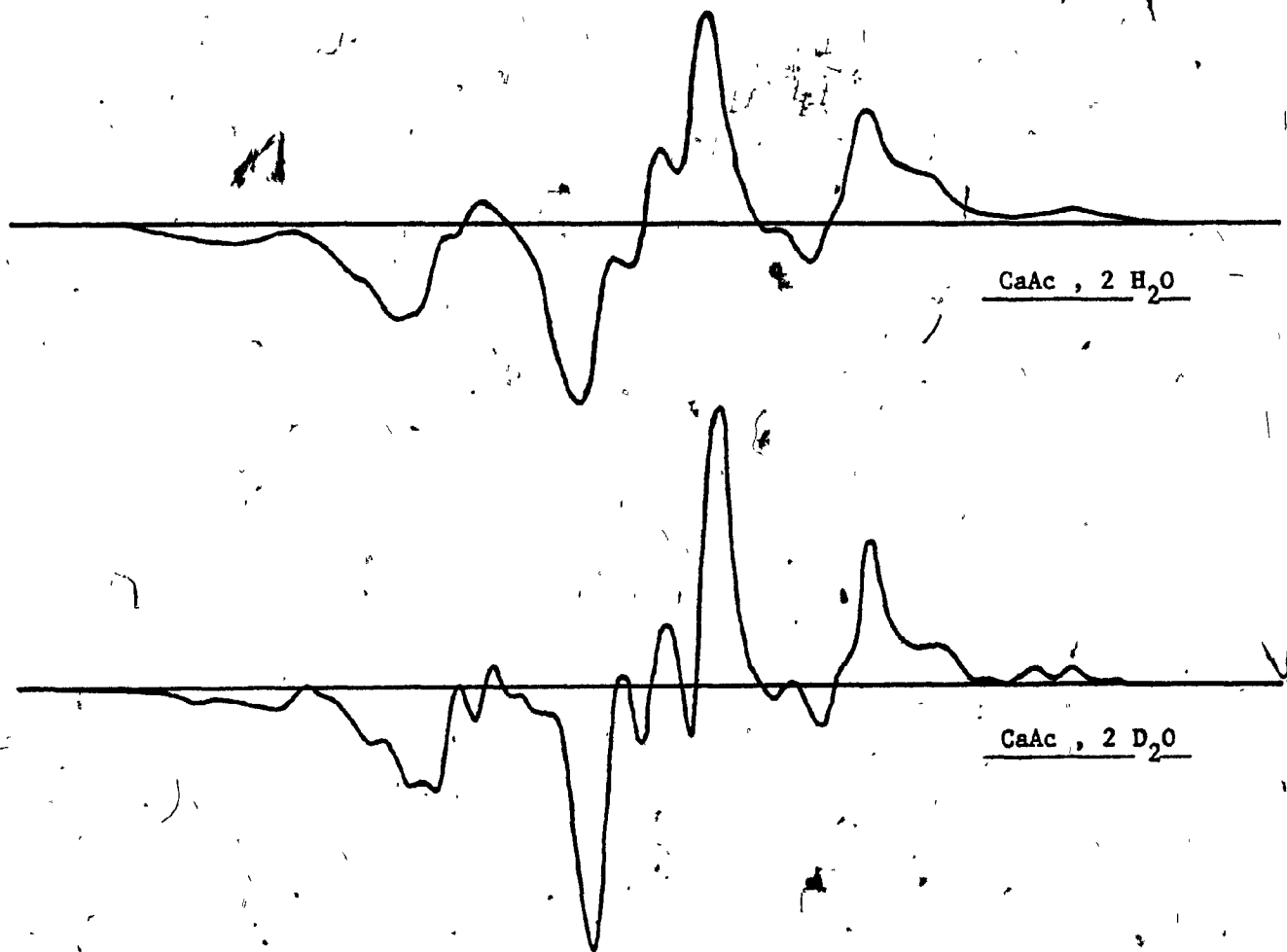
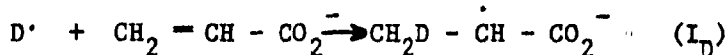
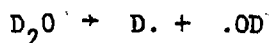


Fig. III-4-7 : Radiochemical involvement of the water of hydration :  
effect of deuteration on the initial ESR spectra at low temperature .

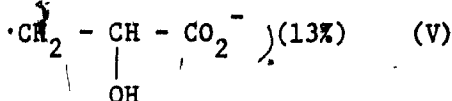
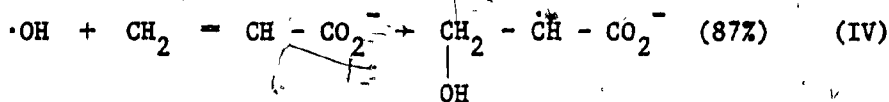
Conditions : - recorded at 77°K immediately after 0.86 Mrad given at 77°K  
- 0.3 mW R.F. power ; 1.6 Gauss modulation amplitude

observed between the two spectra confirm unambiguously that the deuterium of the water has become involved in the formation of type ( $I_D$ ) addition radicals:

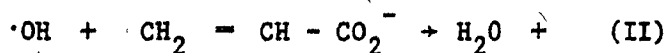


On the other hand, non-deuterated radicals of type ( $I_H$ ) may come either from the same reactions of  $H_2O$ , or from hydrogen abstracted from the acrylate monomer by an ionic homolytic mechanism such as described earlier.

What happens to the  $\cdot OH$  radicals formed by scission of the water may be discussed in the light of the studies by Fischer and Giacometti<sup>(104)</sup> and by Fischer<sup>(105)</sup> on acrylic acid with a  $H_2O_2/Fe^{3+}$  initiator:



Besides the addition onto a monomer, a number of other reactions may be envisaged to explain the fate of the hydroxyl radicals:



Originally, it was the purpose of the use of heavy-water to allow a quantitative measurement of the ratio of the two radical species ( $I_H$ )

and  $(I_D)$  as a function of the hydration level. The aim was to verify whether the extent of the radiochemical involvement of water was proportional to the amount of water present, or not. However, Fig. III-4-7 shows that no suitable peak could be found for a convenient measurement of  $(I_H) / (I_D)$  (such a peak would ideally be rather sharp, specific of one of the two species and located in a region void of peaks from the other species).

An attempt was made to circumvent this difficulty by subtracting the spectrum of Ca-Ac, 2 H<sub>2</sub>O (characteristic of  $(I_H)$ ) from the spectrum of Ca-Ac, 2 D<sub>2</sub>O (characteristic of  $(I_H) + (I_D)$ ). The spectra were digitalized with the help of a curve reader, normalized and subtracted point by point with a computer program developed specially. The difference spectrum was plotted by a Calcomp plotter linked directly to the computer, and is shown on Fig. III-4-8.

Some variations were noted in the shape of the difference spectrum, depending on the precise matching of the two parent spectra along the field abscissa. Exact matching of the field origins proved difficult, because the spacing of the lines were not exactly the same and no rigorous center of symmetry could be found. The use of an external field reference was envisaged, such as chromium, which gives a characteristic sharp singlet suitable for origins matching. It was rejected however, because the position of this singlet interferes with the wings of the acrylate spectra.

The difference spectrum shown is merely intermediate between the shapes of the two parent spectra, and the experiments based on the ESR technique were therefore judged inconclusive, quantitatively speaking. It must be noted that even if the ESR technique had proved successful at

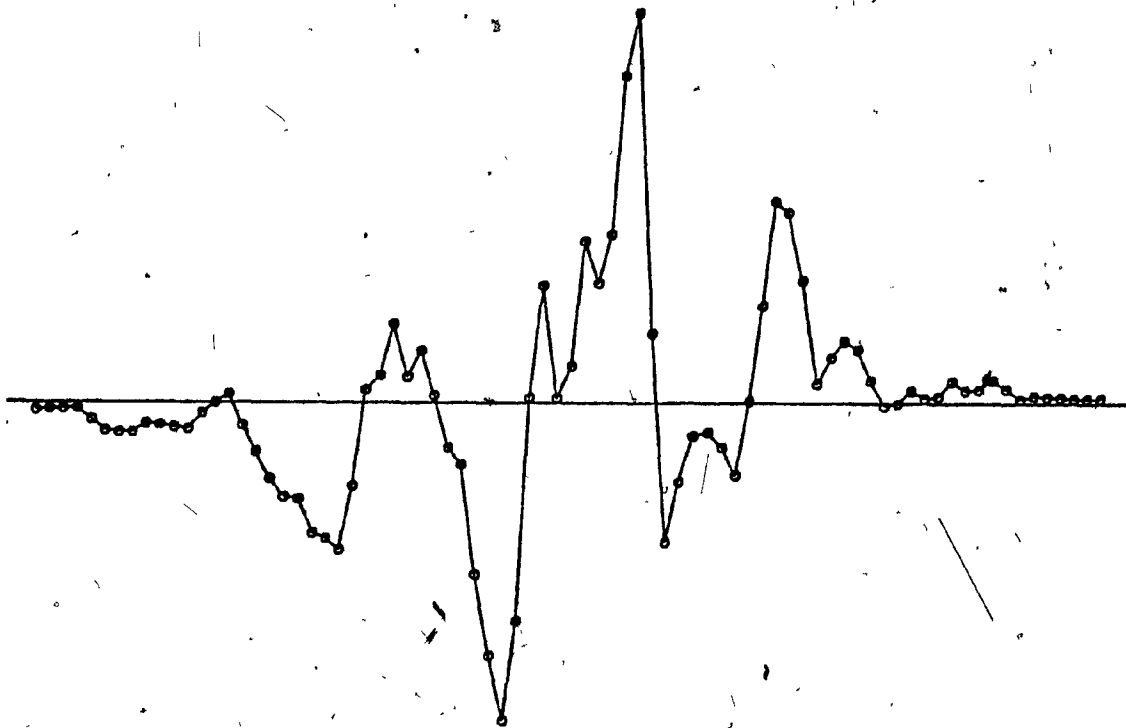


Fig. III-4-8 : Difference spectrum computed from  $\text{CaAc} \cdot 2\text{H}_2\text{O}$  and  $\text{CaAc} \cdot 2\text{D}_2\text{O}$   
Conditions : recorded at  $77^\circ\text{K}$  , immediately after 0.86 Mrad irradiation .

measuring the ratio of the spectra of  $(I_H) / (I_D)$ , the ratio of the radicals themselves would prove difficult to calculate because the radicals of type (I) present a nodal plane going through the methyl group. The frequency of rotation of the methyl will therefore determine how many of the deuterated radicals will exhibit an apparent spectrum identical to that of the regular radical, when the deuterium becomes "invisible" by ESR by falling in the nodal plane.

As a result, it was decided to attempt to obtain an estimate of the extent of the radiochemical involvement of water by another independent method.

#### III-4-2-b Analysis of the radiolysis gases

The mass spectrometric analysis of the vapours above a pre-irradiated sample of  $D_2O$ -dihydrate was undertaken in an attempt to measure quantitatively the extent of the radiochemical involvement of the water of hydration in the formation of the initiating radicals of type (I). It also provided an opportunity to study other chemical species associated with the irradiation in a more systematic way, in the hope that this would improve the understanding of the initiating stages of SSP.

The vapours were expected to consist primarily of  $D_2O$ , with some amount of  $HDO$  and  $H_2O$  as well as traces of organic species resulting from the decomposition of the monomer under the ionizing radiations. In order to interpret such an analysis, preliminary experiments were required, consisting of the analysis of  $H_2O$ ,  $D_2O$  and of a model mixture of the two. These preliminary experiments are presented in Appendix A. A data treatment method was developed to allow the calculation of the fragmentation probabilities of the three kinds of water. Difficulties were encountered, owing

to the continual presence of moisture in the residual background gases of the mass spectrometer, probably adsorbed on the walls of the vacuum chambers.

The analyses of the pre-irradiated sample was performed as described in the experimental section by first measuring the background spectra of the spectrometer, with the sealed sample held at liquid N<sub>2</sub> temperature. The seal was then broken, and further spectra were measured at the same temperature. This allowed one to practically isolate the very light gases such as the hydrogen isotopes, while keeping the heavier gases and the water isotopes frozen at 77°K. Following this, the sample was rapidly heated to room temperature, which released all the species of interest for analysis.

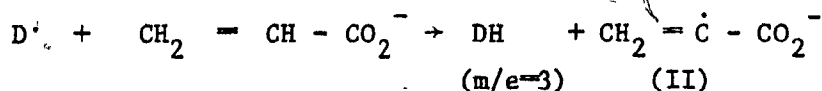
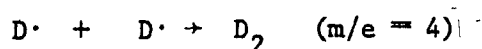
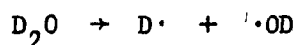
(1) Sample at 77°K

It was observed that the breaking of the seal caused no significant changes in the peak intensities of the usual background gases. This attested to the good vacuum achieved above the sample when it was prepared. The numerical data are presented in tabular form in Appendix B-1.

In view of this result, it was particularly interesting to observe that nevertheless, traces of D<sub>2</sub> and DH were distinctly present. Deuterium could be clearly resolved at m/e = 4, from the helium peak, and a peak appeared at m/e = 3, which could be unambiguously attributed to DH since there exists no other isotope at m/e = 3. Their intensities were of the order of 0.3% referred to m/e = 18, which is far above what could be expected to come from the natural abundance of deuterium in the background water.

These results establish unambiguously that deuterium atoms from the

hydration water have been formed by the irradiation, and subsequently reacted with either themselves or hydrogen atoms abstracted from the acrylate molecules:



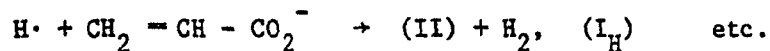
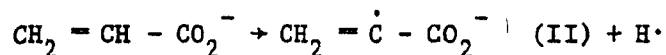
(2) Sample at room temperature

The sample was isolated by a valve from the spectrometer, and heated rapidly to 20°C until thermal equilibrium was established. The valve was then opened and spectra were recorded periodically for some time. The numerical data are presented in Appendix B-2.

The data treatment method developed in Appendix A was used to analyse the results concerning the water isotopes. The ratios  $D_2O / HDO / H_2O$  were calculated to be 6.2/34.0/59.9% initially and 7.6/42.8/49.6% half an hour later. As detailed in the appendix, these calculations involve a number of assumptions and suffer from the harmful effects of the interference produced by the adsorption of the background water on the walls of the spectrometer. Because of the limited amount of sample gases available, it was not proceeded to as many cycles of flushing and reevacuating as ideally desirable for the isotopic equilibration of the background waters of the spectrometer with those of the sample.

However, the lack of major differences between the first and the second analyses seems to indicate that the sample had a water vapour pressure high enough to partially overwhelm the background and make the ana-





This randomization was estimated to be considerable, and possibly total. It is here suggested that the use of a large sample could allow the many cycles of flushing of the spectrometer necessary to reach the isotopic equilibrium of the background and sample waters and measure its value more precisely. Furthermore, the selective deuteration of the acrylate molecule in the  $\alpha$  position and the radioactive labelling of the water oxygen could certainly determine which of the many reactions involved are the most important ones by performing ESR and mass spectrometric analyses of the monomer, as well as making an end-group analysis of the polymer formed (by scintillation counting).

Finally, further analyses of the mass spectra were performed and disclosed the presence of various small concentrations of  $\text{D}_2$ ,  $\text{DH}$ ,  $\text{CO}_2$ ,  $\text{CO}$ ,  $\text{C}_2\text{H}_4$  and  $\text{C}_2\text{H}_2$  in the vapours. These results are presented in the Appendix B-3, and give a general idea of the perturbation imposed on the system by the action of high-energy ionizing radiations.

CHAPTER IV

---

THE POLYMERIZATION MECHANISMS  
AND THE POLYMER

IV-1 Oxygen diffusion and location of the radicals at the limiting conversion stage

The study of the diffusion of oxygen (section III-2) and that of the location of the radicals (section III-4-2) has led to some important conclusions regarding the monomer at the initiation stage. However, a heterogeneous polymerization such as that of calcium acrylate dihydrate is certain to bring a considerable disruption to the lattice, which should alter the diffusion behaviour. Furthermore, the polymer radicals may travel until they reach grain boundaries, where they could remain inactivated by the lack of fresh monomer feed.

Consequently, it was decided to investigate the diffusion of oxygen and the surface inhibition by a liquid scavenger at the limiting conversion stage as well. Dihydrate and anhydrate samples were post-polymerized for one month at 50°C in vacuo. At this time, the rates of radical decay and polymerization had dropped near zero, and the analyses performed then could safely be assumed to be representative of the limiting conversion stage.

The experimental procedure was as follows: the samples were placed in vessels as described in the experimental section (Fig. II-9-1-a). Air from the hammer-magnet compartment was admitted by breaking the seal. The rate of oxygen diffusion was first monitored by following the transformation of the acrylate radical signal into that of the peroxide. The sample tube was then retrieved and cut open. The powder was agitated for 5 min with an excess of inhibitor solution in the open air, filtered out, rinsed with fresh benzene and air-dried by suction. The sample was then returned to the original ESR tube and to the spectrometer.

#### IV-1-1 In the dihydrate

Under vacuum at 25°C, the simple triplet of the propagation radicals was observed (Fig. IV-1-1-a). Traces of a shoulder were noted symmetrically on either side of the central line. These shoulders could therefore not be attributed to a small peroxide signal, as it had been for the initiation stage, because the peroxide signal is dissymmetric.

Immediately after the seal was broken, the central line of the triplet began to be distorted by the increasing peroxide signal (Fig. IV-1-1-b). It was found impractical to measure the intensity of the peroxide signal itself, as it was overlapped by the central acrylate line. However, the concentration of the acrylate radicals could be safely assumed invariant at such a long polymerization time. It was therefore easy to measure the rate of oxidation by monitoring the decay of the acrylate triplet. The peak-to-peak heights were measured from the outer lines, which are relatively insensitive to interference by the peroxide lines, and are shown on the graph of Fig. IV-1-2.

After 50 min, the samples were taken out of the spectrometer for the inhibition treatment, and then returned to the ESR cavity for further analyses. It can be seen that the treatment of the powder in the open air with the scavenger solution led to a step-decrease in the radical concentration. This could be mistaken for an indication that the radicals resided at the surface. However, three arguments may be developed to show that such an interpretation would be false.

First, the experiment done at the initiation stage (section III-2-1) showed that 70% of the surface radicals react with  $O_2$  within 15 minutes at liquid  $N_2$  temperature. Such rate would be expected to be even faster

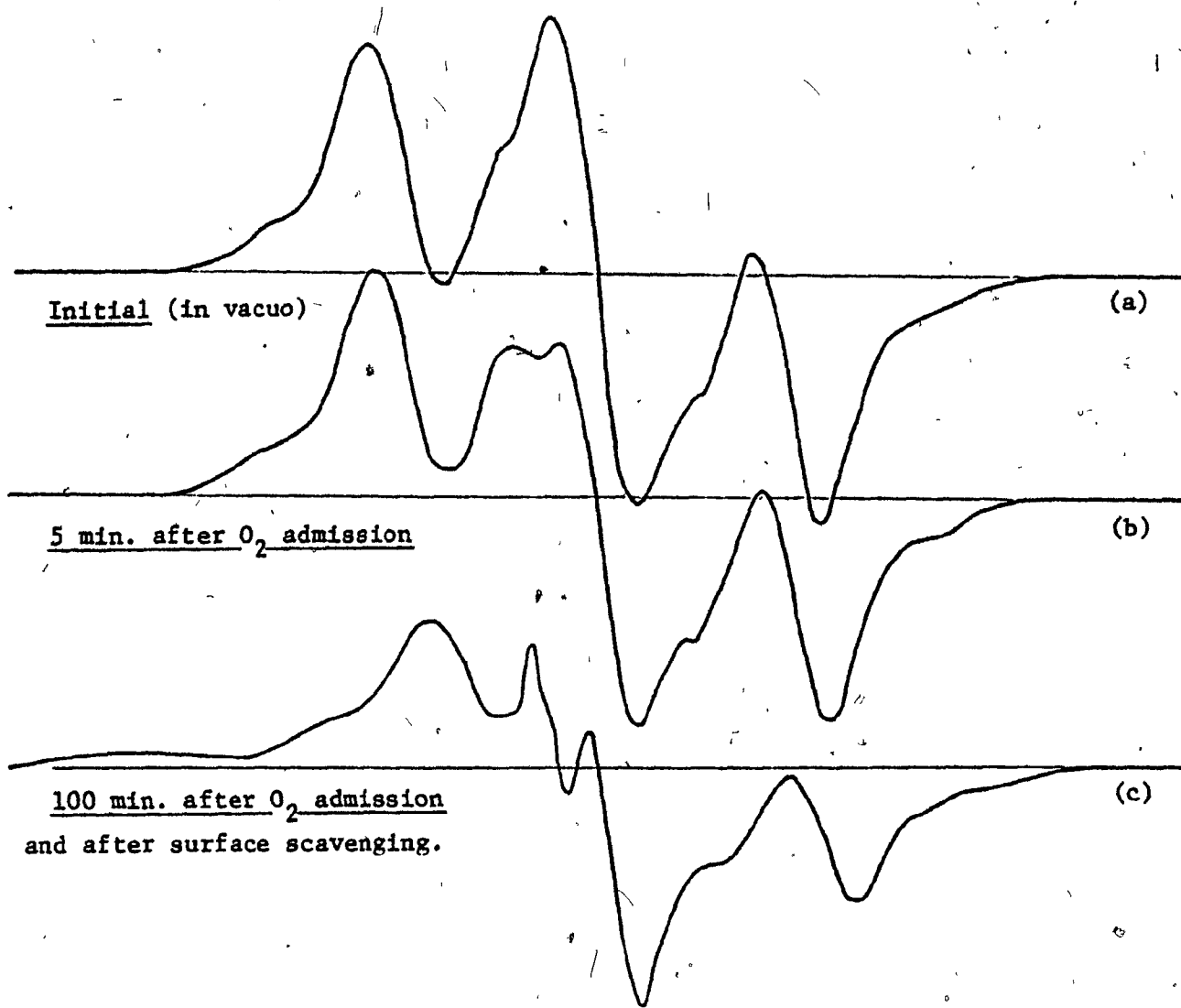


Fig. IV-1-1 : ESR study of oxygen diffusion at 25°C through CaAc , 2 H<sub>2</sub>O  
at the limiting conversion stage .

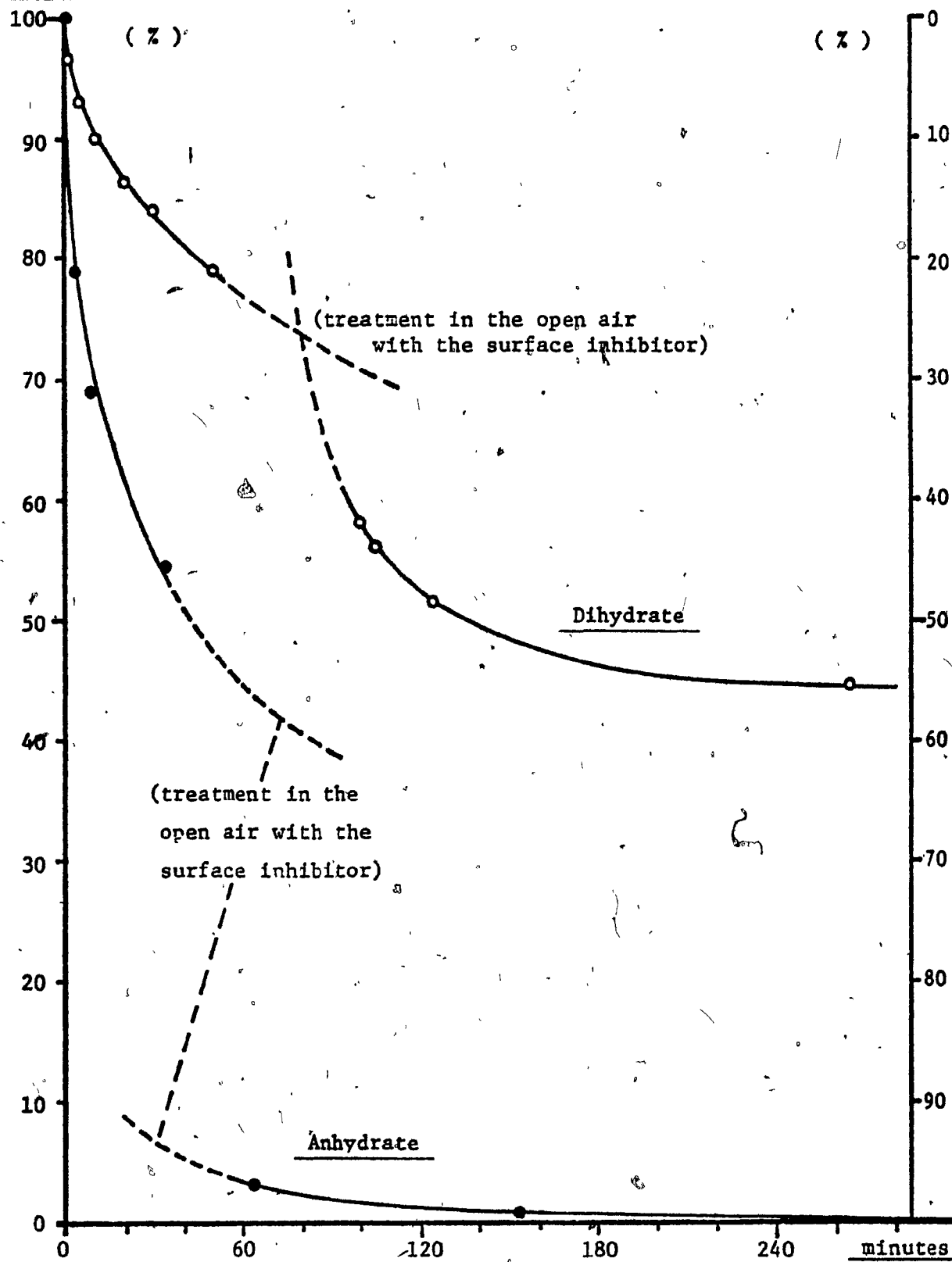
Remaining acrylate radicalsOxidized radicals

Fig. IV-1-2 : Kinetics of oxygen diffusion through CaAc at the limiting conversion stage, as measured by the rate of oxidation of the acrylate radicals at 25°C

at room temperature. On the contrary Fig. IV-1-2 shows a slower rate of oxidation at the limiting conversion stage thereby suggesting that the radicals reside deeper within the solid, and have their supply of oxygen limited by diffusion.

Secondly, the inhibitor treatment of the powder in the open air increased the rate of decay again. This indicated that the amount of air made available to the sample from the break-seal compartment was unfortunately stoichiometrically insufficient (if the inhibitor had been responsible for the sudden decrease in the acrylate radicals, the subsequent decay would have continued at a rate slower than before the treatment, not faster).

Thirdly, the step-decrease in the acrylate radical concentration is effected to the profit of the peroxide signal. Radicals therefore have not been destroyed by the scavenger, but only transformed by the attending oxidation.

Furthermore, a small singlet was observed 14 G lower than the acrylate triplet center, and much narrower (4.7 G width) than the peroxide (10 G) or the acrylate (60 G) (Fig. IV-1-1-c). Its intensity was only about 0.3% of the acrylate signal. This small singlet was attributed to a phenoxy radical formed upon contact with the inhibitor and adsorbed on the solid surface.

We can therefore conclude that the step-decrease in radical concentration observed on Fig. IV-1-2 upon treatment of the sample in the open air with an inhibitor, reflects the more abundant supply of oxygen to the sample rather than any action of the inhibitor itself. Ultimately, 56% of the dihydrate radicals got oxidized.

#### IV-1-2 In the anhydrate

The anhydrate showed the symmetrical triplet characteristic of long polymerization times (Fig. IV-1-3-a). Some differences from the dihydrate were noted: the shoulders on either side of the central line and those on the outside of either wing were much more pronounced.

Within the first minute after breaking the seal a devastating effect was produced on the central line, which vanished rapidly to the profit of the peroxide line (Fig. IV-1-3-b). As for the dihydrate, the rate of oxidation was monitored by the decay of the two outside lines of the acrylate triplet. Results are shown on Fig. IV-1-2.

As in the case of the dihydrate, the same argument may be made to show that most of the radicals were trapped within the bulk of solid rather than at the surface. 97% of the anhydrate radicals got oxidized after 64 min, and 100% ultimately.

#### IV-1-3 Conclusions

The study of the oxidation of the acrylate radicals by ESR has established earlier that the rate of the chemical reaction of oxygen was very fast even at 77°K. As a result, the rates of oxidation were concluded to be diffusion-limited in all cases. The extents and rates of oxidation can therefore be taken as a measure of the openness of each sample to the penetration of oxygen.

The initial rate of oxidation for the anhydrate at the limiting conversion stage was found to be 3.8 times larger than that of the dihydrate. This is easily explainable by their amorphous and crystalline natures, but seems to indicate that although half of the monomer had polymerized in both cases, enough of the dihydrate lattice was left unperturbed to pose a per-

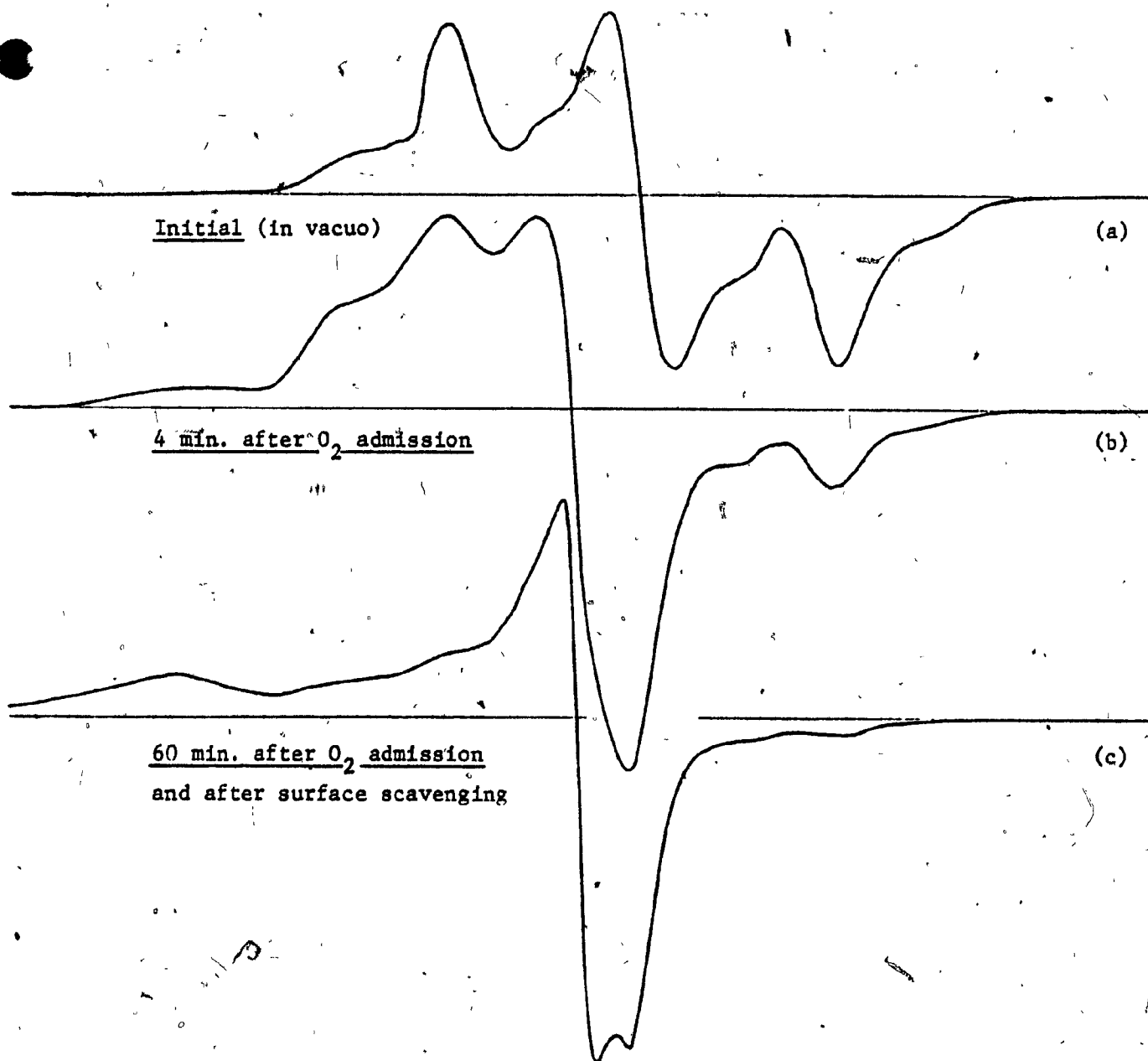


Fig. IV-1-3 : ESR study of oxygen diffusion at  $25^\circ C$  through CaAc anhydrate  
at the limiting conversion stage .

sisting barrier to the penetration of oxygen.

The same conclusion is strongly supported by the limiting extents of oxidation. Although the anhydrate proved 100% diffusible at all stages, the dihydrate was diffusible only to the extent of 2% right after irradiation and 56% after 14 days. An additional measurement after 1 day gave a value of 14%. It is extremely revealing to remark that the fractions of the accessible radicals after 0, 1, and 14 days, were approximately equal to the extents of in-source and post-polymerization respectively at the same times. As the virgin dihydrate was demonstrated to be completely impermeable to oxygen, and as the polymer was demonstrated by X-ray to form a heterogeneous phase, we may safely conclude that in the dihydrate, the oxidizable radicals are polymer radicals.

Alternately, these could be suggested to be dimer radicals placed in a "disruption sleeve" between the polymer phase and the lattice, and where they could be reached by the oxygen diffusing through the polymer phase. However, it will be shown later, by Wide-Line NMR, that this disruption sleeve is a phase of high mobility. Since polymerization in such a phase should prove very easy, dimer radicals should be short-lived, and the above suggestion should be rejected.

Finally, the location of the polymer radicals was determined to be in the bulk of the solid samples. Only an estimated 0.3% of them were accessible to the inhibitor solution brought into contact with the fine powders. This demonstrates that the growth of the polymer does not terminate when the living chain ends become trapped at the grain boundaries by the lack of fresh monomer feed. As the oxidizable radicals in the dihydrate are believed to be polymer radicals, we must therefore conclude that polymeri-

zation in this system does not terminate in the usual chemical sense of the term, but rather, that the chain ends become trapped in the polymer after having exhausted all the monomer molecules accessible at the level of thermal agitation available.

#### IV-2 Molecular motions during polymerization

We have seen in Chap. III that the study of molecular motions in the monomers as a function of dehydration, irradiation and temperature could not offer a satisfactory explanation of the polymerization mechanism, although it had been very informative in itself.

Accordingly, it was felt that a study of molecular motions during the polymerization itself held the hope of shedding more light on its mechanism.

The three di-H<sub>2</sub>O-hydrate, di-D<sub>2</sub>O-hydrate and anhydrate samples which were irradiated for the study discussed in section III-3-3 had disclosed Wide-Line NMR spectra identical at 50°C to those of unirradiated samples.

However, after only 12 hrs post-polymerization at 50°C, the central part of the dihydrate spectra began to show an obvious distortion from the initial shapes. After 1 day, it became apparent that the distortion was due to the presence of a narrow line growing at the center of the broad monomer line (Fig. IV-2-1). The D<sub>2</sub>O-dihydrate showed a sharper and better separated narrow line than that of the H<sub>2</sub>O-dihydrate (Fig. IV-2-2).

By reducing the modulation amplitude of the sweep field below 0.35 Gauss, it was possible to nearly isolate the narrow component from the broad one. Its line width was measured to be 0.86 Gauss for the H<sub>2</sub>O-dihydrate, and 0.40 Gauss for the D<sub>2</sub>O-dihydrate. Such line widths indicate a degree of mobility much higher than in the solid state, but lower than in

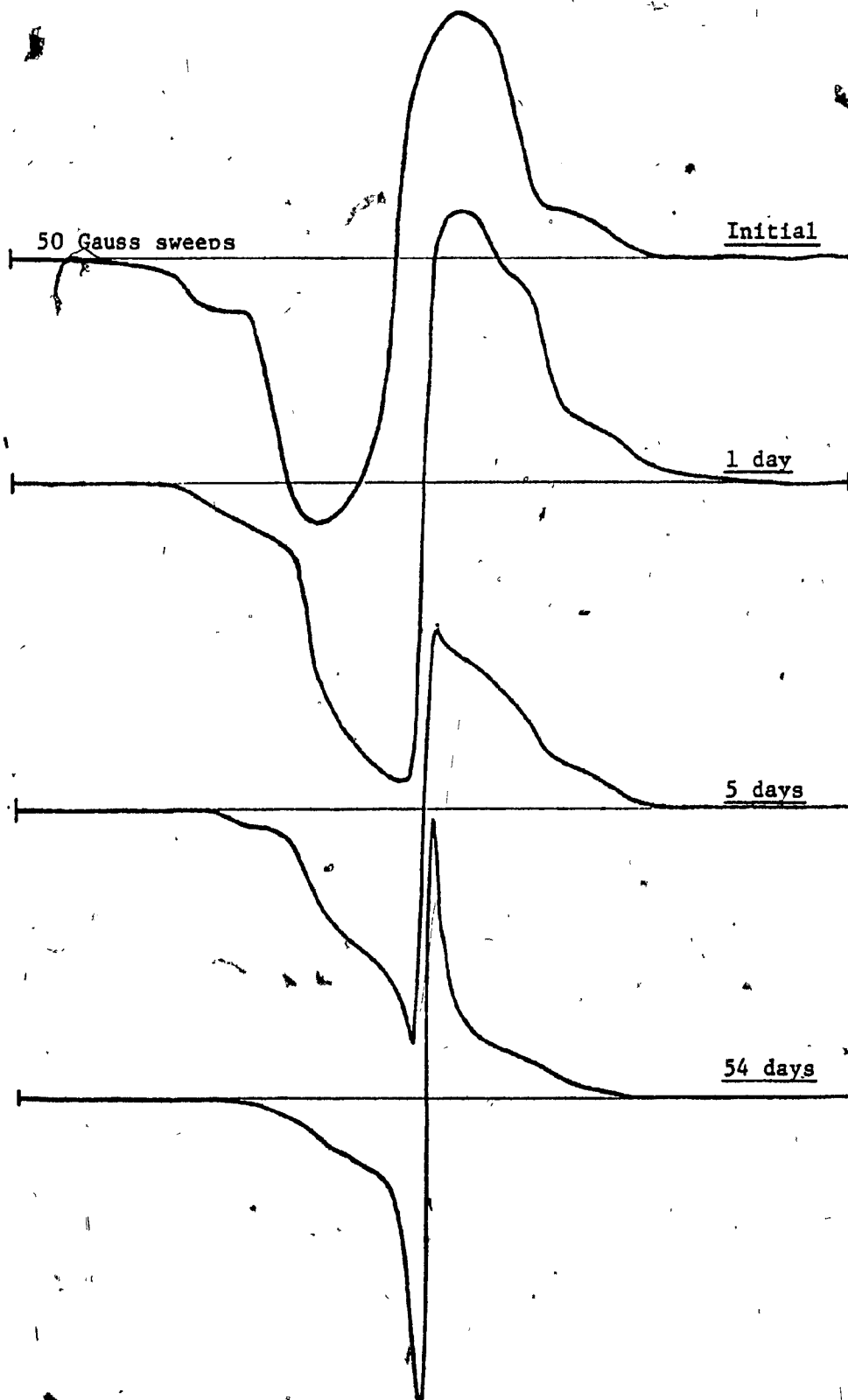


Fig. IV-2-1 : Wide-Line NMR spectra of irradiated calcium acrylate , 2 H<sub>2</sub>O after various times of post-polymerization at 50°C in vacuo (recorded @ 50°C)

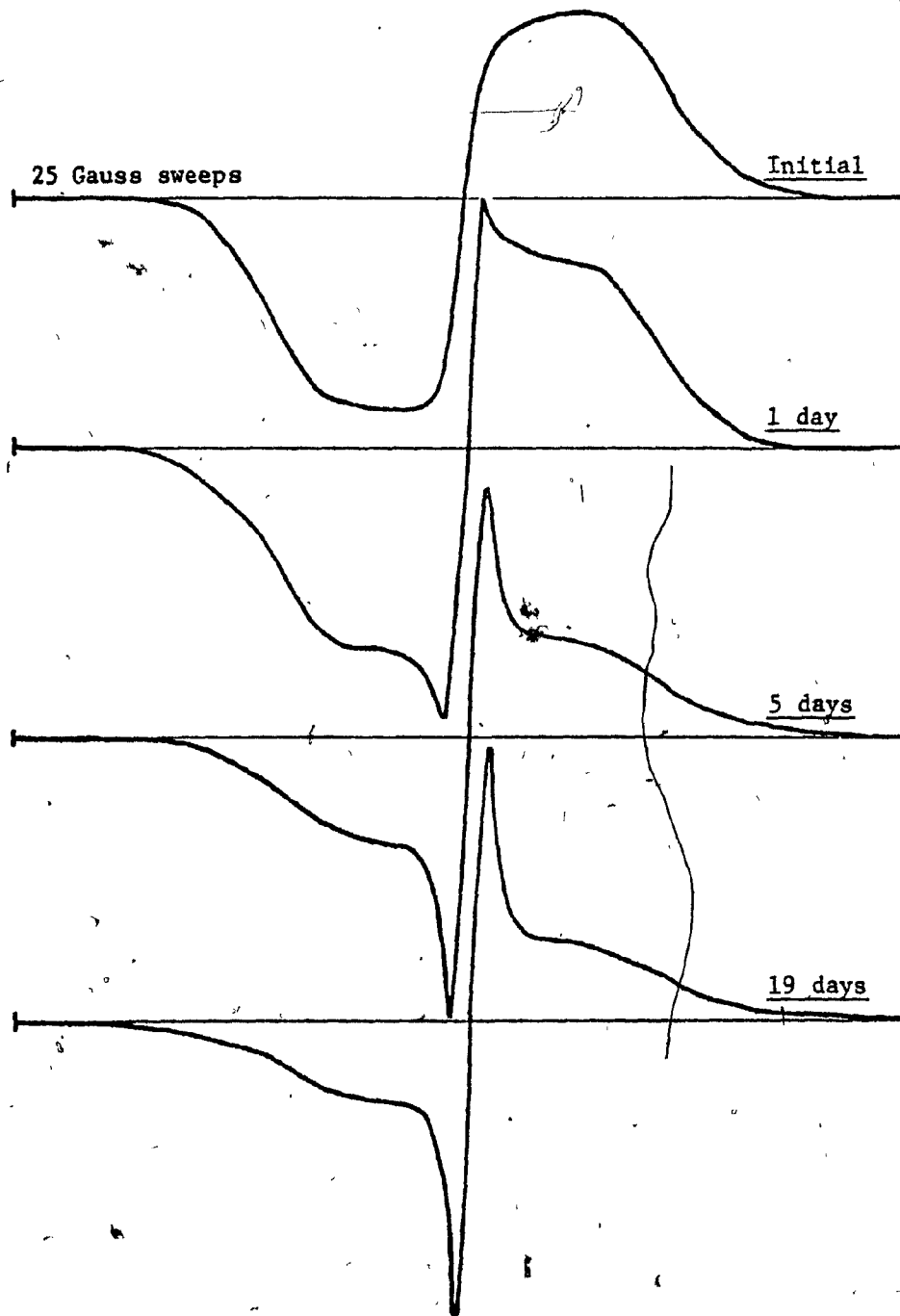


Fig. IV-2-2 : Wide-Line NMR spectra of irradiated calcium acrylate ,  $2\text{ D}_2\text{O}$  after various times of post-polymerization at  $50^\circ\text{C}$  in vacuo (recorded @  $50^\circ\text{C}$ )

the liquid state. The peak-to-peak height of this narrow component was measured, and was found to increase logarithmically with time (Fig. IV-2-3). The  $H_2O$ -dihydrate gave a less accurate fit to the logarithmic line, because the higher intermolecular broadening due to the water imparted a lack of resolution between the spectrum components, especially at short and long times. The growth of the  $D_2O$ -dihydrate line seemed to level off after 300 hrs, whereas that of the  $H_2O$ -dihydrate only slowed down between 300 and 1000 hrs.

At this stage, the presence of a sharp narrow line may be hypothesized as originating from three possible provenances: motions of the water, the monomer or the polymer. The exothermicity of the polymerization reaction may favor either molecular motion locally and temporarily, because of the poor heat dissipation characteristics of solids.

#### IV-2-1 Mobility of the water

Strong support for the water as an origin for the narrow line appears to come from the experiment on irradiated anhydrate. No narrow line was observed there during post-polymerization, and the spectra were identical with those of unirradiated anhydrate for more than 8 days at  $50^\circ C$ . Of course, the presence of a narrow line in the  $D_2O$ -dihydrate goes against this first hypothesis (i.e. that the  $H_2O$  is the origin of the narrow line) but it could still be rationalized since, on the basis of ESR and mass spectrometry evidence presented earlier, irradiation brings about an important randomization of the  $D_2O$  deuterons with the acrylate protons. The HDO present after irradiation would thus be detectable by NMR.

However, narrow lines have been observed (40, 89, 90) superimposed on the irradiated monomer spectra of several other SSP systems where water was

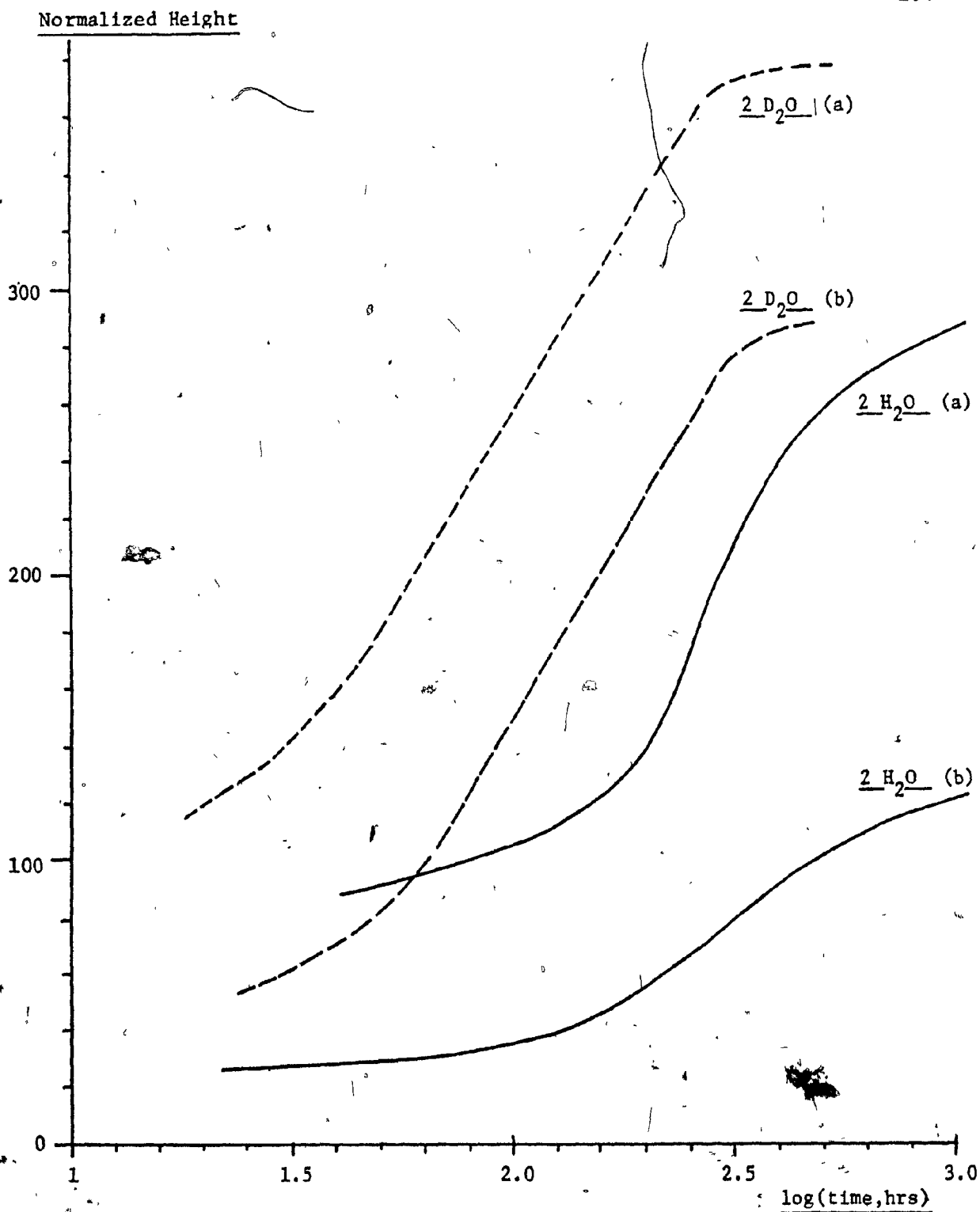


Fig. IV-2-3 : Peak-to-Peak height of the NMR narrow line in CaAc dihydrates , during the post-irradiation polymerization stage at 50°C .

Conditions : (a) 1.4 Gauss modulation amplitude ; (b) 0.5 Gauss mod. amplitude

totally absent. In particular, acrylamide and acrylic acid<sup>(90)</sup> exhibit 0.7 and 0.3 Gauss lines respectively, compared to 0.7 and 3.5 Gauss for the corresponding pure polymers. Consequently, it appears that the origin of these narrow lines should be looked for elsewhere than in the mobility of the water.

Let us now envisage what happens during polymerization. In the case of a heterogeneous SSP such as ours, the making of polymer links much shorter than the intermonomer distances in the lattice results in a polymer density greater than that of the monomer. This has been observed for vinyl SSP in general and for calcium acrylate in particular ( $d_{\text{poly}} = 1.555 \text{ g/cm}^3$ ;  $d_{\text{dihyd.}} = 1.461$ ;  $d_{\text{anhyd.}} = 1.425$ )<sup>(84)</sup>. The ensuing contraction will soon leave the living chain end in a "cavity", such as illustrated on Fig. IV-2-4. At this stage, further polymerization may only proceed by either one or a combination of two mechanisms: the monomer may diffuse towards the reactive chain end, or vice-versa.

#### IV-2-2 Mobility of the monomer

The monomer mobility may assume two forms. In the first form, a monomer might leave the cavity wall and diffuse towards the reactive chain end. This form should be rejected as an origin of the narrow line for three reasons:

- (1) the narrow line should then be highest at the beginning (where polymerization rate and local thermal agitation are maximum), whereas it was found to increase until the end of polymerization.
- (2) the concentration of such diffusing monomer is going to be of the order of that of the growing chains. As the limiting degree of polymerization is  $2 \times 10^3$  and the yield 30%, the order of magnitude of the concen-

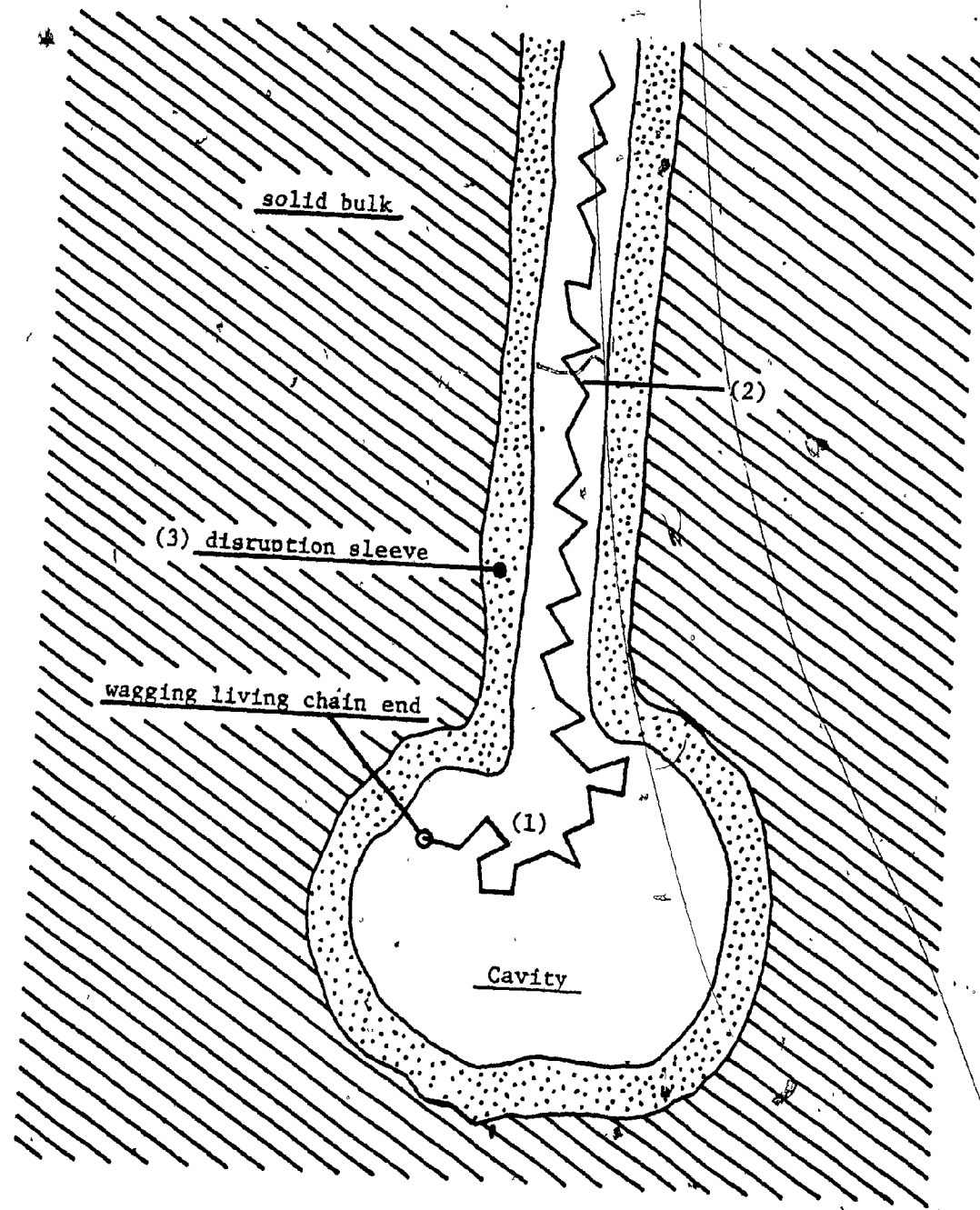


Fig. IV-2-4 : Schematic representation of a physical model of S.S.P.

Zones where the mobility disclosed by the NMR narrow line could take origin :

- (1) : end of the living chain ( wagging in the cavity )
- (2) : macromolecule ( segmental mobility )
- (3) : interfacial disruption sleeve ( monomer mobility )

Zones (1) and (2) may be swollen with water released from the dihydrate lattice.

tration in "adding monomers" is  $10^{-4}$ . This is far too small to be observed, in regard of the low sensitivity of Wide-Line NMR.

(3) the "sublimation" of a monomer requires the severance of strong Ca-CO<sub>2</sub> and hydrogen bonds before the heat of polymerization is available to provide the necessary energy, which is very difficult.

As a result, Fig. IV-2-4 presents a solid-state polymerization model where chain growth is achieved by wagging of the chain end inside the cavity until it hits a wall and abstracts a fresh monomer.

In the second form of monomer mobility, the narrow line observed during post-polymerization would take origin in a new monomer phase located at the interface between the monomer lattice and the polymer chain. This new phase would not be a temporary phenomenon such as local melting, since the narrow line persisted even after polymerization had virtually stopped. On the contrary, a permanent "disruption sleeve" would be created by the exothermicity of the polymerization. A destruction of the calcium coordination polyhedron, and a local dehydration would accompany the reaction.

Such a "sleeve" could very well include the walls of the cavity mentioned earlier, as depicted schematically on Fig. IV-2-4. Whatever the shape of this interphase boundary, its existence may be deduced simply from the crystalline structure of the dihydrate. Of course, the loosening of the lattice bonds along the disruption sleeve would result in an increased monomer mobility and could thus very well account for the observation of a narrow line by NMR.

Two kinds of experimental evidence may be brought to support this hypothesis. Both are based on the fact that if such a disruption sleeve is produced around the polymer chains, the amount of monomer molecules in-

involved in it is going to be proportional to the amount of polymer formed.

The first experimental evidence has been presented in section IV-1, where an empirical proportionality between the polymer yield and the fraction of monomers accessible to the diffusion by oxygen was demonstrated by ESR.

The second experimental evidence was obtained directly by Wide-Line NMR. A curve of the peak-to-peak height of the narrow line versus the polymer yield was constructed at various post-polymerization times, as is shown, on Fig. IV-2-5. They were found to follow a good proportionality line up to the limiting conversion. The fact that the amount of this new monomer phase was proportional to the polymer yield is perfectly consistent with the model of the "disruption sleeve" and/or "cavity" depicted on Fig. IV-2-4.

However, two objections may be opposed to the hypothesis of the monomer-originated narrow line. The first is that the narrow line was not observed in the polymerizing anhydrate. This conspicuous absence may be rationalized by considering that the anhydrate might not require the presence of a high-mobility monomer-polymer interphase. The amorphous nature of the anhydrate, and the intrinsically higher bulk monomer mobility in it, might be responsible for a crumbling and packing of the monomer around the polymer as it grows, thereby quenching the mobility of both monomer and polymer by the establishment of new Van der Waals bonds between them.

The second objection to the hypothesis that the narrow line takes origin in the monomer mobility is that such a line could very well originate in the polymer chain itself, as will be examined below.

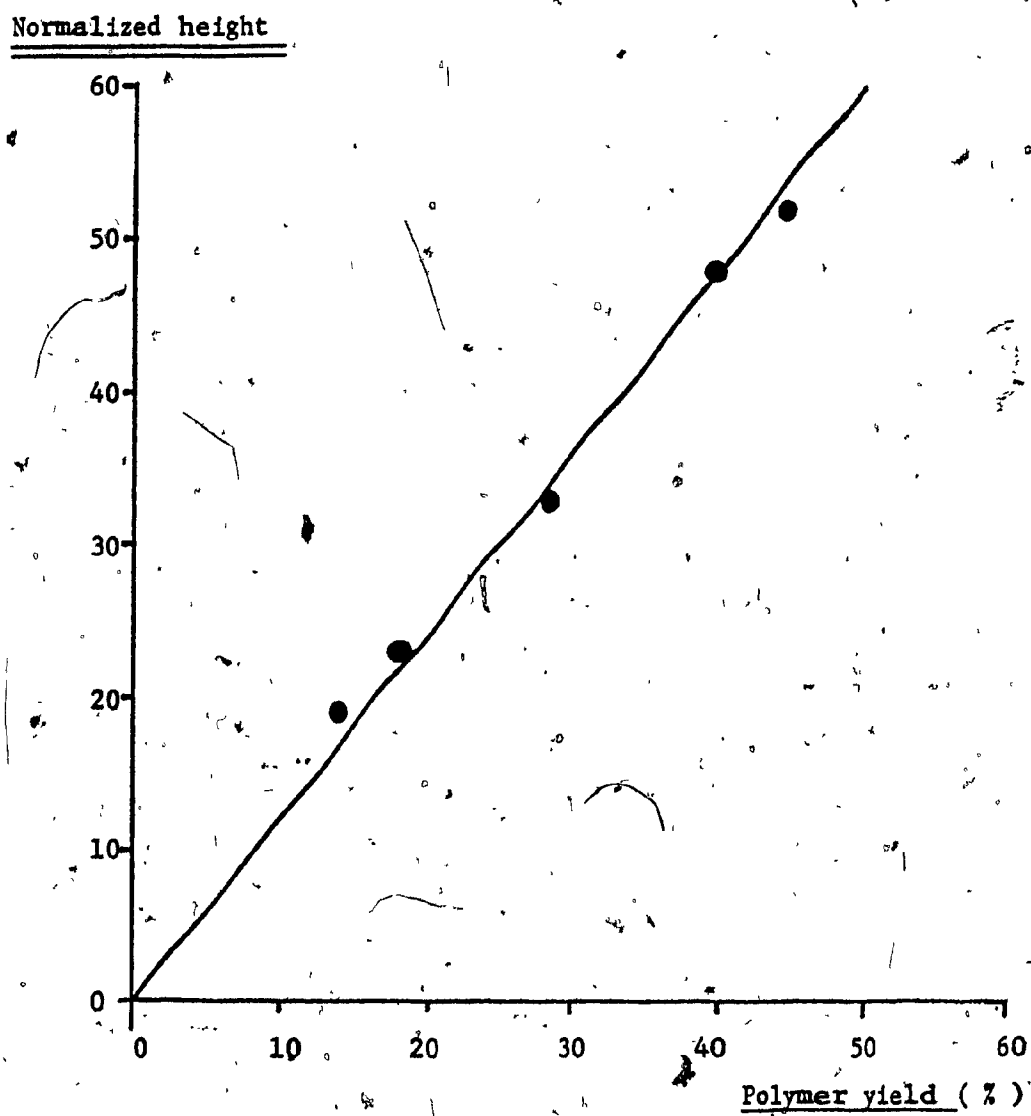


Fig. IV-2-5 : Proportionality between the normalized height of the narrow component of the NMR spectra and the polymer yield.

Sample : dihydrate irradiated to 0.86 Mrad , polymerised at 50°C in vacuo  
Conditions : recorded at 50°C with 0.5 Gauss mod.ampl.

#### IV-2-3 Mobility of the polymer

In order to establish a comparison basis, the motions in the polymer were investigated directly by recording the Wide-Line NMR spectrum of a sample of isolated pure polymer (Fig. IV-2-6). The spectrum was found to consist of a 10 Gauss broad line superimposed on a 1.2 Gauss narrow component (which was measured by reducing the modulation amplitude below 0.35 Gauss).

The origin of the narrow line in the pure polymer is believed to reside in segmental mobility of the chains, as when a macromolecule has already grown to any sizeable length, it is likely to be so embedded in the bulk of the solid phase as to render global diffusion improbable.

The width of the narrow line observed here is 30% larger than that in the polymerizing  $H_2O$ -dihydrate (0.86 Gauss) and three times larger than that in the  $D_2O$ -dihydrate (0.40 Gauss). However, all or part of the difference may be ascribed to a slightly different temperature ( $25^\circ C$  for the polymer instead of  $50^\circ C$ ) and to a different solid environment. As a result, it is quite possible that the narrow line observed in the polymerizing system could come from the polymer mobility rather than from the monomer as suggested earlier.

Whether the mobility disclosed comes from agitation of segments inside a disruption sleeve or from wagging of the chain end inside a cavity, either mechanism would be consistent with the proportionality of the narrow line to the polymer yield.

On the other hand, the absence of a narrow line in the anhydrate might still be rationalized with the argument developed earlier, involving a quenching of the macromolecular segmental mobility by the progressive packing of the anhydrate.

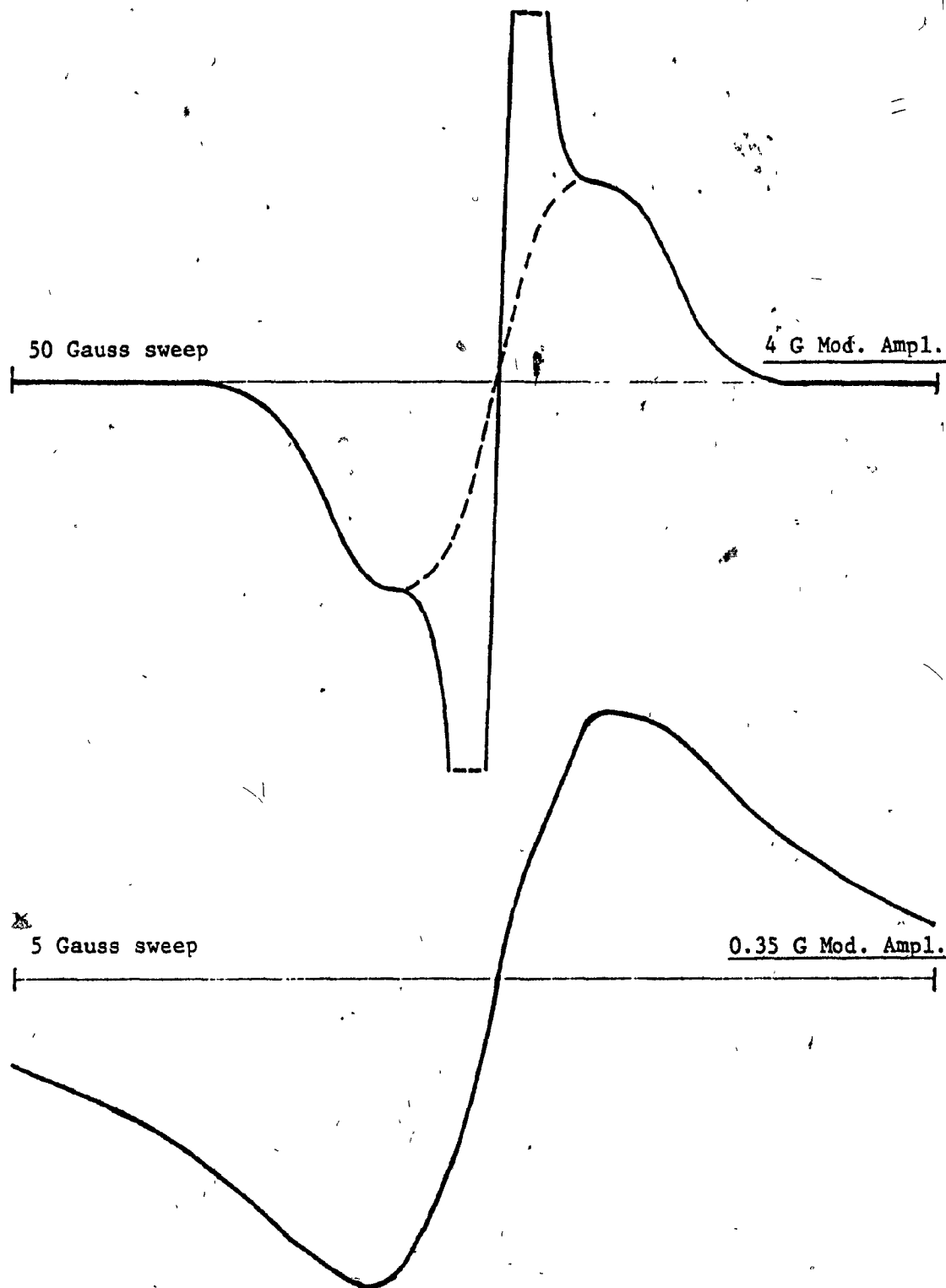


Fig. IV-2-6 : Wide-Line NMR spectra of pure poly(calcium acrylate) at 25°C .

#### IV-2-4 Conclusion: physical mechanism of SSP

The investigation of the molecular mobility by Wide-Line NMR has led to the observation of a new phase during the post-polymerization of hydrated monomers. This new phase is characterized by a mobility intermediate between that of a solid and that of a liquid, and was found to grow proportionally to the amount of polymer formed. It was not observed in the anhydrate.

The reported existence of an identical behaviour in water-less systems was interpreted as meaning that the mobility disclosed was not that of the water of hydration.

The mobility of the monomer in an interfacial "disruption sleeve" or at the surface of a "cavity", and that of segments or of the ends of the polymer chain were envisaged as an origin for the narrow line observed. Both mechanisms can be logically predicted and explained on the basis of the known properties of the system, and both are perfectly consistent with the body of experimental evidence available. No experiment could be devised so far to distinguish between them. On the other hand, it is certainly possible that both mechanisms could coexist.

The absence of this new phase in the anhydrate system was rationalized on the basis that the amorphous anhydrate does not require such transitional phase as the crystalline dihydrate does, because its looser texture is more apt to collapse and fill the voids created by polymerization, thereby quenching any unusual molecular mobility.

Practically, the proportionality observed between the polymer yield and the height of the NMR narrow line makes it the basis for an attractive

( ) non-destructive method for measuring the extent of monomer conversion.

This analytical tool is novel, and one of the very few available so far to the solid-state polymer scientists interested in kinetic studies.

Finally, a solid-state polymerization model was proposed, where chain growth occurs by wagging inside a cavity until it abstracts a new monomer from the wall. Such an abstraction would increase the range accessible to the wagging chain end faster than it would increase the average diameter of the cavity, thus providing for a rapid polymerization to high molecular weights. This model fits the polymerization data available, and predicts that control of the stereotacticity of the polymer by the crystalline lattice should not be observed. Indeed, the  $^{13}\text{C}$ -NMR experiments support this model, as will be developed in the following section.

#### IV-3 Stereotacticity of the polymerization

For a full understanding of the mechanism of SSP, a knowledge of the stereoregularity of the polymer is required. The possibility that the strict order of the monomer crystal could impart a preferential configuration to the polymer by imposing a special orientation to the adding monomer units must be investigated.

Because of the dependence of the chemical shifts upon the steric environment, the NMR signals lend themselves to a stereotacticity analysis.  $^{13}\text{C}$ -NMR is more powerful in this respect than proton-NMR for the following reasons:

- $^{13}\text{C}$  chemical shifts cover a range of 300 ppm compared to only 12 ppm for protons.
- $^{13}\text{C}$  shifts are much more sensitive to steric environment than proton shifts.
- $^{13}\text{C}$  spectra are simpler to interpret because all spin-spin interactions can be removed by heteronuclear decoupling.
- dipolar broadening of peaks is very much reduced in  $^{13}\text{C}$  polymer spectra compared to proton polymer spectra.

The sensitivity of  $^{13}\text{C}$  spectrometry is 5720 times lower than that of proton-NMR, however, because of the low natural abundance of  $^{13}\text{C}$  (1.1%) and of its lower magnetic moment. Fortunately, this sensitivity problem may be offset by the use of larger sample tubes, of the Fourier-Transform method and of a time-averaging computer accumulating thousands of free-induction decays of the pulsed R.F. field. Thus, the availability of modern fast Fourier-Transform spectrometers has made  $^{13}\text{C}$ -NMR a preferred method for the stereoregularity analysis of macromolecules.

Five polymer samples were prepared as described in section II-12.

They were:

- Early polyacrylic acid (15 hours post-polymerization time giving a yield of 14%) from a Ca acrylate di-hydrate under vacuum.
- Late poly-acid (14 days, yield of 50%) also from di-hydrate under vacuum.
- Poly-acid made from anhydrate under vacuum.
- Poly-acid made from di-hydrate in air.
- Poly-acid made from anhydrate in air.

The effects of the pH and of the temperature of observation were

studied, on some samples, and the optimal conditions thus determined were used for the recording of all other spectra.

#### IV-3-1 Effect of the pH of observation

The pH of the sample solution was 1. It could be adjusted by the addition of a few drops of KOH to pH 5 and 9. Changes in the chemical shifts and the shape of the spectra were immediately apparent, as shown on Fig. IV-3-1, but were more drastic for the CH and CH<sub>2</sub> groups than for the CO<sub>2</sub><sup>-</sup>. The chemical shifts measured are listed in Table IV-3-1, in parts per million relative to the internal reference standard of dioxane. The assignments were made after Schaeffer (91).

pH	CO <sub>2</sub>	CH			CH <sub>2</sub>		
	(Singlet)	syndio	hetero	iso	syndio	hetero	iso
1	111.5	-25.0 (singlet)			-31.9	-32.3	-32.7
5	broad	broad singlet			singlet		
9	117.8	-19.6	-20.4	-21.4	-27.8	-29.4	-30.5

TABLE IV-3-1

<sup>13</sup>C chemical shifts (in ppm) of poly-acrylic acid, relative to dioxane

The CH<sub>2</sub> signal changes from a poor triplet at pH 1 to a better resolved triplet at pH 9. The low-field peak (left-hand side) is barely perceptible at pH 1, but grows more intense at pH 9. The high-field peak remains partly merged with the central line at both pH. On the other hand, the CH signal goes from a sharp singlet at pH 1 to a triplet at pH 9.

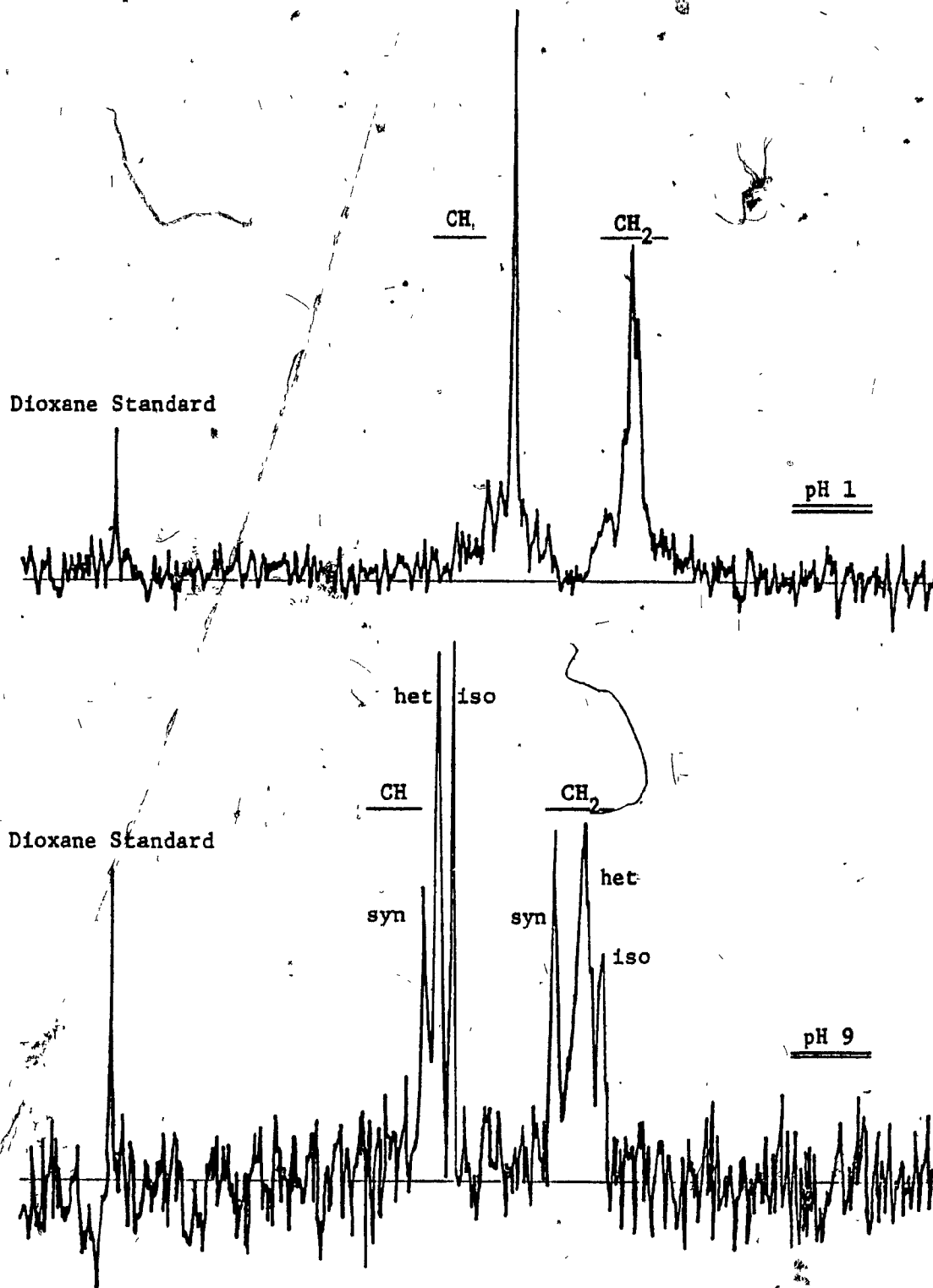


Fig. IV-3-1 : Effect of pH on the  $^{13}\text{C}$ -NMR spectra of poly(acrylic acid) in  $\text{D}_2\text{O}$  at  $353^\circ\text{K}$ . Sample : "early polymer" made from  $\text{CaAc}_2 \cdot 2 \text{H}_2\text{O}$  under vacuum .

2

These changes are believed to be due to conformational changes. It is known that poly-acrylic acid in water approaches a random coil at acidic pH; whereas its being neutralized extends the chain by increasing the coulombic repulsions between the pendant carboxylate groups. This is consistent with the observed sharp increase in the viscosity of the solution upon neutralization.

As a result, the analyses have been made at pH 9, as the spectra thus recorded display much more information about the tacticity of the poly-acid.

#### 4 IV-3-2 Effect of the temperature of observation

As the temperature of the sample was raised from 300. to 353°K, no change in the chemical shifts was observed. The behaviour was similar for pH 1 and 9. The CO<sub>2</sub> peak intensity somewhat decreased relative to the others. The resolution of the CH and CH<sub>2</sub> triplets was noticeably improved, with the iso and syndio peaks increasing on either side of the central hereto peak of each triplet.

The improved resolution is thought to be due to the decrease of the viscosity of the sample. At pH 1, the poly-acid viscosity changes sharply with temperature. At pH 9 however, the viscosity of the extended chains of the high molecular weight poly-salt depends more on segmental mobility than on newtonian behaviour, and decreases only slowly upon heating. The microviscosity is still much reduced, and the best spectra were thus recorded at pH 9 and elevated temperature, which were chosen as the conditions for the rest of this study.

#### IV-3-3 Analysis of the results

The spectra recorded at pH 9 and 353°K, i.e. in the best conditions

found, were identical within the accuracy of the experiment for all five samples regardless of the level of hydration, the presence or absence of oxygen and the extent of polymerization (Fig. IV-3-2).

With the help of Schaeffer's work<sup>(91)</sup> on  $^{13}\text{C}$  of poly-acrylic acid, observation of the ratios of the syndio/hetero/iso peaks could yield information on the triad sequences of the polymer. As these ratios could be measured from either the CH or the  $\text{CH}_2$  signals, an attempt was made to determine which one would give the more consistent results.

One may think of using either the peak heights or the peak areas to measure these ratios. However, it was ascertained that the peak heights were not a valid approximation of the peak intensities. Indeed, the intensity of the iso peak relative to the syndio peak ranged from 1.1 to 1.9 times larger when measured from peak heights than when measured from peak areas. This shows no consistent correlation between the two methods.

The peak areas were used from then on, and the relative percentages of occurrence of syndio, hetero and iso triads were determined from the CH and  $\text{CH}_2$  parts of each spectrum. Uncertainty arose in the drawing of the peak wings and baseline for three different reasons:

- the inherently noisy baseline of the  $^{13}\text{C}$  spectrum.
- the occasional presence of spinning sidebands on either side of each peak. These could not always be suppressed because of the high viscosity of the samples.
- the presence of ill-resolved components of sequences of a higher order. Both CH and  $\text{CH}_2$  groups showed signals that were partly sensitive to tetrads and pentads sequences, although these have a much lower intensity than the main triplets of the triads.

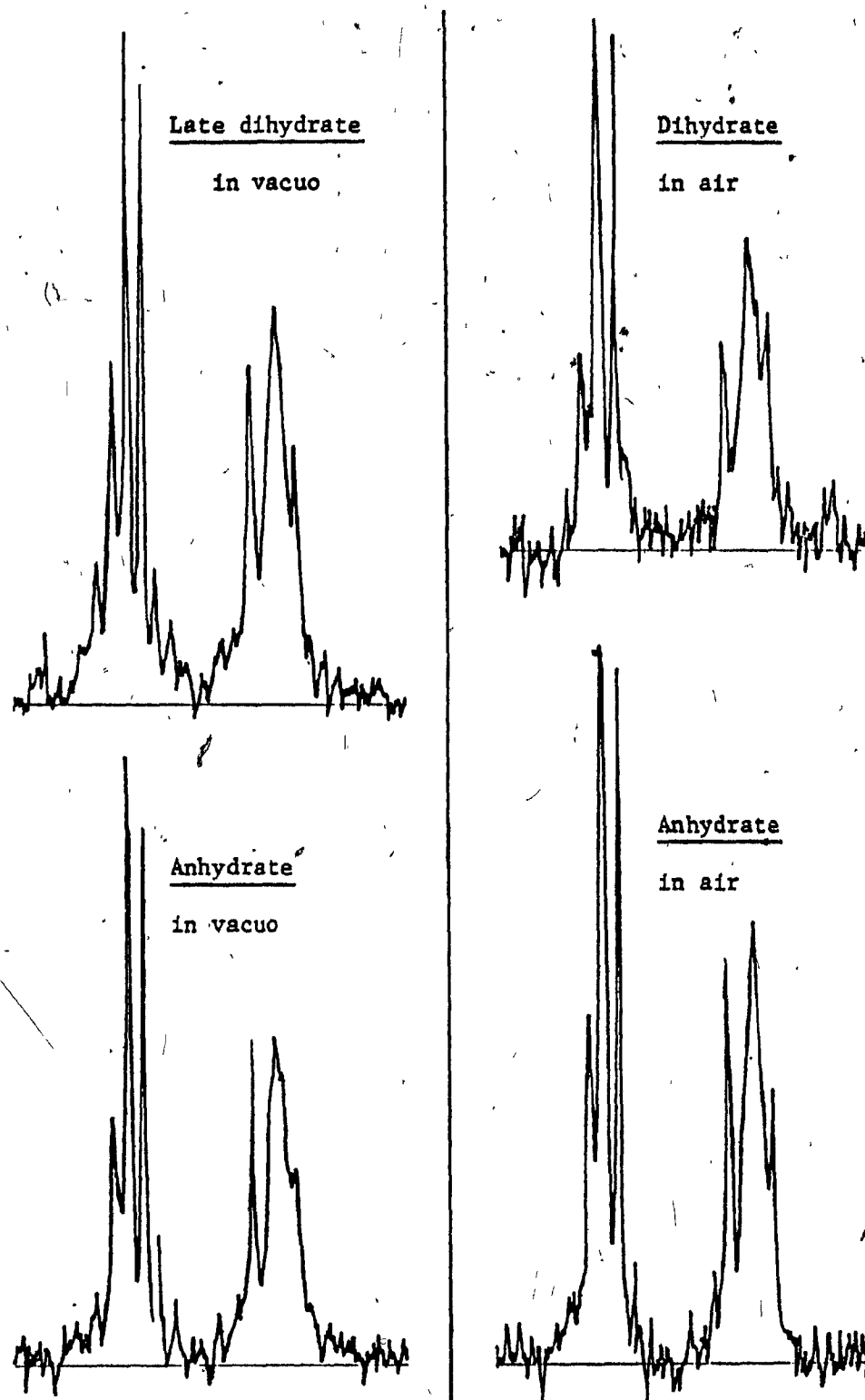


Fig. IV-3-2 :  $^{13}\text{C}$ -NMR spectra of poly(acrylic acid) samples made by SSP from calcium acrylates under different conditions ; recorded in  $\text{D}_2\text{O}$  at pH 9, 353°K.

In order to solve these difficulties, the following tests were made. Two determinations of the syn/het/iso percentages were made on the CH of the "early polymer from dihydrate under vacuum" while drawing broad wings encompassing the aforementioned spinning sidebands and higher order components. They yielded an average of 24.8/44.5/30.7%. Two more determinations were then made on the same sample, but this time drawing wings that excluded the interfering components. They yielded an average of 23.7/46.6/29.8%. The differences between these two methods of measurement appear small and within the normal range of scatter on repeated scans. It was thus decided to draw arbitrarily and consistently the wings midway between these two extremes. The use of electronic integration would obviously prove of no value in alleviating all these problems.

In order to check for a possible systematic difference between the measurements derived from the CH and CH<sub>2</sub> groups, the following test was run. Six determinations of the syn/het/iso percentages were made on the CH group from three different samples, and yielded 23.3/45.7/31.0% with a standard deviation of 1.87, 1.06 and 1.08 respectively. Four more determinations were made on the CH<sub>2</sub> group from the same samples, where the resolution allowed it. They yielded an average of 21.3/55.9/22.8% with standard deviations of 3.97, 1.88 and 3.41 respectively.

It appears that the determinations made from the CH<sub>2</sub> peak areas show an excess of 10 points for the hetero triads, at the expense of the syndio for two points and of the iso for 8 points, over the CH-based determinations. The standard deviations for the CH<sub>2</sub> were nearly double those for the CH groups. It seems possible to explain these results with the observed shapes of the two groups of lines: shoulders on the side of the

syndio and hetero peaks regularly appeared in the CH group, probably manifesting some sensitivity to tetrad sequences. Close scrutiny revealed that although the iso peak appeared to be a pure singlet, the syndio and hetero peaks of the CH signal seem to be in fact nearly coalesced doublets.

The situation is similar for the CH<sub>2</sub> signal, although aggravated by a poorer resolution. The broader and more overlapping peaks result here in a more arbitrary drawing of the wings and a more inaccurate measurement of their relative areas, than in the case of the CH signal.

In consideration of all the preceding arguments, it was finally judged that a systematic difference could not be established between the measurements made from the CH and CH<sub>2</sub> signals, and that accordingly, all 13 determinations made from them should be retained and averaged in the hope of minimizing the influence of arbitrary choices. A confidence level of 95% and a "Student's t factor" of 1.77 were used to calculate the means, standard deviations and error limits shown below:

- syndiotactic:  $22.9 \pm 1.3\%$ ;  $\sigma = 2.6$
- heterotactic:  $48.8 \pm 2.5\%$ ;  $\sigma = 5.1$
- isotactic :  $28.3 \pm 2.1\%$ ;  $\sigma = 4.3$

#### IV-3-4 Fit with Bernoullian statistics

A macromolecule is said to follow Bernoullian statistics when the isotactic placement of the next monomer to be added onto a living chain can be described by a single probability. We shall call this probability  $P_m$  in accordance with the notation of Bovey<sup>(92)</sup>. To say that a polymer is Bernoullian is equivalent to saying that the addition is influenced only by the end-unit of the growing chain. Such a statement should not be

( ) understood to mean that addition is influenced by the stereo-chemistry of the end of the growing chain, for one monomer unit considered alone has no stereo-chemistry, but can of course exert a steric influence.

According to this scheme, the probability to find an isotactic triad will be  $P_m^2$ , that of a syndiotactic triad  $(1-P_m)^2$  and that of an heterotactic triad  $2 P_m (1-P_m)$ . Therefore, experimental results should lie on a single vertical line on the graph of Fig. IV-3-3. It can be visually ascertained that the above experimentally measured probabilities comply with this requirement. Another way to check the fit with Bernoullian trial is to compute the theoretical hetero and syndio percentages from the isotactic one. The  $P_m$  was calculated to be 0.532, which gives syndio and hetero probabilities of 21.9 and 49.8%. These match very well the experimental average values of 22.9 and 48.8% respectively, within the estimated error limit.

It can thus be concluded that in a first approximation, the polyacrylic acid obtained from gamma-initiated solid-state post-polymerization follows Bernoullian statistics regardless of the level of hydration (0 or 2) of the monomer, of the presence or absence of oxygen, and of the extent of conversion.

According to Fordham<sup>(93)</sup>, the kinetic rate constants for the addition of a monomer in the syndio and isotactic placements obey the equation:

$$\frac{k_s}{k_i} = \exp\left(\frac{-\Delta F^*}{R T}\right) = \exp\left(\frac{\Delta S^*}{R}\right) \exp\left(\frac{-\Delta H^*}{R T}\right)$$

where the starred deltas represent the differences between the corresponding free energy, entropy or enthalpy for the syn and iso placements.

## Triad probability

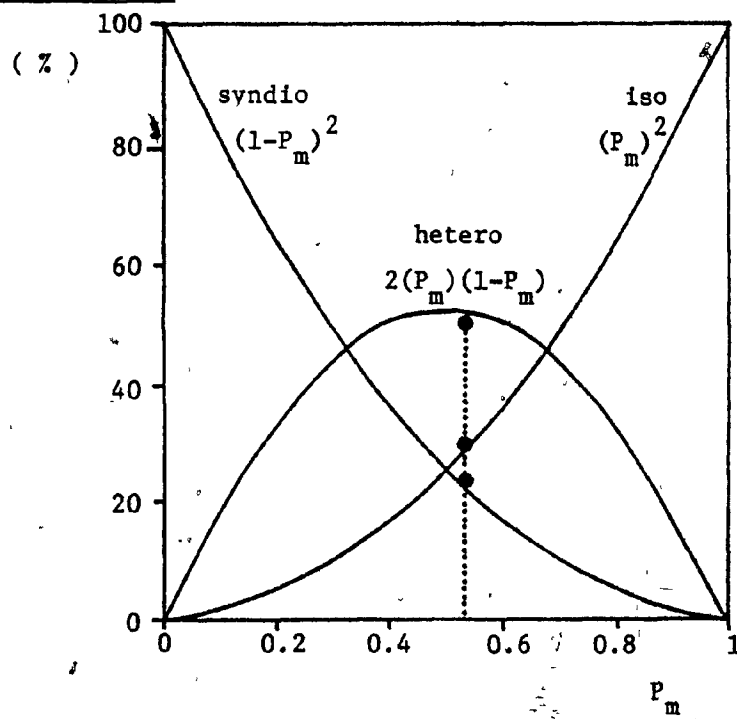


Fig. IV-3-3 : Triad probability ( % ) for a Bernoullian polymer , as a function of the placement probability  $P_m$  of the last adding monomer .

..... calculated values

● experimental values measured by  $^{13}\text{C-NMR}$

Matsuzaki et al.<sup>(94)</sup>, using proton NMR, measured an average  $P_m$  of 0.525 for several samples of poly-methyl acrylate polymerized at various temperatures, in various solvents or in bulk, and initiated by either UV or gamma-rays. None of their samples exhibited significant deviation from the mean, showing a remarkable insensitivity of the polymerization mechanism towards the traditionally important environmental parameters. Fordham's treatment of Matsuzaki's data gives a

$$\Delta H_s - \Delta H_i = 0 \text{ cal/mole} \quad \text{and a} \quad \Delta S_s - \Delta S_i = -0.20 \text{ entropy units.}$$

Bovey<sup>(92)</sup> also states that most alkyl acrylates polymerize by a free-radical mechanism, and show a  $\Delta(\Delta H)$  near zero and a very small  $\Delta(\Delta S)$  regardless of the temperature, of the ester group and of the solvent.

It appeared therefore justifiable to assume in a first approximation a  $\Delta(\Delta H)$  of zero for the calcium acrylate system as well. Fordham's treatment then leads to:

$$\frac{k_s}{k_i} = \frac{1-P_m}{P_m} = 0.880$$

$$\Delta S_s - \Delta S_i = R \ln\left(\frac{k_s}{k_i}\right) = -0.26 \text{ entropy units,}$$

which is consistent with Matsuzaki's and Bovey's findings.

Upon closer scrutiny, however, it is possible to envisage the ionized nature of the acrylate salt altering the activation energy of the intermediate addition complex to give a non-zero  $\Delta(\Delta H)$  in contrast to the

behaviour of all the acrylate esters. Only a study of the possible temperature dependence of  $P_m$  for the solid-state poly-acrylic salts could establish beyond doubt whether  $\Delta(\Delta H)$  is zero or not in this particular system.

#### IV-3-5 Fit with higher-order statistics

It has now been established that poly (calcium acrylate) obeys Bernoullian statistics. This means that only one probability  $P_m$  is necessary to describe the system, because the placement of the adding monomer is only influenced by the last unit added. However, Bovey<sup>(92)</sup> states that mechanisms of a higher order than can be tested can never be ruled out, i.e. those involving the influence of the penultimate or antepenultimate link. Such mechanisms require more than one probability to be described, as for example the Markov or the Coleman-Fox statistics.

An attempt was made at testing the fit with such higher-order statistics. Assuming the 13 determinations of syn/het/iso were randomly scattered, a fuller application of the laws of statistics should enable one to reject those data that fall outside a reasonable error interval defined from the standard deviation. It turns out that three determinations would thus be rejected. The average of the 10 remaining would then be (applying the same 95% confidence level):

- syndiotactic:  $23.8 \pm 1.0\%$ ;  $\sigma = 1.7$
- heterotactic:  $46.4 \pm 1.5\%$ ;  $\sigma = 2.73$
- isotactic :  $29.8 \pm 1.8\%$ ;  $\sigma = 3.30$

These probabilities are slightly different from those determined in section IV-3-3, but their standard deviation sigmas are 40% lower which indicates a greater homogeneity in the data.

A placement probability  $P_m$  of 0.545 was derived and used to check the fit with Bernoulli's statistics. The resulting syndio and hetero probabilities were 20.6 and 49.5% respectively. These calculated values fall outside of the above experimental ones by one to two sigmas. This constitutes a deviation from Bernoullian behaviour which is apparently significant. As a result, the calcium acrylate polymer may thus be postulated to follow some higher order statistics such as Markov and Coleman-Fox. Alternately, it could be argued that these statistics were all derived for liquid-state polymerizations and that possibly, factors specific to the solid-state could dominate the traditional parameters in such a way as to obey a new type of statistics of its own.

However, due caution must be exerted in the interpretation of these results. It turns out that the three determinations rejected on the basis of the so-called statistical arguments were all made from  $\text{CH}_2$  signals, and that the only other  $\text{CH}_2$  determination was also right on the borderline of rejection. Accordingly, the non-random nature of the scattering of the data do not justify a blind application of variance analysis.

In conclusion, we may state that the tacticity analysis of the CH signals indicates a slight deviation from Bernoullian statistics and suggests that poly (calcium acrylate) made in the solid-state may follow a higher-order statistic. On the other hand, the analysis of all data from the  $\text{CH}_2$  together with the CH signals does follow Bernoullian statistics.

The choice between these two hypotheses relies entirely on the arbitrary drawing of the wings of the peaks and on the resolution of the spectra. Unfortunately, higher accuracy in this field is difficult to achieve, as it would require excessively long times to accumulate more scans in the

spectrometer, and a painstaking multiplication of experiments to broaden the statistical basis of the variance analysis.

#### IV-3-6 Conclusion: Tacticity control in SSP

The above discussion has established that poly-calcium acrylate follows a Bernoullian placement statistic in a first approximation, even though higher-order statistics may not be ruled out at the present time, owing to experimental limitations.

Regardless of which hypothesis one chooses to accept, a probability  $P_m$  of isotactic placement of slightly above 0.5 reveals that the orientation of a new adding monomer unit is nearly random. This, together with the fact that the values of  $P_m$  and  $\Delta(\Delta S)$  are the same for the solid-state polymer as for the polymers made in solution or in bulk establishes clearly the absence of topochemical control over the tacticity of the polymer.

Because a highly ordered crystalline lattice such as that of the dihydrate monomer fails to bring about any degree of observably significant order, and because local melting of the monomer is precluded by its extremely high melting point, one is led to envisage a sublimation-like diffusion of the monomer towards the growing chain or vice-versa, resulting in a random orientation of the adding monomer.

This polymerization model is supported by the crystallographic results (which show that polymerization cannot proceed in the perfect lattice) and by the Wide-line NMR results (which show the presence of a high-mobility phase in the polymerizing monomer).

#### IV-4 The molecular weight of the polymer and the chemical mechanism of polymerization

The knowledge of the molecular weight of the polymer produced by

SSP is vital to the understanding of the polymerization mechanisms.

However, more than the absolute value of the molecular weight itself, its distribution and its relative variations as a function of time, temperature and hydration level are likely to hold the clues leading to the mechanisms involved in SSP.

Accordingly, an investigation of the molecular weight distributions was undertaken by exclusion chromatography. However, this technique is only a method of separation, and gives by itself no measurement of the molecular weights. Exclusion chromatography needs therefore to be calibrated against samples whose molecular weights have been independently determined by other methods such as light scattering or viscometry.

#### IV-4-1 Molecular weights measurements by viscometry

In an attempt to obtain a calibration curve for the exclusion chromatography experiments to be presented in section IV-4-2, the viscometric analysis of a sample of poly-acrylic acid was undertaken. The sample was prepared from poly (calcium acrylate) as was described in the experimental section (II-10).

The viscometry was done in two solvent systems, p-dioxane and 0.2 N HCl, which have been reported to be Theta-solvents for poly-acrylic acid. Unfortunately, the relative scarcity of the data available in the literature and their questionable reliability will be seen to leave some degree of uncertainty as to the absolute value of the molecular weight found.

##### IV-4-1-a Viscometry in p-dioxane

Newman et al. <sup>(95)</sup> have found that poly-acrylic acids ranging from 134 to 1220 kg molecular weights exhibited a Theta-point at 30°C in p-dioxane.

A Theta-point is encountered in a polymer solution when the temperature and the solvent system are such that the interactions between the macromolecules and the solvent molecules are balanced with the interactions between the macromolecules themselves. As a result, the polymer chains assume a random coil conformation in a Theta solvent, and are characterized by an unperturbed dimension which is theoretically the same in all possible Theta solvents.

The Mark-Houwink viscometric constants were reported to be  $a = 0.50$  (as expected in a Theta solvent) and  $K = 85 \times 10^{-5}$  dl/g. However, Brandrup and Immergut<sup>(96)</sup> as well as Kurata and Stockmayer<sup>(97)</sup> quoted the value of  $76 \times 10^{-5}$  dl/g for K, although citing Newman et al. as their source. No explanation could be found for this discrepancy.

The dissolution of the sample in dioxane at  $30^{\circ}\text{C}$  was difficult. The swelling of a 0.26 g/100 ml suspension occurred easily, but even after stirring for one week, an apparently large quantity of insoluble gel had deposited on the walls of the flask. Upon close examination, refractive index irregularities were observed throughout the liquid, even though no individual particles could be distinguished. In an attempt to find a better dissolution temperature, it was found that the turbidity of the raw solution increased sharply outside the  $20-40^{\circ}\text{C}$  range, and that massive precipitation occurred outside the  $5-55^{\circ}\text{C}$  range. The solubility gap at this concentration is thus quite narrow.

Titration of the poly-acrylic acid by a standardized solution of sodium hydroxide was performed in order to measure the actual amount of undissolved polymer. The phenolphthalein end-point was found usable, although not very sharp. In order to improve the accuracy and the repro-

ducibility of the titration, two colour standards were made up with the same concentrations of all constituents as those used for the titration. One was left colourless and the other was an over-titrated pink sample. The end-point was assumed to have been reached when a colour intermediate between the two comparison standards developed and remained stable for one minute. This technique yielded very reproducible end-points.

It was used to titrate first 10 ml of the solution drawn in a syringe through an 8 microns paper filter, and subsequently to titrate 10 ml of the whole shaken gel suspension. Adding water to the titration vessel had no other effect than suppressing the milkiness resulting from the insolubility of the sodium salt in dioxane. The same concentration of 0.260 g/dl was found in either case.

This result indicates that the visual observation of a "large amount of gel" had been misleading, as the actual amount was not detectable within the 1% accuracy of volumetric titration.

This gel is thought to be due to either            crosslinking, or ionic interactions. Crosslinking is unlikely, since one would expect a crosslinked gel to be equally insoluble in dioxane and in the other Theta-solvent (0.2 N HCl aq.). However, it has only been observed in dioxane. On the other hand, a very small fraction of  $\text{Ca}^{++}$  ions remaining from an incomplete ion-exchange could easily account for the formation of a gel in dioxane and its solubility in the more polar aqueous solutions.

The relative viscosity of the unfiltered solution decreased markedly upon dilution (30% over one decade in concentration) and gave very scattered points.

The results of the viscosity measurements made on a filtered solution

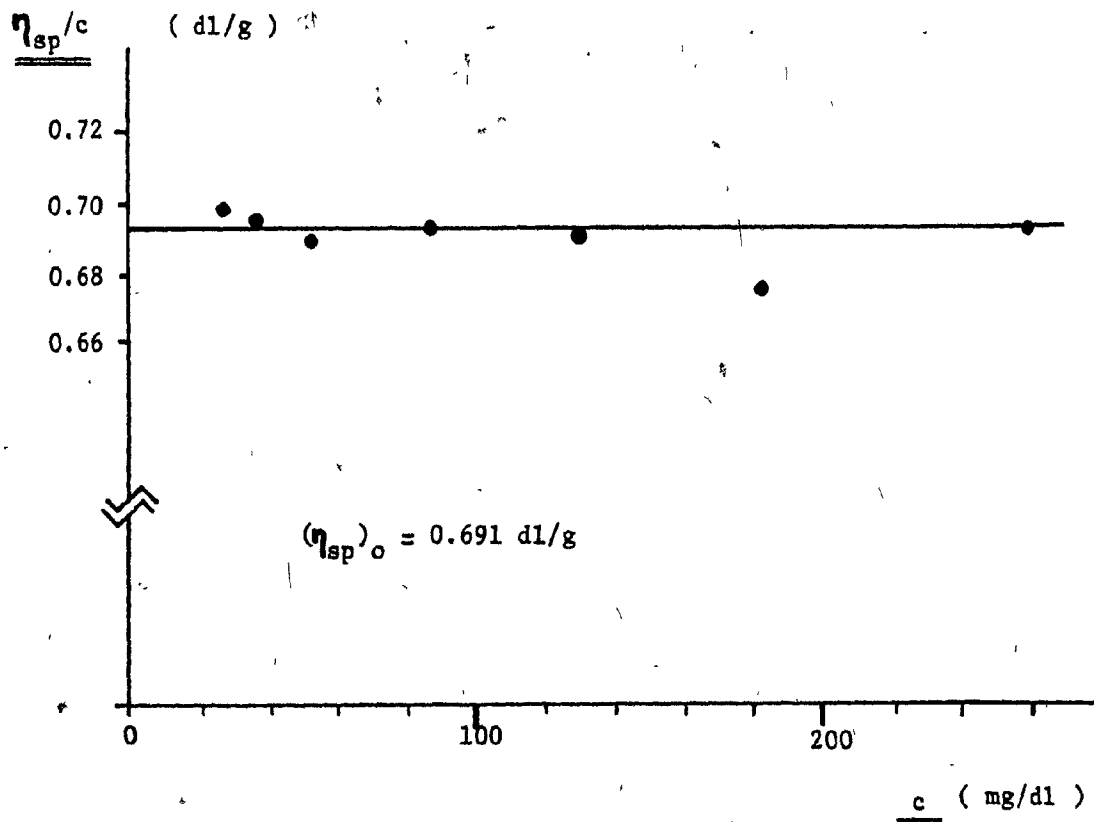


Fig. IV-4-1 : Viscometry of poly(acrylic acid) in p-dioxane at  $30.00 \pm 0.02^\circ\text{C}$

are shown on Fig. IV-4-1. A straight horizontal line is obtained, showing that the polymer is indeed at a Theta temperature. The limiting viscosity number was 0.691 dl/g, which corresponds to  $\bar{M}_v = 661$  kg according to Newman et al., and 827 kg according to either Brandrup and Immergut or Kurata and Stockmayer.

#### IV-4-1-b Viscometry in 0.2 N HCl

Silberberg, Eliassaf and Katchalsky<sup>(98)</sup> have studied polyacrylic acid in 0.2 N aqueous HCl by viscometry and light scattering over a range of 20-30°C. They found a Theta-temperature of 14°C in this solvent and reported the dissolution to have been difficult.

However, the dissolution of the solid-state post-polymer was quite easy (20 min at 25°C). The clear and homogeneous solution was filtered through an 8 microns paper filter before injection. The viscometric results at  $24.00 \pm 0.02^\circ\text{C}$  are shown on Fig. IV-4-2. The points give a good straight line fit of small positive slope (7% over one decade in concentration), showing the proximity to the Theta temperature. By extrapolation to infinite dilution, the limiting viscosity number was found to be 0.688 dl/g (it is interesting to note how close this value is to the previously measured 0.691 dl/g dioxane).

The concentration of the initial solution was found to be 2.292 g/l by two methods, gravimetry and titration. Silberberg et al. stated that gravimetry gave an 8-10% excess in concentration, because the very strongly bound water could not be removed by dessication. However, it was found that the evacuation of the freeze-dried poly-acid at 80°C for 2 hours gave a concentration value identical within experimental error to that measured by titration with sodium hydroxide to the phenolphthalein endpoint.

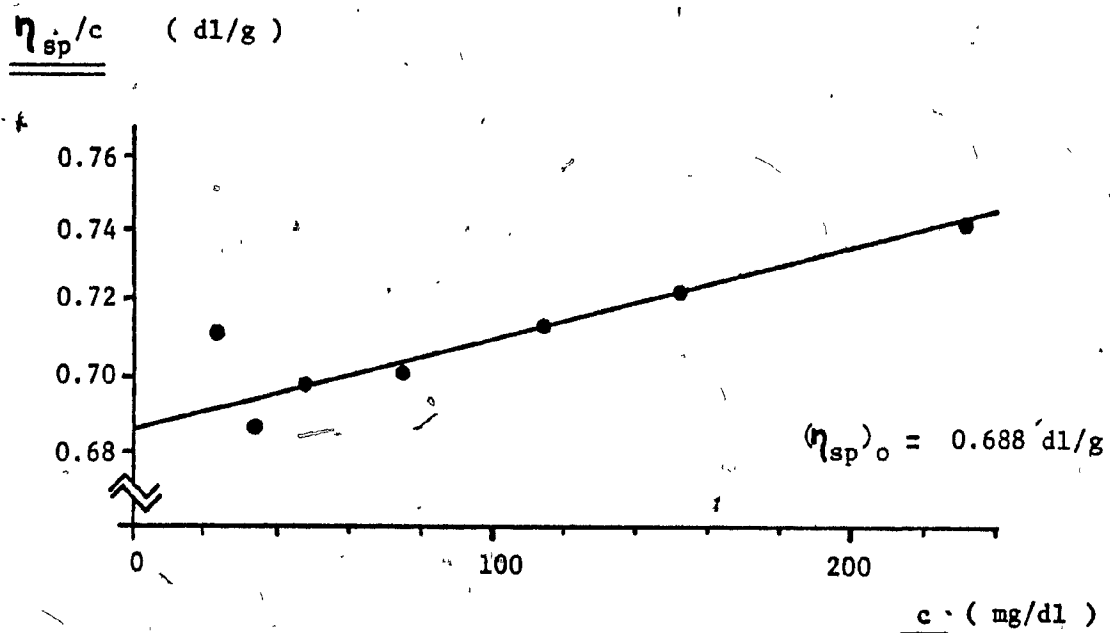


Fig. IV-4-2 : Viscometry of poly(acrylic acid) in 0.2 N HCl at  $24.00 \pm 0.02^\circ\text{C}$  /

In order to derive the molecular weight of the solid-state polymer from its limiting viscosity number, the data of Silberberg et al. were used. In so doing, three problems arose.

First, these authors measured the degree of polymerization of their sample (D.P. = 6000,  $\bar{M}_v = 430$  kg) as a  $\text{Na}^+$  salt in 2 N NaOH, using viscosity constants derived from a 1933 reference. The trustworthiness of constants determined in these indirect conditions is at least open to question. Indeed, it is to be noted that their molecular weight measured by light scattering was  $\bar{M}_w = 1.1$  Mg. As it is known that the viscosity molecular weight  $\bar{M}_v$  is usually much closer to the weight-average molecular weight  $\bar{M}_w$  than to the number average molecular weight  $\bar{M}_n$ , a rough estimate of the  $\bar{M}_n$  of Silberberg et al. would give a value between 10 kg and 50 kg. The polydispersity  $\bar{M}_w/\bar{M}_n$  of their sample would then have been between 110 and 22, which is unheard of for poly-acrylic acid synthesized by any known method.

Secondly, the viscosity data of Silberberg et al. show a rather large amount of scattering ( $\pm 7\%$ ) leading to a somewhat arbitrary extrapolation.

Thirdly, the reported difficulty in dissolving their sample might possibly be blamed on a crosslinked, ████████ or somehow impure sample.

Interpolating the limiting viscosity number between 20 and 30°C for Silberberg's sample gives a value of 1.58 dl/g. The value of K need not be known in this case, since it may be eliminated between the two Mark-Houwink equations:

$$[\eta_1]_{24^\circ\text{C}} = K \times M_1^a \quad \text{for Silberberg et al.}$$

$$[\eta_2]_{24^\circ\text{C}} = K \times M_2^a \quad \text{for this study}$$

$$\frac{M_2}{M_1} = \left( \frac{\eta_2}{\eta_1} \right)^{1/a}$$

Only "a" needs to be estimated. To a first approximation, a value of 0.6 may be used to account for the fact that the system is somewhat removed from the Theta condition. The calculated value for the solid-state polymer would then be around 108 kg/mole, which is unacceptably low when compared to the values inferred from the viscosity in dioxane and from Exclusion Chromatography.

In view of the severe limitations in the credibility of the data of Silberberg et al. it is suggested that unfortunately, although the results of the viscometry in HCl appear to be experimentally satisfying, they should not be taken into further consideration until reliable Mark-Houwink coefficients can be found.

#### IV-4-2 Molecular weights distribution measurements by Exclusion Chromatography

Exclusion Chromatography (E.C.) is a separation technique involving the sorting of the solute molecules according to their sizes. It involves the pumping of the solution at high pressure through columns filled with a

highly porous material similar to molecular sieves, or with an organic crosslinked polymer gel (Gel Permeation Chromatography).

The quantity actually measured by E.C. is the Stokes radius of the macromolecules. Large molecules cannot enter the pores and are quickly flushed by the eluant stream, whereas small molecules spend some time inside the pores and elute later. The Stokes radius depends on the molecular weight of the macromolecule and on its coefficient of expansion  $\alpha$ .

Because of that, the E.C. technique requires a calibration with samples of known molecular weights determined by another method, and places an alternative before the experimenter: either standard samples must be found that belong to the same chemical class as the unknown and which may safely be assumed to have the same expansion coefficient, or the expansion coefficients of both standards and unknowns need to be known, in order to apply the suitable correction.

Unfortunately, neither of these two methods could be successfully followed in the case of aqueous poly-acrylic acid, for the following reasons. First, well characterized samples of poly-acrylic acid to be used as standards for the present study could not be found anywhere in North America. Secondly, the values of the expansion coefficients in the aqueous solvent system selected were not available for the poly-acrylic acid and the standards chosen.

The selection of an aqueous solvent was regarded as mandatory at the time this study was initiated, in order to share the E.C. chromatograph with another member of this department whose polymers were insoluble in organic solvents. This person was planning to study the molecular weights distributions of several SSP systems similar to calcium acrylate, and the

comparison of all these results would have been highly informative.

Unfortunately, he abandoned the project after it was underway.

In order to circumvent the calibration difficulties mentioned above, one may take advantage of a "universal calibration method" developed by Benoit, and which is explained below. This method allows the use of standards and solvent systems different from the samples and solvents under analysis, by correlating their viscosity and molecular weight.

#### IV-4-2-a Benoit's calibration

For work in aqueous solutions, only two kinds of standards appeared to be available: biological material and Dextran. A great many globular proteins, enzymes or viruses such as ribonuclease, myoglobin, alpha-chymotrypsin, ovalbumin, tobacco mosaic virus etc. exhibit a good correlation between their molecular weights and Stokes radii. However, the most commonly employed standards are the Dextran, polysaccharides from Pharmacia Laboratories.

The characteristics of the five Dextran standards and the E.C. columns used have been described in the experimental chapter (II-11-f and -g).

The best attempt that can be made at using the Dextran as standards for the poly-acrylic acids involves the use of the "universal calibration method" developed by Benoit et al.<sup>(99)</sup> and reviewed by Coll and Gilding<sup>(100)</sup>. This method makes use of the fact that the hydrodynamic volume of a macromolecule in solution is proportional to  $[\eta] \times M$ , product of its intrinsic viscosity and molecular weight. A plot of  $\log([\eta] \times M)$  versus the elution volumes gives an empirical linear relationship for data obtained from a great many different types of polymers. Such a plot is shown on Fig. IV-4-3 for the Dextran, using the data given by the manufacturer.

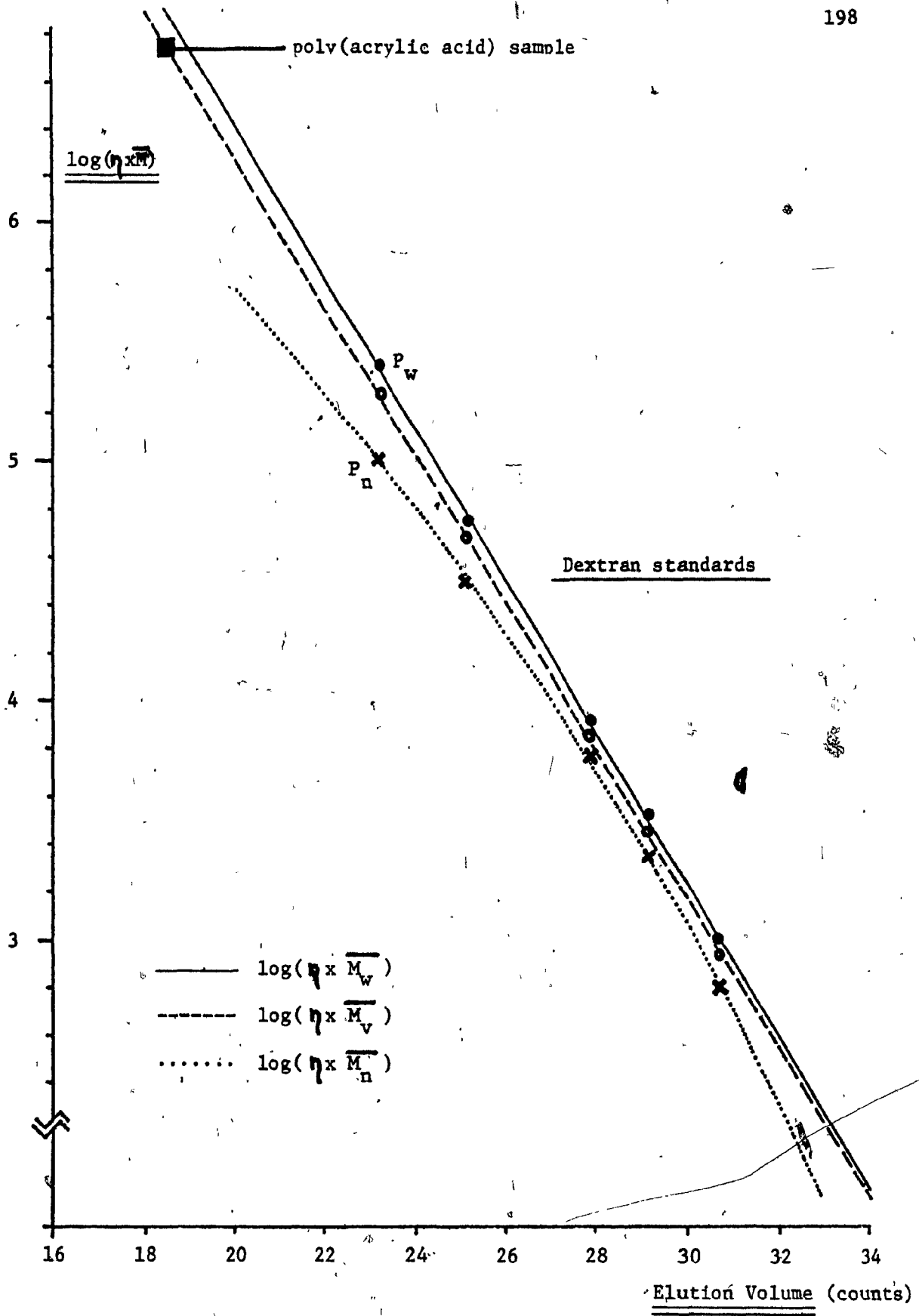


Fig. IV-4-3 : "Benoit calibration plot" for the Dextran standards .

The manufacturer's data were checked by measuring the intrinsic viscosity of the 35 kg Dextran. The value found agreed perfectly with the value given.

Some ambiguity arose when constructing the graph of Fig. IV-4-3, because the Dextrans exhibited broad molecular weights distributions. E.C. measures essentially  $\bar{M}_V$ , whereas only  $\bar{M}_W$  and  $\bar{M}_n$  were given, and they were different by as much as a factor 2.5.

These three molecular weights averages are defined as follows:

$$\bar{M}_n = (\sum N_i M_i) / \sum N_i = \text{Number average}$$

$$\bar{M}_W = (\sum N_i M_i^2) / \sum N_i M_i = \text{Weight average}$$

$$\bar{M}_V = \left[ (\sum N_i M_i^{1+a}) / \sum N_i M_i \right]^{1/a} = \text{Viscosity average}$$

where  $N_i$  is the number of molecules of molecular weight  $M_i$ , and  $a$  is the exponent in the Mark-Houwink equation.

The value of  $\bar{M}_V$  is nearer to  $\bar{M}_W$  than to  $\bar{M}_n$ , and accordingly, the viscosity-average molecular weights have been represented in a first approximation on Fig. IV-4-3 by points dividing the segments  $P_W P_n$  in a ratio of one to three. In accordance with Benoit,  $\log (\eta \bar{M}_V)$  was found to be perfectly linear with the E.C. elution volumes.

The viscosity of the poly-acrylic acid sample (P.A.A.), already measured in dioxane and 0.2 N HCl, needed to be measured again in the phosphoric buffer at pH 3 used throughout the E.C. experiments. The results are shown on Fig. IV-4-4.

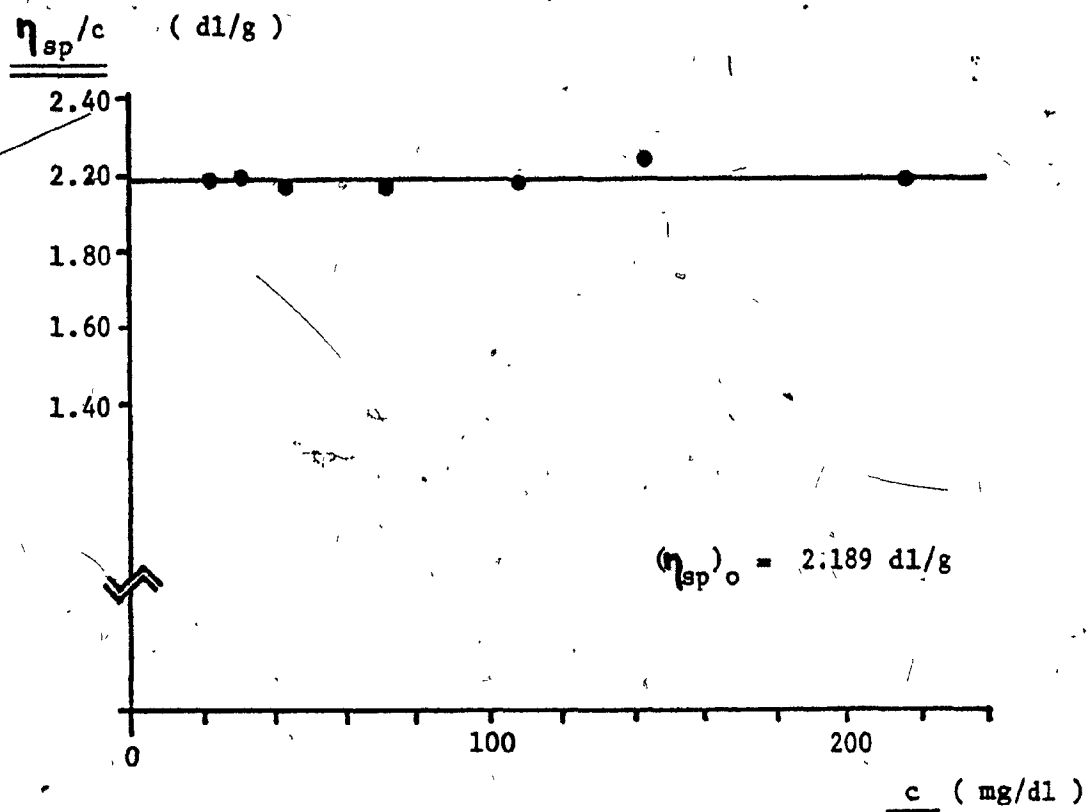


Fig. IV-4-4 : Viscometry of poly(acrylic acid) in the phosphoric buffer used for the exclusion chromatography experiments ( pH 3 and  $24.00 \pm 0.02^\circ\text{C}$  )

The intrinsic viscosity in this solvent was 2.19 dl/g compared to 0.69 dl/g in the other two. This three-fold increase is believed to reflect a more extended conformation of the macromolecule. Indeed at pH 3, the acidity of the solution is much less than in the 0.2 N HCl (pH = 0.7) and this probably allows sufficient ionization of the polyacid to provoke coulombic repulsion between adjacent carboxylate ions.

Using the "Benoit calibration plot", the apparent molecular weight of the P.A.A. sample was then calculated:

$$\bar{M}_V = (1/\eta) \times 10^{6.72} = 2.4 \text{ Mg}$$

This is much larger than the  $\bar{M}_V$  previously measured in dioxane.

This surprising result is thought to be possibly due to interference from adsorption of the Dextran onto the highly divided glass surface. A series of tests were performed to verify this hypothesis. In order to determine the "total permeation volume" of the columns, light monomeric substances were suitably diluted and injected. The retention times were soon found to vary enormously with the chemical nature of these compounds, as is shown diagrammatically on (Fig. IV-4-5). It is clear that the elution order does not follow the order of decreasing sizes, but that the presence of alcohol and particularly of ether functional groups tends to delay the elution because of surface adsorption.

This effect caused a delay ranging between one and five counts compared to the elution volume of calcium acrylate. The oxyhydril- and ether-rich Dextran could thus be delayed by adsorption onto the glass substrate, and artificially shift the calibration curve so as to give apparent molecular weights anywhere between 2 and 17 times heavier than the true ones.

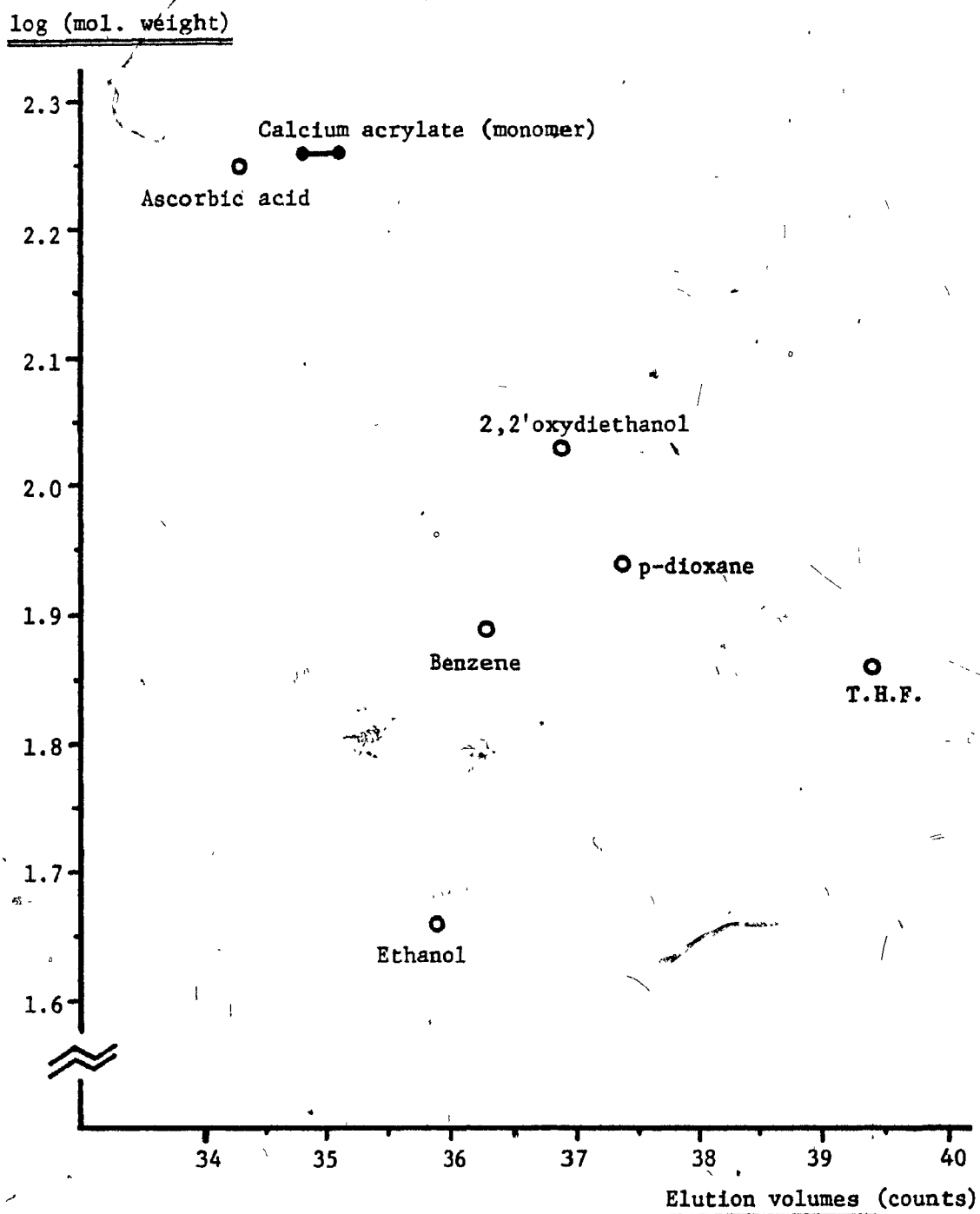


Fig. IV-4-5 : Effect of the chemical nature of the solutes on their elution volumes, in exclusion chromatography over porous glass columns .

As a consequence, the use of Dextrans in the conditions of this study seems to be able to yield deceitful results when the traditional procedures are followed.

In order to circumvent this difficulty, an attempt was made at modifying Benoit's method the following way. The  $\log(\overline{M}_V)$  of the Dextrans were derived from the Benoit's curve of Fig. IV-4-3, and plotted on Fig. IV-4-6 as a function of the elution volumes. A straight line was obtained, which was linearly translated until it passed through the point P defined by the observed elution volume (18.5 counts) and the molecular weight of the P.A.A. sample measured earlier. This molecular weight was derived from the dioxane viscosity data only, and arbitrarily taken as the average of the  $\overline{M}_V$ 's calculated using Newman's constant (661 kg) and Brandrup / Kurata's constant (827 kg), i.e. 744kg.

A justification of this procedure may be found by noting how close the resulting calibration curve passes to the point obtained experimentally for the monomer. Consequently, it is believed that the curve on Fig. IV-4-6 comes as close to a true calibration curve as could be obtained, and is even quite accurate for molecular weights ratios and relative comparisons, although the accuracy of absolute values read from it should still be considered with some caution for the reasons explained above.

#### IV-4-2-b $\overline{M}_V$ distributions of polymers from dihydrate in vacuo and in air

---

The curves of the polymerization yields versus time are first shown on Fig. IV-4-7 for the samples in vacuo and in air. They illustrate the absence of anomalies during these two runs, and reveal the 70% inhibition achieved in the presence of oxygen.

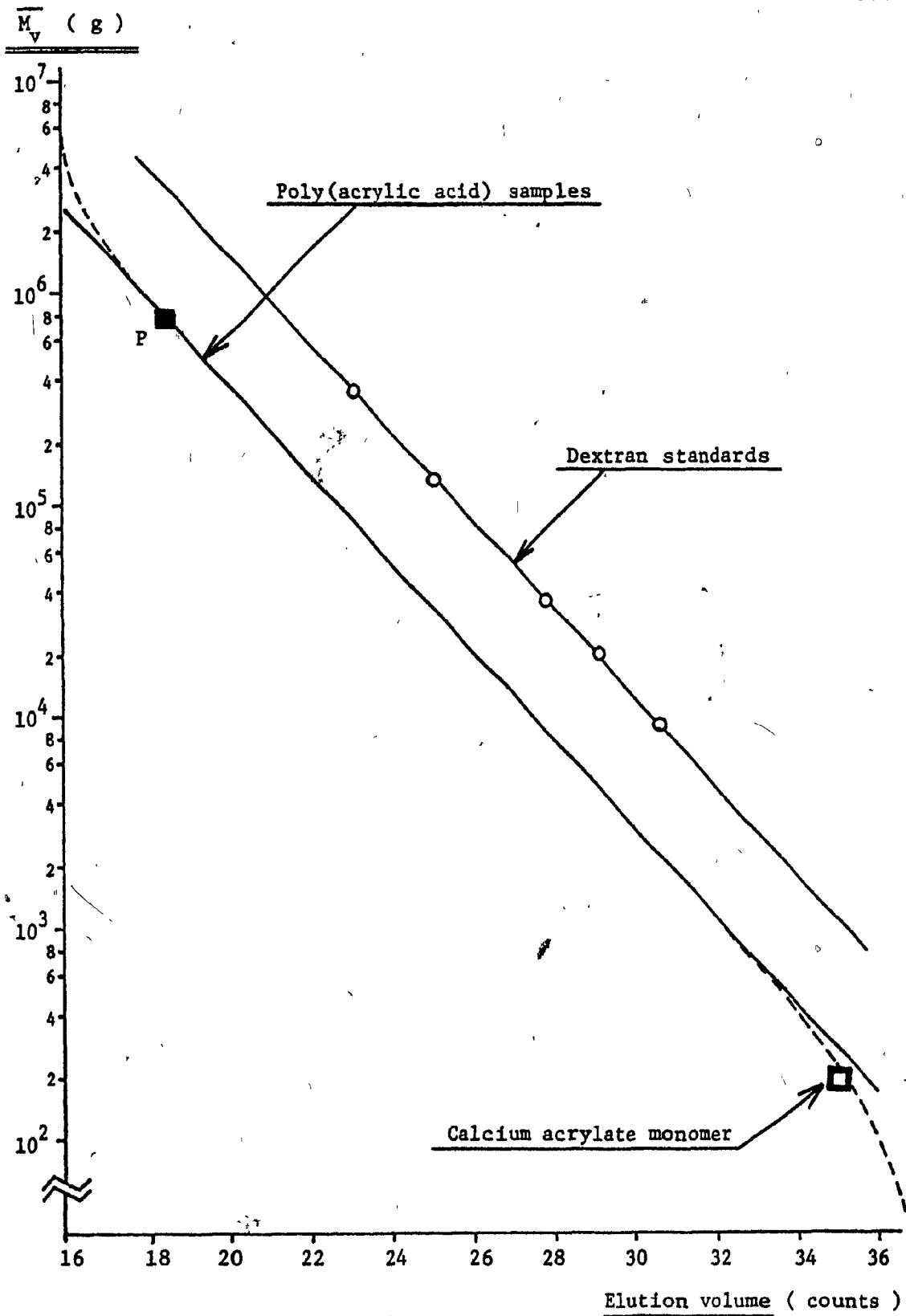


Fig. IV-4-6 : Practical molecular weights calibration curve for the exclusion chromatography experiments , at 25°C in the pH 3 buffer .

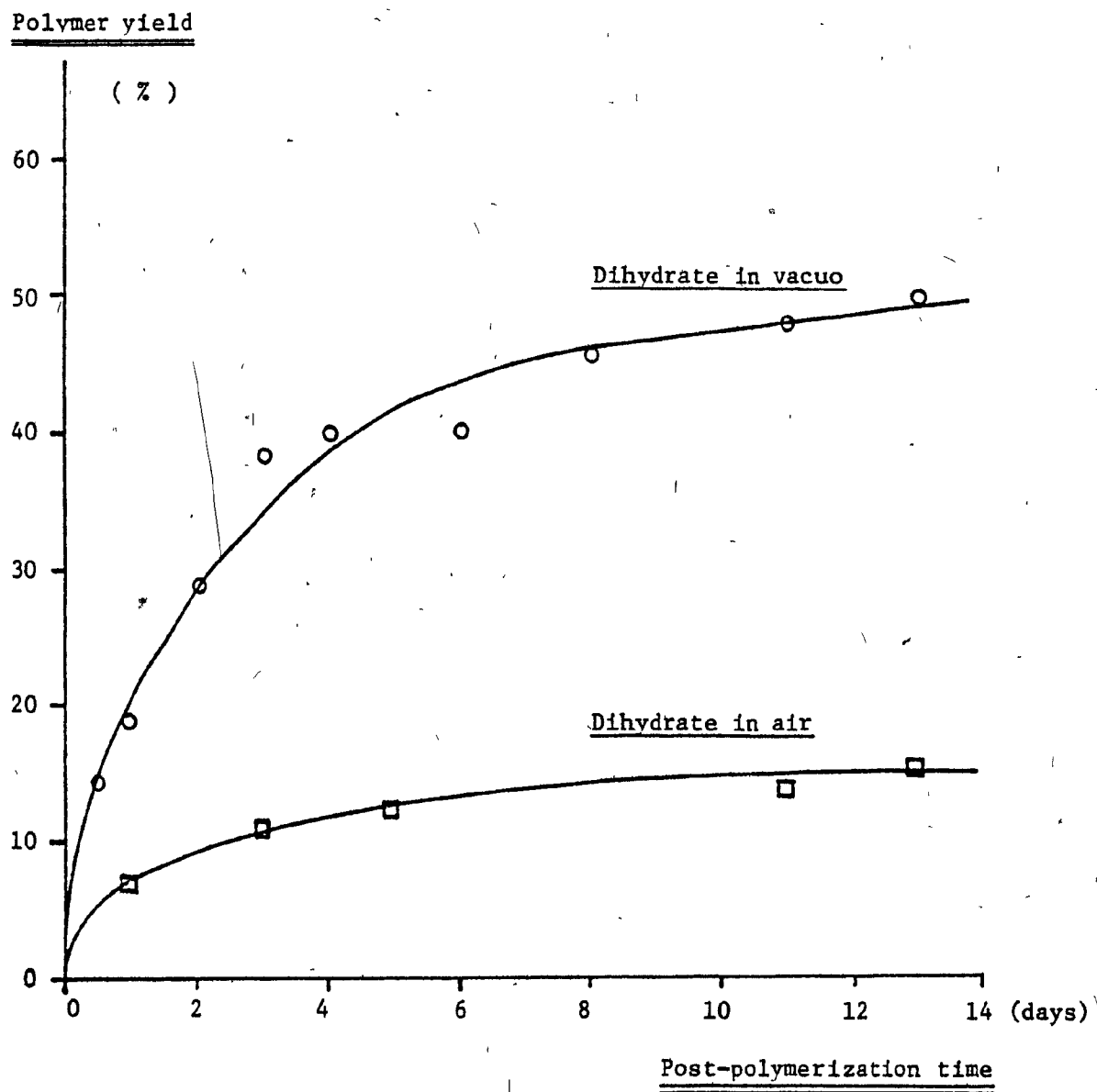


Fig. IV-4-7 : Polymerization curves of calcium acrylate dihydrate in vacuo and in air . Conditions : 0.95 Mrad at  $-78^{\circ}\text{C}$  , post-polymerization at  $50^{\circ}\text{C}$  .

The exclusion chromatograms of the same samples are shown on Fig. IV-4-8 in vacuo and Fig. IV-4-9 in air, and exhibited notable differences of considerable interest. Little variation was observed from 15 hrs to 14 days post-polymerization, and the patterns comprised basically three features.

(1) The very small peak around 32 counts is probably due to a small quantity of oligomers, or of impurities released by the resin during the ion-exchange processing step.

(2) The main peak of the P.A.A. samples in vacuo shifted only little with time, as illustrated on Fig. IV-4-10.

Over an initial period of two days, the molecular weight increased slightly with time (200 kg to 600 kg). The curve then leveled off abruptly, with little change being observed for the remaining 12 days. It is to be noted that this abrupt bend bears no resemblance to the smooth curvature of the yield plot over the full 14 days period, and that the molecular weight extrapolated to zero time is not zero, but instead a high value of 200 kg. The polymer made "in-source" could not be analysed, because the yield was too low to be practically usable.

From this, it can already be concluded that for the dihydrate in vacuo:

- The propagation step proceeds very rapidly until 200 kg Molecular Weight is reached.

- Until approximately 50% of the limiting conversion is reached, the growth of the polymer is limited by a combination of initiation and propagation kinetic factors. However, the disruption of the lattice may play an important role as propagation proceeds during this phase, influ-

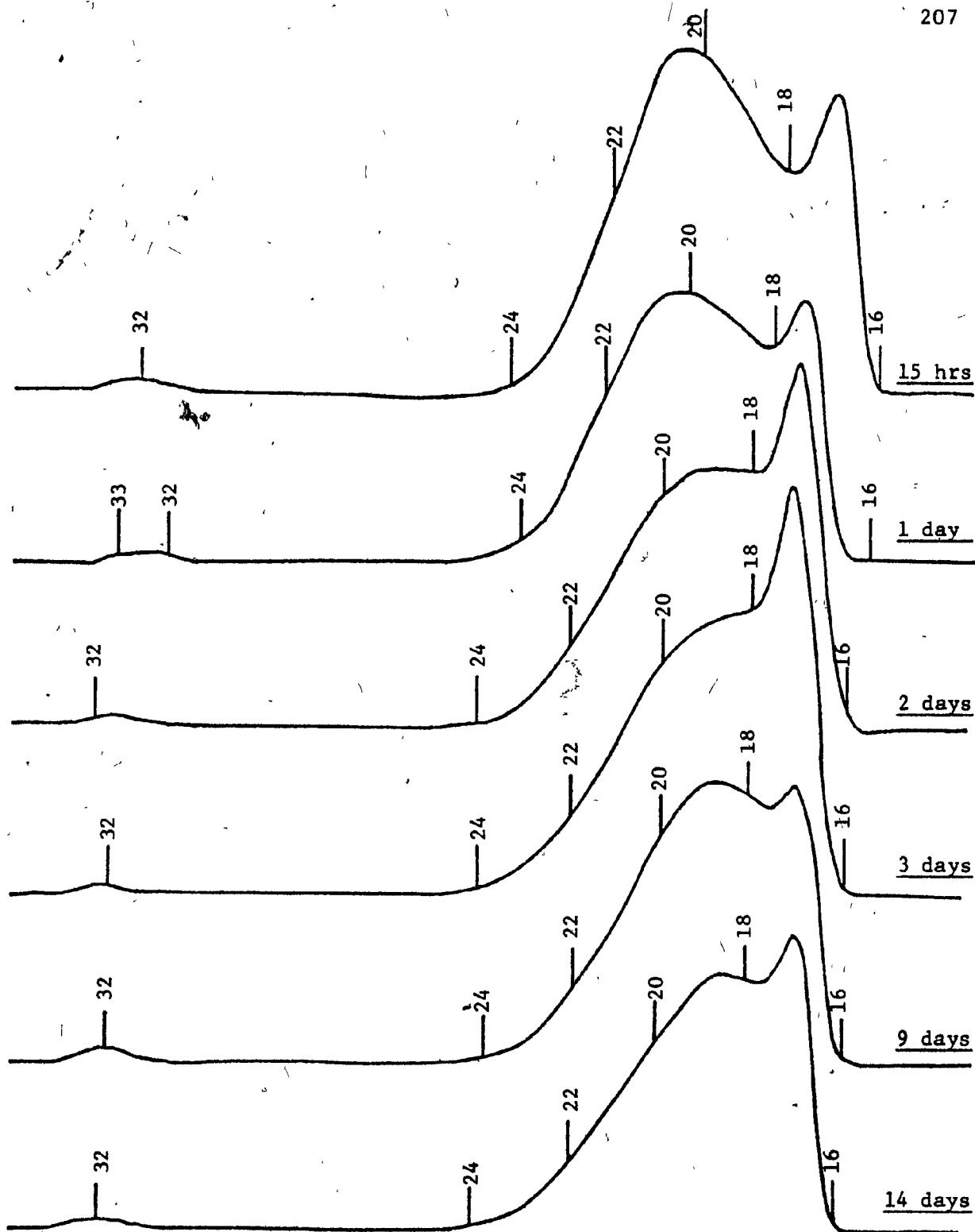
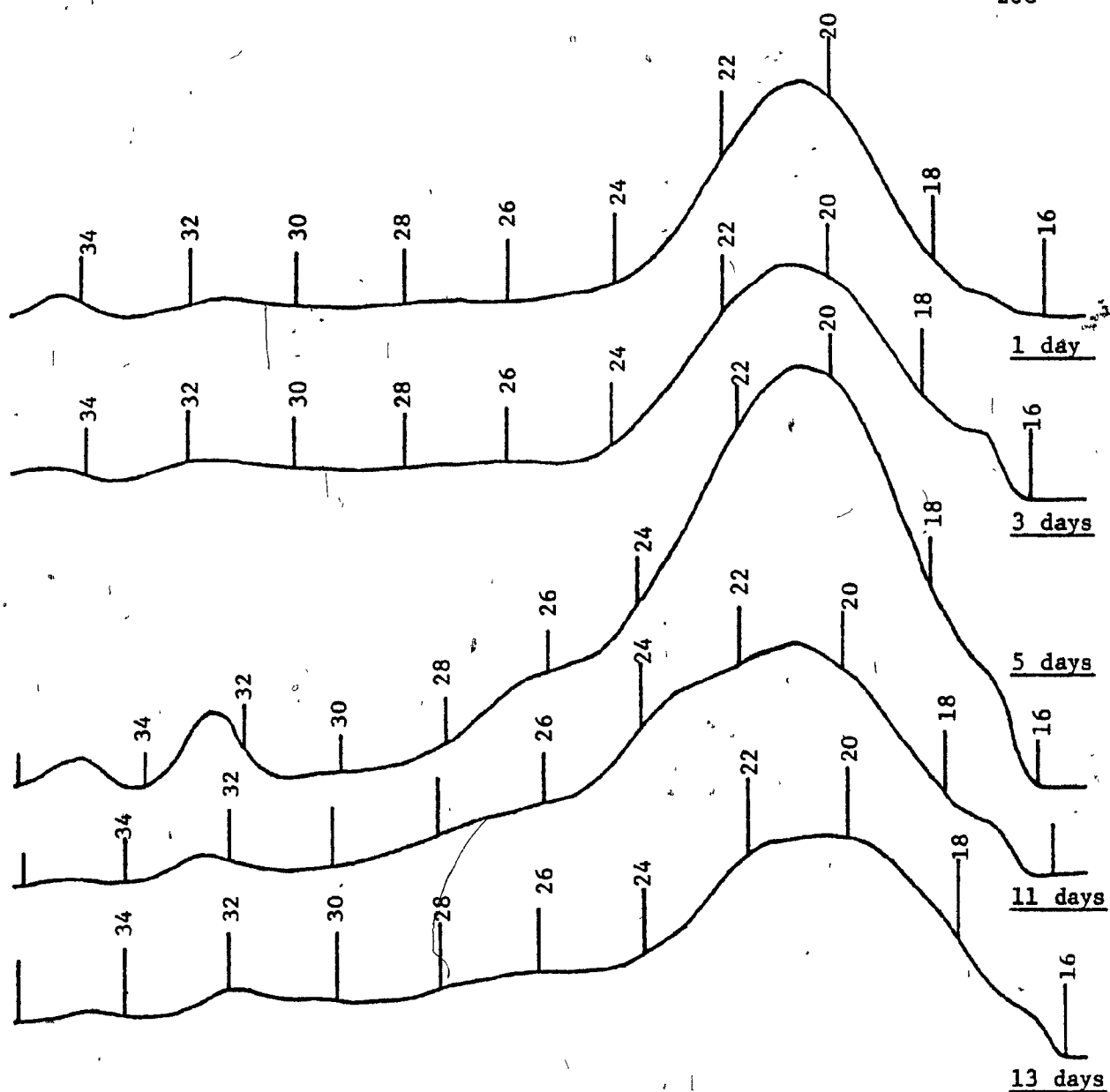


Fig. IV-4-8 : Exclusion chromatograms of polyacids from dihydrate in vacuo , after various times of post-irradiation polymerization at 50°C .



**Fig. IV-4-9 :** Exclusion chromatograms of polyacids from dihydrate in air ,  
after various times of post-irradiation polymerization at 50°C .

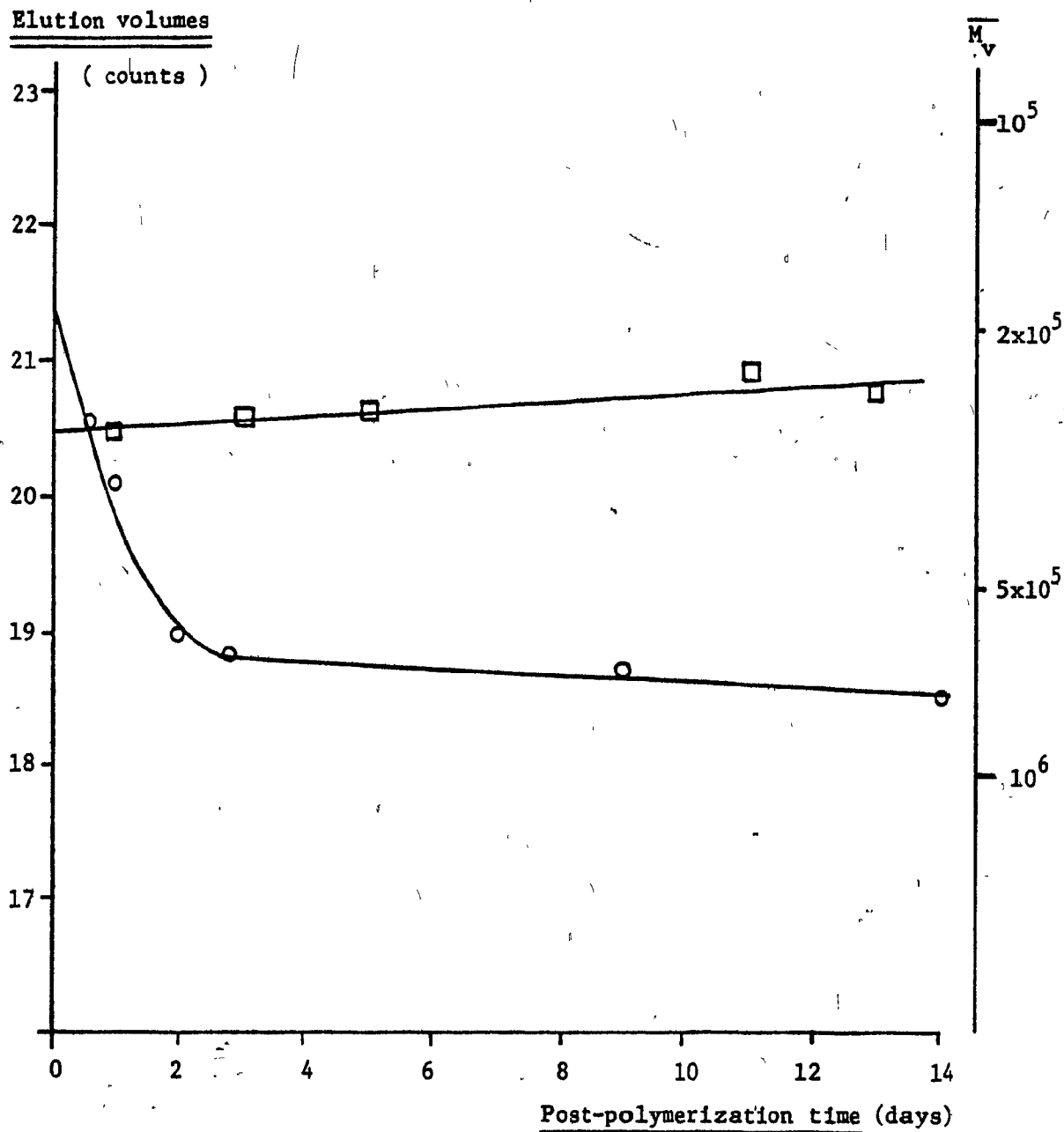


Fig. IV-4-10 : E.C. elution volumes as a function of post-polymerization times. Molecular weights estimated from Fig. IV-4-6 are shown on the right-hand scale.

- polyacid from dihydrate in vacuo (main peak only)
- polyacid from dihydrate in air (main peak only)

encing the initiation rate. The resulting kinetic equations are likely to be very complex.

- The last 50% of the limiting conversion are accomplished solely by increasing the number of chains, but not their length. The growth is then initiation-limited, with the attending simpler kinetic scheme.

(3) On most chromatograms displayed, a shoulder or a sharp peak may be seen at 16.5-17 counts. This is an artefact due to the sharp exclusion limit of the columns. Even the largest pores used (1422 Å) were still too narrow to separate the highest molecular weight fractions. All macromolecules larger than about 2.5 Mg (16 counts) were thus totally excluded from the pores, and massed up around 17 counts. The use of a larger pore column (2000 Å) effectively suppressed this artefact, but degraded the resolution of the other columns so much that it was abandoned.

However, by comparing the chromatograms for the one-day old dihydrate in vacuo and in air, it is obvious that the aforementioned "exclusion artefact" cannot explain all the difference between the two line shapes. Both main peaks are centered on 20.4 counts (302 kg) and the "in air" curve is a symmetric Gaussian with a normal, very weak artefact shoulder around 17 counts (1.5 Mg). Because the exclusion artefact peak on the "in vacuo" curve is stronger by a factor 10 than in air, it indicates that there is a non-gaussian distortion of the main peak on the high-molecular weight side. This is believed to come from an unresolved second gaussian component in the "in vacuo" curves, centered around 16.5 - 17.5 counts, and of an intensity approximately 1/3 of the main component.

On the other hand, the dihydrate in air exhibited a behaviour dif-

ferent from that in vacuo. The initial chromatograms showed a single, symmetrical Gaussian main peak. The exclusion artefact was only a very small shoulder on the far end of the wing. This indicates the absence of the second Gaussian component observed in vacuo.

The overall distribution is thus actually binodal in vacuo, representing two different mechanisms at work in the solid-state polymerization. The selective inhibition of the higher  $\bar{M}_v$  node by oxygen is a strong argument in favour of the existence of an ionic mechanism for the lower node, in addition to the traditionally accepted radical one, and will be discussed further later (IV-4-3).

Contrary to the in vacuo dihydrate, the peak maximum did not shift appreciably with time, but remained constant at 20.6 counts (260 kg). Rather, all the lower molecular weights down to the oligomers gradually increased their concentrations with time. Two shoulders developed progressively at 22 and 26 counts (100 and 20 kg resp.).

It is not clear yet whether the presence of oxygen promotes the formation of such low degree of polymerization components by a chain transfer mechanism, or whether these are produced during the post-recovery stages. It is very possible that heavy macromolecules containing one or more peroxy-ether internal links could be hydrolyzed into smaller fragments during the ion-exchange acidic treatment or in the pH 3 buffer solution. To distinguish between these two possibilities, experiments should be conducted by carrying out a deliberate, controlled, hydrolysis with radio-labelled reagents before the ion-exchange, and then counting the activity incorporated into the end-groups.

However, the fact that the molecular weights of all these samples

were found to increase very little if at all with time suggests that there should be no reason to have more peroxy-ether hydrolyzable links per chain at long times than at short times. Therefore, the intermediate molecular weights appear to have been actually formed during the SSP stage itself.

Finally, an informal analysis was made of a polymer formed from heavy-water dihydrate at the occasion of the Mass Spectrometry experiments. The conditions were different (2.25 Mrad irradiation, 8 days post-polymerization at 22°C in vacuo), but nevertheless, the results were found to be similar to those of the regular samples.

IV-4-2-c IV distributions of polymers from anhydrate in vacuo and in air

The exclusion chromatograms obtained were found to be qualitatively very similar to those of the dihydrate samples, but with remarkable quantitative differences.

The anhydrate in vacuo (Fig. IV-4-11) gave a binodal distribution, as in the case of the dihydrate. However, the two nodes were much better resolved and of comparable intensity. The lower  $\bar{M}_v$  node was found around 22 counts (138 kg), and the higher one around 17.5 counts (1 Mg), but it was difficult to measure accurately because of the exclusion artefact.

The anhydrate in air (Fig. IV-4-12) gave a monodal distribution, as did the dihydrate. It was centered around 22.2 - 23 counts (126-86 kg), except for the in-source sample which stood apart at approximately 17.5 counts (1 Mg). Again, as for the dihydrate, the shape of this distribution was Gaussian at short times, and became distorted by the presence of an increasing amount of low-molecular weight fractions at longer times.

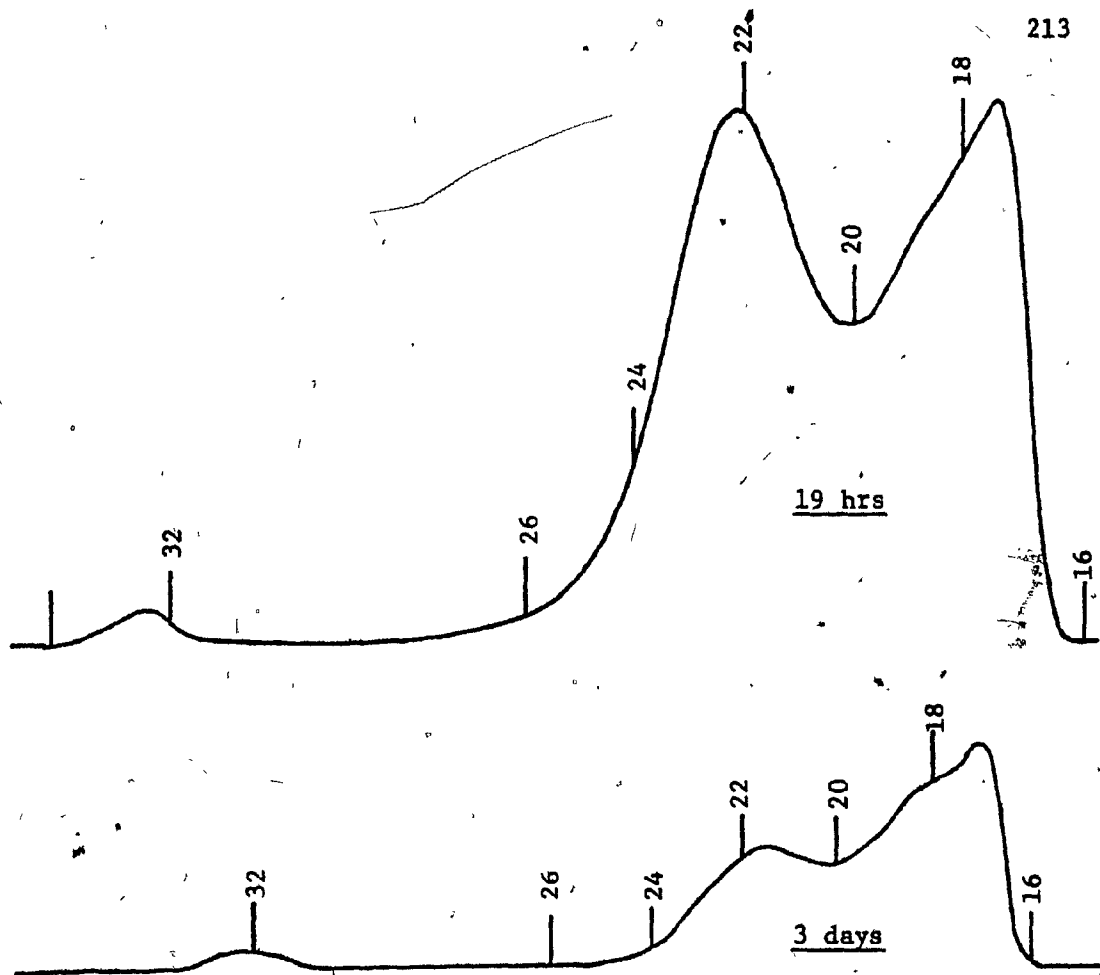


Fig. IV-4-11 : Exclusion chromatograms of polyacids from anhydrate in vacuo ,  
 after various times of post-irradiation polymerization at 50°C .

continued ../..

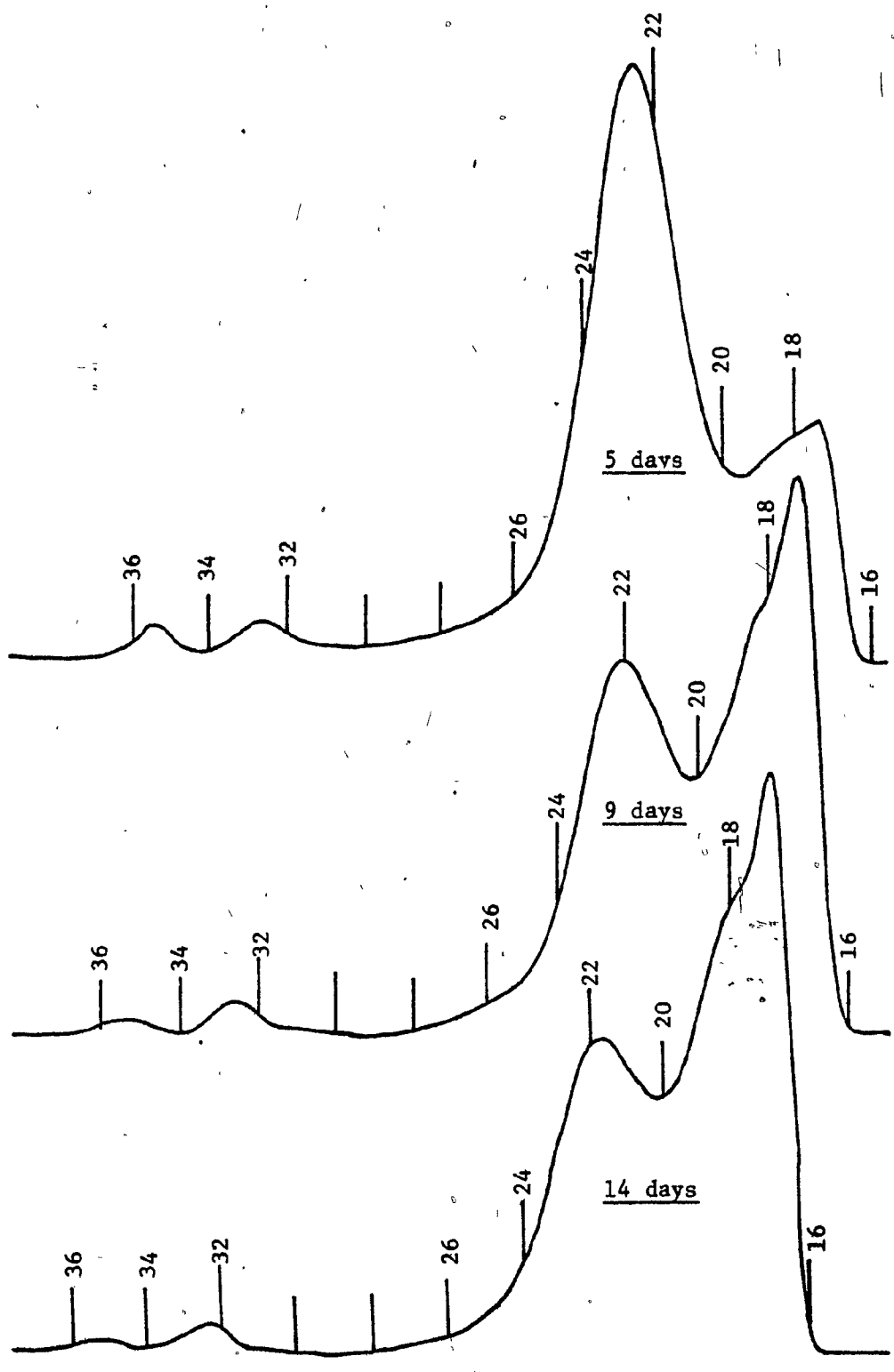


Fig. IV-4-11 (continued) : Exclusion chromatograms of polyacids from anhydrate in vacuo after various times of post-irradiation polymerization .

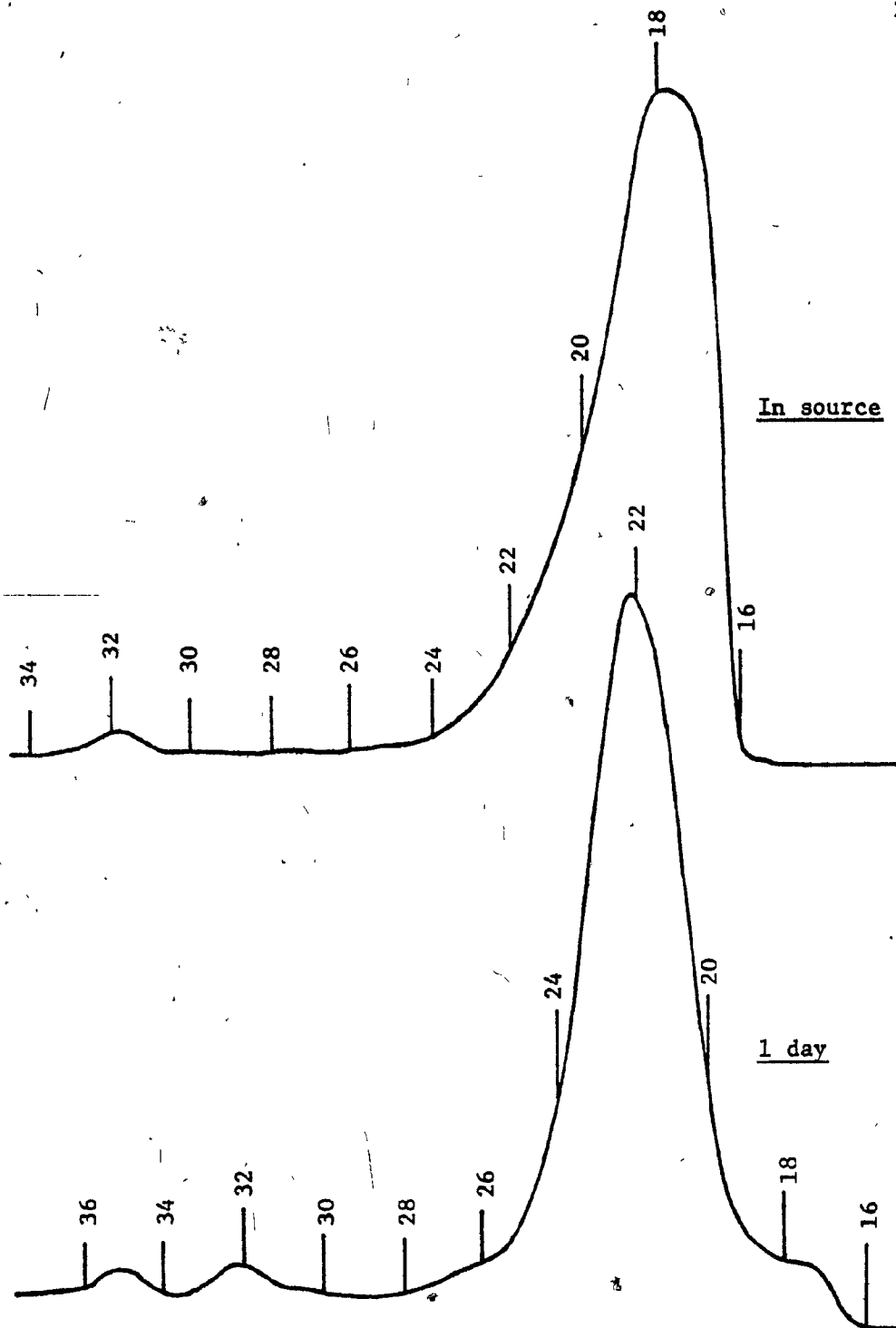


Fig. IV-4-12 : Exclusion chromatograms of polyacids from anhydrate in air ,  
 after various times of post-irradiation polymerization at 50°C .

continued ..//..

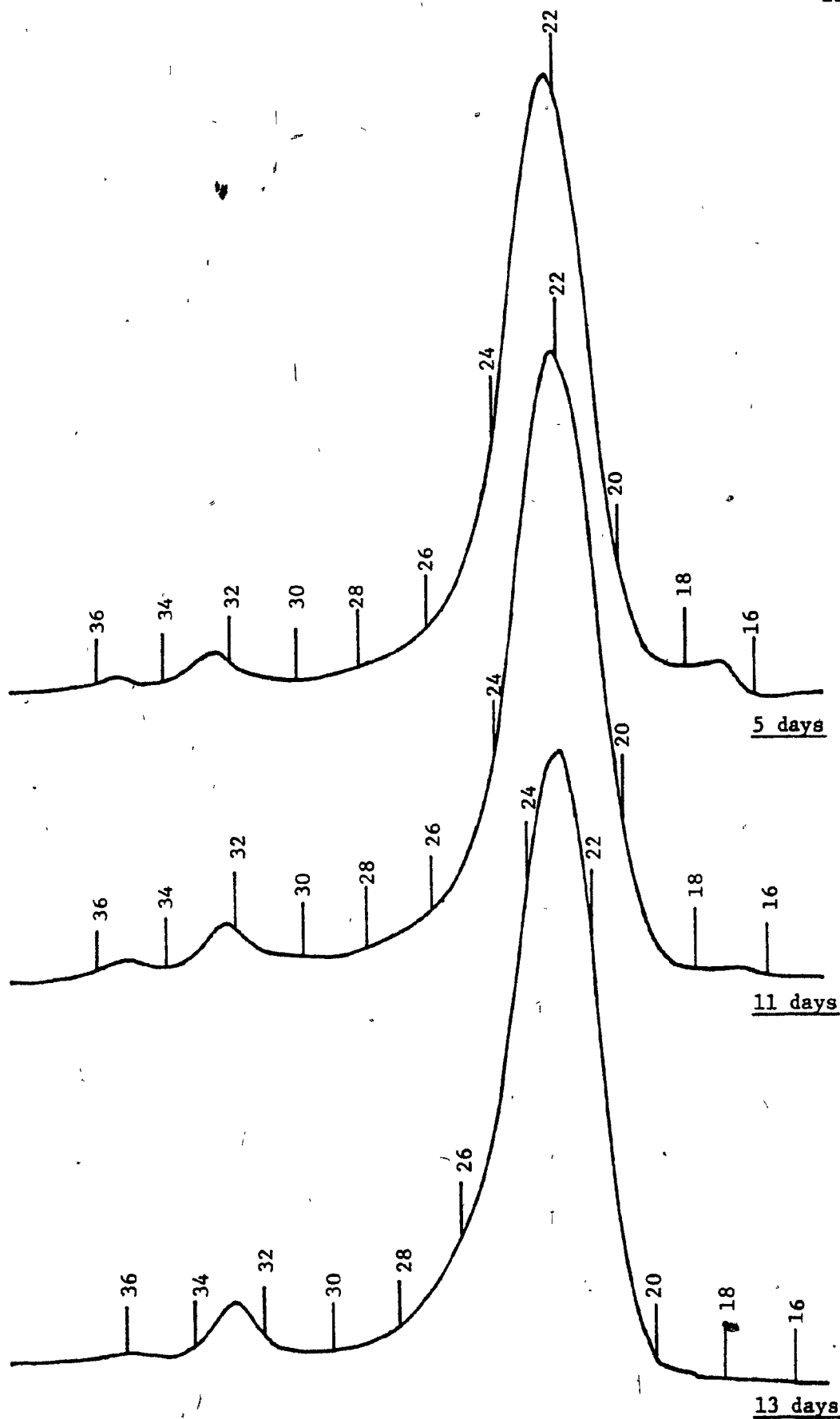


Fig. IV-4-12 (continued) : Exclusion chromatograms of polyacids from anh. in air

The two small shoulders observed in the dihydrate were absent in the anhydrate, however.

The evolution of the molecular weights with time is illustrated on Fig. IV-4-13. All peaks maxima remained at the same position during the whole polymerization time, except at zero time (in-source), where the molecular weight was markedly higher. This constancy of the  $\overline{M}_V$  held to a much greater extent than for the dihydrate samples, where the  $\overline{M}_V$  were seen to completely stabilize only after two days.

Contrary to the dihydrate samples, the anhydrates gave rise to an unusual variability in the polymer yields (Fig. IV-4-14) and in the shape of the chromatograms (Fig. IV-4-11). An explanation for these inconsistencies will be proposed below, along with the interpretation of the molecular weights distributions.

#### IV-4-3 Conclusion : chemical polymerization mechanisms and kinetic parameters

---

##### IV-4-3-a Chemical polymerization mechanisms

One feature of the exclusion chromatography results emerges as being of capital significance : the presence of binodal distributions. In vacuo, both the dihydrate and the anhydrate samples exhibited two peaks, representing molecular weights differing by as much as an order of magnitude. In itself, this finding is considered a very strong indication that at least two different mechanisms of polymerization are at work in the CaAc system.

But the observation that air inhibited selectively the higher  $\overline{M}_V$  peak in both samples strongly supports this conclusion as well, and points towards an ionic mechanism as the one responsible for the lower  $\overline{M}_V$  peak, which remained little affected by oxygen.

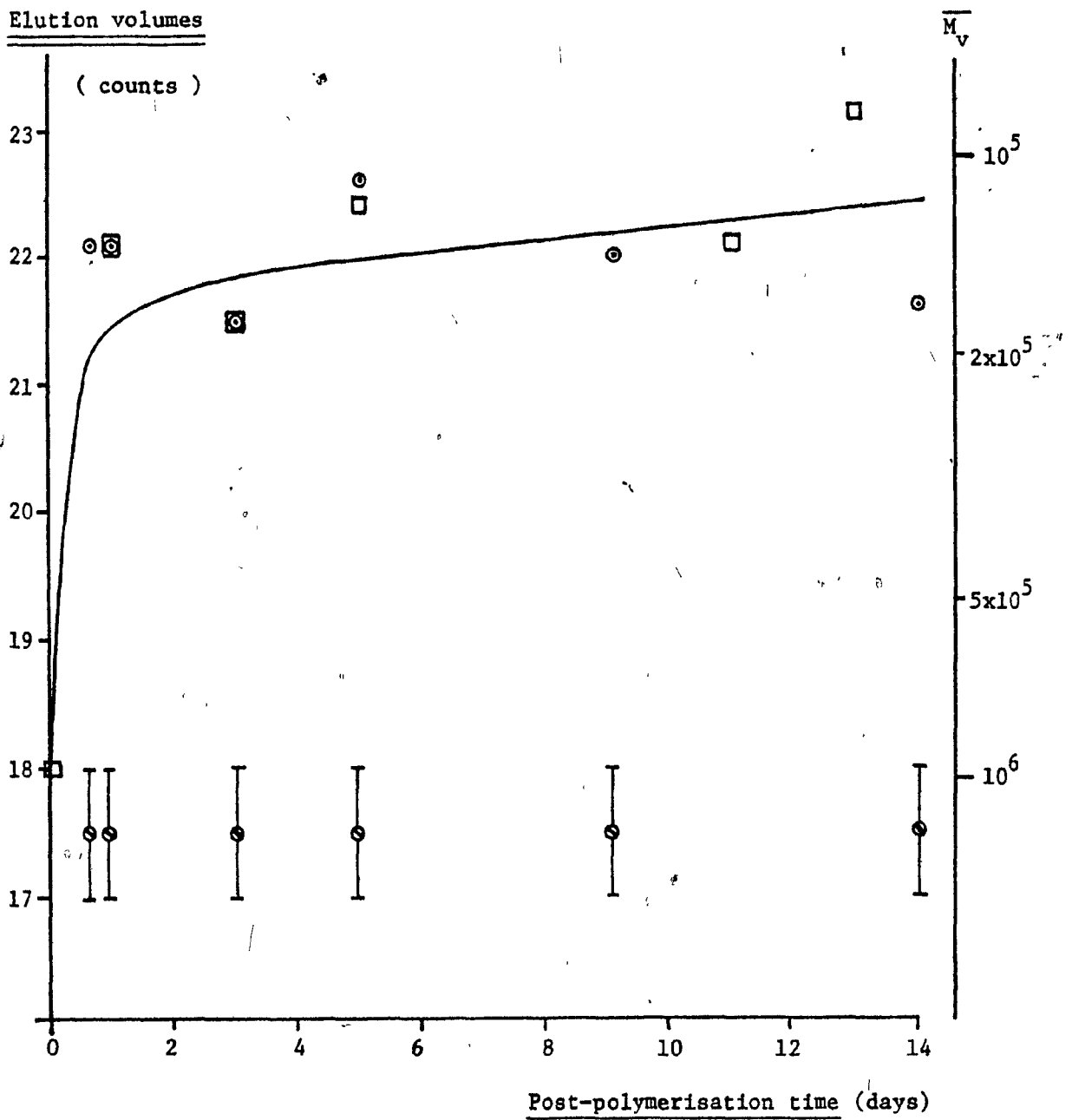


Fig. IV-4-13 : E.C. elution volumes as a function of post-polymerization times.

Molecular weights estimated from Fig. IV-4-6 are shown on the right-hand scale.

- ⊙ ⊙ polyacid from anhydride in vacuo (both peaks shown)
- polyacid from anhydride in air (main peak)

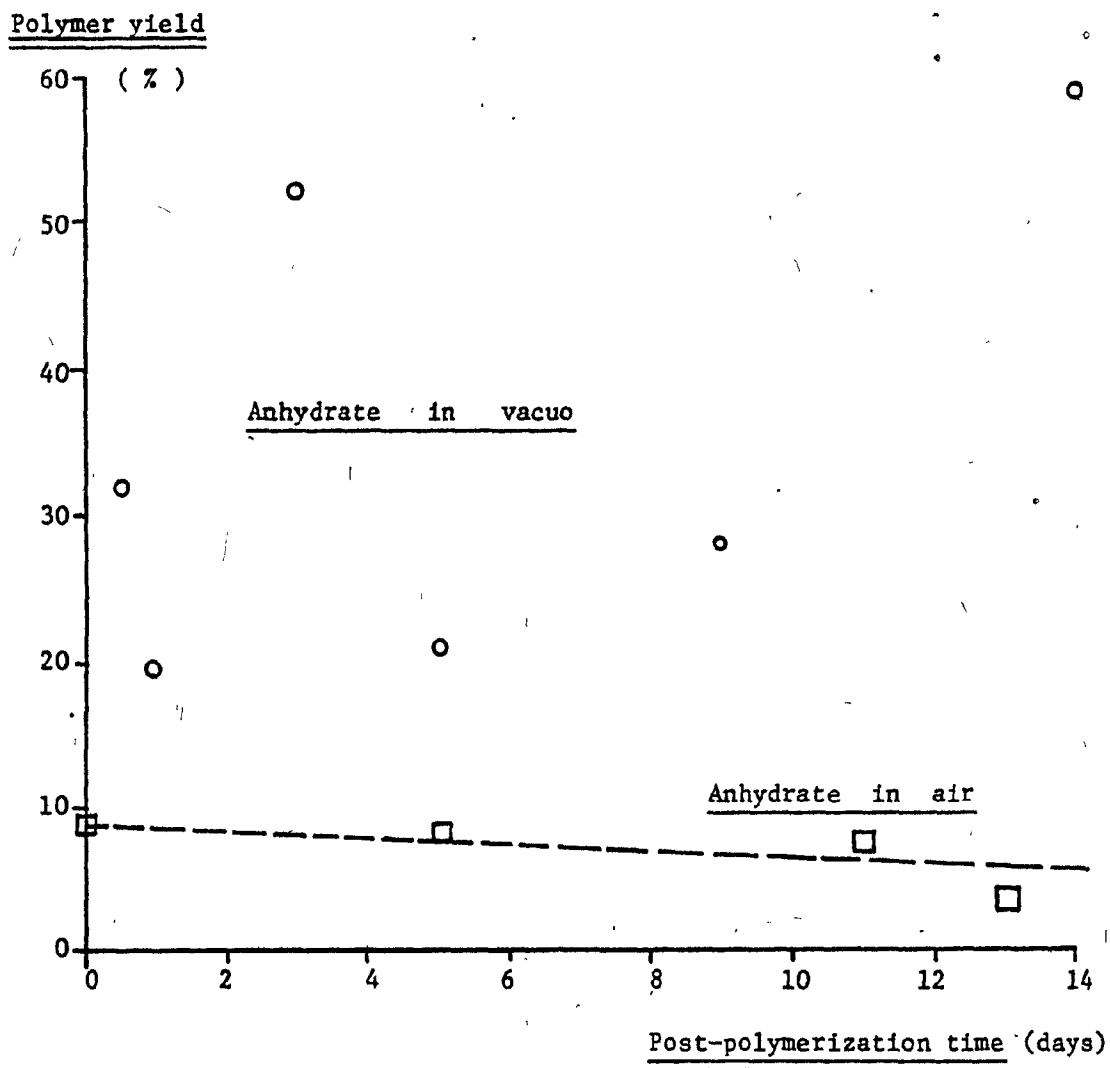


Fig. IV-4-14 : Polymerization curves of calcium acrylate anhydrate in vacuo and in air . Conditions : 0.95 Mrad at  $-78^{\circ}\text{C}$  , post-polymerization at  $50^{\circ}\text{C}$  .

Further support comes from the fact that oxygen, although able to diffuse totally and rapidly through the anhydrate, failed to provoke a total inhibition (Fig. IV-4-14) whereas it was able to do so in the 0.5 hydrate<sup>(84,85)</sup>. Furthermore, Watine<sup>(85)</sup> has observed a surprising effect of  $N_2O$  (which is an ionic inhibitor) whereby the polymer yield of the dihydrate was enhanced 25% over the yield in vacuo .

The unusual variability in the yields and  $\overline{M}_v$  distributions shapes of the anhydrate samples is also considered to reflect the existence of an ionic mechanism . Small differences in water content between regular dry and carefully prepared "super dry" monomers are known to profoundly affect ionic polymerizations<sup>(32,60-65,111)</sup>. The absence of these inconsistencies in the dihydrate is perfectly logical, since water is present there in a large excess anyway . This remark suggests that further experiments should be performed to compare the behaviour of "dry" and "super dry" anhydrates .

In source at  $-78^\circ C$ , the molecular weight of the polymer was found to be an order of magnitude larger than that of polymers made at  $50^\circ C$  at any later time . Costaschuk<sup>(84)</sup> also measured that the yields in source at  $-78^\circ C$  amounted to 2-3%, whereas no additional polymer was formed even after 10 days at the same temperature . These two observations tend to show the possible existence of a particular mechanism under the irradiation conditions , but nothing yet allows us to distinguish whether it is a particular case of the already known radical or ionic mechanism, or yet a third one such as one of those mentioned in the introduction, i.e. a collective "electronic" or "hot track" mechanism (I-4-2) .

It is therefore concluded that at least two polymerization mechanisms are at work in the SSP of the calcium acrylate system . The presence of an

ionic as well as of a radical mechanism appears to be clearly established by the several independent types of experimental evidence available. A third special mechanism might also exist at low temperatures under the irradiation, but other experiments are required to determine its exact nature.

#### IV-4-3<sup>b</sup> Kinetic parameters

The presence of high molecular weight fractions in samples having been post-polymerized for only very short times indicates that propagation is not the rate-limiting step, but that it takes place on the contrary quite rapidly.

This statement goes against the conclusions of Costaschuk<sup>(84)</sup>, but he reported having made his study of the molecular weights by dissolving his poly(acrylic acid) samples in benzene. However, P.A.A. is known<sup>(96)</sup> and has been verified here to be insoluble in this solvent. As a result, it is believed that all his conclusions about chain transfer, branching and kinetic equations of polymerization were unfortunately unfounded.

No evidence for chain transfer could be found in the present study, except possibly in the presence of air. On the other hand, bimolecular termination is believed to be virtually absent in most SSP systems, because of the low probability that two macroradicals embedded in a solid phase would encounter each other. In this particular system as well, the ESR study of radical oxidation, coupled with the NMR study of molecular motions at long polymerization times, concluded to the virtual "immortality" of most polymer radicals (section IV-1-3).

By elimination, we may therefore conclude that it is the "initiation" which is the rate-controlling step of the radical part of the mechanism. By "initiation", it is here understood the thermal unlocking of dimers trapped

in the solid, the heat of polymerization being subsequently sufficient to promote the monomer diffusion or chains motions necessary to aliment propagation . Such a kinetic model is entirely consistent with the frequently observed "reanimation" phenomenon by which a SSP system, having reached its limiting conversion, may be activated again by raising the temperature . This model also accounts for the fact that the last 50% of the limiting conversion are accomplished by increasing the number of macromolecules without increasing their length (Fig. IV-4-10 and IV-4-13) .

However, during the first 50% of the polymerization, the heterogeneous polymer growth will interfere with the "initiation" rate by accumulating stresses in the dihydrate lattice, which will certainly result in a more complex kinetic scheme . Indeed, dual-range kinetics have recently been reported in other similar acrylic SSP systems<sup>(39)</sup> .

CHAPTER V

---

SUMMARY AND CONCLUSIONS

## V-1 Summarizing discussion

Owing to the multidisciplinary nature of this thesis, it was felt desirable to gather in a summarizing discussion the main points pertaining to the three mechanisms investigated (dehydration, chemical and physical polymerization mechanisms). Short conclusions will be presented in section V-2 .

### V-1-a Dehydration mechanisms

Previous authors have presented two dynamic dehydration mechanisms, that were compared on Fig. III-1-1 . Costaschuk proposed a model involving two phases (crystalline dihydrate, amorphous anhydrate) and a thin boundary, while Watine proposed a three-phase model . In this model, the dihydrate would lose water to the profit of an intermediate "active volume phase" of constantly varying composition  $x$  , until around  $0.5 \text{ H}_2\text{O}$  where this "x phase" would permeate the whole volume of each particle . Upon further dehydration, this "x phase" would then progressively give way to the anhydrate .

The reinvestigation of this problem led to the conclusion that Watine's model should be rejected for the following 4 reasons :

(1) The finding that the water's oxigens lent a strong negative contribution to the intensity of the diffraction lines chosen by Watine to measure the percentage crystallinity as a function of the hydration levels, led to the conclusion that the non-linearity observed by Watine in the  $0.7$  to  $2 \text{ H}_2\text{O}$  range was actually an artefact . On the basis of Watine's own measurements, it was estimated that the amounts of dehydration the lattice could tolerate without crumbling was limited to less than approximately 2 % .

(2) Costaschuk's observation of a reduced, but clear dihydrate X-ray pattern all the way down to the very low  $0.28 \text{ H}_2\text{O}$  level goes directly against Watine's

contention that the last traces of dihydrate disappear below  $0.5 \text{ H}_2\text{O}$  to the profit of an "active volume" x phase .

(3) The fall of the crystallinity percentage below linearity, observed by Watine for hydration levels below  $0.5 \text{ H}_2\text{O}$  , may be simply reinterpreted as an indication that the dehydration proceeds by an abundant nucleation of small centers . Another artefact results of this, since the fall of their average diameter below  $1000 \text{ \AA}$  broadens their diffraction lines and thus leads to the misleading observation of a reduced intensity .

(4) The accumulation of the saturated solution and vapour phases present during equilibrium dehydration conditions (such as encountered during differential scanning calorimetry in a sealed sample pan) was concluded to be very unlikely under dynamic dehydration conditions, because water is believed to diffuse relatively easily through the dihydrate (and very easily through the anhydrate) at these temperatures .

Accordingly, it was decided to retain the dynamic dehydration model of Costaschuk, involving the dihydrate and anhydrate phases, and a thin boundary susceptible to play a crucial role in the physical polymerization mechanism . The existence of such a boundary was further supported by the finding of a maximum in radical concentration at the  $0.3 \text{ H}_2\text{O}$  level, since the abundant nucleation logically leads to a maximization of the interfacial area at this composition, and since the higher local molecular mobility at the interface decreases the "local cage recombination" of the initial radicals .

On the other hand, equilibrium dehydration was concluded from the thermal analysis experiments (in a sealed sample pan with a pinhole) to present an invariant quadruple point at  $79.6^\circ\text{C}$ , involving 4 phases (sharp endotherm): dihydrate, anhydrate, saturated solution and water vapour . The loss of water

occured only at higher temperatures, and progressively (broad endotherm) .

Finally, although no direct evidence of its existence could be found so far, the existence of an unstable intermediate hydrate under certain special conditions cannot be totally discounted . The presence of two slightly different types of water molecules in the dihydrate lattice and of a small unexplained feature in the DTA dehydration endotherm are indications to this effect.

#### V-1-b Chemical polymerization mechanisms

Up to this date, the SSP mechanism of calcium acrylate had always been assumed to be a free radical one . However, the existence of at least two polymerization mechanisms was indicated by the failure of oxygen to provoke a total inhibition in the anhydrate, although it was demonstrated to be totally diffusible by oxygen .

The existence of a second mechanism was conclusively established by the finding of a binodal molecular weights distribution by exclusion chromatography, and it was demonstrated to be ionic by the observation that oxygen inhibited selectively the higher  $\overline{M}_V$  node . The poor reproducibility of the polymer yields and ratios of the two  $\overline{M}_V$  nodes in the anhydrate was taken as a further argument in favour of an ionic mechanism, since the active ionic species are known to be very sensitive to the differing amounts of residual moisture traces found in "dry" and "super dry" samples (32,60-65,111) .

The coexistence of ionic and radical mechanisms is not a rare occurrence in the solid state, but has been reported along with binodal  $\overline{M}_V$  distributions for a few common vinyl monomers (63-65) . The inhibiting action of polar molecules such as water on the ionic species, usually total in the liquid phase polymerizations, has been reported to be sometimes sharply curtailed or suppres-

sed altogether in the solid state<sup>(63,64)</sup>. Indeed, large differences can be found in solids between average and local water concentrations, and can easily account for this behaviour .

As regards the acrylate radicals, the study of their concentration as a function of hydration levels and that of their decay behaviour upon annealing and oxygen inhibition disclosed the presence of three chemically equivalent types of radicals, to be distinguished according to their fate during the post-irradiation solid-state polymerization :

- active radicals, leading eventually to polymerization ;
- inert radicals, trapped in the dihydrate lattice under the form of dimers ;
- radicals doomed to bimolecular recombination and disappearance .

The observation of a small maximum in radical concentrations at the 0.3 H<sub>2</sub>O level is the second most important finding of this work, and will be related to the physical polymerization mechanism in the next section .

Finally, two observations have been made, that indicate the presence of a special polymerization behaviour at low temperatures under the gamma rays :

- a small percentage of conversion to polymer was observed "in source" at a temperature too low for post-polymerization to occur ;
- the  $\overline{M}_v$  distribution of the "in source" polymer was found in one case to be monodal and ten times heavier than that of post-polymers made under any other conditions .

This appears to leave open the possibility of finding yet a third polymerization mechanism . Whether it be a particular case of ionic or radical, or still another one among those suggested by Tabata<sup>(110)</sup> (i.e. "collective electronic" or "energetic chain"), the particular behaviour taking place "in source" warrants further investigation .

### V-1-c Physical polymerization mechanism

(1) In the dihydrate, the polymerization was shown by crystallography to be impossible within the perfect lattice . Since the ESR study of oxygen inhibition and the surface scavenging study have shown that the initiating and propagating species were entrenched in the bulk of the solid, we must conclude that propagation takes place at lattice defects, at least initially .

The polymerization itself, being heterogeneous, will engender and accumulate stresses in the lattice . Attention must be drawn to the possibility that the water of hydration could play a role in relieving those stresses by acting like a plasticizer in the migration of dislocations, or by being involved in a concerted vacancy diffusion process .

The ESR study of radical oxidation at the limiting conversion stage concluded to the "immortality" of the majority of the polymer radicals . As a result, polymerization was concluded to terminate physically by the exhaustion of all the monomers accessible at the level of thermal agitation available , rather than chemically by bimolecular recombination . The study of the molecular weights distribution as a function of time also led to the conclusion that the propagation occurred quite rapidly, and was initiation-limited over most of the range (initiation is here meant as the thermal release of trapped dimers radicals) . Such behaviour has also been reported for other vinyl SSP systems. (64) .

The interplay between the generation of stresses by polymerization and their relief by a thermal annealing process which tends to initiate more chains in turn, is certainly conducive to complex kinetic schemes .

The formation of a new phase , of molecular mobility intermediate between that of a solid and that of a liquid, was observed by Wide-Line NMR in the polymerizing dihydrate . This phase was found to be permeable by oxygen,

and to grow proportionally to the amount of polymer formed . Accordingly, a physical polymerization model was proposed in which the macromolecule grows inside a "disruption sleeve" or a "cavity" by such motions as wagging the chain end until it abstracts a monomer from a nearby wall (Fig.IV-2-4). To date, no direct evidence could be found to distinguish whether the mobility / observed stemmed from the motions of macromolecular segments or from those of the monomers lining the disruption sleeve or the cavity .

However, it must be stressed that polymerization and dehydration are inextricably connected in the dihydrate, which may lead to some clues as to what the new phase is . Not only does dehydration help polymerization by providing increased mobility at the boundaries, but polymerization conversely promotes dehydration by destroying the coordination polyhedron of the calcium ion, and liberating water molecules from the lattice bonds with the help of the reaction heat .

It is therefore suggested that the new "intermediate mobility phase" is made up of polymer swollen with either water or a saturated monomer solution, which would explain why this phase was not observed in the anhydrate . The similar observation of such a phase in other water-less systems can be rationalized by noting that some polymers are capable of swelling in their own monomers .

(2) In the intermediate hydrates , the interphase boundaries are, of course, the most obvious of the defects to be considered . Although the study of the average molecular mobility disclosed no particular increase at the 0.5 H<sub>2</sub>O hydration, the presence of a maximum in radical concentration at that level was explained in the light of the dehydration model proposed, as follows .

The abundant nucleation of the dehydration centers leads logically to the maximization of the surface area of the interphase boundaries between the

dihydrate crystallites and their anhydrate shells, just before total dehydration. The greater looseness in these regions certainly provides for an increased local mobility, which escapes detection by NMR because their molar concentration is below the sensitivity limit of this technique. The mobility and looseness at the interphase boundaries are the keys to a reduced "cage effect recombination" (resulting in the radical concentration maximum observed) as well as to an easier polymerization. Both factors combine, of course, to increase the polymer yield in the form of the maximum observed around 0.5 H<sub>2</sub>O.

The great similarity of the partially dehydrated system with a eutectic mixture must be recognized, for both are constituted by the juxtaposition of finely divided phases, and as such exhibit a maximal boundary area at certain compositions. Indeed, a maximum in polymerization rates has often been reported around eutectic compositions<sup>(36,48-50)</sup>, probably for the reasons expounded above.

(3) The above physical polymerization model is perfectly consistent with the finding that the average stereotacticity of the polymers made under any SSP conditions tried was the same as the tacticity of polymers made in the liquid phase, i.e. the solid state imparts no preferential orientation to the adding monomer.

## V-2 Short conclusions

a) The main conclusion pertains to the chemical polymerization mechanism, which was found to consist of at least 2 elements, radical and ionic, whose proportions vary with the degree of hydration and the effect of inhibitors.

b) The second most important conclusion pertains to the physical polymerization mechanism.

In the dihydrate, polymerization was found to be impossible in the perfect lattice, but to proceed by the creation of a new phase of intermediate mobility, either in the form of a "disruption sleeve" or of a "cavity", and involving motions such as the wagging of the chains ends to aliment the growth.

"Initiation" occurs by the thermal release of trapped dimers, and was concluded to be the rate-limiting step over most of the polymerization range. The rate of thermal stress annealing and stress generation by the polymerization itself will be the principal factors of the initiation rate.

Termination was concluded to occur primarily by entrapment and exhaustion of monomer, rather than by chemical recombination.

At all hydration levels, the polymerization was found to proceed in the bulk of the solids rather than at the surface, and without any stereotactical control.

c) The dynamic dehydration was concluded to involve 2 phases (dihydrate and anhydrate) separated by a thin boundary.

The equilibrium dehydration was concluded to proceed via an invariant quadruple point at  $79.6^{\circ}\text{C}$  (involving dihydrate, anhydrate, saturated solution and water vapour) followed by a subsequent loss of water at higher temperatures.

d) Finally, all the above conclusions were used to explain the heretofore puzzling maximum in polymer yield around the  $0.5 \text{ H}_2\text{O}$  hydration, and which had

been the prime motivation behind the undertaking of the present work . It was concluded to be the result of a maximum in the concentration of initiating radicals, and of a local increase in molecular mobility at the boundary . Both these factors are directly associated with the preeminent role played by the interphase boundaries, whose areas are maximized shortly before total dehydration .

V-3 Contributions to original knowledge

a) The crystal structure of calcium acrylate dihydrate was reinvestigated in cooperation with Drs G. Donnay and Y. Lepage, and S. Fortier. Dimerization was shown to be easy, but polymerization impossible within the perfect lattice since the latter destroys the coordination polyhedron of the calcium ions. The existence\* of two<sup>f</sup> different types of water molecules was demonstrated.

The anhydrate was confirmed to be amorphous, but to have nevertheless retained some interatomic distances from the parent dihydrate.

b) Oxygen was found to be unable to diffuse through the dihydrate, but to have an easy access inside the anhydrate.

c) The location of the radicals produced by gamma-irradiation was determined to be in the bulk of the dihydrate and anhydrate solids, both at the initiation and at the limiting conversion stages.

d) The water of hydration was found to be radio-chemically involved in the formation of the initiating species, and to a large extent.

e) The average molecular mobilities of water and of the monomer over the hydration range were found to be unrelated to the presence of a polymerization maximum at the 0.5 H<sub>2</sub>O level. A new phase of mobility intermediate between that of a solid and that of a liquid was discovered to form during post-polymerization. Its amount was found to be proportional to the polymer yield, which led to the development of a non-destructive analytical technique for measuring polymerization kinetics.

f) The presence of a radical concentration maximum was discovered at the same hydration level where a polymer yield maximum occurs. The existence of three chemically equivalent types of radicals was derived from their decay characteristics, depending on their fate during post-polymerization.

g) The existence of a dual polymerization mechanism (ionic/radical) was established by the finding of a binodal molecular weights distribution and of the selective inhibition of the higher node by oxygen .

h) The stereotacticity of the polymers produced under various SSP conditions was measured to be Bernoullian, and identical to that of the poly(acrylic acids) made in the liquid phase . The absence of topotactical control by the solid state was thus demonstrated in this system .

V-4 Suggestions for further work

a) The nature of the chemical mechanisms of polymerization should be investigated further .

In particular, the sign of the ionic mechanism involved should be determined . Practically, a more thorough study of inhibition should be undertaken, if possible with specific inhibitors such as  $\text{NH}_3$  .

All inhibitors should be introduced by a break-seal after irradiation, to prevent their degradation during this phase . Their effect on the polymer yields and  $\overline{M}_V$  distributions should be evaluated; and the same applies to a comparison between "dry" and "super dry" anhydrates .

The polymers made "in source" at 77 and 195°K should be prepared in quantities large enough to allow  $^{13}\text{C}$ -NMR and  $\overline{M}_V$  distribution analyses .

All exclusion chromatography experiments are now believed to be best conducted at 30°C in p-dioxane, which corresponds to Theta conditions for poly(acrylic acid), and would allow the use of the accurate and easily available polystyrene standards .

b) The physical factors of SSP should also be the objects of deeper study:

- the effects of particle size and defects concentration on the polymer yields and  $\overline{M}_V$  distributions should be measured . Dihydrate samples should be prepared as large monocrystals, and under widely varying conditions such as slow or fast crystallization, seeding, co-crystallization and addition of "inert additives" (carbon black, silica, alumina etc...) .
- a "reanimation" experiment should be attempted .
- since SSP and dehydration are so tightly linked together, a dynamic dehydration should be undertaken on irradiated dihydrate, in the hope that it would result in extreme conversion rates as the interphase boundary sweeps through the solid .

c) The dehydration mechanism should be further investigated by performing a XXXXXXXXXX thermal analysis of  $\text{CaAc}_2 \cdot 2 \text{H}_2\text{O}$  samples covering a broad particle size range, with simultaneous effluent analysis, and by recording X-ray patterns at intermediate temperatures .

Tagging with  $^{18}\text{OH}_2$  should be used to determine whether the fast exchange of the hydration  $\text{D}_2\text{O}$  with atmospheric moisture at room temperature, results from the diffusion of the water molecules themselves<sup>(85)</sup> or from a fast chain-exchange of protons .

d) The Wide-Line NMR spectra of samples of a saturated monomer solution as well as of polymer swollen in water should be recorded, in order to compare their linewidths with those of the dry polymer and of the new phase discovered in this thesis .

REFERENCES

1. J.V. SCHMITZ and E.J. LAWTON: Science, 113, 718 (1951).
2. R.B. MESROBIAN, P. ANDER, D.S. BALLANTINE and G.J. DIENES:  
J. Chem. Phys., 22, 565 (1954).
3. A. HENGLEIN and R. SCHULZ: Z. Naturforsch., 9-B, 617 (1954).
4. G.M.J. SCHMIDT: Publications of G.M.J. SCHMIDT 1957-1972:  
Israel J. of Chemistry, 10, 67-72 (1972).
5. M. MAGAT: Polymer, 3, 449 (1962).
6. S. OKAMURA, K. HAYASHI and Y. KITANISHI:  
J. Poly. Sci., 58, 925 (1962).
7. S. NAKASHIO, M. KONDO, H. TSUCHITA and M. YAMADA:  
Makromol. Chem., 52, 79 (1962).
8. A. CHAPIRO and S. PENCZEK: J. Chim. Phys., 59, 696 (1962).
9. K. HAYASHI, S. OKAMURA and H. WATANABE:  
J. Poly. Sci., Bl, 397 (1963).
10. M. MIURA, T. HIRAI and KAWAMATSU:  
Bull. Chem. Soc. Jap., 38, 344 (1965).
11. S. OKAMURA, K. TAKAKURA and K. HAYASHI:  
Pure Appl. Chem., 12, 387 (1966).
12. R.H. BAUGHMAN: J. Poly. Sci. (Physics), 12, 1511-1535 (1974).
13. J. KAISER, G. WEGNER and E.W. FISCHER:  
Israel J. Chem., 10, 157-171 (1972).
14. G. WEGNER: Makromol. Chem., 154, 35 (1972).  
Makromol. Chem., 145, 85 (1971).  
Makromol. Chem., 134, 219 (1970).  
Z. Naturforschung, 24b, 824 (1969).

15. M. HASEGAWA, Y. SUZUKI and T. TAMAKI:  
Chem. Soc. Japan, (Bull.), 43, No. 9, 3020 (1970).
16. B. KEGGENHOF and G. WEGNER: J. Poly Sci., 11 (1973),  
Part I: 759-769; Part II: 769-784.
17. H. KAYE and S.H. CHANG: Macromolecules, 5 (4), 397-401 (1972).
18. K. HAYASHI, H. WATANABE and S. OKAMURA:  
Polymer Letters 1, 397 (1963).
19. Y. TABATA, B. SAITO, H. SHIBANO, H. SOBUE and K. OSHIMA:  
Makromol. Chem., 76, 89 (1964).
20. H. MORAWETZ: J. Poly. Sci., C-12, 79 (1966).
21. G.M.J. SCHMIDT: "The Photochemistry of the Solid State" in  
"Reactivity of the Photoexcited Organic Molecule".  
Interscience, p. 227, (1967).
22. F.L. HIRSHFELD and G.M.J. SCHMIDT: J. Poly. Sci., A2, 2181 (1964).
23. C.H.S. Chen and D.G. GRABAR: J. Poly. Sci., C4, 869 (1963).
24. M. MAGAT: Pure Applied Chem. (London), 5, 487 (1962).
25. R. BENSASSON, A. DWORKIN and R. MARX: J. Poly. Sci., C4, 881 (1964).
26. Y. TABATA and K. OSHIMA: Intern. Symp. Macromol. Chem. Prague (1965).
27. T.A. FADNER and H. MORAWETZ: J. Poly. Sci., 45, 475 (1960).  
J. Poly. Sci., 40, 475 (1960).  
Makromol. Chem., 34, 162 (1959).
28. G. ADLER, D.S. BALLANTINE and B. BAYSAL:  
J. Poly. Sci., 48, 195 (1960). International Sympos. Macromol.  
Chem. Moscow (1960).
29. R. BENSASSON and R. MARX: J. Poly. Sci., 48, 53 (1960).
30. C. CHACHATY: Thèse, Paris (1962).
31. S. OKAMURA and K. HAYASHI: J. Chim. Phys., 59, 429 (1962).

32. A.S. CHAWLA: McGill University Thesis (1970).
33. W. BOLLMANN: "Crystal Defects and Crystalline Interfaces", Springer-Verlag (1970).
34. N.B. HANNY: "Solid State Chemistry", Prentice-Hall (1967) U.S.A.
35. A. BENNETT, D. HAMILTON, A. MARADUDIN, R. MILLER and J. MURPHY: "Crystals; Perfect and Imperfect", Walker & Co., New York (1965).
36. A. CHAPIRO: "Encyclopedia of Polymer Science", John Wiley & Sons, Vol. 11, 725-735 (1969).
37. A. FAUCITANO and G. ADLER: J. Macromol. Sci. Chem., A4, (2), 261-275 (1970).
38. I. VOIGT-MARTIN: Makromol. Chem., 175, 2669-86 (1974).
39. P.P. SAVIOTTI: McGill University Ph.D. Thesis (1975).
- 40a. C. CHACHATY and A. FORCHIONI: J. Poly. Sci., A1, 10, 1905-1922 (1972).
- 40b. A. FORCHIONI and C. CHACHATY: J. Poly. Sci., A1, 10, 1923-1943 (1972).
- 40c. C. CHACHATY, A. FORCHIONI and M. LATIMIER: J. Poly. Sci., A1, 13, 189-199 (1975).
41. A.M. KAPLAN, A.I. MIKHAILOV, D.P. KIRYOUCHIN, I.M. BARKALOV and V.I. GOLDANSKY: Tihany 3rd Symp. on Radiation Chemistry, (1971), 485-492 (Budapest).
42. A.I. MIKHAILOV, A.I. BOL'SHAKOV, I.M. BARKALOV and V.I. GOLDANSKY: Tihany 3rd Symp. on Radiation Chemistry, (1971), 493-501 (Budapest).
43. J.M. THOMAS and J.O. WILLIAMS: Trans. Farad. Soc., 63, 1922-28 (1967).
44. B. BAYSAL, G. ADLER, D. BALLANTINE and P. COLOMBO: J. Poly. Sci., 44, 117 (1960).
45. A. CHAPIRO and Z. MANKOWSKY: Europ. Poly. J., 7, 1073-1090 (1971).
46. J.R. PUIG and R. GOULOUBANDI: J. Chimie Phys., 72 No. 6, 702-718 (1975).

47. J.B. LANDO and J. SEMEN:  
J. Poly. Sci., Polymer Chem., 10, 3003-3016 (1972).
48. A. CHAPIRO and P. LESAULNIER: Europ. Poly. J., 9, 863-876 (1973).
49. A. CHAPIRO and P. LESAULNIER: Europ. Poly. J., 10, 171-191 (1974).
50. Z. MANKOWSKI: J. Chimie Phys., 70 (9), 1299-1304 (1973).
51. C.H. BAMFORD, G.C. EASTMOND and J.C. WARD:  
Proc. Roy. Soc. (London), A271, 357 (1963).
52. Y. TABATA and T. SUZUKI: Makromol. Chem., 81, 223 (1965).
53. T. SUZUKI, Y. TABATA and K. OSHIMA: J. Poly. Sci., C16, 1821 (1967).
54. Y. TABATA, S. SHU and K. OSHIMA:  
Mol. Cryst. Liq. Cryst., 9, 435 (1969).  
Makromol. Chem., 109, 120 (1967).
- 55a. J.F. BROWN and D.H. WHITE: J. Am. Chem. Soc., 82, 5671 (1960).
- 55b. D.M. WHITE: J. Am. Chem. Soc., 82, 5678 (1960).
56. Y.B. AMERIK and B.A. KRENTSEL: J. Poly. Sci., C16, 1383 (1967).
- 57a. A. CHAPIRO and L. PEREC:  
Compt. Rend. Acad. Sci. Paris, 264, 285 (1967).
- 57b. A. CHAPIRO, L. PEREC and S. RUSSO: Europ. Poly. J., 10, 71-75 (1974).
58. A.I. BOL'SHAKOV, A.I. MIKHAILOV, I.M. BARKALOV and V.I. GOLDANSKY:  
Dokl. Phys. Chem., 205 (1-3), 594-597 (1972).
59. I. KAETSU, H. OKUBO, A. ITO and K. HAYASHI:  
J. Poly. Sci., A-1, 10, 2203-2214 (1972) Part I.  
J. Poly. Sci., A-1, 10, 2661-2675 (1972) Part III.
60. T. GILLBRO: J. Poly. Sci., B(11), 309-312 (1973).
61. S. LIYAMA, S. ABE and K. NAMBA: J. Poly. Sci., B11 (2), 81-85 (1973).
62. R. BENSASSON, A. BERNAS, M. BODARD and R. MARX:  
J. Chim. Phys., 60, 950 (1963).

63. J.F. WESTLAKE and K.Y. HUANG:  
J. Poly. Sci., A-1, Part III: 8, 49-61 (1970).  
Part IV: 10, 1429-1441 (1972); Part V: 10, 1443-1466 (1972).  
Part VI: 10, 2149-2158 (1972); Part VII: 10, 3053-3066 (1972).
64. S. MACHI, J. SILVERMAN and D. METZ:  
J. Phys. Chem., 76 (6), 930-937 (1972).
65. S. TERAMACHI and H. USHIYAMA: Polym. J. 5 (3), 243-247 (1973).
66. G. HARDY, K. NYITRAY, G. KOVACS, N. FEDOROVA and J. VARGA:  
Proceedings of the Tihany Symp. on Radiation Chem.,  
Akademiai Kiado, Budapest, Reprint No. 6459176.
67. A. BOL'SHAKOV, A. MIKHAILOV, I. BARKALOV and V. GOLDANSKY:  
Vysokomol Soyed., A15 (3), 470-477 (1973) Transl. in:  
Poly. Sci. USSR, 528-537.
68. A. CHAPIRO: Proc. 22nd Nobel Symposium (June 1972, Sweden), 117-127.
69. H. MORAWETZ: J. Poly. Sci., C1, 65 (1963).
70. N.N. SEMENOV: J. Poly. Sci., 55, 563 (1961).  
J. Poly. Sci., 35, 159 (1961).
71. I. GUSAKOVSKAYA, T. LARKINA, V. TRUKHTANOV, Yu. SHCHERBININ and  
V. GOLDANSKY: Vysokomol Soyed. A14 (6), 1390-95 (1972).  
Transl. J. Poly. Sci. USSR.
72. A.J. RESTAINO, R.B. MESROBIAN, H. MORAWETZ, D.S. BALLANTINE,  
G.J. DIENES and D.J. METZ: J. Am. Chem. Soc., 78, 2939 (1956).
73. H. MORAWETZ and I.D. RUBIN: J. Poly. Sci., 57, 687 (1962).  
J. Poly. Sci., 57, 669 (1962).
74. V.A. KARGIN, V.A. KABANOV and G.P. ANDRIANOVA:  
Poly. Sci. USSR, 1, 106 (1960).

75. V.A. KARGIN, V.A. KABANOV and N. Ya. RAPAPORT-MOLODTSOVA:  
Poly. Sci. USSR, 3, 657 (1962).
76. H.C. HELLER, S. SCHLICK, H.C. YAO and T. COLE:  
Mol. Cryst. Liq. Cryst., 9, 401 (1969).
77. J.B. LANDO: Polytechnic Inst. of Brooklyn. Ph.D. Thesis,  
June (1963).
78. J.B. LANDO and H. MORAWETZ: J. Poly. Sci., C4, 789-803 (1964).
79. J.H. O'DONNELL, B. MCGARVEY and H. MORAWETZ:  
J. Am. Chem. Soc., 86, 2322 (1964).
80. N.W. ISAACS, C.H.L. KENNARD and J.H. O'DONNELL:  
Nature, 216, 1104 (1967).
- 81a. M.J. BOWDEN and J.H. O'DONNELL: Macromol., 1, 499 (1968).
- 81b. M.J. BOWDEN and J.H. O'DONNELL: J. Phys. Chem., 72, 1577 (1968).
- 81c. M.J. BOWDEN and J.H. O'DONNELL: J. Phys. Chem., 73, 2871 (1969).
82. M.J. BOWDEN, J.H. O'DONNELL and R.D. SOTHMAN:  
Makromol. Chem., 122, 186 (1969).
- 83a. J.H. O'DONNELL and R.D. SOTHMAN: J. Poly. Sci., A-1, 6, 1073 (1968).
- 83b. J.H. O'DONNELL and R.D. SOTHMAN:  
J. Macromol. Sci. Chem., A6 (4), 745 (1971).
- 84a. F.M. COSTASCHUK: McGill University, Ph.D. Thesis, Chemistry, May (1970).
- 84b. F.M. COSTASCHUK, D.F.R. GILSON and L.E. ST. PIERRE:  
Macromolecules, 3 (4), 393 (1970).
- 84c. F.M. COSTASCHUK, D.F.R. GILSON and L.E. ST. PIERRE:  
J. Phys. Chem., 74, 2035 (1970).
- 84d. F.M. COSTASCHUK, D.F.R. GILSON and L.E. ST. PIERRE:  
Macromolecules, 4 (1), 16 (1971).

85. F.B. WATINE: McGill Univ., M.Sc. Thesis, Chemistry, July (1971).  
F.B. WATINE and L.E. ST. PIERRE:  
J. Poly. Sci. Symp. No. 42, 123-133 and 135-145 (1973).
86. SCHWARZKOPF MICROANALYTICAL LABORATORY:  
56-19, 37th Avenue, Woodside, New York 11377, USA.
87. ELECTRO-NUCLEONICS, INC.:  
368 Passaic Avenue, P.O. Box 803, Fairfield, New Jersey 07006 USA.
88. A. FARKAS: "Light & Heavy Hydrogen", Cambridge Univ. Press (1935).
- 89a. V.A. TOLKACHEV: Tihany 3rd Symp. (1971), 441-451.
- 89b. V.A. TOLKACHEV: Review, Khimia Vysokih Energii, Vol. IV, 322 (1970).
- 90a. C. CHACHATY, A. FORCHIONI and Buu BAN: Proc. of 3rd Symp. on  
Radiation Chemistry, Tihany, Budapest (1971), 589.
- 90b. C. CHACHATY, S. FORCHIONY and B. BAN: J. Poly. Sci., B9, 483 (1971).
91. J. SCHAEFER: Macromolecules, 4, 1, 98-104 (1971).
- 92a. F.A. BOVEY:  
"Polymer Conformation and Configuration", Acad. Press, (1969).
- 92b. F.A. BOVEY: "High Resolution NMR of Macromolecules" (includes <sup>13</sup>C),  
Academic Press (1972).
93. J.W.L. FORDHAM: J. Poly. Sci., 39, 321 (1959).
- 94a. K. MATSUZAKI, T. URYU, A. ISHIDA and M. TAKEUCHI:  
J. Poly. Sci., A-1, 5, 2167 (1967).
- 94b. K. MATSUZAKI, T. URYU, A. ISHIDA and M. TAKEUCHI:  
J. Poly. Sci., C16, Part 4, 2099-2110 (1967).
95. S. NEWMAN, W.R. KRIGBAUM, C. LAUGIER and P.J. FLORY:  
J. Poly. Sci., 14, 451 (1954).
96. J. BRANDRUP and E.H. IMMERGUT: "Polymer Handbook",  
Interscience, New York (1966).

97. M. KURATA and W.H. STOCKMAYER: "Intrinsic Viscosities and Unperturbed Dimensions of Long Chain Molecules" (Review) Fortschritte der Hochpolymeren Forshung 3, 196-312 (1961-64).
98. A. SILBERBERG, J. ELIASSAF and A. KATCHALSKY: J. Poly. Sci., 23, 259 (1957).
99. H. BENOIT, P. REMPP and Z. GRUBISIC: Polymer Letters 5, 753 (1967).
100. H. COLL and D.K. GILDING: J. Poly. Sci., A-2, 8, 89 (1970).
101. A. CARRINGTON and A.D. McLACHLAN: Introduction to Magnetic Resonance, Harper & Row (1967).
102. R. MARX and S. FENISTEIN: J. Chim. Phys., 64, 1424 (1967).
103. D.E. O'REILLY and J.H. ANDERSON: Physics and Chemistry of the Organic Solid State, Vol. II: Magnetic properties, Interscience (1965).
104. H. FISCHER and G. GIACOMETTI: Polymer Smyposia IUPAC Prague (1965) Part 5, Vol. 16, 2763-2771.
105. H. FISCHER: Z. Naturforsch. 19a, 267 (1964).
106. THERMAL ANALYSIS NEWSLETTER No. 7 (1967), Perkin Elmer Corporation, Norwalk, Connecticut 06852, USA.
107. B. BAN and C. CHACHATY: Can. J. Chem., 51, 3889 (1973).
108. R. ARNOLD and G.C. EASTMOND: Trans. Farad. Society, 67, 772 (1971).

Selected reviews on SSP:

109. A. CHAPIRO: "Polymérisation en phase solide amorcées par les radiations" in "Actions Chimiques et Biologiques", 10<sup>e</sup> série, M. Haissinsky ed., Masson et Cie, Paris, pp. 187-312 (1966).
110. Y. TABATA: "Vinyl Polymerizations" G.E. Ham ed. (1969).
111. A. CHAPIRO: "Initiation & propagation steps in SSP of vinyl monomers" Israel J. of Chem. 10, 129-141 (1972).

112. C.H. BAMFORD and G.C. EASTMOND: Q. Rev. 23, 271 (1969).
113. A. CHARLESBY: Rep. Prog. Phys. 28, 463 (1965).
114. J. Poly. Sci. Part C: (Polymer Symposia) 765-966 (1964).

O

---

APPENDICES

O

A

APPENDIX A: Preliminary mass spectrometric experiments

The vapours above irradiated calcium acrylate di-deuterohydrate were expected to consist primarily of  $D_2O$  and possibly of HDO and  $H_2O$  as well. Consequently, preliminary experiments were devised with water,  $D_2O$  and a model mixture of the two, in order to gain the expertise necessary to perform the experiment, and to develop a method for the treatment of the data and their interpretation.

A-1 Analysis of water

First, the exact positions of  $m/e = 4,3,2,1$  were ascertain by admitting He in the spectrometer. Secondly, a sample of degassed distilled water was analysed, and the spectra compared to the background spectrum. The average of the intensities measured on 3 successive spectra are shown in Table A-1. The variations in the intensity of the same peak measured on successive scans or on different lines of the spectra were of the order of 10%.

Particular attention has to be paid to the Argon peak (40). It is apparent from this experiment that the introduction of a large quantity of water vapour does not affect the intensity of the Ar peak. As no "masking" was apparent, this peak was chosen as a reference for the subsequent studies.

It can also be seen from this table that the relative intensities of the water peaks agree with those found in the literature. The slight increase in the air gases ( $m/e = 32,28,14$ ) and the doubling of the  $CO_2$  peak are believed to be due to residual traces of air dissolved in the water.

Species	m/e	background	Water (Average of 3)	Water Relative Abundance (%)	
				Experimental	Literature
CO <sub>2</sub>	44	80	170	-	-
Ar	40	110	110	-	-
O <sub>2</sub>	32	1200	1400	-	-
N <sub>2</sub>	28	3500	3900	-	-
Ethylene	27	5	14	-	-
Acetylene	26	3	16	-	-
H <sub>2</sub> <sup>18</sup> O, D <sub>2</sub> O	20	6	280	0.20	-
HDO, H <sup>18</sup> O	19	4	2300	1.64	-
H <sub>2</sub> O	18	2100	140,000	Reference	100%
HO <sup>+</sup>	17	420	29,000	20.7	21.1
O <sub>2</sub> <sup>++</sup> , O <sup>+</sup>	16	37	1030	0.74	-
N <sub>2</sub> <sup>++</sup>	14	70	83	-	-
He, D <sub>2</sub>	4	-	-	-	-
DH	3	-	-	-	-
H <sub>2</sub> , D, He <sup>++</sup>	2	-	58	0.041	-
H	1	3	510	0.35	-

TABLE A-1

Mass spectrometric analysis of water: Peak intensities and relative abundances of the ions.

A-2 Analysis of D<sub>2</sub>O

The analysis of a sample of freshly outgassed D<sub>2</sub>O was performed in order to obtain comparison data for the later analysis of the gases above the irradiated heavy-water dihydrate.

Due to problems of adsorption of the three types of water, it was found necessary to remove the 3 l Pyrex expansion flask. The spectrometer was then flooded with D<sub>2</sub>O vapour and re-evacuated several times. This procedure bore two consequences: the background air had been flushed away (Ar, O<sub>2</sub> and N<sub>2</sub> were reduced 8 to 12 times), and the water, as measured by the peak (17) of OH<sup>+</sup> was reduced more than 2.1 times. This makes it meaningless to subtract the background spectrum, as usually done, from the sample spectrum.

Table A-2 presents the experimental results. The analysis of these results is somewhat complicated by the presence of 15% HDO (as referred to D<sub>2</sub>O = 100%). The presence of HDO seems to be inevitable, as it persisted after more than six cycles of flooding the spectrometer with D<sub>2</sub>O vapour and re-evacuating. It is believed that this HDO is the result of a chemical exchange taking place on the walls of the spectrometer between the adsorbed background H<sub>2</sub>O and the passing D<sub>2</sub>O vapour. Assuming that the 1% of OH<sup>+</sup> comes totally from H<sub>2</sub>O, the latter could be present to a maximum of only 5%, which shows that the background H<sub>2</sub>O is negligible as compared to D<sub>2</sub>O, and nearly so in comparison to HDO. The consequence is that OH<sup>+</sup> is formed from HDO to the extent of 6.7% or even less if we allow for some traces of water.

If we now assume that the sum of the probabilities of forming an OH and an OD fragment from HDO is nearly equal to that of forming an OH

Species+		Background		D <sub>2</sub> O		D <sub>2</sub> O
m/e	sensitivity+	1x	51x	1x	51x	Relative Abundances (%)
22	D <sub>2</sub> <sup>18</sup> O	-	8	47	2400	1.57
21	HD <sup>18</sup> O	-	2	11	600	0.38
20	D <sub>2</sub> O	1	80	3000	153,000*	100% (Reference)
19	HDO	19.5	1000	450	22,950*	15.0
18	H <sub>2</sub> O	350	17,800*	-	-	19.6 from D <sub>2</sub> O
18	OD	-	-	650	33,150*	(Total: 21.7) 2.1 from HDO
17	OH	70	3000	30	1600	1.0
16	O	4.5	250	13	700	0.45
4	D <sub>2</sub>	-	-	2.5	140	0.09
3	HD	-	0.25	0.5	40	0.03
2	H <sub>2</sub> ,D	-	1.5	16.5	700	0.45
1	H <sup>+</sup>	-	0.25	0.25	19	0.014

\* (calculated with the 51x sensitivity factor).

TABLE A-2 Mass spectrometric analysis of heavy water:  
peak intensities and relative abundances of the ions.

H <sub>2</sub> O		HDO		D <sub>2</sub> O	
OH <sup>+</sup>	20.7	OH <sup>+</sup>	<6.7	-	-
-	-	OD <sup>+</sup>	≥14	OD <sup>+</sup>	19.6

TABLE A-3 Fragmentation probabilities (%) of the three isotopes of water in the mass spectrometer.

fragment from  $H_2O$  (which is 20.7%), we can deduce that the percentage of OD formed from HDO is greater than or equal to:  $20.7 - 6.7 = 14\%$ . We can then split peak 18 between  $14\% \times 15\% = 2.1\%$  OD coming from HDO, and  $21.7\% - 2.1\% = 19.6\%$  OD coming from  $D_2O$ .  $^{18}O$  Oxygen contributions to the peaks 18,19,20 were neglected.

To summarize, this experiment has yielded quantitative data on the fragmentation probabilities of the three isotopes of water, which are shown in Table A-3.

These results follow the expected pattern because of the isotopic effect of deuterium. The deuterium requires more kinetic energy than the lighter hydrogen to be ejected, and the O-D bond vibrational ground state is lower than that of the O-H bond. It is therefore logical to expect the ionization efficiency of  $D_2O$  to be slightly lower than that of  $H_2O$ , and also HDO to give more OD than OH fragments.

#### A-3 Analysis of a model mixture $H_2O/D_2O$

A model mixture of 50%  $H_2O$  and 50%  $D_2O$  was allowed to equilibrate for two days, outgassed by repeated freezing and thawing under vacuum, and then analysed. The results are presented below in Table A-4. The first analysis was performed 5 min after the first background, then the spectrometer was evacuated and flooded again with the vapours (6 times). After a thorough evacuation, an "intermediate background" was recorded, followed by the second analysis.

The species analysed being either the same as, or readily exchangeable with the background water in the spectrometer, it is again meaningless to subtract the background spectrum from the sample spectrum. As in the case of  $D_2O$ , we can neglect the contribution of  $^{18}O$  to the peaks

Species+		First Background		1st Analysis		Intermed. Background		2nd Analysis	
m/e	sensitivity →	1x	52x	1x	52x	1x	52x	1x	52x
22	D <sub>2</sub> <sup>18</sup> O	0	7.5	5	380	0	9	3.5	290
21	HD <sup>18</sup> O	0	3.5	13	900	1	46	13	750
20	D <sub>2</sub> O	1	105	800	41,600*	49	2400	650	33,800*
19	HDO	31	1700	1400	72,800*	210	10,900*	1400	72,800*
18	H <sub>2</sub> O; OD	315	16,400*	900	46,800*	310	16,100*	1000	52,000*
17	OH	65	3000	200	10,400*	58	2900	230	11,960*
16	O	4	240	10	500	4	250	9.5	500
4	D <sub>2</sub> (He)	0	7	0.5	34(2)	0	1(7)	0.5	30(2.5)
3	DH	0	0.5	1.5	80	0	3	1	85
2	H <sub>2</sub> ,D	0	1	6.5	320	0	2	5	290
1	H	0	0.5	0.5	47	0	0	0.5	47

\* (Calculated with the 52x sensitivity factor)

TABLE A-4

Mass spectrometric analysis of a model mixture of 50% H<sub>2</sub>O + 50% D<sub>2</sub>O:  
relative peak intensities at equilibrium

18, 19 and 20.  $D_2O$  and HDO abundances are then given by the peaks 20 and 19, respectively.

Using the fragmentation probabilities measured previously (see Table A-3) we can calculate the fractions of the OD fragments coming from  $D_2O$  and HDO. By subtracting these from the  $m/e = 18$ , we can calculate the part of its intensity due to  $H_2O$  alone. The abundances of the various water isotopes relative to one another are shown on Table A-5.

A good test of the validity of these assumptions and of the exactness of the results can then be made by comparing the calculated and experimental intensity of peak 17 ( $OH^+$ ). They were 207 and 200 respectively for the first analysis, and 234 and 230 respectively for the second analysis. This excellent agreement justifies "a posteriori" the method used.

However satisfactory the numerical method is, one should be aware of the shortcomings of the experimental method, which is undermined by two main sources of error. The first one is the great sensitivity of the  $D_2O/H_2O$  ratio to relatively minor changes in the heights of peaks 20 and 18, as evidenced by comparing the first and second analysis.

The second shortcoming is the presence of a background signal due to water on the walls of the spectrometer. This water can be neither fully removed, nor fully exchanged with the isotopes of the sample, nor simply deducted from the sample spectrum. The only hope lies in flooding the spectrometer with an overwhelming amount of the sample vapour. Failing this, the ratios of  $D_2O/HDO/H_2O$  will be shifted towards the isotope last present in the ion chamber, usually  $H_2O$ .

Isotope	First Analysis	Second Analysis	Theoretical (*)
$D_2^{18}O$	0.91% (re: $D_2O$ )	0.86% (re: $D_2O$ )	-
$HD^{18}O$	1.24% (re: HDO)	1.03% (re: HDO)	-
$D_2O$	29.1%	23.8%	26.4%
HDO	51.0	51.4	47.2
$H_2O$	19.9	24.8	26.4

TABLE A-5

Relative abundances of the 3 isotopes of water at equilibrium in a model mixture of 50%  $H_2O$  + 50%  $D_2O$ .

(\*) Theoretical values calculated with an equilibrium constant  $K = 3.2 @ 20^\circ C$ , after Farkas (38).

APPENDIX B:

The data presented in Appendix B refer to the analysis of the vapours above calcium acrylate di-deuterohydrate, pre-irradiated at 77°K to 2.25 Mrad. The experimental technique has been described in section II-8.

B-1 Analysis at 77°K

The background spectrum was recorded after prolonged evacuation of the hammer-magnet compartment. The seal was then broken, and spectra recorded again with the sample immersed in liquid nitrogen. Table B-1 presents the numerical data gathered, by order of decreasing mass numbers.

No change was observed in the concentration of the usual background gases, within the accuracy of this type of measurements (variations of the order of 10-15% were frequently registered among successive spectra). This attested to the good vacuum achieved above the sample, and to the fact that the waters were effectively frozen at this temperature.

As a result, the appearance of traces of  $D_2^+$  and  $DH^+$  may be concluded to demonstrate the presence of molecular  $D_2$  and  $DH$  in the vapours, since they could not possibly be fragments of the frozen waters.

B-2 Analysis at 20°C

Following the analysis at 77°K, the sample was isolated by a valve from the spectrometer and heated rapidly to 20°C until thermal equilibrium was established. The valve was then opened and spectra recorded periodically for some time.

Table B-2 presents the numerical data gathered, by order of decreasing mass numbers. Spectra were recorded with various sensitivities, in

Species	m/e	Background relative intensities of peaks	After breaking the seal
CO <sub>2</sub> <sup>+</sup>	44	56	47
Ar <sup>+</sup>	35	35	33
O <sub>2</sub> <sup>+</sup>	32	600	600
CO <sup>+</sup> , N <sub>2</sub> <sup>+</sup>	28	2100	2000
Ethylene	27	15	9
Acetylene	26	9	5
-	25	2	1.5
-	24	0	0
D <sub>2</sub> O <sup>+</sup>	20	2	2
HDO <sup>+</sup>	19	0	0
OD <sup>+</sup> , H <sub>2</sub> O <sup>+</sup>	18	300	330
OH <sup>+</sup>	17	80	80
O <sub>2</sub> <sup>++</sup> , O <sup>+</sup>	16	60	60
N <sub>2</sub> <sup>++</sup>	14	120	140
-	13	4	2
D <sub>2</sub> <sup>+</sup>	4	0	0.9
He <sup>+</sup>	4	320	310
HD <sup>+</sup>	3	0	1
H <sub>2</sub> <sup>+</sup> , D <sup>+</sup> , He <sup>++</sup>	2	50	52
H <sup>+</sup>	1	1	1.5

TABLE B-1

Mass spectrometric analysis at 77°K of the gasses above irradiated calcium acrylate di-deuterohydrate.

Time after warm-up→ Multiplier gain setting→		Initial 5	20 min. 5	24 min. 3.5	26 min. 2.5
Species	m/e	Background Analysis	Sample at 20°C		
CO <sub>2</sub> <sup>+</sup>	44	56	2100	460	110
Ar <sup>+</sup>	40	35	170	22	5
O <sub>2</sub> <sup>+</sup>	32	600	1500	190	41
CO <sup>+</sup> , N <sub>2</sub> <sup>+</sup>	28	2100	>4000	650	230
Ethylene	27	15	170	23	5.5
Acetylene	26	9	320	35	7
-	25	2	53	6	1.5
-	24	0	16	1	0.5
D <sub>2</sub> O <sup>+</sup>	20	2	1200	750	290
HDO <sup>+</sup>	19	0	>4500	-	1600
OD <sup>+</sup> , H <sub>2</sub> O <sup>+</sup>	18	300	-	-	3100
OH <sup>+</sup>	17	80	-	2300	650
O <sub>2</sub> <sup>++</sup> , O <sup>+</sup>	16	60	500	120	30
N <sub>2</sub> <sup>++</sup>	14	120	180	24	4
-	13	4	16	1.5	0.5
D <sub>2</sub> <sup>+</sup>	4	0	5	-	0
He <sup>+</sup>	4	320	80	-	1
HD <sup>+</sup>	3	0	16	-	0
H <sub>2</sub> <sup>+</sup> , D <sup>+</sup> , He <sup>++</sup>	2	50	150	-	8
H <sup>+</sup>	1	3	-	-	27

TABLE B-2

Mass spectrometric analysis at 20°C of the gasses above irradiated calcium acrylate di-deutero hydrate.

order to encompass the totality of the extreme range of concentrations present. The multiplier detector gain setting is mentioned at the head of each column. Unfortunately, this gain control operates in a non-linear manner, and some adjustments of the collector slit width were required from time to time to maintain the resolution. As a result, it is best to make comparisons of the relative intensities only (peak ratios) rather than of the absolute intensities, which would be misleading.

The presence of larger amounts of  $D_2^+$ ,  $HD^+$ ,  $H_2^+$  and  $D^+$  than at  $77^\circ K$  cannot be interpreted the same as they were then, since these ions are also fragments of the three kinds of water which are present in abundance at  $20^\circ C$ .

As the vacuum above the sample had been shown to be very good by the analysis at  $77^\circ K$ , the apparent large increase in the air gases was interpreted as reflecting the higher efficiency of ionization which results from the sample pressure being much higher than the residual background pressure. To account for this effect, all subsequent calculations were referred to the intensity of the Ar peak which was taken as a standard for relative comparisons.

### B-3 Miscellaneous irradiation products

The data already presented in Table B-2 were analysed to determine the presence of several miscellaneous irradiation products. As mentioned earlier, all peak intensities were normalized by referring to the Argon peak serving as a standard.

#### B-3-1 Carbon dioxide and $N_2O$

The intensity of the  $CO_2$  peak ( $m/e = 44$ ) relative to that of the Ar

peak ( $m/e = 40$ ) is shown on Table B-3-1 after various times. It is evident that the spectrometer registered a 14-fold increase in  $CO_2$  concentration over that of the background.

The possibility that this increase could be due to the presence of  $N_2O$  (which also comes at  $m/e = 44$ ) and could be an irradiation product of the air has been discounted on the basis of a control experiment. In this test, moist air was irradiated to 3 Mrad at  $77^\circ K$  and analysed. Although  $N_2O$  can be resolved from  $CO_2$ , no increase in its concentration was noted when the seal was broken.

Spectrum	Time (min) at $20^\circ C$	$CO_2/Ar$	Average $CO_2/Ar$
Background	-	1.6	1.5
Sample at $77^\circ K$	-	1.4	
Sample at $20^\circ C$	0	12.3	discounted (not stabilized)
"	4	20.9	21.5
"	6	22.0	

TABLE B-3-1 Carbon dioxide

B-3-2 Carbon monoxide

The CO peak could be partially resolved from the  $N_2$  peak at  $m/e = 28$ . Its concentration was estimated to be approximately 14% of that of the nitrogen. Although the exact measurement of the CO peak had not been performed in the background beforehand, it is clear that

this concentration of 14% that of  $N_2$  is at least one order of magnitude larger than what can be expected from the usual residual air in the spectrometer.

### B-3-3 Ethylene

The molecular peak  $m/e = 28.031300$  of ethylene was completely resolved from that of nitrogen (28.006148) and of carbon monoxide (27.994914). It had an intensity of 4% of that of the nitrogen, a marked increase (three-fold) over that of the background. In order to illustrate this point further, the intensities of the peak  $m/e = 27$  relative to argon are listed as a function of time, in the Table B-3-3 below. Peak (27) was chosen because it suffers no interference from the acetylene peaks, and its intensity is strong enough (63% of the molecular peak 28).

Spectrum	Time (min)	(27)/Ar	Average (27)/Ar
	at 20°C		
Background	-	0.43	0.35
Sample at 77°K	-	0.27	
Sample at 20°C	0	1.00	discounted (not stabilized)
"	4	1.05	1.08
"	6	1.10	

TABLE B-3-3 Ethylene

### B-3-4 Acetylene

No single fragment of acetylene could be easily analysed in the presence of ethylene as these two compounds share in common most of their fragments. However, the evolution of the peak  $m/e = 26$  is depicted below

in Table B-3-4.

A 7.4 fold increase in the peak at  $m/e = 26$  is shown. This peak represents 100% of the acetylene, but only 63% of the ethylene present in the sample gases. In view of the previously established increase of the ethylene concentration by a factor of only 3, it seems reasonable to conclude that the acetylene itself increased by a factor of more than 7.4.

Thus the acetylene was more abundant in the sample gases than the ethylene. This result is confirmed by the study of the relative intensities of the peaks 26, 25, 24 and 13. Their ratios are 100/17/5/5 and match closely the theoretical 100/20/6/6 especially if one takes into account the interference from the ethylene fragments.

Spectrum	Time (min) at 20°C	(26)/Ar	Average <sup>(26)</sup> /Ar
Background	-	0.26	0.20
Sample at 177°K	-	0.15	
Sample at 20°C	0	1.88	discounted (not stabilized)
"	4	1.59	
"	6	1.40	1.50

TABLE B-3-4 Acetylene

APPENDIX CNotes on the direct synthesis of calcium acrylate anhydrate

Lando and Morawetz<sup>(77,78)</sup> reported to have synthesized different varieties of CaAc anhydrate, by dehydration of the dihydrate or of the monohydrate, and by recrystallization from an anhydrous solution in methanol.

The monohydrate, although obtainable by partial dehydration of the dihydrate, appears to be simply a mixture of 50% dihydrate and 50% anhydrate, and has escaped isolation as a definite entity thus far (cf. section III-3-1).

The synthesis of the anhydrate by recrystallization of an anhydrous methanolic solution was attempted. When dry nitrogen was used as a purge gas, the same problems as for the synthesis of D<sub>2</sub>O-dihydrate were encountered, i.e. some spontaneous polymerization took place. Accordingly, dry air was used instead. The solubility of the anhydrate in methanol was observed to be low, and some heating was required.

In one instance, parallelepipedic transparent crystals were obtained, and they were stored in a vacuum oven overnight at 60°C. It was found subsequently that these crystals had decomposed into an opaque whitish material presenting very weak mechanical resistance. Analysis of a fresh batch of crystals by I.R. displayed a band attributed to one of the fundamental MeOH vibration frequencies, that was absent from the spectrum of the anhydrate prepared by dehydration.

These observations suggest that an unstable methanolate might have been formed, with MeOH either included in the lattice (like H<sub>2</sub>O in a hydrate) or occluded in lattice voids. Although O'Donnell and Sothman<sup>(83)</sup> did not

report similar problems during the recrystallization of Ba-methacrylate, these observations point towards the need for further investigation. The synthesis of a true crystalline anhydrate would present a considerable interest by allowing the comparison of its polymerization behaviour with that of the amorphous variety.

In case only a methanolate could be obtained, the probably amorphous material made by removing the methanol could still be fruitfully compared with the dehydrated variety, as it would not necessarily display an identical Debye-Scherrer pattern.

Appendix D : Tables of supporting dataTable of data for Fig. III-3-7Wide-Line NMR second moments (in Gauss<sup>2</sup>) of CaAc hydrates at 77 and 295°K .

D <sub>2</sub> O Hydrates			H <sub>2</sub> O Hydrates		
Hydration Level	at 77°K	at 295°K	Hydration Level	at 77°K	at 295°K
0	9.19; 9.48	4.37; 5.43	0	-	4.66; 5.21
0	9.09; 9.86	4.17; 5.07	0	-	4.43; 5.92
0.16	9.67; 9.47	5.96; 5.46	0.27	10.70; 10.88	5.42; 6.14
0.16	9.17; 9.22				
0.34	11.12; 8.68	5.97; 6.15	0.51	12.51; 11.90	7.51; -
0.41	9.73; 8.72	6.13; 5.86	0.51	-	7.16; 6.78
0.61	9.70; 8.79	5.21; 7.16	0.72	13.16; 12.90	6.79; 10.80
0.99	9.66; 8.72	5.85; 7.01	1.03	14.10; 15.57	10.05; 10.15
1.00	-	5.44; 5.01	1.57	16.85; 18.03	13.30; 12.60
1.10	9.63; 9.56	6.16; 5.73	1.72	17.47; 19.46	12.39; 13.15
1.47	9.81; 9.20	5.36; 7.17	1.72	-	14.75; 14.25
2.00	10.00; 11.09	7.28; 6.94	1.72	-	15.95; 11.79
2.00	-	6.47; 6.37	2.00	-	14.81; 15.06
2.00	-	6.37; 6.70	2.00	-	15.24
2.00	-	6.67; 6.09			

## Data for Fig. III-3-8

Wide-Line NMR second moments of CaAc hydrates as a function of temperature

D <sub>2</sub> O dihydrate				Anhydrate			
Temp. (°K)	R.F. power (db)	Modul. Ampl. (Gauss)	Second Moment (Gauss <sup>2</sup> )	Temp. (°K)	R.F. power (db)	Modul. Ampl. (Gauss)	Second Moment (Gauss <sup>2</sup> )
77	-50	2	10.0;11.1	77	-53	1	9.19;9.48
115	-50	2	10.3;9.11	"	-53	1	9.09;9.86
136	-48	2	10.6;9.77	106	-53	2	9.17;8.67
153	-45	2	10.1;9.84	135	-53	2	7.46;8.59
186	-45	2	10.3;9.46	159	-53	2.8	6.25;7.73
202	-44	2	8.64;9.66	165	-40	2.8	7.96;6.92
218	-44	2	9.30;9.90	174	-40	2.8	6.66;6.80
232	-43	2	8.61;8.69	200	-35	2.8	5.64;6.06
244	-40	2	7.78;7.92	214	-35	2	6.06;6.65
256	-40	2	7.40;7.72	239	-35	2	5.80;6.22
267	-40	2	6.25;7.26	259	-33	2	5.13;5.94
281	-40	2	6.61;6.55	275	-33	2	4.74;6.00
295	-23	2.8	6.47;6.37	295	-35	2	4.17;5.07
"	-23	2.8	6.37;6.70	"	-33	2.8	4.66;5.21
"	-23	2.8	6.67;6.09	"	-33	1.4	4.43;5.92
"	-33	1.4	7.27;6.94	"	-33	1.4	4.37;5.43
				"	-23	2.8	3.87;5.06
				"	-23	2.8	3.66;4.08
				"	-23	2	4.46;5.77
				"	-23	0.5	5.87;5.94
				321	-30	1.4	4.42;5.15
				332	-30	1.4	4.55;5.56
				354	-30	1.4	4.04;4.49
				373	-30	1.4	4.13;4.42
				407	-30	1.4	3.49;3.61

Data for Fig. III-4-2

Effect of R.F. power on the saturation of the ESR signals at 77°K, initially. Signal intensities were normalized with respect to a pitch standard and to the packing density of each sample (in mg/cm in the tube).

<u>D<sub>2</sub>O hydration level</u>	<u>0.1 mW R.F.</u>	<u>0.3 mW R.F.</u>	<u>5 mW R.F.</u>
2.00	-	0.968	-
"	0.311	1.21	2.26
"	-	1.23	-
1.75	0.559	1.23	2.11
1.62	-	1.32	-
1.22	0.857	1.73	2.86
1.10	-	1.90	-
1.00	0.908	1.92	3.16
0.82	-	2.03	-
0.71	0.961	2.04	3.14
0.51	1.29;1.05	2.47	3.54
0.32	1.50	2.81	3.96
0.14	1.35	2.60	3.54
0.00	1.23	2.34	3.25

Data for Fig. III-4-5

Effect of annealing and hydration level on the ESR signal intensity, at 77°K and 0.1 mW R.F. power.

<u>D<sub>2</sub>O hydration level</u>	<u>immediately after irradiation</u>	<u>1 week anneal<sup>g</sup> at -78°C</u>	<u>4 weeks anneal<sup>g</sup> at -78°C</u>	<u>at 22°C</u>
2.00	0.311	0.277	0.278;0.210	0.230
1.75	0.559	-	0.312	0.242
1.22	0.857	-	-	-
1.00	0.908	-	0.465	0.340
0.71	0.961	0.720	0.569	0.387
0.51	1.29;1.05	-	0.694	0.478
0.32	1.50	0.886	0.825	0.587
0.14	1.35	-	-	-
0.00	1.23	0.858	0.701	0.544

Data for Fig. IV-1-2

Oxygen diffusion at the limiting conversion stage, studied by ESR

Polymerized Dihydrate			Polymerized Anhydrate		
Time (min)	Triplet height (mm)	Height loss (%)	Time (min)	Triplet height (mm)	Height loss (%)
0	186	0	0	147	0
1	179	3.5	4	116	21.1
5	173	7.0	9	102	30.6
10	167	10.2	34	80	45.6
20	161	13.7	<u>Treatment in the open air</u>		
30	156	16.1	<u>with a scavenger solution</u>		
50	147	21.0	64	4	97
<u>Treatment in the open air</u>			154	1	>99
<u>with a scavenger solution</u>					
100	108	42.0			
105	104	44.0			
125	96	48.4			
275	83	55.4			

The origin of the times given corresponds to the admission of the oxygen of the break-seal compartment.

Data for Fig. IV-2-3

Wide-Line NMR study of irradiated CaAc dihydrates samples as a function of post-polymerization time : reduced height of the narrow line signal (in mm).

Time (days)	log(time) (in hrs)	<u>D<sub>2</sub>O - dihydrate</u> Modulation Amplitude		<u>H<sub>2</sub>O - dihydrate</u> Modulation Amplitude	
		1.4 Gauss	0.5 Gauss	1.4 Gauss	0.5 Gauss
1	1.38	132	57	-	23
2	1.68	170	85	92	33
5	2.08	274	160	107	39
6	2.16	302	210	114	44
7	2.23	316	201	125	48
8	2.28	328	234	133	49
9	2.33	346	238	140	52
12	2.46	375	267	176	74
13	2.49	365	262	213	74
14	2.53	378	287	226	83
15	2.56	370	272	226	83
16	2.58	378	282	237	95
19	2.66	370	280	252	97
20	2.68	-	-	250	98
22	2.72	-	-	257	104
23	2.74	-	-	265	105
26	2.80	-	-	267	107
33	2.90	-	-	280	119
40	2.98	-	-	285	119
54	3.11	-	-	330	149

Data for Fig. IV-2-5

Reduced height of the NMR narrow component vs. polymer yield, for CaAc<sub>2</sub>H<sub>2</sub>O.

14.1% : 18mm ; 18.6% : 23mm ; 28.6% : 33mm ; 39.7% : 48mm ; 45.0% : 52mm .

Data for Fig. IV-4-1 , IV-4-2 , and IV-4-4Viscometry data for poly(acrylic acid) made from CaAc, 2H<sub>2</sub>O under vacuum .

	Total Volume ( ml )	Average Elution Time ( sec. )	$\eta_{sp}$	Concentration c ( mg/dl )	$\eta_{sp}/c$ (dl/g)
<u>p-dioxane at 30.00±0.02°C :</u>		576.2	(pure solvent)		
<u>Sample :</u>	10	679.8	0.1799	260	0.692
	15	643.7	0.1172	173	0.676
	20	627.9	0.0897	130	0.690
	30	610.7	0.0599	86.7	0.691
	50	596.8	0.0358	52.0	0.689
	70	591.0	0.0258	37.1	0.693
	95	587.2	0.0191	27.4	0.698
<u>0.203 N HCl at 24.00±0.02°C :</u>		493.3	(pure solvent)		
<u>Sample :</u>	10	577.3	0.1703	229.2	0.743
	15	547.9	0.1107	152.8	0.724
	20	533.7	0.0819	114.6	0.715
	30	519.8	0.0537	76.4	0.703
	50	509.1	0.0320	45.8	0.699
	70	504.5	0.0227	32.7	0.693
	95	501.7	0.0170	24.1	0.706
<u>pH 3 buffer at 24.00±0.02°C :</u>		478.1	(pure solvent)		
<u>Sample :</u>	10	702.2	0.4687	214.4	2.186
	15	629.9	0.3175	142.9	2.221
	20	589.8	0.2336	107.2	2.179
	30	552.2	0.1550	71.5	2.169
	50	522.8	0.0936	42.9	2.183
	70	510.2	0.0671	30.6	2.192
	100	500.5	0.0470	21.4	2.190

Data for Fig. IV-4-5

Elution volumes of various small molecules as a function of molecular weights.

Compound	Mol. weight (g)	lbg(mol. weight)	Elution volume ( counts )
Tetra-Hydro-Furane	72	1.86	39.4
p-Dioxane	88	1.94	37.4
2,2'-oxydiethanol	106	2.03	36.9
Benzene	78	1.89	36.3
Ethanol	46	1.66	35.9
Ca Acrylate monomer	182	2.26	35.1;34.8
Ascorbic Acid	176	2.25	34.3
HCl ; KBr	-	-	32.5 (negative peak)

Data for Fig. IV-4-7 and IV-4-14

Polymer yield kinetics for dihydrate and anhydrate, in vacuo and in air, at 50°C.

Dihydrate ( Fig. IV-4-7 )				Anhydrate ( Fig. IV-4-14 )			
In Vacuo		In Air		In Vacuo		In Air	
Time	Yield (%)	Time	Yield (%)	Time	Yield (%)	Time	Yield (%)
15hrs	14.1	-	-	19hrs	32.7	0 hrs	8.6
1 day	18.3	1 day	7.0	1 day	19.5	5 days	7.0
2 "	28.6	3 "	11.0	3 "	51.9	11 "	6.6
3 "	38.4	5 "	12.6	5 "	20.5	13 "	2.8
4 "	39.7	11 "	13.6	9 "	26.9		
7 "	39.7	13 "	14.9	14 "	58.1		
9 "	45.0						
12 "	47.0						
14 "	49.8						